22-st INTERNATIONAL CONFERENCE ON THE METHODS OF AEROPHYSICAL RESEARCH

July 1 – 5, 2024
Novosibirsk, Russia

Abstracts
Part I

Ministry of Science and Higher Education of the Russian Federation
Russian National Committee on Theoretical and Applied Mechanics
Siberian Branch of the Russian Academy of Sciences
Khristianovich Institute of Theoretical and Applied Mechanics
of the Russian Academy of Sciences
Central Aerodynamic Institute
Novosibirsk State University

International Conference on the Methods of Aerophysical Research

July 1–5, 2024
Novosibirsk, Russia

Abstracts
Part I

Edited by E.I. Kraus

Novosibirsk
Siberian Branch of the Russian Academy of Sciences
2024

INDEPENDENT ELECTRONIC PUBLICATION

UDK 533.6+532.5.013.4+551.5:371.3
BBK B253.33я431(0)

ICMAR-2024 is sponsored by:
Siberian Branch of the Russian Academy of Sciences
Novosibirsk State University

International Conference on the Methods of Aerophysical Research, Novosibirsk, Russia, July, 1 – 5, 2024: Abstracts. Pt. I / Ed. E.I. Kraus; Ministry of Science and Higher Education of the Russian Federation: on [et al.]. – Novosibirsk: SB RAS, 2024. – 177 p.

The 22th International Conference on the Methods of Aerophysical Research (ICMAR 2024) is to be held on July 1–5, 2024. The Conference is devoted to the 110th anniversary of academician V.V. Struminsky, who led ITAM SB RAS from 1966 to 1971.
This collection contains the abstracts of the conference. It includes the following main topics of ICMAR 2024:

- Physical modeling and mathematical simulation of aerogasdynamics of internal and external flows;
- Wind tunnels, gasdynamic facilities and methods of flow diagnostics;
- Hydrodynamic stability, turbulence and flow separation;
- Methods of aerophysical research in interdisciplinary problems.

A special section of ICMAR deals with artificial intelligence and mechanics in medicine.

The papers are printed by direct reproduction from the authors' originals. The authors are responsible for possible misprints and the quality of translations.

ISBN 978-5-6049901-3-1 (ч. 1)
ISBN 978-5-6049901-2-4

DOI 10.53954/9785604990131_3

AN EXPERIMENTAL STUDY OF THE MUTUAL CORRELATION CHARACTERISTICS OF BOUNDARY LAYER DISTURBANCES AND PULSATIONS OF AN INCOMING SUPERSONIC FLOW

L.V. Afanasev, A.D. Kosinov

Khristianovich Institute of Theoretical and Applied Mechanics SB RAS
630090, Novosibirsk, Russian Federation

This report presents the results of an experimental study of the relationship between pulsations of supersonic incoming flow and disturbances of the boundary layer of flat plates at Mach numbers 2 and 2.5, single Reynolds numbers $Re_1 = 5.6\times10^6$ m^{-1} and $Re_1 = 11\times10^6$ m^{-1}. Correlation characteristics such as cross-correlation, the square of the coherence function and the phase of disturbances are used to assess the relationship. The pulsations of the flow were recorded using constant temperature anemometers. Two hot-wire sensors with a tungsten wire with a diameter of 10 microns and a thread length of 1.7 mm were used. One of the sensors is located under the model, the other sensor is located on the coordinate device above the upper surface of the model. In the experiments, models of a flat plate with a sharp leading edge and a model with a cylindrical leading edge with a blunt radius of 0.5 mm were used.

Using digital signal processing, the spatial-temporal distributions of the correlation coefficient and the spatial-frequency distributions of the square of the coherence function and the mutual phase for the boundary layer section are obtained. A detailed description of the technique is presented in [1].

The results obtained allow us to estimate the frequency range of the interconnection of disturbances of the free flow and the boundary layer – 0.8–4 kHz, for the Mach 2.5 number and the Reynolds unit number Re1 = 5.6×106 m^{-1}. An estimate of the size of the boundary layer region in which there is a relationship with the pulsations of the incoming flow is obtained.

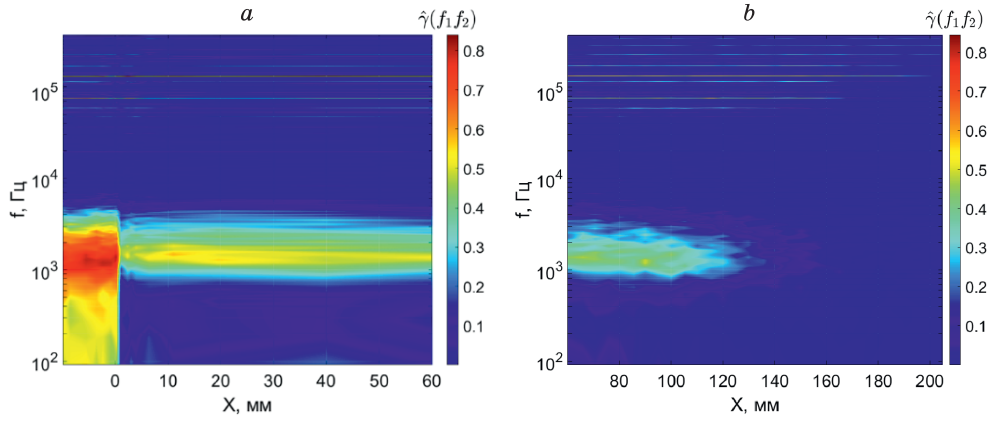

Fig. 1. Spatial-frequency distributions of the square of the coherence function (*a*) in the section above the boundary layer along the flow, (*b*) in the section of the boundary layer along the flow.

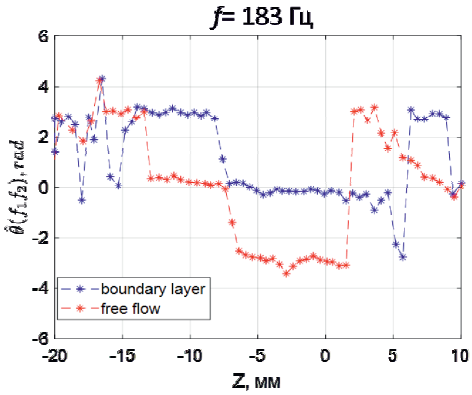

Fig. 2. Spatial distribution of the mutual phase for a frequency of 183 Hz in the area of the impact of weak shock waves on the leading edge.

An experimental study of the mutual correlation characteristics of the incoming flow and the boundary layer of a sharp plate was also carried out on the leading edge of which an N-wave falls at Mach 2 and a single Reynolds number $Re_1 = 11 \times 10^6$ m^{-1}. These experimental results demonstrate a shift in the phase of disturbances by ~π radians in the area of incidence of weak shock waves on the leading edge of the model.

The study was conducted at the Equipment Sharing Center «Mechanics» of ITAM SB RAS. The research was supported by the Russian Science Foundation № 22-19-00666, https://rscf.ru/project/22-19-00666/ .

REFERENCES

1. **Afanasyev L.V., Kosinov A.D., Yatskikh A.A., Shipul S.A., Semionov N.V.** On the Methodology for Estimating the Relationship of Disturbances Using Digital Signal Processing in Relation to Measurements in Supersonic Flows. Siberian Journal of Physics, 2022, vol. 17, no. 4, pp. 58–71. (in Russ.) DOI 10.25205/2541-9447-2022-17-4-58-71

DOI 10.53954/9785604990131_5

EFFECT OF INTERNAL CONVECTION ON THE TEMPERATURE FIELD OF TWO-LIQUID DROPLETS BEFORE THEIR MICRO-EXPLOSION

D.V. Antonov, P.A. Strizhak

National Research Tomsk Polytechnic University
634050, Tomsk, Russia

Two-liquid droplets are a significant alternative to emulsified and homogeneous fuels [1, 2]. The presence of a dispersed phase, for example, water, leads to the appearance of micro-explosion effects, significantly increasing the combustion efficiency of fuel compositions and reducing the concentration of anthropogenic emissions (sulfur and nitrogen oxides) [3, 4]. Micro-explosion (Fig. 1) is a process in which the initial two-liquid droplets (parent droplets) disintegrate into smaller secondary fragments (child droplets) due to local boiling of the dispersed phase (water) with the formation of a steam-air mixture [5, 6]. The characteristics of a micro-explosion depend on a set of parameters: the size and concentration of the dispersed phase, the composition of the shell of two-liquid droplets, the size of the parent droplets, their shape, the temperature of the external gas-air environment and droplets, the heating pattern and rate, heat flow, etc. It is known that the efficiency of a micro-explosion is higher in the case of unmixed two-liquid droplets compared to emulsified fuels.

This paper presents the results of numerical studies of the characteristics of heating and evaporation of two-liquid droplets before micro-explosion under conditions of forced and natural convection, determining the role of internal convection in the formation of the temperature field of droplets. The fundamental case of heating and evaporation of an isolated two-liquid droplet (water/two-component kerosene surrogate) is considered, taking into account the internal forced and natural convection in it when heated in a heated gas-air environment. Numerical calculations of heating and evaporation of two-liquid droplets with and without internal convection were carried out using the COMSOL Multiphysics software package. A comparison is presented of the characteristics of heating and evaporation of two-liquid droplets to the limiting conditions of micro-explosion with and without internal convection under identical initial and boundary conditions. In Fig. 2 presents a quantitative

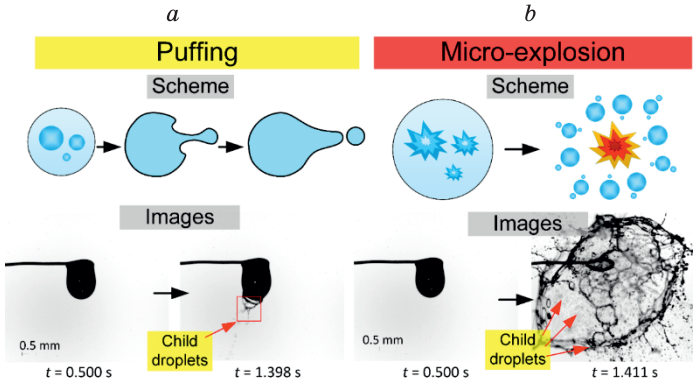

Fig. 1. Typical dynamics of «puffing» (*a*) and «micro-explosion» (*b*) in two-liquid droplets (rapeseed oil (90%) + water (10%)).

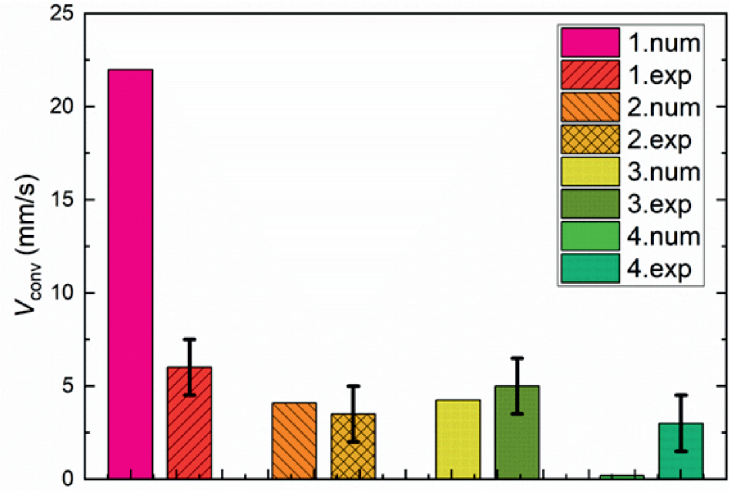

Fig. 2. Column diagrams of maximum (1), average (2) in the fuel shell and maximum (3), average (4) in the water core convection velocities in two-liquid droplets (R_{d0} = 1 mm, T_g = 773 K, water concentration 10 %) based on the results experimental studies (exp) and numerical modelling (num).

comparison of the results of experimental studies and modelling. A good agreement between the results of modelling and experiments was obtained for the average and maximum values of convection velocities. However, there is also some discrepancy (for example, 1 and 2) in the maximum convection velocities in the fuel shell. This is due to the fact that in the experiment, when an air flow flows around two-liquid droplets, their oscillations are observed, which make a significant contribution to the registration of the maximum values of convection velocities.

It has been established that internal convective flows are the root cause of the shift of the core of two-liquid droplets relative to their centre. It was determined that under conditions of natural convection, two large-scale toroidal vortices are formed inside two-liquid droplets, and at the same time, local maximums of the speed of natural convection corresponded to the zone above the core of two-liquid droplets. Mathematical processing of the results of numerical studies was carried out in order to determine the influence of internal convection on the micro-explosion of droplets under various initial and boundary conditions.

The research was supported by the Russian Science Foundation (project No 23-69-10006, https://rscf.ru/project/23-69-10006/).

REFERENCES

1. **Antonov D.V., Kuznetsov G.V., Strizhak P.A., Rybdylova O., Sazhin S.S.** Micro-explosion and autoignition of composite fuel/water droplets // Combust. Flame. 2019. Vol. 210. P. 479–489.
2. **Vellaiyan S.** Recent advancements in water emulsion fuel to explore efficient and cleaner production from various biodiesels: A retrospective review // Renew. Sustain. Energy Rev. 2023. Vol. 187. 113704.
3. **Shinjo J, Xia J.** Combustion characteristics of a single decane/ethanol emulsion droplet and a droplet group under puffing conditions // Proc. Combust. Inst. 2017. Vol. 36. P. 2513–2521.
4. **Watanabe H., Matsushita Y., Aoki H., Miura T.** Numerical simulation of emulsified fuel spray combustion with puffing and micro-explosion // Combust. Flame. 2010. Vol. 157. P. 839–852.
5. **Antonov D.V., Kuznetsov G.V., Strizhak P.A.** The micro-explosive fragmentation criteria of two-liquid droplets // Int. J. Heat Mass. Transf. 2022. Vol. 196. 123293.
6. **Wang C.H., Hung W.G., Fu S.Y., Huang W.C., Law C.K.** On the burning and microexplosion of collision-generated two-component droplets: Miscible fuels // Combust. Flame. 2003. Vol. 134. P. 289–300.

DOI 10.53954/9785604990131_7

STUDY OF LOCAL HEAT TRANSFER IN TRANSVERSE SUPERSONIC FLOW PAST A CYLINDER IN A SHOCK TUBE

E.V. Babich[1], A.V. Masyukevich[2], E.V. Kolesnik[1], P.A. Popov[2]

[1]Peter the Great St.Petersburg Polytechnic University, 195251, Saint Petersburg, Russia

[2]The Ioffe Physical-Technical Institute of the RAS, 194021, Saint Petersburg, Russia

The study of gas dynamic phenomena, which occur in high-speed viscous gas flows past obstacles mounted on the streamlined surface, is of great importance for designing various air-craft elements and for power engineering [1]. In experimental studies of such flows, one of the challenges is the accurate measurement of heat flux to the streamlined surface. At the same time, three-dimensional numerical simulations are required nowadays for a more detailed analysis of local heat transfer characteristics in a complex flow near the obstacle.

The experiments were conducted using a shock tube of the Ioffe Institute with a rectangular section of 50 mm × 150 mm (Fig. 1). A transversally streamlined cylinder with a length of 50 mm and a diameter of D = 12 mm was located in the middle longitudinal plane between the tube walls (Fig. 1a). A flow behind the incident shock wave with a growing boundary layer flows past the cylinder. The working gas is air at an initial pressure of 1.33 kPa, the Mach number of the incident shock wave is $M_1 = 4.8$. The parameters of the flow calculated using one-dimensional shock tube theory are the following: the Mach number is M = 1.8, the unit Reynolds number is $Re = 2.5 \cdot 10^6$ [1/m] (the Reynolds number based on cylinder diameter is $Re_D = 3 \cdot 10^4$). The local heat flux towards the tube wall in the separation region in front of the cylinder was measured. The heat flux measurement was conducted using sensors based on anisotropic bismuth thermoelements [3]. The sensor was mounted in the median longitudinal plane; the position of the cylinder was varied (by changing the length of the retainer) to provide different distances between the sensor and the cylinder (Fig. 1). A series of experiments showed good repeatability of results.

In order to analyze the flow structure in detail, numerical simulations of supersonic flow past a cylinder mounted on a plate were carried out. The incoming flow parameters corresponded to the flow behind the incident shock wave in the shock tube. Calculations were performed using the SINF/Flag-S program code developed at St. Petersburg Polytechnic University; the resources of the supercomputer center of St. Petersburg Polytechnic University (www.scc.spbstu.ru) were used.

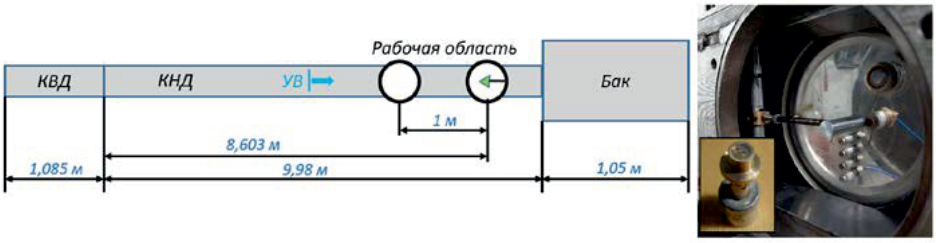

Fig. 1. Scheme of rectangular shock tube, cylinder location in channel and heat flux sensor.

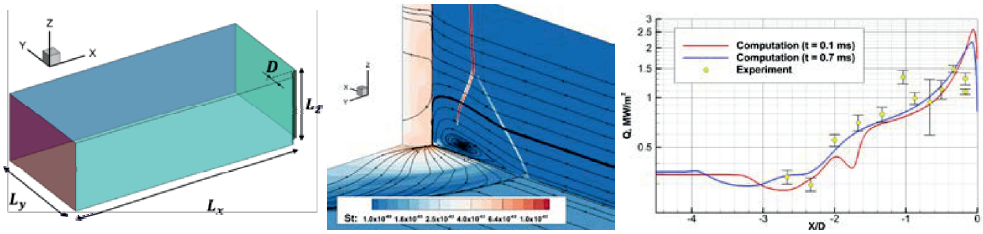

Fig. 2. Computation domain, 3D flow structure and comparison of calculation and experimental values of heat flux in front of the cylinder

The computational domain covered half of the experimental configuration (Fig. 2), the size $L_y = 6.25D$ corresponded to half the width of the low-pressure chamber, other sizes were $L_z = 4D$ and $L_x = 13D$. The Reynolds-averaged Navier-Stokes equations for perfect gas were solved numerically. The k-ω SST turbulence model was used. The AUSM scheme of the second order of accuracy was used to convective fluxes evaluation (the numerical scheme is described in detail in [2]). The quasi-structured mesh consisted of 4 million cells and met the requirement $y^+ < 1$. The cylinder surface and the plate were maintained at a constant temperature, $T_w = 273$ K. The non-reflecting boundary conditions were specified on the lateral and upper boundaries and the zero-gradient condition was set at the outlet. The quasi-stationary simulation was performed: at the inlet, profiles of local parameters of the flow were specified, corresponding to several moments within the shock tube test time. These profiles were obtained using auxiliary unsteady two-dimensional calculation of shock wave propagation in the shock tube without a cylinder.

Fig. 2 illustrates the 3D flow structure, corresponding to the moment 0.1 ms after the front of the shock wave passes the point where the cylinder was located. One can see a bow shock and a large separation area, consisting of a single horseshoe vortex (for the time-averaged flow), in front of the body. The bow shock intersects the shock wave emanating from the separated-flow region in a triple point.

Cylinder and boundary layer viscous-inviscid interaction results in local high heat flux regions on the plate. In Fig. 2, the heat flux distributions along the symmetry line calculated for two inlet profiles are compared with experimental data. The latter are obtained by averaging the interval of 100 μs, the figure also shows the standard deviations. It can be noted that the results are in good agreement, which, in particular, confirms the presence of a quasi-stationary time interval in the experiment.

This research was funded by the Russian Scientific Foundation, grant number 23-29-00286.

REFERENCES

1. **Sabnis K., Babinsky H.** A review of three-dimensional shock wave–boundary-layer interactions. Prog. Aerosp. Sci., 2023, vol. 143, art. no. 100953.
2. **Kolesnik E.V., Smirnov E.M., Smirnovsky A.A.**, Numerical solution of a 3D problem on a supersonic viscous gas flow past a plate-cylindrical body junction at M 2.95, St. Petersburg Polytechnical State University Journal. Physics and Mathematics. 12 (2) (2019) 7–22. DOI: 10.18721/JPM.12201
3. **Sapozhnikov S.Z., Mityakov V.Yu., Mityakov A.V.** Heatmetry: The Science and Practice of Heat Flux Measurement: Heat and Mass Transfer. Springer International Publishing, 2020, pp. 209. https://doi.org/10.1007/978-3-030-40854-1

DOI 10.53954/9785604990131_9

JUSTIFICATION OF THE CHOICE OF TURBULENCE MODEL FOR MODELLING OF WORKING PROCESSES IN POWER PLANTS

B.Y. Bendersky, A.A. Chernova

Kalashnikov Izhevsk State Technical University
426069, Studencheskaya str., 7, Izhevsk, Russia

The issues of research and modelling of turbulent flows remain topical during the last decades. New methods and approaches to numerical modelling of turbulent flows are being developed. At the same time, due to insufficient study of turbulence itself, there are no universal approaches to its modelling [1–7]. That is, the application of each approach, as well as individual models, requires not only the use of appropriate forms of the conservation equation system [2, 3, 4, 6], but also a different degree of resolution of the mesh domain and, as a consequence, different computational resources. As a consequence, the problem of assessing the correctness and admissibility of a particular approach to modelling turbulent flows and/or a particular model is required for each problem to be solved. Thus, the questions of justification of correctness of turbulence model selection for numerical modelling of gas-dynamic and thermophysical processes occurring in the combustion chamber of power plants are considered. Since the Reynolds turbulence models [1, 8–11] are the least demanding for discretization of the computational domain in space and for computational capacity, the choice of models will be made from their class.

We consider the coupled problem of heat transfer in the combustion chamber of a power plant, where a spatial, turbulent ($Re \geq 105$) flow of compressible heat-conducting gas is realised. The first stage of validation of RANS models of turbulence – testing of correctness of turbulence models is carried out on the experimental description [12] of the problem of heat transfer on the inlet surface of a recessed nozzle of a power plant. It is found that the application of the RNG k-ε, k-ε and Spalart-Allmaras turbulence models leads, on the one hand, to an overestimation of the heat transfer intensity in the high-speed flow region by 95 %, 44 % and 24 %, respectively, and, on the other hand, to a significant underestimation of the heat transfer coefficient in the return flow region by 80 %, 85 % and 96 %, respectively. Therefore, the use of the RNG k-ε, k-ε and Spalart-Allmaras models for numerical modelling of working processes in combustion chambers of power plants is not reasonable.

The second stage of validation of RANS models of turbulence is testing of turbulence models k-ω SST, k-ω and SST on the problem of gas flow in flow paths of power plant, which has a detailed experimental description [13]. It is revealed that all considered turbulence models allow to obtain correct distributions of heat transfer coefficient in the region of braking points and return flows, but, at used model coefficients, do not correlate with experimental data in the regions of transonic flows. In the subsonic region, the heat transfer coefficient distributions obtained in the framework of the considered turbulence models are close to the experimental ones.

Thus, the analysis of applicability of RANS turbulence models for modelling of spatial quasi-stationary intrachamber processes in flow paths and pre-flow volume of a power plant has been carried out. Validation of the most widespread turbulence models as applied to the problems of conjugate heat transfer on the known experimental data has been carried out. It is shown that the turbulence model SST k-ω allows to obtain the local distributions of the

heat transfer coefficient closest to the experimental data: the discrepancy of the model with the experimental data does not exceed 8 %.

REFERENCES

1. **Bardina J.E., Huang P.G., Coakley T.J.** Turbulence Modeling Validation, Testing, and Development, NASA Technical Memorandum 110446, 1997.
2. **Garbaruk A.V.** Current Approaches to Turbulence Modeling, St. Petersburg: SPbPU, 2016 (Russian).
3. **Garbaruk A.V.** Viscous Fluid Flows and Turbulence Models: Methods for Calculating Turbulent Flows, St. Petersburg: SPbPU, 2010 (Russian).
4. **Isaev A.I., Skorobogatov S.V.** Hydrodynamic Verification and Validation of Numerical Methods of the Flow Calculation in Combustion Chamber of a Gas Turbine Engine, Trudy MAI, 2017, no. 97, 28 pp. (Russian).
5. **Volkov K.N., Emelyanov V.N.** Mass-Driven Gas Flows in Channels and Ducts of Power Plants, Moscow: Fizmatlit, 2011 (Russian).
6. **Volkov K.N., Emelyanov V.N.** Large Eddies Simulation in Turbulent Flow Calculations, Moscow: Fizmatlit, 2011 (Russian).
7. **Wilcox D.C.** Turbulence Modeling for CFD, California: DCW Industries La Canada, 1998
8. **Jagadeesh P., Murali K.** Application of Low-Re Turbulence Models for Flow simulations past Underwater Vehicle Hull Forms Journal of Naval Architecture and Marine Engineering, 2005, June, pp. 41–55.
9. **Menter F.R.** Multiscale Model for Turbulent Flows, 24th Fluid Dynamic: Proc. Conf., American Institute of Aeronautics and Astronautics, 1993, pp. 128–143.
10. **Menter F.R., Kuntz M., Langtry R.** Ten years of industrial experience with the SST turbulence model, Proc. 4th. Int. Symp. on Turbulence, Heat and Mass Transfer, Begell House, 2003, pp. 625–632.
11. **Spalart P.R., Allmaras S.R.** A One-Equation Turbulence Model for Aerodynamic Flows, AIAA Paper, 1992, № 0439, pp. 5–12.
12. **Shishkov A.A., Panin S.D., Rumyantsev V.V.,** Workflows in Solid Propellant Rocket Engines, Moskow: Mashinostroenie, 1989 (Russian).
13. **Saveliev S.K., Emelyanov V.N., Benderskiy B.Ya.,** Experimental Methods of SRM Gas Dynamics Research, St. Petersburg: Nedra, 2007 (Russian).

DOI 10.53954/9785604990131_11

GENERATION OF ATMOSPHERIC TURBULENCE IN A MULTIFAN WIND TUNNEL

G.A. Berkon, P.A. Polivanov

Institute of Theoretical and Applied Mechanics SB RAS
630090, Institutskaya 4/1, Novosibirsk, Russia

Atmospheric turbulence can have a significant effect on the flight trajectory of small unmanned aerial vehicles (UAVs) [1]. Improving the flight dynamics of a UAV is often done in flight tests by adjusting the flight controller. In this case there is a high probability of losing the aircraft. In addition flight tests do not allow monitoring all the required parameters of the incoming flow. To carry out such tests in laboratory conditions it is necessary to have an wind tunnel capable of creating flows that simulate atmospheric turbulence. One of the ways to solve this problem is a multifan aerodynamic wind tunnel [2–5]. The low inertia of individual fans makes it possible to simulate gusts of wind close to real ones. The ability to control each fan individually makes it possible to implement the necessary velocity defects distribution in space. In this paper the capabilities of the multifan wind tunnel for modeling atmospheric turbulence are determined experimentally and numerically.

In Fig. 1 shows a photo of a multifan wind tunnel, the parameters of which were studied in this paper. The stand consists of 81 server fans located parallel to each other in a 9 by 9. The cross-sectional area of the test section of the wind tunnel is 0.5 m^2, the maximum flow velocity is 10.5 m/s. The rotation frequency of each individual fan is adjusted independently of each other, which makes it possible to simulate non-uniformity velocity in space and different unsteady process. A honeycomb was installed at the exit from the wind tunnel, which made it possible to decrease a value of root-mean-square velocity up to about 4–6 %. During preliminary tests it was

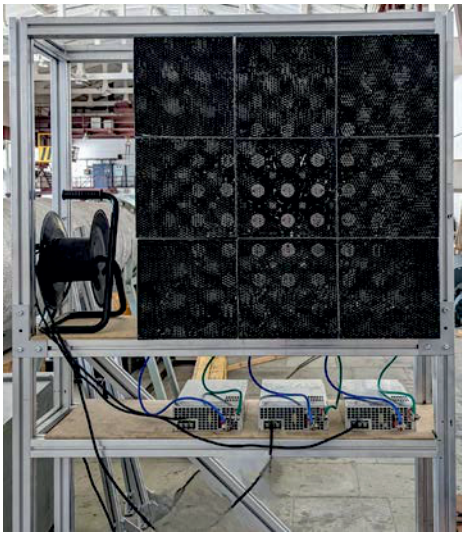

Fig. 1. Photo of a multifan wind tunnel

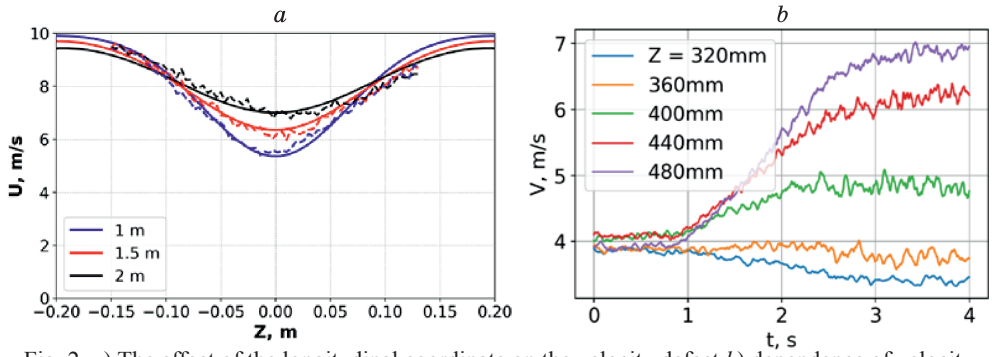

Fig. 2. *a*) The effect of the longitudinal coordinate on the velocity defect *b*) dependence of velocity on time when generating a gust of wind in a shear layer

found that the aerodynamic characteristics of multirotor aerial vehicles measured in multifan wind tunnel do not differ significantly from the results found in classical wind tunnels.

An example of the data can be seen in Fig. 2. In Fig. 2a shows the velocity profiles found for the case in which one vertical line of fans of the wind tunnel was turned off, all other fans operated in a regime generating a flow velocity of about 10 m/s. The dashed line was obtained experimentally and the solid line was found numerically. The paper proposes a simplified algorithm for calculating the velocity profile based on the conservation of mass law with the assumption of a of a constant mixing angle in shear layer. This algorithm makes it possible to find regimes for each fan (solve inverse problem) that are necessary to obtain a given velocity non-uniformity in space. In Fig. 2a shows good agreement between the numerical and experimental data. In Fig. 2b shows an example of a change of velocity at various points of an non-uniformity flow with a sharp change in the fan rotation frequency. Based on the data found dependencies were derived that made it possible to determine the optimal size of fans to achieve a given non-uniformity of velocity in space at a given distance from the wind tunnel to the experimental model.

The capabilities of the multifan wind tunnel in simulating the frequency and spatial scales of atmospheric turbulence were determined. Algorithms for controlling a multifan wind tunnel were developed and tested, which make it possible to generate various wind gust scenarios. A work plan for further improvement of the wind tunnel was drawn up.

REFERENCES

1. **Polivanov P.A., Markin V., Kislovsky V.A., Sidorenko A.A.** Results of flight experiments on the detection of a separated flow by unsteady sensors on UAVS // XXI International Conference on the Methods of Aerophysical Research (ICMAR – 2022) (Novosibirsk, 8–14 Aug. 2022): Abstr. Pt. I. – Novosibirsk: SB RAS, 2022. – P. 159–160. DOI: 10.53954/9785604788967_159
2. **Greenblatt D., Wygnanski I.D.** The control of flow separation by periodic excitation // Progress in Aerospace Sciences. – Vol. 36, No. 7. 2000. P. 487–545.
3. **Songqi Li, Yutong Liu, Zhutao Jiang, Gang Hu, Bernd R. Noack.** Aerodynamic Characterization of a Fan Array Wind Generator. 1 Sep 2023.
4. **Guillaume Catry, Nicolas Bosson, Luca J. Bardazzi, Sergio Márquez, and Albéric Gros.** Wind and Weather Facility for Testing Free-Flying Drones. 2019.
5. **Shigehira Ozono, Hiroshi Ikeda.** Realization of both high-intensity and large-scale turbulence using a multi-fan wind tunnel. 2018.

DOI 10.53954/9785604990131_13

STABILITY OF THREE-DIMENSIONAL BOUNDARY LAYER WITH REVERSAL OF CROSSFLOW

A.V. Boiko[1], N.V. Demidenko[1, 2]

[1]Khristianovich Institute of Theoretical and Applied Mechanics SB RAS, 630090, Novosibirsk

[2]Novosibirsk State University, 630090, Novosibirsk

An aircraft with a fully turbulent boundary layer has a significantly higher drag than a partially laminarized vehicle that leads to increased fuel consumption and reduced flight range. At the stage of optimizing structural elements with natural laminar flow it is important to determine the laminar–turbulent transition region. The existing universal gas-dynamic packages (ANSYS Fluent, OpenFOAM, etc.) have no means for theoretically justified modeling of the laminar–turbulent transition and depend entirely on empirical models based on the transport equations (see, e.g., [1]).

To analyze the growth of small perturbations, the theory of hydrodynamic stability is usually applied. The success of its application depends to a large extent on the accuracy of specifying the profiles and first derivatives of the streamwise and crossflow velocity components in the boundary layer, which are parameters in the linearized Navier–Stokes equations [2]. Previously, the stability of the flow in the boundary layer of a swept wing in the region of flow deceleration preceding the flow separation has not been systematically investigated. Note that the profiles of the crossflow velocity component of the pre-separated boundary layer are characterized by a peculiar S-shape.

In the authors' previous work [2], two-parameter family of Gaster profiles [2] was used to approximate the flow in this region. It was shown that the pre-separated profiles observed in experiments and calculations are reproduce well by the family [3]. In the present work, these profiles were used to analyze the stability of the boundary layer with reversal of the crossflow velocity component (Fig. 1*a*).

The computations were performed using the local approximation of the theory of hydrodynamic stability in time [4]. By the Stuart transformation, the problem was reduced to an effectively two-dimensional one along the direction of the wave vector of the considered disturbance (Fig. 1*b*). It turned out that, in contrast to the Falkner–Scan–Cook self-similar profiles, the considered effective velocity profiles of retarded flow have two inflection points at certain angles of the wave-vector direction, and, respectively, up to four critical layers (coordinates η at which the local flow velocity coincides with the velocity at the inflection points), see Fig. 2*a*.

Hence, two growing disturbances (with imaginary part of the frequency (eigenvalue) $\mathrm{Imag}(\omega)>0$) can occur, see Fig. 2*b*. Thus, the possibility of simultaneous growth of two different disturbances with the same wave numbers α and β in the three-dimensional boundary layer with velocity described by the profiles of two-parameter Gaster family has been shown for the first time.

The work was supported by Russian Science Foundation grant 23-19-00644 ("Development of new methods for controlling the swept-wing boundary layer").

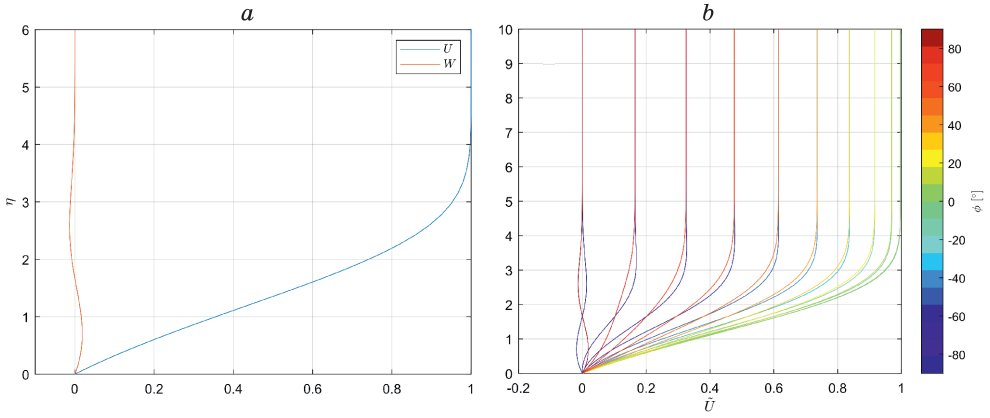

Fig. 1. Profiles of streamwise and crossflow velocity components in self-similar coordinates η.

a – U – streamwise velocity component, W – crossflow velocity component with different flow direction near and far from the wall at the family parameters $\beta_G = 0.2$, $\gamma_G = 0.05$ and flow rotation angle $\theta = 30^o$ (см. [2]); b – examples of effective two-dimensional profiles depending on the angles of the disturbance wave vector ϕ

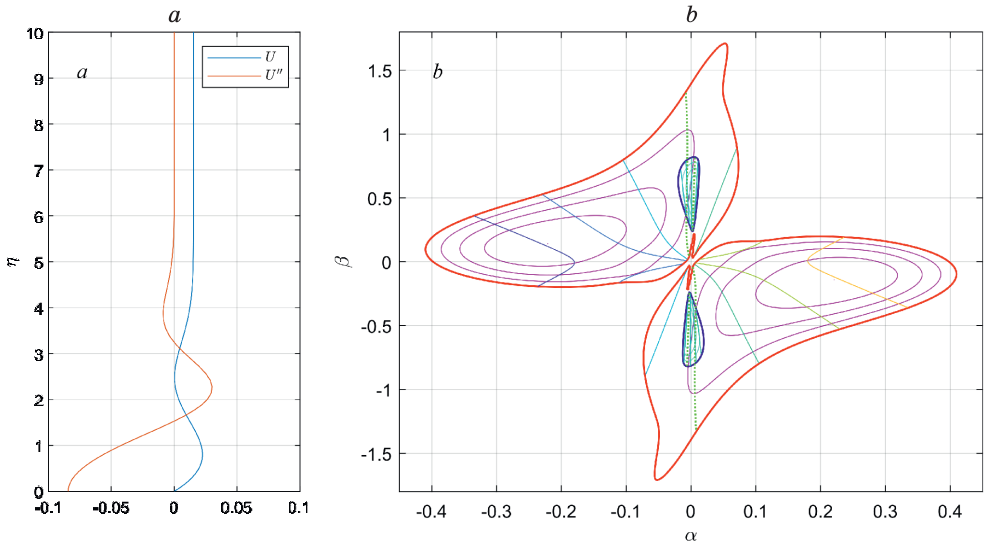

Fig. 2. Stability analysis in the case of retarded pre-separated flow with $\beta_G = 0.2$, $\gamma_G = 0.05$, $\theta = 30^o$ (see [2]).

a – $\tilde{U}$ and $\widetilde{U''}$ – effective velocity and its second derivative by η; *b* – slice of neutral surfaces (red and blue contours), contour lines of increments and phase velocities of disturbances at $\mathrm{Re}_\eta = 5000$.

REFERENCES

1. **Boiko A.V., Kirilovskiy S.V., Maslov A.A., Poplavskaya T.V.** Engineering modeling of the laminar–turbulent transition: Achievements and problems (Review) // Journal of Applied Mechanics and Technical Physics. 2015. Vol. 56, No. 5. P. 761–776.
2. **Demidenko N.V., Boiko A.V.** Using two-parameter velocity profiles for three-dimensional boundary layers // Journal of Applied Mechanics and Technical Physics. 2023. Vol. 64, No. 6. P. 1068–1077.
3. **Boiko A.V., Kirilovskiy S.V., Poplavskaya T.V.** Computational grids for engineering modeling of the laminar–turbulent flow // Journal of Applied Mechanics and Technical Physics. 2022. Vol. 63, No 6. P. 984–987.
4. **Boiko A.V., Dovgal A.V., Grek G.R., Kozlov V.V.** Physics of transitional shear flows // Berlin, Heidelberg: Springer-Verlag. 2012. 272 p.

DOI 10.53954/9785604990131_15

NUMERICAL SIMULATION OF THE FLOW AT A SWEPT WING WITH A SURFACE RELIEF

A.V. Boiko, S.V. Kirilovskiy, T.V. Poplavskaya

Khristianovich Institute of Theoretical and Applied Mechanics of SB RAS, 630090, Novosibirsk, Russia

The problem of reducing the aerodynamic drag of modern subsonic commercial aircraft forces researchers to find new ways to reduce it by developing various methods of controlling the flow structure in the boundary layer. For subsonic flows such control methods as blowing or suction of the flow through the wing surface [1, 2] (active control) and application of different discrete roughness elements (structured surface reliefs) [3–5] (passive control) are actively investigated.

In this paper a swept wing with a sweep angle of 45° and the chord length of 0.7 m exposed to airflow of velocity $Q_\infty = 30$ m/s at an angle of attack $\alpha = -5°$ is considered. The crossflow in the boundary layer at the upper (windward) surface of the swept-wing leads to the laminar-turbulent transition dominated by the crossflow instability vortices (CFVs) [6]. In experiments [5], a method of delaying the transition with a structured surface relief consisted of striped protrusions of rectangular cross-section was tested.

In this study, a numerical simulation of laminar-turbulent flow in the sweep-wing boundary layer with surface relief elements of various configurations at subsonic flow velocities in order was performed to identify and visualize the mechanism of laminar-turbulent transition (LTT) delay and to determine effective geometries and methods of surface relief arrangement. As elements of the surface relief are considered the striped protrusions of rectangular cross-section and their combinations. The protrusions with the height less than one third of the boundary-layer displacement thickness covered the entire wing span. They were located parallel or at an angle to the leading edge of the wing at distances varying from 10 % to 20% of the chord length (Fig. 1).

The numerical simulation was carried out using the computational technology [7] proposed by the authors, which combines the ANSYS Fluent fluid simulation software (to obtain the characteristics of the main flow) with the LOTRAN 3 LTT prediction module (to analyze the stability of the main flow velocity profiles aiming to determine distributions of *N*-factors of disturbance developing in the boundary layer). The computations were carried out for the wing both with and without the surface relief elements. Using the experimental

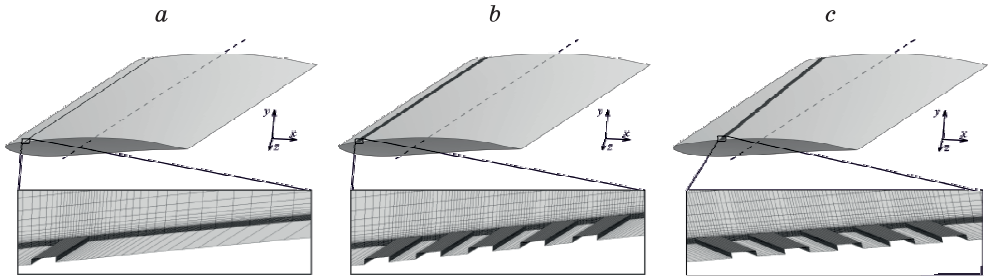

Fig. 1. Schematic imaging of reliefs of different configuration on the upper surface of the swept-wing.

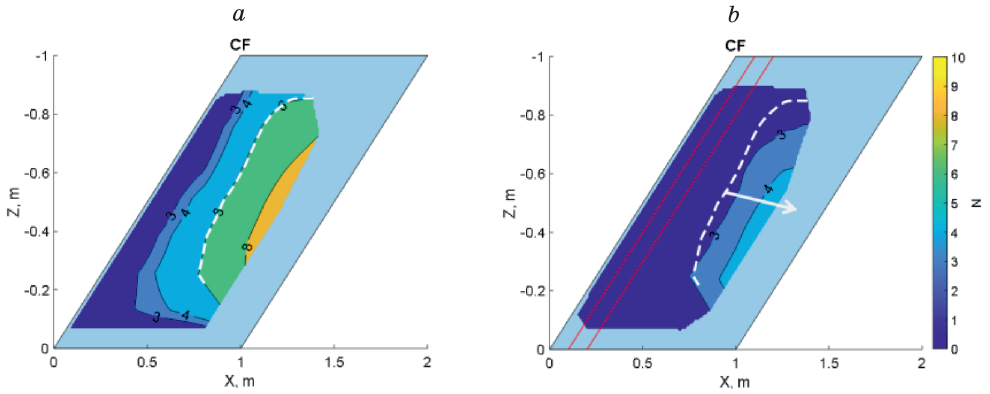

Fig. 2. Isosurfaces of CFVs *N*-factors on the upper surface of smooth wing (*a*) and the wing with two single-stripe reliefs at 10 % and 20 % of the wing chord (red solid lines) (*b*). $Q_\infty = 30$ m/s, $\alpha = 5°$.

data on the LTT position obtained from the analysis of thermograms based on the difference of cooling velocities of the heated wing surface in the laminar and turbulent flow regions [8], the value of the critical *N*-factor of the CFVs $N^*_{CF} = 6$ was determined for a smooth wing at $\alpha = -5°$ and $Q_\infty = 30$ m/s (shown in Fig. 2 by the white dashed line).

The influence of the relief is clearly seen by comparing the *N*-factor isosurface patterns. In the case of the wing with a single-stripe relief and with a combination of two single-strip reliefs (as shown e.g. Fig. 2), the level of $N^*_{CF} = 6$ shifts significantly downstream in respect to the base case (smooth wing). Thus, numerical simulation shows that the surface protrusions under consideration oriented both parallel and at an angle to the leading edge attenuate the CFVs, the sequential installation of several relief elements leading to an increase in the stabilizing effect. The mechanism of such an effect is illustrated: extended zones of weakened transverse flow appear near the vertical walls of the protrusions, contributing to the slowing down of CFVs growth.

This research was funded by the Russian Science Foundation (grant No. 23-19-00644).

REFERENCES

1. **Kornilov V.I., Boiko A.V.** Flat-plate drag reduction with streamwise noncontinuous microblowing // AIAA J. 2014. V. 52, No. 1, P. 93–103.
2. **Boiko A.V., Kirilovskiy S.V., Poplavskaya T.V.** Numerical simulation of laminar-turbulent flow at a sweep wing under the effect of blowing or suction sources // Thermophysics and Aeromechanics. 2024. V. 31, №. 2.
3. **Saric et al.** Stability and Transition of Three-Dimensional Boundary Layers // Annual Reviews of Fluid Mechanics. 2003. V. 35. P.413–440
4. **Kurz H., Kloker M.J.** Mechanisms of flow tripping by discrete roughness elements in a swept-wing boundary layer // JFM. 2016. V. 796. P. 158–194.
5. **Ivanov A.V, Mischenko D.A.** Delay of laminar-turbulent transition on swept-wing with help of sweeping surface relief // AIP Conf. Proc. Vol. 2125, pp. 030041 (2019).
6. **Boiko A.V. et al.** Engineering modeling of the laminar–turbulent transition: Achievements and problems (Review) // J. Appl. Mech. Tech. Phys. 2015. Vol. 56, No. 5. P. 761–776.
7. **Boiko A.V. et al.** Modeling of transonic transitional 3D flows with a general-purpose CFD code using the eN-method // AIAA J. 2021. V. 59, № 9. P. 3598–3610.
8. **Boiko A.V. et al.** Quantification technique of transition to turbulence in boundary layers using infrared thermography // Int. J. Heat Mass Transf. 2022. Vol. 183, Part A. P. 122065.1-122065.11.

DOI 10.53954/9785604990131_17

INVESTIGATION OF TWO-DIMENSIONAL FLAME AND DETONATION WAVES WITH THEIR SIMULTANEOUS REGISTRATION BY A PHOTO CAMERA AND A HIGH-SPEED CAMERA

A.A. Boriskin, A.A. Vasil'ev

Lavrentyev Institute of Hydrodynamics SB RAS
630090, Russia, Novosibirsk, Lavrentyev Ave., 15

It is known that in combustible mixtures both limiting self-sustaining propagation modes–subsonic flame with velocities at the level of deeply subsonic values and supersonic detonation–are unstable, as a result of which their fronts acquire a significantly non-one-dimensional shape. This indicates the classical one-dimensional steady-state models of flame and detonation are too idealized. Since between the limiting regimes there are a large number of non-stationary modes of propagation of flame and detonation waves (including the deflagration to detonation transition), along with the construction of mathematical two-dimensional and three-dimensional models, experimental studies of the characteristics of such non-stationary waves are required. Such studies will make it possible to more adequately simulate the propagation of flame and detonation waves.

In this work, studies were carried out of non-stationary processes occurring with a flame or detonation wave during its transition from a narrow channel to a wide one (so-called wave diffraction). What is new is the simultaneous use of two photographic recording methods: the "open shutter" method of a digital photo camera, which makes it possible to record the trajectories of transverse waves of multifront detonation, and the method of frame-by-frame high-speed registration of the luminescence front using the «NANOGATE-22/16» electron-optical camera. The studies were carried out in quasi-flat channels in the form of a gap between two parallel plates with the condition that the gap size is much smaller than any other characteristic size of the process and the geometric size of the channel. In such a channel, the wave turns from three-dimensional form into two-dimensional, more convenient for research. A stoichiometric mixture of acetylene and oxygen was chosen as the combustible mixture.

Typical time-lapse photographs of the diffraction process for various non-stationary processes are presented in the following figures.

The first frame of Fig. 1 shows the flame front in a narrow channel – significantly curved and inconsistent with model concepts. In subsequent frames, the flame front emerges from a narrow channel into a wide one and burns out the mixture in an expanding flame wave. As the wave propagates further, the wave front smoothes out. In the last frame, the flame front has reached the side walls of the wide channel.

Fig. 1. Propagation of the flame front followed by diffraction.

Fig. 2. Propagation of a diffracting detonation wave with subsequent attenuation.

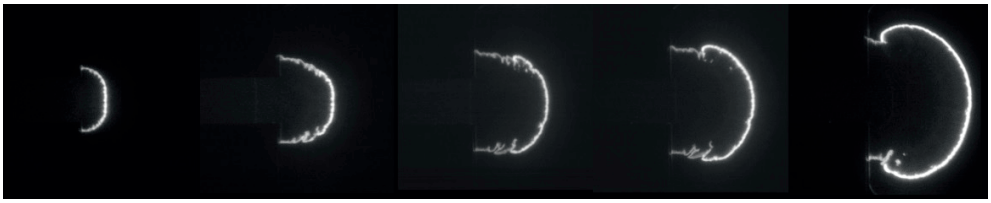

Fig. 3. Propagation of a diffracting detonation wave with subsequent reinitiation.

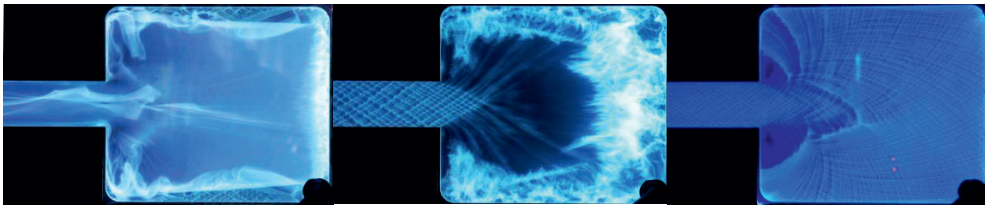

Fig. 4. Pictures of non-stationary processes obtained using the open shutter method. Each photograph (from left to right) corresponds to the processes shown in Fig. 1–3.

Figure 2 shows the process of failure of the initial quasi-stationary multifront detonation during its diffraction. The subsequent frames show the complex shape of the flame front after the detonation decouples into the leading shock and the flame front lagging behind it. This front, lagging behind the shock, burns the mixture in a wide channel.

Figure 3 shows the process of diffraction of a multifront detonation wave during the transition from a narrow channel to a wide one with restoration (reinitiation) of the detonation regime. In this case, the leading shock and the flame front do not "spread away" from each other, but the expanding detonation wave burns out the mixture in a wide channel, including propagating upstream.

These photographs represent the most characteristic, but not the only non-stationary processes in two-dimensional channels. Frames of the non-stationary processes described above obtained by the open shutter method are shown in Fig. 4.

The obtained photographs of the evolution of diffracting waves of flame and detonation help to understand the mechanism of formation of non-stationary waves. The results must be taken into account when making recommendations to reduce the risk of occurrence and development of emergency situations when working with flammable gases in the conditions of the actual location of process equipment in industrial buildings and residential premises.

DOI 10.53954/9785604990131_19

DISTRIBUTED VORTEX RECEPTIVITY OF A SWEPT-WING BOUNDARY LAYER IN PRESENCE OF SURFACE NONUNIFORMITIES. PART 1. METHOD AND VORTEX RECEPTIVITY COEFFICIENTS

V.I. Borodulin, A.V. Ivanov, Y.S. Kachanov

Khristianovich Institute of Theoretical and Applied Mechanics SB RAS
630090, Novosibirsk, Russia

A method of experimental determination of receptivity coefficients describing the efficiency of excitation of cross-flow disturbances in the boundary layer on a swept wing under the combined effect of the streamwise vorticity of the incident flow and the surface waviness (hereinafter referred to as '*surface-vortex receptivity*') is proposed.

In experiments [1, 2], it was shown that the effective transformation of streamwise vorticity into cross-flow perturbations ('*vortex receptivity'*) is not localized in space, but is distributed streamwise. It has been suggested that in the presence of surface waviness, the distributed generation of perturbations could be very significant due to wavenumber resonance. Unfortunately, direct obtaining of receptivity coefficients for this case is not possible because the spatial evolution of the measured quantities is an intricate superposition of already existing (growing or decaying) vortices and newly generated ones. The goal of this work was to develop a method for obtaining the *surface-vortex* receptivity coefficients in experiment.

The method is based on an evolutionary equation for three-dimensional cross-flow instability waves, which describes the growth (or decay) of the amplitudes of boundary layer perturbations, distributedly generated both directly by vortices of the incident flow and due to their scattering on flow inhomogeneities created by surface waviness. In deriving this equation, several simplifying assumptions were made, the validity of which was verified by measurements. The sought *surface-vortex* receptivity coefficients are included in the equation along with the *vortex* receptivity coefficients. All parameters of surface waviness and nonuniformity of the boundary layer (due to its growth), as well as growth rates and streamwise wavenumbers of 'pure' instability waves (in the absence of their distributed generation) can be obtained by direct measurements in complementary experiments. To find the receptivity coefficients, it is necessary to solve the inverse problem. For this purpose, an analytical solution of the evolutionary equation in general form has been written out. It was assumed that the susceptibility and waviness functions are homogeneous in magnitude, harmonic along the longitudinal coordinate, with exponentially varying amplitude. It was assumed that the receptivity and waviness functions are spanwise uniform, harmonic in streamwise direction, and their amplitudes evolve streamwise exponentially. Having this, the solution can be of several types, depending on the ratio of wave numbers of existing and generated disturbances. For each type, we propose procedures for approximating the measured evolution of cross-flow disturbance amplitudes by analytical solutions. The coefficients giving the best approximation will be the sought distributed receptivity coefficients.

The minimum procedure for obtaining receptivity coefficients includes: (1) measuring the stability characteristics on a wavy surface without vortex perturbations in the incoming flow; (2) measuring the evolution of cross-flow perturbations as external vortices scattering on the wavy surface. To obtain more reliable results, it is desirable to repeat the previous two experiments on a smooth surface as well.

The proposed method was applied to the study of flow on a swept-wing model installed in the low-turbulence wind tunnel T-324 of ITPM SB RAS. The model was a flat plate with a sweep angle of 25° equipped with a displacement body with the same sweep angle inducing a pressure gradient in the direction perpendicular to the leading edge of the model, and a pair of sidewalls providing the sweep condition (constancy of the velocity component parallel to the leading edge) in the entire measurement area in the vicinity of the center of the model along the span. Measurements of the mean flow velocity vector components and the streamwise component of velocity perturbations were carried out with a hot-wire anemometer. The base flow both in and out of the boundary layer was carefully documented. A detailed description of the experimental setup and data acquisition system is given in [1]. The velocity of the incident flow was 11.24 m/s, its background turbulence level in the frequency range above 1 Hz did not exceed 0.06 %.

Stability characteristics on smooth and on wavy surfaces were obtained under controlled perturbations introduced by a point source of pulsating blow-in-blow-out built into the model. Vortex perturbations of the incoming flow were generated by a thin (0.05 mm in diameter) vibrating wire installed in front of the model parallel to the leading edge. The wire wake, a two-dimensional vortex street, touched the outer part of the boundary layer. A swelling at the center of the wire created streamwise vortices that were highly repeatable and carefully measured. The alternating activation of the point source and the vibrating wire made it possible to perform the two necessary measurements (stability and receptivity) in one session. Thus, the influence of drift of atmospheric parameters (temperature, density, and viscosity) on the final results was eliminated.

The surface waviness on the model was set using thin appliqués on the model. They had a sinusoidal profile in the chordwise direction and were spanwise uniform. It turned out that small-amplitude surface waviness practically does not affect the velocity profiles in the boundary layer and the development of 'pure' instability modes. At the same time, its influence on the distributed receptivity and the evolution of distributedly generated cross-flow instability waves was quite significant. The paper presents the coefficients of the distributed *vortex* receptivity obtained in the present experiments and their comparison with previous experimental results [1, 2]. The analysis of the mechanism of distributed *surface-vortex* receptivity and comparison of the efficiency of both of the above mechanisms are presented in the second part of this paper [3].

The scope of operated parameters in this work: Reynolds number based on the displacement thickness – 656...774; frequency parameter of disturbances – $14/10^6$...$31/10^6$; waviness amplitudes less than 0.12 of the displacement thickness; chordwise component of waviness wave numbers – about 0.03 rad/mm.

The data obtained using the proposed method for determining the vortex and surface-vortex receptivity coefficients will be useful for the development of engineering methods for transition prediction on swept wings and in other three-dimensional boundary-layer flows. They may also be useful in developing methods for transition control by managed wall waviness.

REFERENCES

1. **Borodulin V.I., Ivanov A.V., Kachanov, Y.S., Roschektayev A.P.** Distributed vortex receptivity of swept-wing boundary layer. Part 1. Efficient excitation of CF modes // J. Fluid Mech. 2020. Vol. 908, A14.
2. **Borodulin V.I., Ivanov A.V., Kachanov, Y.S., Roschektayev A.P.** Distributed vortex receptivity of swept-wing boundary layer. Part 2. Receptivity characteristics// J. Fluid Mech. 2020. Vol. 908, A15.
3. **Borodulin V.I., Ivanov A.V., Kachanov, Y.S.** Distributed vortex receptivity of a swept-wing boundary layer in presence of surface nonuniformities. Part 2. Coefficients of surface-vortex receptivity // ICMAR 2024. Abstracts. – Novosibirsk: ITAB SB RAS, 2024.

DOI 10.53954/9785604990131_21

ASPECTS FLOWING OF THE LONG-RANGE AIRCRAFT TAIL IN LANDING REGIME

N.N. Bragin, G.V. Biryukov, M.F. Garifullin, A.V. Zabrodin, E.A. Zavarzina

Central Aerohydrodynamic Institute named after Prof. N.E. Zhukovsky (TsAGI) 140180 Zhukovsky St. 1, Zhukovsky, Moscow Region, Russia

Experimental investigations of the model long-range aircraft in landing configurations with three variations of spoilers and airbrakes deflection with and without the landing gear with the rake array of static and dynamic pressure (ГПДД32) and tuft method visualization were made.

Amplitude spike of relative power spectrum (relative spectral density of velocity signal) was indicated at frequency $f \sim 12^{\circ}$, airspeed of 50 m/s with airbrakes deflection equal 55°.

Pressure pulsations measurements were made by the rake array of static and dynamic pressure standing beyond the vertical tail in plane the horizontal tail symmetrically. These measurements can be estimated degree of symmetry (antisymmetry) of pressure pulsations acting on the horizontal tail.

The flow visualization was showed pressure pulsations acting with the outboard of wing and generating bending moment in root of the horizontal tail more effect in loading of the horizontal tail. The same pressure pulsations act on the vertical tail. When spoilers and airbrakes deflection equal intensity of flow separation decreases. Based on results obtained the flow visualization has been discovered that spoilers and airbrakes deflection bring about extension wake and intensification of velocity pulsations.

DOI 10.53954/9785604990131_22

SELF-EXCITING PITCH OSCILLATIONS OF A CONE WITH A REAR HEMISPHERICAL PART AT MACH NUMBER M = 1.75

E.A. Chasovnikov

Khristianovich Institute of Theoretical and Applied Mechanics SB RAS, 630090, Novosibirsk, Russia

When the cones move freely along the pitch angle, self-excited oscillations are often induced, which, after the end of the transition process, culminate in the formation of undamped oscillations (self-oscillations). Currently, this complex phenomenon cannot be adequately modeled using numerical methods based on solving continuum equations, so there are no alternatives to experimental research methods in wind tunnels or ballistic tracks. Due to the great technical and fundamental difficulties of these methods, the mechanisms of self-oscillations of axisymmetric bodies have not yet been sufficiently studied.

In works [1, 2], self-excited oscillations of a circular cone with a rear hemispherical part were discovered (Fig. 1) during tests in the T-313 wind tunnel of the ITAM SB RAS on a free oscillation installation at Mach number M = 1.75 and two moments of inertia relative to axis of rotation. This paper examines the results of a study of self-excited oscillations of this cone over a wider range of oscillation frequencies. Changing the oscillation frequency of the cone was carried out by installing additional weights inside the cone, as well as changing the flow parameters. Tests were also carried out on a cone with a slight rounding of the nose to a sphere.

It was found that in all tests, after the completion of transient processes, undamped oscillations of the cone are formed (Fig. 2). At high reduced frequencies, undamped oscillations become irregular. The initial angle of attack does not affect the amplitude of undamped oscillations. The dependence of the amplitude of undamped oscillations on the reduced frequency is of a resonant nature (Fig. 3). Maximum amplitudes are observed at reduced frequencies $\overline{\omega} \approx 0.02$. In the same region, the greatest sensitivity of the amplitude to changes in the reduced frequency is observed.

The following are the various characteristics of the pitch moment coefficient. Methods for obtaining them can be found in [3].

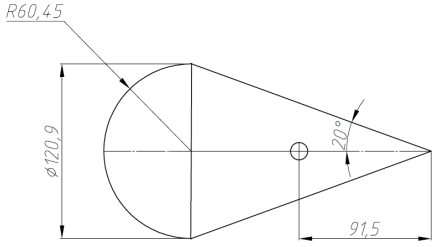

Fig. 1. Scheme of the model.

Dimensions in mm. A round marker on the symmetry axis marks the position of the rotation axis.

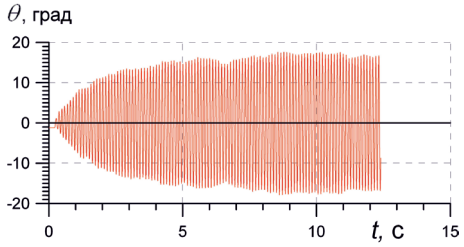

Fig. 2. Dependence of pitch angle on time.

Moment of inertia $I_Z = 14 \cdot 10^{-3}$ kg·m^2.

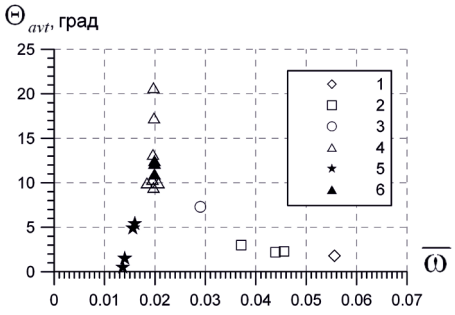

Fig. 3. Dependence of the amplitude of undamped oscillations on the reduced frequency.

1 – 4 – I_Z = 2,2·10^{-3} – 14·10^{-3} kg·m^2. 5, 6 – I_Z = 23,3·10^{-3}, 14·10^{-3} kg·m^2 (the nose of the cone is rounded).

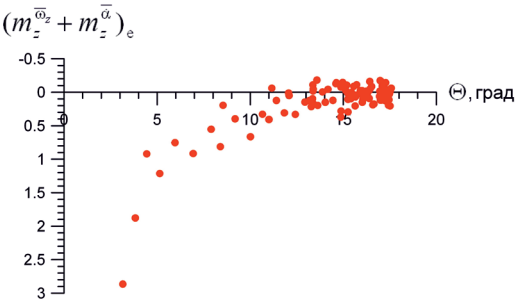

Fig. 4. Dependences of the equivalent pitch damping coefficient on the oscillation amplitude.

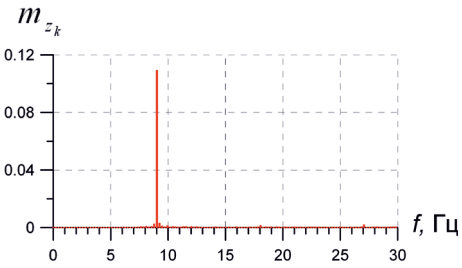

Fig. 5. Spectrum of the pitch moment coefficient during undamped oscillations.

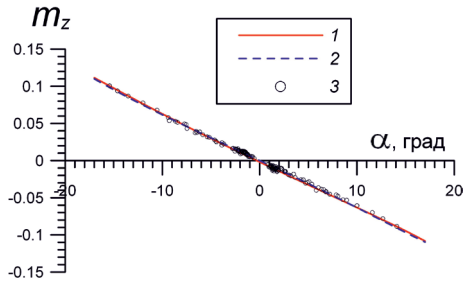

Fig. 6. Dependence of the pitching moment coefficient on the angle of attack.

1 – positive angular velocity, 2 – negative angular velocity, 3 – stationary dependence.

Processing of the initial data showed that the dependence of the equivalent pitch damping coefficient on the oscillation amplitude is hyperbolic in nature (Fig. 4). Everywhere below we provide data for the implementation shown in Fig. 2.

Analysis of the frequency spectrum of the pitch angle and the pitch moment coefficient during undamped oscillations of the cone showed the dominance of the first harmonic (Fig. 5).

It was revealed that in the modes of undamped oscillation of the cone, the values of the pitch moment coefficient at positive and negative angular velocity practically coincide with each other and are close to stationary values (Fig. 6).

It is shown that the probable mechanism of self-exciting oscillations of the cone, proposed in [4], does not contradict the results obtained in the work.

The author expresses gratitude to Adamov N.P. and Chistyakov M.V. for assistance in preparing and conducting the experiments.

The work was carried out within the framework of the Program of Basic Scientific Research of State Academies of Sciences for 2021-2023. The experiments were carried out on the basis of the Mechanika Shared Use Center.

REFERENCES

1. **Adamov N.P., Chasovnikov E.A.** Self-induced oscillations of a cone with a hemispherical rear part at low supersonic velocities // American Institute of Physics Conf. Proceedings. 2018. V. 2027. P. 030150-1–030150-5.
2. **Mishchenko N.A., Chasovnikov E.A.** Study of self-excited pitch oscillations of a conical-spherical body at Mach number M = 1.75 and two moments of inertia // Siberian Physical Journal. 2023. T. 18, No. 1. P. 43–52.
3. **Chasovnikov E.A., Chasovnikov S.A.**. Methods for determining the equivalent aerodynamic damping of reentry vehicle models tested in a setup with free oscillations // Thermophysics and Aeromechanics, 2019, Vol. 26, No. 1. P. 1–8.
4. **Chasovnikov E.A.** Mathematical modeling of self-excited oscillations over the pitch of a conical-spherical body at Mach number M = 1.75 using the forced-oscillation hypothesis // Thermophysics and Aeromechanics, 2023, Vol. 30, No. 5. P. 951–964.

DOI 10.53954/9785604990131_25

STATISTICAL MODEL OF LAMINAR-TURBULENT TRANSITION DUE TO ATMOSPHERIC PARTICULATES

P.V. Chuvakhov[1, 2], A.V. Fedorov[2]

[1]Central Aerohydrodynamic Institute named after N.E. Zhukovsky (TsAGI)
140180, Zhukovsky, Moscow Reg., Russia
[2]Moscow Institute of Physics and Technology (National Research University) (MIPT)
141701, Dolgoprudny, Moscow Reg., Russia

Based on the amplitude method and linear stability theory, a statistical model for prediction of laminar-turbulent transition onset due to atmospheric particulates striking through the boundary layer has been developed. The model accounts for boundary layer receptivity to particulates and makes use of the asymptotic of wave packets of an unstable mode that propagate downstream from the particle-surface collision station. Particles are supposed to be solid spheres, with the concentration distribution law with respect to radius known.

The measurements of the atmospheric particles' characteristics [1, 2] point to the fact that the particles are mainly the products of solid rocket exhaust, having sizes less than 10 μm, which is much less than length scale of both receptivity region and corresponding boundary layer thickness. Such particles can excite the unstable modes directly via the mechanism of dynamic interaction with the boundary layer. A model of this kind of interaction was proposed in [3], and its three numerical implementations [4–6] give quantitively close results.

Model formulation. Consider a steady compressible continuous medium with solid spherical particles with volume-averaged concentration C^* m^{-3} ("*" denotes dimensional quantity). The particles are also steady and distributed randomly with a constant distribution function. A sharp wedge-like body of infinite span and local surface inclination angle $\theta(x)$ with respect to axis r_1 moves through the medium at supersonic speeds. Coordinate systems and schematic of particle-surface collision are given in Fig. 1 relative to the body. Particle strikes excite wave packets in the boundary layer. The packets evolve downstream and reach some critical amplitude some distance apart from the leading edge $x = x_t$, at which transition to turbulence begins and which is to be found.

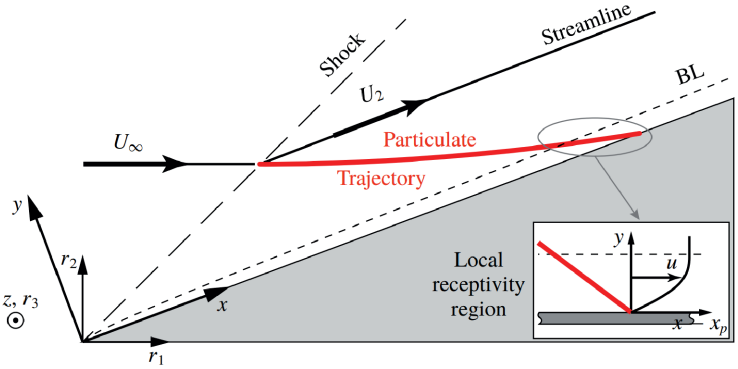

Fig. 1. Schematic of the problem. «BL» is the upper edge of the boundary layer.

The model is based on the following assumptions.

1) Each particle generates a wave packet independent of other particles. The statistically averaged specific frequency ν of particle-surface collisions is equal to that of generation of wave packets in the boundary layer.
2) Undisturbed flow field over the body does not depend on z. Then, ν depends on $\theta(x)$. In particular, in the case of straight-line trajectories $\nu^*(x) = C^* U_\infty^* \sin\theta(x)$.
3) Collisions are random, and excited wave packets are not coherent. Then, the mean square of disturbance amplitude is the sum of squares of all wave packet amplitudes.
4) Receptivity weakly depends on the coordinate x_c of particle-surface collision. Excited wave packets have broadband initial spectral content with amplitude density $\varepsilon(\omega, \beta, x_c)$.
5) Wave packet disturbances amplify selectively downstream. Then, in the far field from the collision station ($x \gg x_c$) each wave packet has a spectrum of gaussian shape. Transition to turbulence begins in the far field as well.

To solve the formulated problem, one needs to: a) solve receptivity problem in order to obtain initial spectrum of wave packets ε; b) solve linear stability problem in order to obtain the dependence of wave packet amplitude on x; c) compute statistically averaged contribution of all wave packets to the disturbance amplitude as function of the observation point x; d) formulate amplitude criterion of transition onset in order to find x_t based on the results of item (c). The present work solves the problem of item (c) in analytic form.

Following asymptotic analysis of [7] for a single wave packet, integration of all the contributions of wave packets born in the region $[0, x]$ by using the steepest descent method gives

$$\left\langle p_w'^2 \right\rangle(x) = \frac{e^{2N(x_0,x)}}{\sqrt{\pi N_{xx}}\sqrt{N_{\omega\omega}N_{\beta\beta} - N_{\omega\beta}}} \int_{R_{p,\min}}^{R_{p,\max}} \varepsilon_s^2(x_0, R_p) \frac{d\nu(x_0)}{dR_p} dR_p \qquad (1)$$

Here $x_0 = x_0(\omega_s, \beta_s)$ is neutral point for the wave of frequency ω_s and wave number β_s that dominates in the observation station x. They are computed using e-N method of linear stability theory along with N_{xx}, $N_{\beta\beta}$, $N_{\omega\omega}$, $N_{\omega\beta}$ which are the second derivatives of N-factor of the wave dominant at x; N-factor is computed from x_0 to x (see details in [7]). Physical meaning of (1) is that the main contribution to the intensity of disturbances is due to the particles striking the surface in a strip $x_0 \pm \Delta x_0/2$ near the neutral point, with $\Delta x_0 = \left(\pi / N_{xx}\right)^{0.5}$. This contribution is due to the disturbances from the spectral band $\Delta\omega\Delta\beta = \pi \Big/ \left(N_{\omega\omega}N_{\beta\beta} - N_{\omega\beta}^2\right)^{0.5}$ near (ω_s, β_s). Thus, the band $\Delta\omega\Delta\beta$ is the effective spectral width of the particle-generated wave packets. It worth noting that in the case of second mode instability we have $N_{\omega\beta} = 0$, $\beta_s = 0$, while the right-hand side of (1) should be multiplied by the factor of 0.5.

Reported during presentation will be the results of the application of the developed model to the case of a sharp wedge flying at supersonic speeds in atmosphere with natural particle content.

The work has been done in MIPT under the support of Russian Science Foundation (project no. 19-79-10132).

REFERENCES

1. **Turco R.** Upper-atmosphere aerosols: Properties and natural cycles // NASA RP-1272, pp. 63–91, 1992.
2. **Habeck J.B., Flaten J., Candler G.V.** High-altitude balloon measurements of atmospheric particulates // AIAA-2020-1794, 2020.

3. **Fedorov A.V.** Receptivity of a supersonic boundary layer to solid particulates. // J. Fluid Mech., Vol. 737, pp. 105–131, 2013.
4. **Chuvakhov P.V., Fedorov A.V., Obraz A.O.** Numerical modeling of supersonic boundary-layer receptivity to solid particulates. // J. Fluid Mech., Vol. 859, pp. 949–971, 2019.
5. **Browne O.M., Al Hasnine S.M., and Brehm C.** Numerical Method for Particulate-Induced High-Speed Boundary-Layer Transition Simulations. // AIAA Journal, Vol. 59, No. 4, pp. 1196–1213, 2021.
6. **Habeck J.B., Kroells M.D., Knutson A.L., Candler G.V.** Numerical study on the role of aerosol particles in hypersonic boundary layer transition // AIAA Paper no. 2024-0702, 2024.
7. **Chuvakhov P.V., Fedorov A.V.** Asymptotic boundary condition for numerical modeling of wave packets in a supersonic boundary layer // Computers & Fluids, Vol. 271, paper no. 106181, 2024.

DOI 10.53954/9785604990131_28

MATHEMATICAL MODELS AND METHODS OF RADIATION MECHANICS IN APPLICATION TO NUCLEAR MEDICINE

N.V. Denisova, M.A. Gurko

Khristianovich Institute of Theoretical and Applied Mechanics
630090, Novosibirsk, Russia

Nuclear medicine is a branch of clinical medicine that uses radiopharmaceuticals (RPs) to diagnose and treat diseases. Single photon emission computed tomography combined with computed tomography (SPECT/CT) is a nuclear medicine diagnostic technique in which the patient is injected with a radiopharmaceutical that emits gamma rays. Gamma radiation passes through biological tissues of different densities (bones, air, soft and fatty tissues), then passes through a lead collimator and is recorded by the detectors of a gamma camera rotating around the patient. After mathematical processing of the measured ("raw") data, reconstruction algorithms produce images of the distribution of the administered radiopharmaceutical in the patient's biological tissues and organs. The radiopharmaceutical is selected in such a way that its accumulation in pathological areas differs significantly from accumulation in healthy tissues. As a result, images with high contrast of pathological foci are obtained. Despite the widespread use of SPECT/CT in clinical practice, there are unresolved problems that lead to errors and a decrease in the diagnostic accuracy of the SPECT/CT method. Research is needed to explore and solve these problems. In vivo clinical trials with real patients are limited due to radiation exposure and the lack of a reference for comparison and evaluation of the reconstructed image. Studies using in vitro material phantoms do not cover the diversity of clinical cases and are limited by high costs. Therefore, the most suitable approach is a mathematical simulation method using in silico digital patient models. To conduct such studies, the development of the software package (PC) "Virtual platform for computer simulation tests of the SPECT/CT method" was developed [1, 2]. Computer modeling involves solving the direct problem of collecting raw projection data and the inverse problem of image reconstruction. A physical and mathematical model was built based on a description of the transfer of gamma radiation from a spatially distributed stationary radiation source in media of different densities. Such models are well known in radiation mechanics and their solutions are constructed either on the basis of a system of integro-differential equations of radiation transfer, or using the Monte Carlo statistical modeling method. The software package consists of the following modules:

1) The "Virtual Patient" software module creates a digital model (phantom) of a patient with a given distribution of radiopharmaceuticals. In radiation mechanics, a similar model describes a spatially distributed stationary source of monochromatic radiation.

2) The "Virtual Tomograph" software module simulates SPECT/CT scanning of a "virtual patient". Based on the statistical Monte Carlo method, the stochastic process of emission of gamma quanta with the same initial energy is simulated, as well as the transfer of radiation in matter of different densities, taking into account Compton scattering and the photoelectric effect.

3) The "Image Reconstruction Algorithms" software module includes a library of modern iterative algorithms for image reconstruction using Poisson data. These algorithms are based on comparing the calculated "pseudo-projection" data for the image obtained at

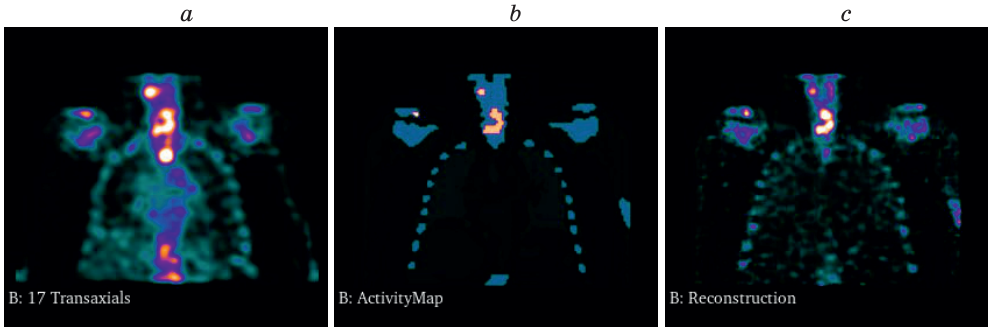

Fig. 1. Comparison of the clinical reconstructed image (a), the phantom (b) and the reconstructed image obtained by simulation modeling (c). Coronal slices of 3D images are shown.

the current iteration with the measured "raw" data. In simulation modeling, projections calculated by the Monte Carlo method in the "Virtual Tomograph" module are used as measured "raw" data. The calculation of "pseudo-projection" data is carried out at each iteration based on the numerical solution of a system of integro-differential equations for the transfer of gamma radiation, written in a discrete representation.

In this work, simulation computer tests of the examination procedure using SPECT/CT with 99mTc-phosphotech of a patient with metastatic lesions of the spine in Th2 were performed. Clinical results were obtained at the National Medical Research Center (NMRC) named after Academician E.N. Meshalkin. Based on the clinical images, a digital twin of the patient was built (the "Virtual Patient" module), projection data was calculated using the Monte Carlo method (the "Virtual Tomograph" module) in accordance with the clinical protocol, and then the image was reconstructed (the "Image Reconstruction Algorithms" module) using the standard OSEM (Ordered Subsets Expectation Maximization) algorithm.

Figure 1 shows a comparison of the clinical reconstructed image (a), the constructed phantom (b), and the simulated reconstructed image (c). There is good agreement between these images.

REFERENCES

1. **Gurko M.A., Denisova N.V.** Modeling of the collection of "raw" projection data in single-photon emission computed tomography JTF 2022 century 5, p. 747–75. http://dx.doi.org/10.21883/JTF.2022.05.52381.264-21
2. **Denisova N.V., Gurko M.A., Minin S.M., Anashbaev Zh.Zh., Zheravin A.A., Samoilova E.A., Krasilnikov S.E.** Possibilities of computer modeling of tumor lesions of the lungs when compared with SPECT/CT data with 99mTc-MIBI Siberian Journal of Oncology 2023 22 14–25 doi: 10.21294/1814-4861-2023-22-2-14-25

DOI 10.53954/9785604990131_30

INVESTIGATION OF FLOW OSCILLATIONS BEHIND THE CIVIL AIRCRAFT WING WITH A WORKING REVERSING DEVICE

D.I. Dugin, D.V. Liverko

140180, TsAGI FAU, Zhukovsky, Moscow region, Russian Federation

In this paper, the parameters of the flow oscillations behind the aircraft wing in landing mode are given. The model geometry includes a glider, a pylon and a nacelle. At that, the wing mechanization, consisting of slats, flaps and brake flaps, is released to the maximum angle, and the reversing device of the engine is turned on. Numerical simulation of the flow is performed using unsteady Navier-Stokes equations averaged by Reynolds (URANS) [1]. The flow simulation is performed by the ZEUS module of the EWT-TSAGI software package [2].

To compare the numerical results with the experiment in wind tunnel, the aircraft model of full-scale Reynolds numbers and a model for the experiment in wind tunnel are investigated. At that, each model has its own features. So, the reversing device in the full-scale model is represented as an air flow with given flow parameters, that is blown out of the reversing device. The runway movement relative to the aircraft is also taken into account. In part of the calculations, a landing gear under the wing is added to study its influence on the flow.

As a result of calculations, the characteristics of flow oscillations at a number of points behind the aircraft wing are obtained. The influence of various factors on the frequency parameters of the flow is investigated. The numerical results for a model without a symmetry plane (full model) and a symmetric model are analyzed. It is obtained that the flow around the full model is not symmetrical, and the difference in the amplitudes of pressure oscillations at prescribed points can be up to two times. Also, for models of different scales (a model for full-scale flight and a model for an experiment in wind tunnel), aerodynamic forces and moments are compared.

REFERENCES

1. **Vlasenko V.V.** On the mathematical approach and principles of developing numerical methodologies for the EWT-TsAGI application software package // Proceedings of TsAGI, issue No. 2671, 2007.
2. **Bosnyakov S.M., Vlasenko V.V., Engulatova M.F., Kazhan E.V., Matyash S.V., Troshin A.I.** Industrial solvers of the EWT-TsAGI package and their verification on a series of standard tests // Proceedings of TsAGI, issue No. 2735, 2015.

DOI 10.53954/9785604990131_31

THE INFLUENCE OF THE WIND TUNNEL NOZZLE ON THE AERODYNAMIC CHARACTERISTICS OF THE WING MODEL WITH DISTRIBUTED POWER UNIT AND COMPARISON WITH THE FREE FLOW

A.A. Ermakov, E.V. Kazhan, D.V. Liverko, R.R. Machin, V.V. Orekhovskii, D.A. Rakhmanin

140180, TsAGI FAU, Zhukovsky, Moscow region, Russian Federation

When testing aerodynamic models in wind tunnels (WT), compliance with similarity criteria is required [1]. The similarity of the Reynolds number Re may require an increase in the geometric dimensions of the model and, as a result, an increase of blockage of the test section of the tunnel. Replaceable WT nozzle (Fig. 1) may reduce blockage effect [2]. The purpose of this work is an estimation of the effect on the aerodynamic characteristics of a large wing model with a distributed power unit (DPU) placed on the flap - the blockage value was 11 %. The influence of any other elements of the facility, that are absent in the real vehicle can be evaluated in a similar way.

The model was tested in a subsonic open-circuit, variable-density open-type WT equipped with an Eiffel Chamber. A direct comparison with the data, obtained in the tests, is given. CFD simulation of the flow was carried out as in WT conditions either in free flow condition, it was based on Reynolds equations and the finite volume method, using the SST turbulence model. These problems are presented in [3]. As conditions of the free flow around the model, the parameters at the far boundary obtained in tests are given: the NPR is measured at the WT chamber at the control point $P_{*WT} / P_{control} = 1.277$ (it corresponds to the Mach number of the flow $M_\infty = 0.6$, total temperature $T_{*for} = T_{MCA}$. The static pressure in the WT outlet section is selected empirically to correspond to the value at the control point placed on the wall of plenum (Fig. 1). On the surfaces of the model and WT elements the conditions “solid insulated” are set, mass flow rate of the DPU’s inlet corresponds to the value $q\left(\lambda_{eng}\right) = 0.78$, like WT test (Fig. 1). Unstructured computational grids contained 3 million polyhedral cells for flow in the WT and 2.5 million polyhedral cells for free flow case.

CFD results showed that taking into account the flow features in WT case leads to a difference in the pressure coefficient C_p along the upper surface of the wing near the sym-

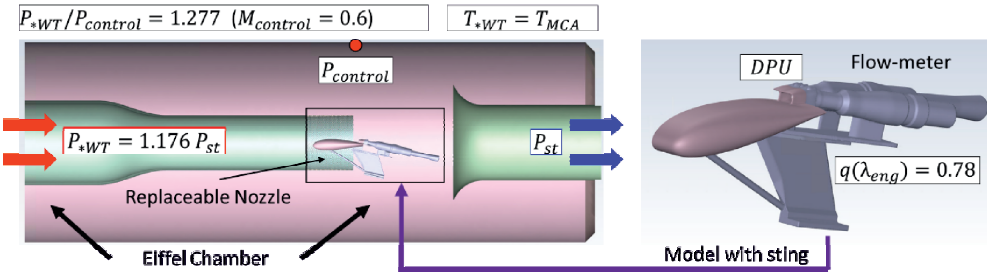

Fig. 1. Test scheme

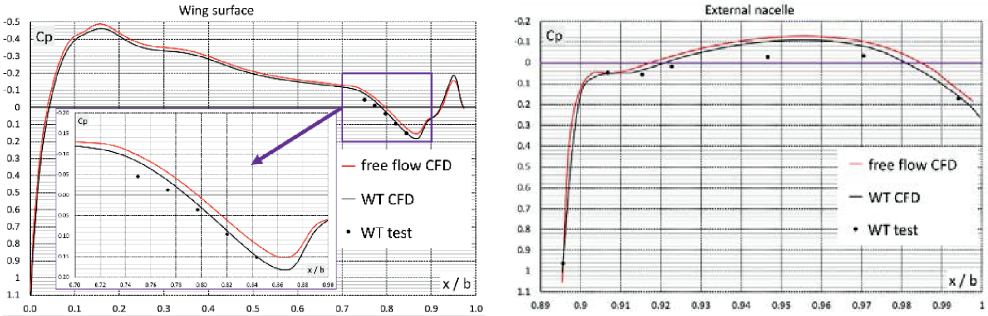

Fig. 2. Pressure coefficient C_p distribution along wing chord (left) and external nacelle surfaces (right)

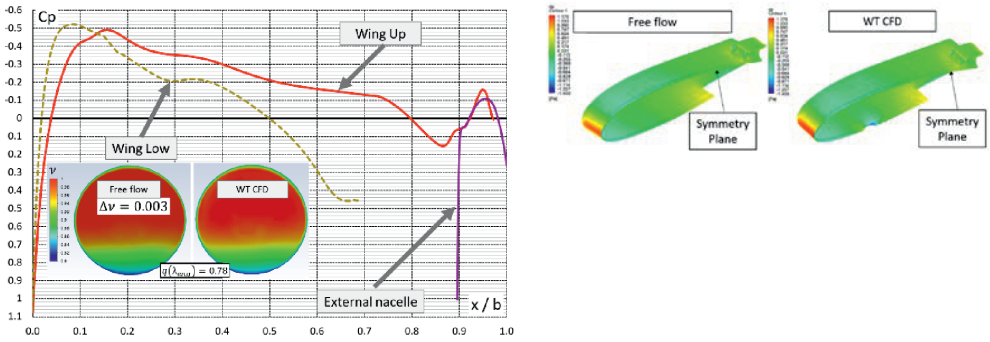

Fig. 3. Pressure coefficient C_p distribution along chord (left) and surface model (right). Distribution of total pressure recovery coefficient ν at control plane in free flow and WT cases

metry plane less than 0.02 C_p value (Fig. 2). The difference in the values of the total pressure recovery coefficient ν for the DPU engine is small (Fig. 3), namely, $\Delta\nu = \nu_{WT} - \nu_{freeflow} = 0.003$.

Based on the provided data, it can be concluded, that for studying of aerodynamic characteristics of wing model with DPU and parameters of the flow in inlet, test with significant blockage value was possible if a simulated Mach number $M_\infty \le 0.6$.

REFERENCES

1. **Martynov A.K.** Eksperimental`naya aerodinamika // OboronGIZ, 1950. pp. 115–117.
2. **Bondarev A.V., Bragin N.N., Bykov A.P., Lavruxin G.N., Skomoroxov S.I., Talyzin V.A., Talyzina A.A.** Eksperimental`nye issledovaniya effekta supercirkulyacii v integral`noj komponovke ploskix sopel s krylom // Uchonye zapiski TsAGI, 2021, vol. 52, № 2, pp. 63–74.
3. **Buj V.T., Kalugin V.T., Lapygin V.I., Xlupnov A.I.** Chislennoe issledovanie vliyaniya stepeni zagromozhdeniya potoka na aerodinamicheskie koefficienty modelej v ae`rodinamicheskix trubax malyx skorostej // Teplofizika i aeromexanika, 2017, vol. 24, № 6.

DOI 10.53954/9785604990131_33

MODEL OF THE CHILD DROPLETS FORMATION DURING MICRO-EXPLOSIVE BREAKUP OF TWO-LIQUID DROPLETS

R.M. Fedorenko, D.V. Antonov, P.A. Strizhak

National Research Tomsk Polytechnic University
634050, Tomsk, Russia

Secondary atomization of multicomponent liquid droplets is considered one of the most relevant areas in the development of fuel technologies. Among the known methods of secondary atomization, micro-explosive breakup is considered the most productive due to the significantly greater increase in the surface area of the liquid per unit time [1]. Determining the conditions necessary for the formation of child droplets with certain sizes and velocities will make it possible to achieve optimal operating conditions of technological equipment. Most existing models of micro-explosive breakup make it possible to predict with a high degree of accuracy the delay time of micro-explosive breakup, but at the same time do not provide information about the number and average sizes of child droplets due to the lack of experimental information and computational difficulties. In this work, a mathematical model of the child droplets formation during the micro-explosive breakup of two-liquid droplets has been developed.

The experimental technique on registration of characteristics of micro-explosive breakup of two-liquid droplets was similar to that used in [2]. The main attention is paid to the registration of the number and sizes of child droplets during micro-explosive breakup. Two-liquid droplets were generated using two electronic dispensers. At the first stage, a water droplet with a known volume was produced and suspended on a holder. After that, a fuel was formed which enveloped the water droplet, forming a fuel film. The two-liquid droplets were heated using Leister CH 6060 hot-air blower (air velocity 0.5–10 m/s) and a Leister LE 5000 HT air heater (temperature range 20–1000 °C). These elements allowed us to generate a hot air flow with required velocity and temperature. Video recording of droplet micro-explosions was performed using a Phantom Miro M310 high-speed camera. Storage and analysis of images was performed using specialised Phantom Camera Control software. Video recording took place at 5400 frames per second. The characteristics of child droplets are presented in the form of $N(r_{cd})$ distributions, as well as the ratio of the areas after and before the breakup S_1/S_0. Water, kerosene, diesel fuel, and rapeseed oil were used as droplet components in the experiments.

In this work, the numerical model was based on a CLS-VOF method (hybrid of Level Set and VOF method) [3] to study the breakup of a two-liquid droplet. It considers the solution of full Navier-Stokes equations to ensure the conservation of mass and momentum in conjunction with the advection of the scalar value known as the fractional volume of fluid $F(x, y, z, t)$. The gaseous and liquid phases are considered to be a single multicomponent medium. The volume fraction $F(x, y, z, t)$ is defined as the percentage of volume occupied by the liquid phase in a computational cell with respect to the total volume of the cell. The volume fraction of a phase in a computational cell is taken as $F(x, y, z, t) = 0$ if the cell is empty, $F(x, y, z, t) = 1$ if the cell is occupied by fluid, and $0 < F(x, y, z, t) < 1$ if the interface between the two fluids crosses the cell. In each control volume, the volume fractions of all phases sum to unity.

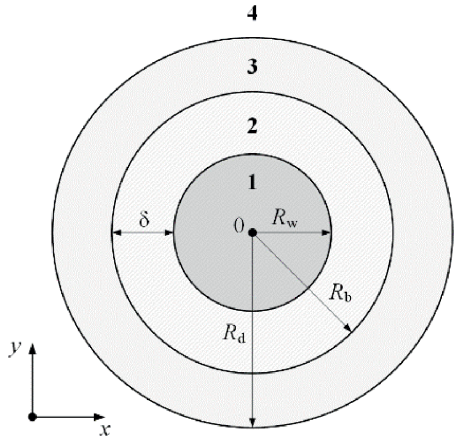

Fig. 1. Schematic of the computational domain of the two-liquid droplet breakup.

1 – water, *2* – water vapor, *3* – fuel, *4* – air, δ – vapor layer thickness.

Fig. 1 shows a schematic of the solution domain for the micro-explosive breakup of the two-liquid droplet. When modeling the breakup of the two-liquid droplet, it was assumed that water inside the droplet reached the overheating state, i.e., the conditions of micro-explosive breakup [4], resulting in the formation of a vapor layer near the water/fuel boundary. The droplet size increase was due to a constant inflow of vapor from the "water/fuel" boundary; the vapor pressure was set as a constant value.

When considering the problem of micro-explosive breakup of a two-liquid droplet, it was assumed that only the fuel film was involved in the formation of child droplets, i.e., the breakup of the water core was not considered in the present study.

The obtained results were verified by comparing the average sizes of child droplets at varying the gas flow temperature. Simulations were carried out at a concentration of 90 vol% for two fuel compositions: water/diesel fuel and water/rapeseed oil. Average radii of child droplets generated during micro-explosive breakup of two-liquid droplets shown to decrease with increasing gas temperatures. According to the results of calculations satisfactory agreement of experimental and theoretical data was established. Maximum deviations do not exceed 10 %. The average sizes of child droplets obtained from the results of simulations have slightly smaller values than in the experiment.

Results of experimental investigation of micro-explosive breakup of two-liquid droplets are presented. The model was developed to predict the consequences of micro-explosive breakup of two-liquid droplets. When compared with experimental data, the model shows good agreement. The present model can be used to create new integrated approaches to modeling micro-explosive breakup, allowing to predict not only the breakup delay time, but also its consequences in the form of child droplets average radii.

The research was supported by the Russian Science Foundation (project No 23-69-10006).

REFERENCES

1. **Antonov D.V., Fedorenko R.M., Strizhak P.A.** Child droplets produced by micro-explosion and puffing of two-component droplets // Applied Thermal Engineering. 2020. Vol. 164. Art. 114501.
2. **Antonov D.V., Volkov R.S., Fedorenko R.M., Strizhak P.A., Castanet G., Sazhin S.S.** Temperature measurements in a string of three closely spaced droplets before the start of puffing/micro-explosion: Experimental results and modelling // International Journal of Heat and Mass Transfer. 2021. Vol. 181. Art. 121837.
3. **Hirt C.W., Nichols B.D.** Volume of fluid (VOF) method for the dynamics of free boundaries // Journal of Computational Physics. 1981. Vol. 39, No. 1. P. 201–225.
4. **Fedorenko R.M., Antonov D.V., Strizhak P.A., Sazhin S.S.** Time evolution of composite fuel/water droplet radii before the start of puffing/micro-explosion // International Journal of Heat and Mass Transfer. 2022. Vol. 191. Art. 122838.

DOI 10.53954/9785604990131_35

INTERACTION OF ELECTRIC DISCHARGE IN MAGNETIC FIELD WITH SUPERSONIC BOUNDARY LAYER

V.P. Fomichev, M.A. Yadrenkin

Khristianovich Institute of Theoretical and Applied Mechanics SB RAS
630090, Novosibirsk, Russia

Investigation is conducted on various types of combined surface electric discharges induced in a supersonic flow over a plate using narrow electrodes with a solid cathode. The objective is to identify the parameter ranges necessary for implementing surface discharges in an aerophysical experiment. Furthermore, the impact of gas-discharge plasma in a magnetic field on the aerophysical characteristics of the wall flow during supersonic flow around the plane is examined.

To investigate the combustion process of a surface gas discharge in a supersonic flow and in a magnetic field, a magnetohydrodynamic (MHD) test rig based on a shock tube is employed. The supersonic flow around a plate mounted at a zero angle of attack is specifically considered in this study. The air flow in the working chamber possesses the following parameters: Mach number (M) of the flow is 4.9, flow velocity is approximately 1800 m/s, static pressure in the flow (P) is 15 Torr (2 kPa), and flow density is 0.02 kg/m^3. These flow parameters are calculated based on the nozzle geometry and stagnation parameters in the pre-chamber. Additionally, the flow Mach number is determined by the angle of inclination of the oblique shock attached to the leading edge of the plate model.

The discharge initiation was carried out using a high-frequency pulse generator. The generator combines two voltage sources: a source of short high-voltage nanosecond pulses necessary for gas breakdown, and a source of rectangular voltage pulses with adjustable duration, superimposed on the short igniting pulses. Both sources have the ability to stepwise adjust the voltage, as well as smoothly adjust the frequency of pulse occurrence. Thus, the generator allows obtaining combined discharges with a frequency of up to 25 kHz.

The surface electric discharge experiment was conducted according to the schematic diagram depicted in Fig. 1*a*. One of the electrodes, the negative electrode, was connected to a conductive sheeth located beneath a non-conductive surface. Fig. 1*b* presents a photograph

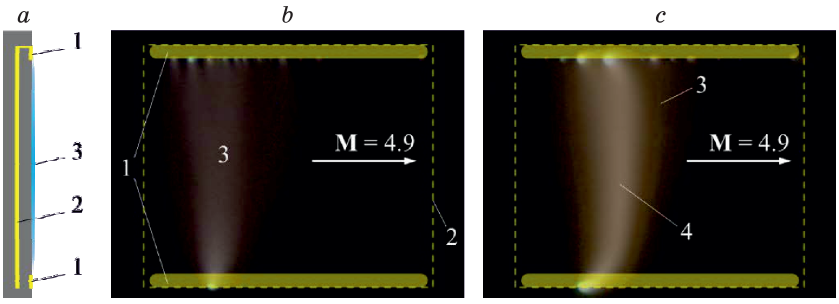

Fig. 1. Diagram of the organization of a sliding discharge on the surface of the plate (a) and photographs of the discharge area in a supersonic gas flow without a magnetic field (b, c).

1 – electrodes, *2* – substrate, *3* – surface discharge zone, *4* – discharge contraction zone

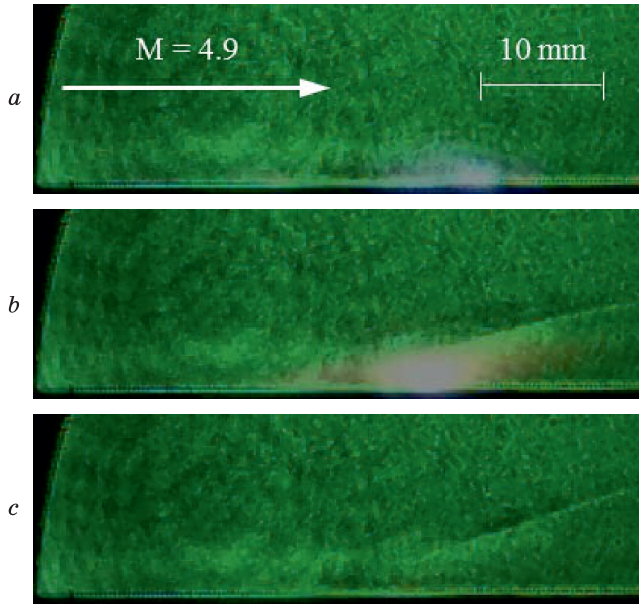

Fig. 2. Visualization of the discharge above the plate surface in a supersonic air flow in a magnetic field of 0.15 T: 0.25 microseconds (a), 10.25 microseconds (b) and 20.25 microseconds after breakdown (c).

captured 0.25 microseconds after the gas breakdown, showcasing the discharge with a uniformly distributed shape over the surface in zone 3. This shape is characteristic of a sliding surface discharge. After 10 microseconds from the breakdown (Fig. 1c), a contraction zone of the discharge (zone 4) becomes evident.

To observe the movement of this discharge in a flow above the formation's surface, a Schlieren system was employed. The system captured sequential frames at a frequency of up to 400 kHz, with each frame having an exposure time of 1 microsecond. Fig. 2 displays the sequential frames obtained from high-speed recording, illustrating the interaction between the gas-discharge plasma and a nighttime current in a magnetic field of 0.15 T.

The discharge region after breakdown, having a diffuse shape, does not cause significant changes in the flow (Fig. 2a). After 10 μs, a hanging oblique jump of compression was formed over the discharge area (Fig. 2b). After 20 μs (Fig. 2c), after the discharge ceased (voltage pulse duration 15 μs), the hanging jump of compression continued to exist over the heated boundary layer region with subsonic flow, that is, above the sonic line with a Mach number M = 1 in supersonic flow.

The research was carried out within the state assignment of Ministry of Science and Higher Education of the Russian Federation.

The study was conducted at the Equipment Sharing Center «Mechanics» of ITAM SB RAS.

DOI 10.53954/9785604990131_37

INTERFERENCE OF CIRCULAR CYLINDER WITH SIDE BLOCKS LOCATED IN THE HORIZONTAL PLANE

A.Y. Germamo, V.A. Frolov

Samara National Research University
34, Moskovskoye Shosse, Samara, Russia, 443086

The work is devoted to the experimental determination of the values of the derivative normal force coefficients $C_{L\alpha}$ versus angle of attack (AoA) α, the interference coefficients of the side blocks (SB) on the fuselage (body) and the fuselage on the SB and their dependences on the relative diameter of the SB in model of the combination of a multi-block aircraft (MBA), presented in Fig. 1.

The studies were carried out with MBA models at the Samara National Research University in a subsonic wind tunnel [1]. Models of the MBA fuselage (body) and SB were cylindrical bodies of rotation of large aspect ratio with elliptical head parts. To measure aerodynamic forces, a standard strain gauge method was used with the installation of sensitive elements inside the fuselage model. Taking into account the linear nature of the dependence of C_L on the AoA, the derivatives of $C_{L\alpha}$ with respect to the AOA were studied depending on the relative diameters of the blocks ($\overline{d} = d/D$, where d – diameter of the block; D – diameter of the fuselage). The area of research was limited to Mach numbers M < 0.1 and Re ≈ 7×10^5, characterizing the initial stage of movement of such MBA [2]. The experimental data were approximated using the least squares method. The results of experimental data processing are presented in Fig. 2–4 using the results of works [2–6] in the form of a power polynomial up to the second-degree. A feature of the presented studies is that the authors used, to determine additional interference forces, the original scheme for attaching the SB to the fuselage and vice versa. Let us introduce the interference coefficients using the following formulas:

$$K_{f(b)} = \frac{\Delta C_{L_\alpha f(b)}}{C_{L_\alpha f}}, \quad K_{b(f)} = \frac{\Delta C_{L_\alpha b(f)}}{C_{L_\alpha b}}, \tag{1}$$

where $C_{L_\alpha f}, C_{L_\alpha b}$ are lift-curve slope of the isolated fuselage and isolated one side block; $\Delta C_{L_\alpha f(b)}, \Delta C_{L_\alpha b(f)}$ are lift-curve slope of the influence fuselage from blocks and the influ-

Fig. 1. Model of the combination of the MBA

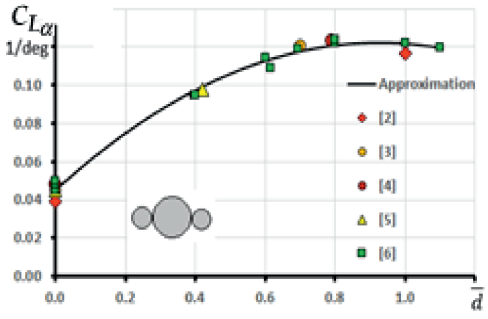

Fig. 2. $C_{L\alpha}$ vs relative diameter of the SB

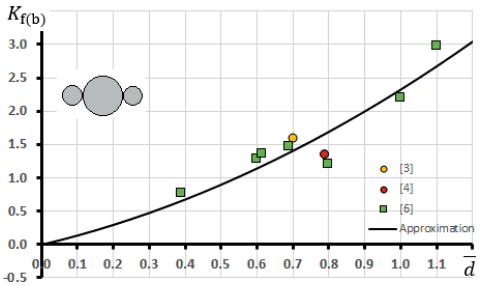

Fig. 3. Interference coefficient from the SB to the fuselage

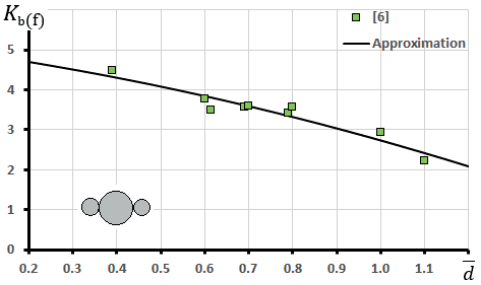

Fig. 4. Interference coefficient from the fuselage to the SB

ence of the blocks from fuselage. The lift-curve slope of the MBA $C_{L\alpha}$ can be written as the formula

$$C_{L_\alpha} = C_{L_\alpha f}\frac{1}{1+\overline{d}^2}\left(1+K_{f(b)}\right)+C_{L_\alpha b}\frac{\overline{d}^2}{1+\overline{d}^2}\left(2+K_{b(f)}\right),\ where\ \frac{1}{1+\overline{d}^2}=\frac{S_{m.f}}{S_m};\ \frac{\overline{d}^2}{1+\overline{d}^2}=\frac{S_{m.b}}{S_m},\quad (2)$$

$S_{m.f}$, $S_{m.b}$ and $S_{m.}$ are cross-sectional areas of the fuselage, side blocks and the combination as a whole. Measuring the normal force when mounting the SB on a special bracket allows us to determine the interference coefficient $K_{f(b)}$ using the first formula (3), then the coefficient $K_{b(f)}$ is determined by the second formula (3) from equation (2)

$$K_{f(b)}=\frac{C_{L_\alpha f}+\Delta C_{L_\alpha f(b)}}{C_{L_\alpha f}}-1,\quad K_{b(f)}=\frac{C_{L_\alpha}-C_{L_\alpha f}\left(1+K_{b(f)}\right)/\left(1+2\overline{d}^2\right)}{C_{L_\alpha b}\left[\overline{d}^2/\left(1+2\overline{d}^2\right)\right]}-n. \quad (3)$$

On Fig. 3 and 4 presented the results obtained for the coefficients.

Conclusions: the presented results allow us to evaluate the lift characteristics of the MBA combination as a whole depending on the relative diameters of the side blocks.

REFERENCES

1. **Komarov V.A.** and others. University educational and research wind tunnel // All-Russian scientific and technical journal "Flight". – 2006. No. 10. – P. 34–41.
2. **Petrov K.P.** Aerodynamics of transport space systems. Moscow, 2000. – 368 pp.
3. **Novikova A.A., Frolov V.A.** Experimental study of the interference of side accelerators located in perpendicular planes of symmetry of the body launch vehicle // All-Russian Conf. of Youth Mechanical Scientists (YSM-2020). Sochi, 2020. P. 112.
4. **Savinov D.I.** and others. Study of the interference of a launch vehicle body with side accelerators and wings // Proceedings XIV Korolev Readings. International Youth Scientific Conference. Samara, 2017. pp. 220–221.
5. **Veremchuk V.A.** and others. Study of the influence of side accelerators on the aerodynamic characteristics of the launch vehicle // Proceedings XIII Korolev Readings. International Youth Scientific Conference. Samara, 2015. pp. 142–143.
6. **Germamo A.Y., Frolov V.A.** Experimental determination of the lifting characteristics of body combination with two blocks located in a horizontal plane of symmetry // Proceedings XXVI All-Russian Seminar on Motion Control and Navigation of Aircraft. Samara, 2023. pp. 147–153.

DOI 10.53954/9785604990131_39

A COMPREHENSIVE STUDY OF A SHARP CONE IN A SHOCK TUBE

A.R. Gorbusin, S.A. Glazkov, M.S. Gribkova, D.I. Dugin, A.D. Epikhin, A.E. Kozik, V.E. Mosharov, V.N. Radchenko

Central Aerohydrodynamic Institute
140180, Zhukovsky, Russia

Experimental studies of canonical bodies in wind tunnels are carried out to verify computational methods and to study the characteristics of the boundary layer on their surface. Experimental studies of the canonical body – a 10° sharp cone with length 0.96 m (Fig. 1) were carried out in the TsAGI shock tube UT-1M in the range of $Re = (7–26)\cdot10^6$ at $M = 6$. Preliminary calculations of the flow over the cone in the facility were performed using EWT-TsAGI software to determine cone optimal position in the test section. The following parameters were measured simultaneously: unsteady aerodynamic loads using internal six-component strain-gauge balance, dynamic behaviour of the cone and strain-gauge balance using three-axis Dytran accelerometers, unsteady pressures on the cone surface and Pitot-Prandtl-type probe by means of Kulite sensors, cone surface temperature by means of TSP [1], temperature fluctuations by means of a constant-voltage thermoanemometer with a film sensor and Schlieren flow visualisation. The readings of all transducers were recorded simultaneously by a Siemens SCL2E20 LMS SCADAS Lab measurement system with a sampling rate of 204.8 kHz/channel. The position of the laminar-turbulent transition and its fixation by means of transition strip were determined using TSP (Fig. 2). The Stanton number was determined using the TSP results. A transition strip located at a distance of 0.3 m from the cone nose with a height of 0.32 mm fixed the transition at $Re > 17\cdot10^6$ and, at the same time, created shock wave (Fig. 3). Typical results of pressure measurements by a Pitot-Prandtl-type probe during the UT-1M run are shown in Fig. 4. The total pressure after the shock wave and static pressure are kept approximately constant for about 40 ms. The high level of the total pressure fluctuations measured by the Pitot probe are caused by oscillations in the probe orifice, which forms a Helmholtz resonator [2] together with the internal cavity with the natural

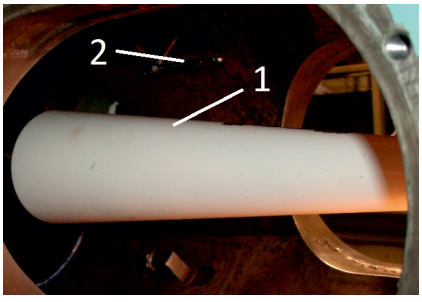

Fig. 1. Cone in the test section of UT-1M shock tube.

1 – cone, *2* – Pitot-Prandtl-type probe.

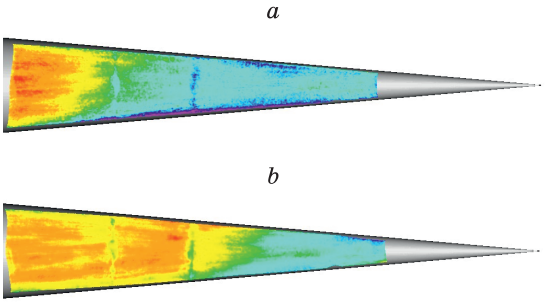

Fig. 2. Stanton number distribution of the cone surface at $Re=8.1\cdot10^6$ (*a*) and $12.2\cdot10^6$ (*b*).

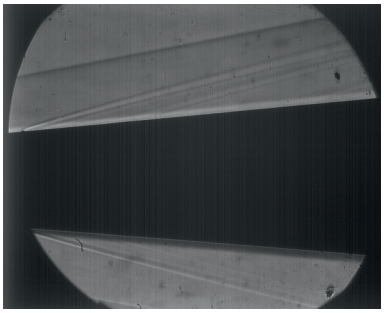

Fig. 3. Schlieren flow visualisation of the cone.

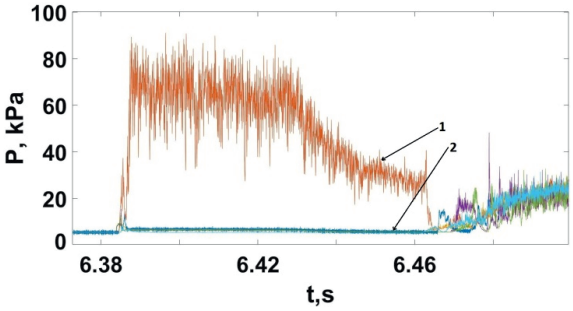

Fig. 4. Pressure measurements by a Pitot-Prandtl-type probe during the UT-1M run.

1 – total pressure, *2* – static pressure.

resonator frequency of 5.03 kHz. The readings of the total pressure probe were corrected for the effect of the resonator natural oscillations according to [2]:

$$P_e = P + \beta \dot{P} / \omega_0^2 + \ddot{P} / \omega_0^2, \quad (1)$$

where P is the readings of the sensor located in the cavity of the total pressure probe; P_e is the pressure in front of the total pressure probe; ω_0 is the circular resonant frequency; β is the damping coefficient.

The resonance frequency and damping coefficient were determined using the results of free damped oscillations generated by the rupture of a rubber ball located near the Pitot-Prandtl-type probe [2]. The correction was applied for the effect of inertial forces on the readings of the axial force component of the strain-gauge balance, according to [3], as follows:

$$AF_a = AF + M \cdot A\ddot{F} / k + \beta_{AF} \cdot A\dot{F} / k + M \cdot \ddot{x},$$

where AF_a is the drag force; AF is the balance axial force; M is the sum of cone and balance metric part masses; k is the balance stiffness coefficient; β_{AF} is the balance damping coefficient; $\ddot{x}$ – acceleration of the balance ground part, measured by accelerometer. The damping coefficient β_{AF} and stiffness coefficient k were determined using the results of free damped oscillations generated by applying a step force [3]. Accelerometer readings were used to determine the trajectory of the cone during the facility run.

The results of this research represent a test case and may be used for validation of computer codes.

The research was supported by the Russian Science Foundation, grant No. 23-19-00041.

REFERENCES

1. **Borovoy V, Mosharov V, Noev A, Radchenko V.** Temperature sensitive paint application for investigation of boundary layer transition in short-duration wind tunnels // EUCASS Proceedings Series – Advances in Aero-Space Sciences. 2012. 3, 15-24. doi.org/10.1051/eucass/201203015.
2. **Gorbushin A, Anokhina E, Stolyarov E.** Unsteady pressure measurement in the presence of a cavity between the sensor and the flow // Sensors and Actuators A: Physical. 2023. 349, 114095. doi.org/10.1016/j.sna.2022.114095.
3. **Gorbushin A.R., Bolshakova A.A.** Unsteady axial force measurement by the strain gauge balance // Measurement. 2020. 152C, 107381, 1–8. doi.org/10.1016/j.measurement.2019.107381.

DOI 10.53954/9785604990131_41

HEAT TRANSFER AND GAS FLOW IN A VIBRATING RECTANGULAR CHANNEL WITH DIFFERENTLY HEATED WALLS

A.A. Gubaidullin, A.V. Pyatkova

Tyumen Branch of the Khristianovich Institute of Theoretical and Applied Mechanics SB RAS, 625026, Tyumen, Russia

In the case of vibration of a cavity or closed channel filled with gas, in addition to the oscillatory motion of the gas, the so-called acoustic streaming develops. Acoustic streaming is the average flow over the period of oscillations and represents stable vortices with a certain direction of rotation [1, 2]. Acoustic streaming can lead to intensification of heat transfer, promote fluid mixing in engineering applications, and be used in biomedical research [3]. The presence of a temperature difference between the channel walls can lead to distortion of the streaming pattern. This, in turn, will lead to a change in the heat flow through the isothermal walls of the channel and the character of the period average distributions of temperature.

Consider a two-dimensional channel with impenetrable walls (Fig. 1). The channel is filled with a perfect viscous gas (air). The system is disturbed from the equilibrium by a vibration effect $A\cos(\omega t)$ with constant amplitude A and frequency ω, causing harmonic oscillations of the entire channel along the abscissa axis. No-slip boundary conditions are specified on the walls of the channel. The vertical walls of the channel are thermally insulated; the horizontal walls are maintained at a constant temperature. In this case, the temperature difference of horizontal walls can vary.

To describe the process, a system of gas dynamics equations is used, written taking into account viscosity, thermal conductivity and viscous dissipation. This system of equations is solved numerically in dimensionless variables in the frame of reference associated with the vibrating cavity. The calculation method described in [4] for the axisymmetric case is used to solve the problem numerically. To discretize the equations, the finite volume method with an implicit staggered grid scheme are used, within which the values of the velocity and mass flow components are calculated on the faces of the main control volumes.

Acoustic streaming and heat transfer in the vibrating rectangular channel are studied. As an example, in the results presented below, the vibration frequency of the channel is taken to be lower than the resonant frequency of the system ($\Omega = 2.5$ with the dimensionless resonant frequency $\Omega_0 \approx \pi$), and the vibration amplitude is small. As a result, nonlinear effects are weakly manifested; only the influence of boundary conditions is shown. In the case when the

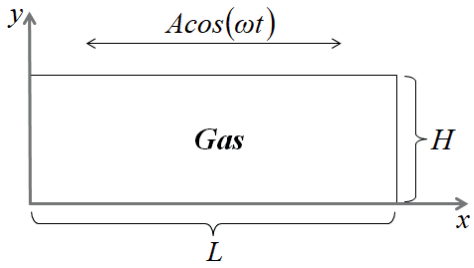

Fig. 1. Schematic of the problem.

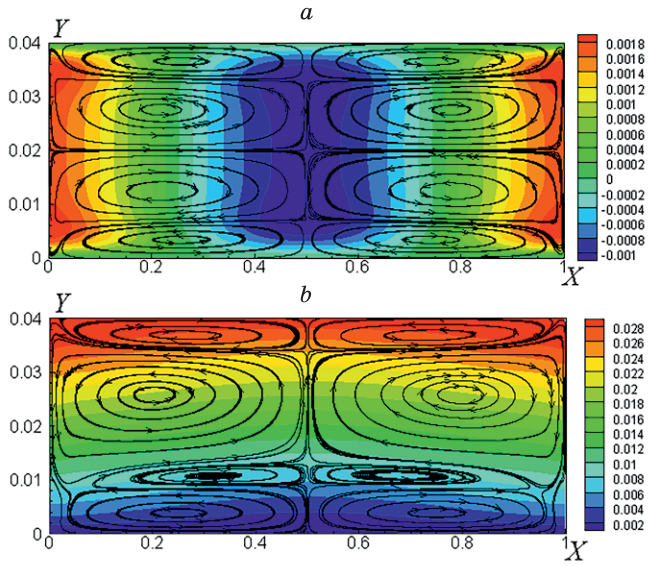

Fig. 2. Streamlines of acoustic streaming and period average distributions of dimensionless temperature, (*a*) $\Delta\Theta = 0$, (*b*) $\Delta\Theta = 0.03$

upper and lower walls of the channel have the same temperature ($\Delta\Theta = 0$), the streaming vortices are symmetrical relative to the central axis of the channel (Fig. 2(a)). The direction of rotation of the vortices is in good agreement with the theoretical concept of Schlichting and Rayleigh vortices [1]. Near the upper and lower walls there are Schlichting vortices, in which fluid is transferred from the oscillatory velocity node to the antinode near the channel walls. The Rayleigh streaming vortices are located in the central part of the channel and have the opposite direction of rotation. The Fig. 2 shows in color the field of the period average dimensionless temperature in the channel. Without the temperature difference between the horizontal walls, the period average temperature in the center of the channel becomes lower than the initial temperature (negative values of the dimensionless temperature). Near the vertical walls, on the contrary, heating of the gas is observed on average over the period.

In the presence of the temperature difference between the upper and lower walls of the channel ($\Delta\Theta = 0.03$), the acoustic streaming vortices lose their symmetry (Fig. 2(b)). The Rayleigh vortices located closer to the more heated wall increase in size, while those located in the lower part of the channel decrease. We also note that a pronounced stratification of the period average temperature is visible, and the period average temperature no longer becomes lower than the initial temperature.

This research was funded by the Russian Science Foundation, grant number 24-29-00394.

REFERENCES

1. **Zarembo L.K.** Acoustic streaming. High-intensity ultrasonic fields, edited by L.D. Rozenberg, New York: Plenum, 1971. Part III. P. 156–164.
2. **Nyborg W.L.** Acoustic streaming. Physical acoustics, edited by W.P. Mason, New York: Academic Press, 1965. Vol. 2, Chap. 11. P. 265–331.
3. **Wu J.** Acoustic streaming and its applications // Fluids. 2018, Vol. 3, 108.
4. **Gubaidullin A.A., Pyatkova A.V.** The effects of heat transfer through the ends of a cylindrical cavity on acoustic streaming and gas temperature // Mathematics. 2023, Vol. 11, 1840.

DOI 10.53954/9785604990131_43

GAS DYNAMIC ANALYSIS OF INLET AND EXHAUST VALVES FOR A SMALL DISPLACEMENT OPPOSITION ENGINE

E.R. Habibullin, K.S. Vakhrushev

M.T. Kalashnikov Izhevsk State University,
Izhevsk, Russia, 7 Studencheskaya St., 426069

The issues of designing medium-range airplane-type unmanned aerial vehicles [1] remain topical up to the present time. The tasks of ensuring uninterrupted production of such systems are associated with the issues of development, production and development of specialized small internal combustion engines. Until 2022 such engines [2] were purchased by the companies-manufacturers of unmanned systems under import programs from foreign partners, which is extremely complicated in the current international situation. In this regard, the current task is to design and produce domestic small-capacity internal combustion engines for airplane unmanned systems. At the same time, the specifics of internal combustion engine operation in the conditions of air flight have a number of characteristic features of functioning of such power plants: – peculiarities of engine starting in the conditions of impulse altitude gain; – cooling of internal combustion engine; – mass and dimensional characteristics of internal combustion engine; – increased requirements to resource and efficiency of operation. This work is devoted to the issues of numerical modeling of working processes in the paths of a small-capacity opposition internal combustion engine, which is the power plant of an unmanned aerial vehicle of medium-range aircraft type.

The conjugate problem of heat transfer in the combustion chamber of an opposition small-capacity internal combustion engine is considered (Fig. 1). The gas dynamics of combustion products at the intake and exhaust stages is considered, including the features of the organization of working processes in a four-stroke opposition combustion engine.

Unsteady spatial turbulent flow of compressible heat-conducting gas in the combustion chamber of an oppositional engine is described by the following system of equations:

$$\begin{aligned}
&\frac{\partial \rho}{\partial t} + \nabla \rho v = 0, \\
&\rho \frac{dv}{dt} = \rho F - \nabla p + DivP, \\
&\rho \frac{d}{dt}\left(C_v T + \frac{v^2}{2} \right) = \rho F v + \nabla \left(Pv \right) + \nabla q, \\
&\frac{\partial T}{\partial t} = \lambda \nabla^2 T, \\
&\frac{p}{T} = \rho R,
\end{aligned} \tag{1}$$

where ρ – gas density, p – pressure, **v** – velocity vector, $P = \frac{1}{2}\text{ì}\left(\frac{\partial V_i}{\partial x_j} + \frac{\partial V_j}{\partial x_i} \right) - \frac{2}{3}\mu\delta_{ij}\text{div}\mathbf{v}$ – stress tensor, F – volume force, T- temperature, **q** – heat flux density vector, R – gas constant;

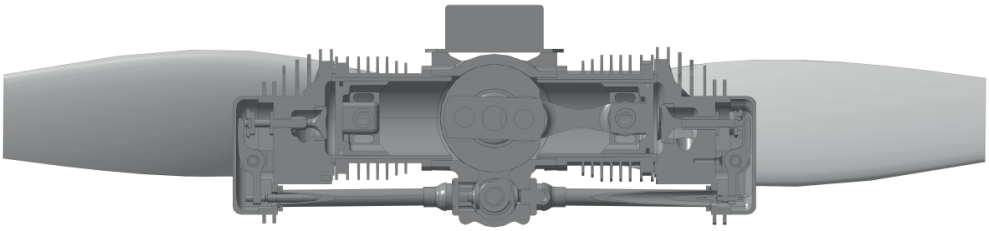

Fig. 1. Structural diagram of a small internal combustion engine in cross-section.

1 – crankcase, 2 – cylinder, 3 – piston, 4 - cylinder head, 5 – valve.

μ – dynamic viscosity, λ – thermal conductivity coefficient, δ_{ij} – Kronecker symbol. Для замыкания системы уравнений (1) используется двухзонная модель турбулентности Ментера SST. The working body is air. Soft boundary conditions are set at the inlet of the combustion chamber of the opposition combustion engine, and non-reflective boundary conditions are set at the outlet. Inlet/outlet of the working body is realized by the motion of valves. The stroke of the valves is defined by a functional relationship. Between the body of the engine and the working body are set the boundary condition of IV kind, on the outer boundary of the body are defined boundary conditions of III kind. The system of equations constructed in this way is solved by the finite volume method. Discretization of the obtained system of equations in space is carried out by hexahedral elements.

As a result of calculations the distributions of fields of physical quantities in the combustion chamber of the opposition internal combustion engine have been obtained. The analysis of the obtained results made it possible to evaluate the influence of changes in altitude and momentum on the engine performance characteristics. The obtained results can be used to improve the efficiency of the engine and the overall performance of the unmanned aerial vehicle.

REFERENCES

1. **Shatalov N.V.** Peculiarities of classification of airplane-type UAVs, Perspektivy razvitiya informatsionnoi tekhnologii No. 30, 2016.
2. **Seriakov V.I.** Designing the engine of an unmanned aerial vehicle, XXIV Tupolev Readings (School of Young Scientists) 2019, pp. 102–104.

DOI 10.53954/9785604990131_45

BOUNDARY LAYER CONTROL ON THE TEST SECTION WALLS IN THE TASKS OF THE WIND TUNNEL TESTING TECHNIQUE

A.I. Ivanov

Federal Autonomous Enterprise "Central Aerohydrodynamic Institute n.a. prof. N.E. Zhukovsky" (FAE "TsAGI"), 140180, Zhukovsky, Moscow reg., Russia

In traditional wind tunnel testing, the presence of a boundary layer on the walls of the test section is usually a factor that negatively affects the accuracy and reliability of the aerodynamic results. When testing straight and swept wing compartment models in wind tunnels to design new wing airfoils, direct balance measurement of the aerodynamic characteristics of the models leads to significant errors due to boundary effects. Indirect methods using pressure distributions in the model cross sections and in the model wake are usually used to determine forces and moments, but even in this case the boundary layer on the side walls can introduce distortions in the quasi-2D flow pattern. This effect is especially noticeable at transonic flow velocities, when the viscous layer interacts with the shock wave closing the supersonic zone on the model.

Methodological materials of the research performed during the preparation for the test section No. 3 of T-128 operation and in tests of wings of «infinite» elongation, including optimization of parameters of boundary layer suction on the side walls and application of the system of tangential flow acceleration at the walls by supersonic high-pressure jets, are presented. The choice of optimal geometric and gas-dynamic parameters of the suction system allowed to reduce the values of integral boundary layer thicknesses by 5–10 times with minimal distortion of the flow field in the model location zone [1, 2]. The tests made it possible to obtain aerodynamic characteristics of single- and double-element airfoil models at transonic flow regimes.

The development of a viscous layer on the side walls during tests of swept wings of «infinite» elongation can lead to a violation of flow similarity in different sections along the model span. To localize the effect of the viscous layer at subsonic velocities [3], a splitter plate on the leading edge near the wing root was used, which made it possible to obtain a «slipping» effect on a model with a span-to-chord ratio of 1:1. In transonic tests of a swept wing [4], boundary layer control was not applied, and the similarity of the flow in the middle sections of the model could be realized only due to its large elongation, with the perturbed zone of interaction between the closing shock wave and the boundary layer on the wall reaching 30% of the model span.

The influence of the near-wall boundary layer cannot always be evaluated unambiguously. In some cases, controlling the flow near the wall provides an opportunity to include an additional tool that affects the quality of the obtained data. The presence of flow boundaries in the test section of the wind tunnel is one of the most significant factors that distort the model flow and lead to discrepancies between the results of wind tunnel and flight experiments. Regardless of the type of boundaries, a viscous layer is formed at the edge of the flow core, which has a noticeable effect on the physical picture of the flow. In facilities with solid walls the displacement effect of the near-wall viscous layer is usually compensated by means of the cross-section increase in the downstream direction of the test section. The boundary layer makes a significant contribution to the formation of the boundary condition, and the

control of this layer can be a useful tool to organize low-interference flow over the model. The proposed concept of a controlled boundary layer on solid walls, which is a development of the idea of jet boundaries, has been realized in T-112 TsAGI wind tunnel [5]. After a number of experimental and computational studies, the optimal boundary layer parameters were selected for different models and different flow regimes at high subsonic and transonic flow velocities, which allowed to significantly reduce all known types of induction.

Traditionally, since the late 40's of the last century, permeable (perforated or slotted) walls of test sections are used in transonic wind tunnels. The influence of the boundary layer developing on the perforated walls is manifested mainly in the change of the effective permeability of the walls. A change in the thickness of the boundary layer displacement in the presence of mass transfer at the wall leads to an increase in the modulus of the normal component of velocity from the wall to the outer boundary of the boundary layer [6], changing the effective permeability of perforated walls.

The computational and experimental studies have also shown the promising application of combined jet-perforated boundaries (perforated walls with a controlled boundary layer on them) [7].

The possibility of damping by combined boundaries of reflected wave disturbances at low supersonic velocities is considered. The results of detailed measurements of viscous layer parameters near permeable walls of different geometry in T-128 and T-125 wind tunnels are given.

REFERENCES

1. **Ivanov A.I., Verkhovsky V.P., Smirnov D.E.** Technology of the flow parameters optimization during the 2D tests in the T-128 wind tunnel // Proc. of the IX conference "Aerodynamics of flying machines", TsAGY ed., 1998, P. 17 (in Russian).
2. **Verhovskij V.P., Ivanov A.I., Mihajlov N.K., Paryshev S.E., Smirnov D.E.** Issledovanie polya techeniya i razrabotka metodiki ispytanij v transzvukovoj aerodinamicheskoj trube profilej kryla i modelej na flatter // Uchenye zapiski TsAGI, 2002, t. XXXIII, No. 1–2, pp. 111–119.
3. **Chernyshev S.L., Ivanov A.I., Kiselev A.Ph., Kuzminsky V.A., Sboev D.S., Zhigulev S.V.** Investigation of influence of free-stream turbulence and acoustic disturbances on the laminar-turbulent transition on LV6 airfoil and swept wing models // Collection of Technical Papers – AIAA/ASME/ASCE/AHS/ASC Structures, Structural Dynamics and Materials Conference, 2011, No. 210.
4. **Gorbushin A.R., Ivanov A.I., Petronevich V.V., Biryukov V.I., Mihajlov N.K., Paryshev S.E.** Eksperimental'nye issledovaniya strelovidnogo kryla beskonechnogo razmaha v usloviyah baftinga // Sb. materialov X SHkoly-seminara «Aerodinamika letatel'nyh apparatov» – Izd. TsAGI, 1999, pp. 31–32.
5. **Ivanov A.I., Streltsov E.V.** Controlled boundary layer on the solid walls of wind tunnels: new approach to the boundary interference problem. Proc. of the 29th Congress of the International Council of the Aeronautical Sciences (ICAS 2014), St. Petersburg, 2014.
6. **Ivanov A.I.** Experimental investigation of gas flow near the perforated walls of a transonic wind tunnel// Scientific Notes of TsAGI, 1987, Vol. XVIII, No. 3, pp. 131–136. (in Russian)
7. **Chernyshev S.L., Ivanov A.I., Streltsov E.V., Volkova A.O.** Application of the combined boundaries to reduce wall interference for NACA 0012 airfoil tests // 31st Congress of the International Council of the Aeronautical Sciences (ICAS 2018), 2018.

DOI 10.53954/9785604990131_47

DISTRIBUTED VORTEX RECEPTIVITY OF A SWEPT-WING BOUNDARY LAYER IN PRESENCE OF SURFACE NONUNIFORMITIES. PART 2. COEFFICIENTS OF SURFACE-VORTEX RECEPTIVITY

Y.S. Kachanov, V.I. Borodulin, A.V. Ivanov

Khristianovich Institute of Theoretical and Applied Mechanics of SB RAS
630090, Novosibirsk, Russia

This paper represents the second part of our work, the first part of which is given in [1]. Our work is experimental basically and is devoted to a detailed investigation of two distributed receptivity mechanisms observed in a swept-wing boundary layer with predominance of the cross-flow (CF) instability. These mechanisms are responsible for distributed (in the chordwise direction) excitation CF-waves and vortices due to scattering of free-stream vortices on either (*i*) the natural nonuniformity of a growing boundary layer or (*ii*) the base-flow distortions produced by surface roughness (waviness) distributed in the chordwise direction, as well. The first of these mechanisms we call hereafter: *'the vortex receptivity'*, while the second one: *'the surface-vortex receptivity'*. Part 1 of our study [1] describes the experimental setup, the base-flow characteristics, the methodology of performing the measurements and obtaining the distributed receptivity coefficients, as well as the results of measurements of the *vortex* distributed receptivity coefficients and their comparison with those obtained in previous experiments [2, 3] carried out on smooth surface. Meanwhile, the present paper (Part 2 of our study) is devoted to description of the results of measurements of the *surface-vortex* distributed receptivity coefficients and to a comparative analysis of relative efficiency of these two receptivity mechanisms.

The experiments were performed in a low-turbulence subsonic wind-tunnel T-324 of ITAM at the incident flow velocity of 11.24 м/с and rms intensity of the streamwise velocity fluctuations (above 1 Hz) of about 0.06 %. The experimental model represented a 25-degree flat swept plate equipped with a swept displacement body inducing a chordwise pressure gradient and with two sidewalls providing better satisfaction of the sweep condition. All measurements were carried out at fully controlled disturbance conditions with excitation of streamwise elongated freestream vortices by a vibrating wire having a spanwise nonuniformity and application onto the swept-wing model surface of controlled wavinesses (with amplitudes h_1/δ_1 below 0.12) which were sinusoidal in the chordwise direction and uniform in span. All measurements were performed with single-wire and double-wire anemometry. The base-flow structure and the shapes of the excited vortices were measured in detail and are described in [2, 3]. The surface waviness was measured accurately as well [1].

The boundary-layer receptivity characteristics were investigated for three disturbance frequencies and three kinds of controlled surface waviness, as well as in absence of waviness. The measurements have shown that the presence of the surface roughness is able to lead to a streamwise-wavenumber resonance of the freestream vortices, boundary-layer perturbations, and the distributedly excited CF-instability waves. In contrast to the smooth-surface cases (studied in [2, 3]), the resonance was possible for the most amplified CF-instability modes (having positive spanwise wavenumbers). This circumstance leaded to the possibility of either more rapid amplification of the CF-waves or to their suppression depending on the phase relationship between previously and newly excited boundary-layer

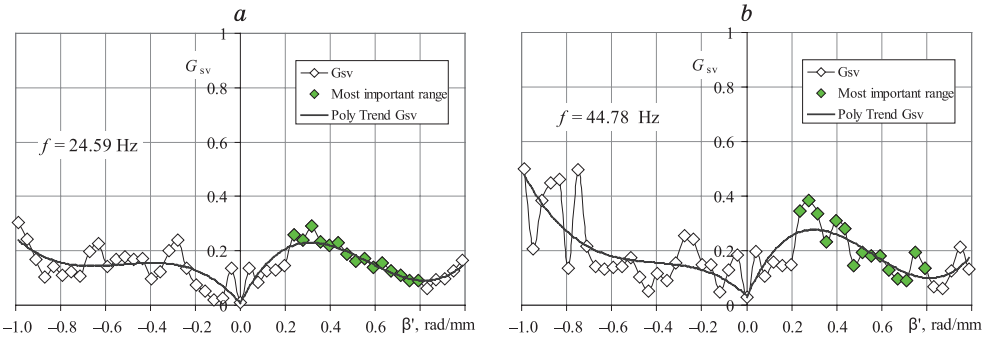

Fig. 1. Surface-vortex receptivity coefficients estimated for frequencies f = 24.59 (*a*) and 44.78 (*b*) Hz

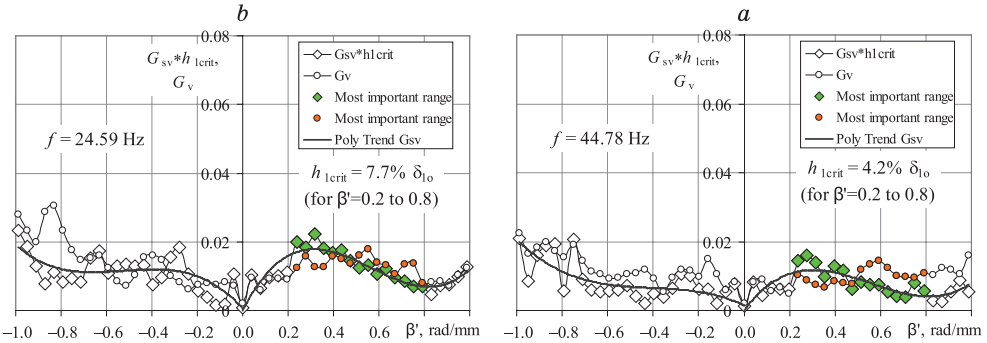

Fig. 2. Comparison of surface-vortex receptivity coefficients multiplied by critical roughness amplitude with vortex receptivity coefficients estimated for frequencies f = 24.59 (*a*) and 44.78 (*b*) Hz

disturbances. However, as was expected, the resonances did not affect the values of the distributed *surface-vortex* receptivity coefficients. These coefficients were estimated by means of a rather complicated procedure of the experimental data analysis described in [1] and compared with the distributed vortex receptivity coefficients estimated there. The following most important results were obtained.

Amplitudes of the distributed surface-vortex receptivity coefficients G_{sv} estimated for two (of three) studied frequencies are shown in Fig. 1 as functions of the spanwise wavenumber. The stability measurements have shown that for the present experimental conditions, the most important range of the spanwise wavenumbers with the most amplified CF-instability waves is approximately between $\beta' \approx +0.2$ to $+0.8$ rad/mm. The distributed surface-vortex receptivity is seen to decrease in this range with β' for all studied cases (Fig. 1, closed symbols). This circumstance can lead to a more significant role of the CF-modes with low spanwise wavenumbers.

A question about relative efficiency of the *vortex* distributed receptivity mechanism (coefficients G_v) in comparison with the *surface-vortex* one is of great importance. Which one is stronger? The answer to this question can be obtained only for particular fixed values of amplitudes the surface waviness h_1. We have estimated critical roughness amplitudes h_{1crit} below which the *vortex* receptivity is stronger in average, while above which the *surface-vortex* receptivity dominates. The 'average strength' of the receptivity mechanism was estimated as mean value of the receptivity coefficient in the spanwise-wavenumber rage of the most amplified (important) CF-waves. Critical values of the waviness amplitudes estimated

for two studied frequencies are indicated in Figs. 2*a,b* together with the corresponding distributions of functions $G_{sv}h_{1crit}$ and G_v. In average for all three studied frequencies, we have estimated that the *surface-vortex* distributed receptivity is weaker than the *vortex* one if the waviness amplitude does not exceed about 5÷6% of δ_1 otherwise the *surface-vortex* receptivity mechanism dominates.

REFERENCES

1. **Borodulin V.I., Ivanov A.V., Kachanov Y.S.** Distributed vortex receptivity of a swept-wing boundary layer in presence of surface nonuniformities. Part 1. Method and vortex receptivity coefficients // Intl. Conf. on Methods of Aerophysical Research. Abstracts. – Novosibirsk: Inst. Theor. and Applied Mech. 2024.
2. **Borodulin V.I., Ivanov A.V., Kachanov, Y.S., Roschektayev A. P.** Distributed vortex receptivity of swept-wing boundary layer. Part 1. Efficient excitation of CF modes // J. Fluid Mech. 2020. Vol. 908, A14.
3. **Borodulin V.I., Ivanov A.V., Kachanov, Y.S., Roschektayev A. P.** Distributed vortex receptivity of swept-wing boundary layer. Part 2. Receptivity characteristics // J. Fluid Mech. 2020. Vol. 908, A15.

DOI 10.53954/9785604990131_50

INTERACTION OF ARTIFICIAL LOCALIZED FREE-STREAM DISTURBANCES WITH THE BLUNTED WING LEADING EDGE

M.M. Katasonov, V.V. Kozlov

Khristianovich Institute of Theoretical and Applied Mechanics, SB RAS, 630090, Novosibirsk, Russia

Abstract. In a model experiment under controlled conditions, the non-stationary interaction processes of artificial external flow disturbances with the blunt leading edge of a straight wing model were studied. It was discovered that localized disturbances generated in the incoming flow give rise to longitudinal streaky structures and wave packets in the boundary layer. Features of boundary layer disturbances arising near a strongly blunted leading edge are revealed. It is shown that under these conditions a transition of the flow from a laminar to a turbulent state is possible due to the spatial growth of wave packets.

Experimental set-up. The experiments were carried out in the subsonic wind tunnel MT-324 of the ITAM SB RAS. The incoming flow velocity was $U_\infty = 3.2$ m/s with the turbulence degree no more than 0.18 %. A model of a straight wing with a span of $L = 200$ mm and a chord of $C = 290$ mm was used. The radius of curvature of the leading edge was 6 mm. The model was positioned under the angle of attack $\alpha = 0°$. Disturbances were generated by pulsed air injection through a source-tube with an outer diameter of 2.5 mm and an inner diameter of 2 mm, Fig. 1. The duration of air blowing from the tube (200 ms) was set by a high-speed electromagnetic valve (EM valve). The measurements were carried out with a constant temperature hot-wire anemometer (CTA) equipped with a single-wire sensor. Signal recording from CTA was synchronized with opening of EM valve.

Results. Unlike studies in natural conditions [1], here a nonstationary localized disturbance is modeled in the free-stream flow Fig. 2a. Due to interaction of the incoming flow disturbance with the insipient boundary layer of the wing model, an several types of disturbances are formed in the boundary layer: longitudinal localized disturbance (streak) Fig. 2b, Fig. 3, Fig. 4, Tollmien-Schlichting (T-Sh) wave packet [2] near its leading front Fig. 3b, Fig. 4b and a small upper vortex, Fig. 3a. A similar pattern was observed in [3–5]. In the present experiment, in the region of a favorable pressure gradient, high-frequency disturbances are damped, including the upper vortex and streak. In the region of an unfavorable pressure gradient, only generated T-Sh wave packets leads to the laminar-turbulent transition. A peculiarity was discovered in the interaction of an external disturbance with the blunt leading edge of the model. When a thin jet interacts with the leading edge, the size of the disturbance in the boundary layer along the transversal coordinate Z becomes 4.6 times larger than the transverse size of the air jet generating it Fig. 2. As a result, the leading edge of the streak becomes quasi-two-dimensional. Accordingly, the T-Sh wave packet that appears near the front of this streak is also quasi-two-dimensional Fig. 4b. As shown in other works, for example in [6], two-dimensional T-Sh waves, in contrast to oblique waves, show the greatest spatial growth.

The authors of the present studies suppose that the appearance of wave packets occurs due to the dispersion properties of the boundary layer. The velocity gradient at the leading edge of the longitudinal structure in this case is a necessary condition ensuring their appearance. The transverse vortex observed in the experiment is the result of the interaction of an

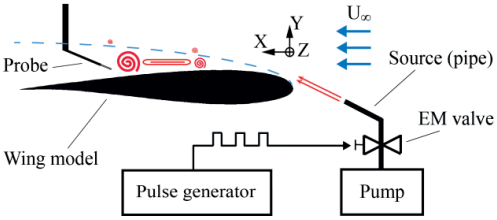

Fig. 1. Experimental scheme.

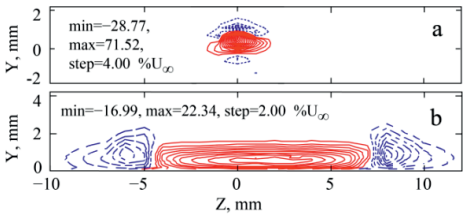

Fig. 2. Isocontours of the velocity fluctuations u' in the $Y - Z$ plane at $t = 200$ ms; a – in the incoming flow, $X/C = -0.003$; b – in the boundary layer, $X/C = 0.14$.

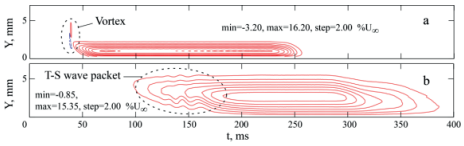

Fig. 3. Isocontours of the velocity fluctuations u' in the $Y - t$ plane at $Z = 0$;
a – $X/C = 0.21$; b – $X/C = 0.76$.

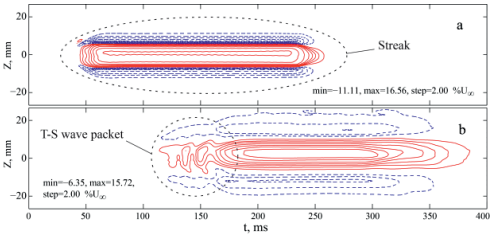

Fig. 4. Isocontours of the velocity fluctuations u' in the $Z - t$ plane at $Y = Yu_{max}$;
a – $X/C = 0.21$; b – $X/C = 0.76$.

unsteady jet and the leading edge, and does not cause the formation of a wave packet inside the boundary layer. All disturbances detected in the experiment are formed almost simultaneously in the region of the leading edge, while the boundary layer amplifies the most unstable of them – these are their own disturbances (T-S wave packets).

The research was supported by the Russian Science Foundation 23-29-00670, https://rscf.ru/en/project/23-29-00670/

REFERENCES

1. **Alfredsson P.H., Matsubara M.** Free-stream turbulence, streaky structures and transition in boundary layer flows // AIAA Paper. 2000. 2534.
2. **Gorev V.N., Katasonov M.M.** Origination and development of precursors on the fronts of streaky structures in the boundary layer on a nonswept wing // Thermophys. and Aeromech. 2004. Vol. 11, No. 3. P. 391–403.
3. **Durbin P.A., Wu X.** Transition beneath vortical disturbances // Ann. Rev. of Fluid Mech. 2007. Vol. 39, P. 107–128.
4. **Zaki T.A., Durbin P.A.** Mode interaction and the bypass route to transition // J. Fluid Mech. 2005. Vol. 531, P. 85–111.
5. **Yao H., Alves-Portela F., Papadakis G.** Evolution of conditionally averaged second-order structure functions in a transitional boundary layer // Phys. Rev. Fluids. 2020. Vol. 5. Paper 093902
6. **Boiko A.V., Grek G.R., Dovgal A.V., Kozlov V.V.** The Origin of Turbulence in Near-Wall Flows, Springer, Berlin. 2002. 263 p.

DOI 10.53954/9785604990131_52

EVOLUTION OF A STALL VORTEX IN THE VICINITY OF A DIHEDRAL CORNER AT MACH NUMBER M = 2.27

I.N. Kavun, A.N. Konopleva, A.I. Maksimov

Khristianovich Institute of Theoretical and Applied Mechanics SB RAS
630090, Novosibirsk, Russia

When bodies and their elements are streamlined by gas or liquid, in many cases flow separations occur, which are accompanied by vortex flows of different complexity and intensity. Considerable attention has always been paid to the study of flow separations and vortex formation processes. Since the formation of vortex systems leads to redistribution of pressure on the streamlined surface and a significant change in the aerodynamic characteristics of aircraft, special importance has been attached to both experimental and computational studies of wings at different flight regimes [1–3].

The computational and experimental studies of the supersonic flow near the external dihedral corner conducted at ITAM SB RAS, and allowed us to identify the main features of the evolution of the stall vortex at small pressure difference between the upper and lateral surfaces of the model [4, 5]. At the same time, a significant similarity with vortex formations arising during the flow of delta wings was found. However, their interesting difference is the gas flow direction in the core of the main vortex: toward the core center in the case of a wing and outward from the core for a dihedral corner. To clarify the results obtained at large pressure difference between dihedral corner surfaces, which are specific for delta wings with sharp leading edges, additional studies were carried out. The new 300 mm long model had a width of 175 mm and a side edge height of 90 mm. The model had the ability to modify the angle of attack between $\alpha = 0 – 20°$ and yaw angle $\beta = 0 – 15°$. Experiments were conducted in wind tunnel T-313 of ITAM SB RAS at Mach number M = 2.27 and Reynolds number $\mathrm{Re} \sim 28 \cdot 10^6$ м$^{-1}$.

In the calculated case, the height of the side edge was increased to 250 mm to eliminate the influence of side effects on the area of the stall vortex location. The calculations were performed with the ANSYS Fluent software package using the *k*-ω SST model of turbulence. To simplify the calculations, it was assumed that the flow was turbulent starting from the leading edge of the model. The number of computational grid cells was 12 million. The calculation methodology is described in more detail in [5].

Figure 1 shows a comparison of the limiting streamlines on the surface of the lateral face in the area of the stall vortex location. Here, the letters *S* and *A* denote the lines of flow separation and reattachment. Numbers 1 and 2 refer to primary and secondary separations and flow reattachments, respectively.

Figure 2 shows a comparison of the flow patterns of a dihedral corner obtained in the experiment and computation with the experimental flow patterns of a delta wing taken from [3]. As can be seen, while the limiting streamlines are practically identical to each other (taking into account the differences in the configurations of the models), the structures of vortex systems differ significantly both in their configurations and in the directions of the streamlines forming the vortex systems.

The research was carried out within the state assignment of Ministry of Science and Higher Education of the Russian Federation with using the equipment of the Equipment Sharing Center “Mechanics” of ITAM SB RAS

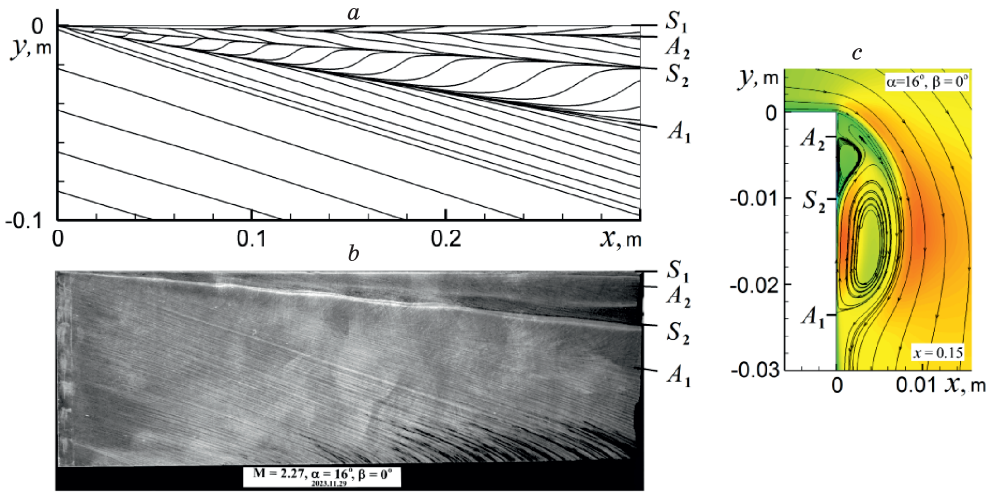

Fig. 1. Stall vortex structure at angle of attack α = 16° and yaw angle β = 0°.

a – calculated and *b* – experimental patterns of the limiting streamlines on the lateral surface of the model, *c* –structure of the stall vortex in the cross section *x* = 150 mm.

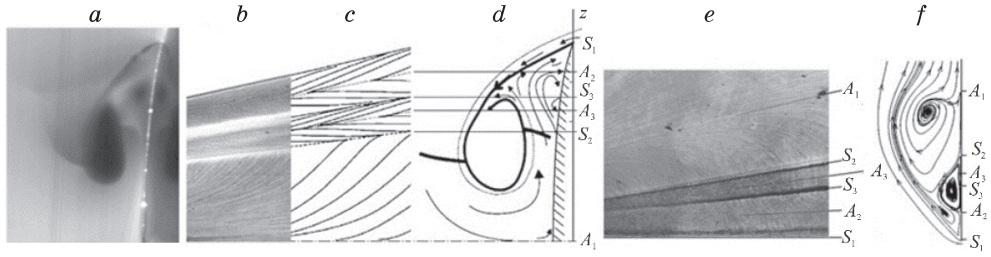

Fig. 2. Comparison of the flow patterns of the delta wing with a leading edge sweep of 78° at M = 2 and α = 14° (*a*, *b*, c, *d*,) and a dihedral configuration at M = 2.27, α = 16°, β = –15° (*e, f*).

a – laser knife image, *b* and *c* – experimental pictures of the limiting streamlines, *d* – interpretation of the flow pattern, *e* – calculated and *f* – experimental structures of vortex systems.

REFERENCES

1. **Luckring J.M.** The discovery and prediction of vortex flow aerodynamics/The Aeronautical Journal. 2019. Vol. 123, No. 1264. P. 729–804.
2. **Maikapar G.I.** Separated flows on the leeward side of delta wing and body of revolution in a supersonic flow. Uch. zap. TsAGI. 1982. Vol. 23, No. 4. P. 22–33.
3. **Brodetsky M.D., Krause E., Nikiforov S.B., Pavlov A.A., Kharitonov A.M., and Shevchenko A.M.** Evolution of vortex structures on the leeward side of a delta wing. J. Appl. Mech. and Tech. Phys. 2001. Vol. 42, No. 2. P. 243–254.
4. **Maksimov A.I. and Kavun I.N.** Evolution of a stall vortex over an external dihedral corner in a supersonic flow. Thermophysics and Aeromechanics. 2020. Vol. 27, No. 5. P. 655–670.
5. **Maksimov A.I. and Kavun I.N.** Formation of a separation vortex in the vicinity of a dihedral corner configuration at $M_\infty = 2.27$ and $\alpha \le 6°$. Thermophysics and Aeromechanics. 2023. Vol. 30, No. 5. P. 787–807.

DOI 10.53954/9785604990131_54

EXPERIMENTAL STUDY OF THE LEVEL OF PEDESTRIAN COMFORT FOR THE COMPLEX CONFIGURATION BLOCK

E.A. Khomenok, E.F. Khrapunov, V.V. Sokolov, S.Yu. Solovev

Federal State Unitary Enterprise «Krylov State Research Centre» 196158, St. Petersburg, Russia

Currently, due to the increasing density of urban development, the growing variety of forms and locations of buildings and structures, the task of ensuring a comfortable stay for people in the urban environment is becoming increasingly urgent. One of the factors influencing the level of comfort is the wind effect on a person in pedestrian and recreational areas. At the same time, improving wind conditions in already built blocks turns out to be difficult to implement, therefore, at the design stage of residential and administrative complexes, studies are increasingly being carried out aimed at determining the characteristics of the flow in spaces near the structures in question. For such work, as a rule, specialized wind tunnels and large-scale models are used. The purpose of this work was to measure the flow speed on the model of urban development with the complex configuration, followed by an assessment of the level of pedestrian comfort.

There are a large number of ways to measure flow velocity, however, in relation to the indicated tasks, the most convenient method is the use of Irwin`s surface wind sensors [1]. Such sensors are relatively simple to manufacture and allow one to measure the mean and pulsating components of air flow velocity.

To test the measurement method, experimental studies were carried out to determine the characteristics of the flow around an object of simplified geometry. In this work, a cube mounted on the horizontal impenetrable surface was used as such an object. The features of flow around such a configuration are well studied, which made it possible to compare the obtained experimental distributions of flow velocity in space near the cube with the results of earlier studies [2]. During testing, good agreement was obtained between the data of this study and the data of the works of other authors.

The determination of the velocity field in pedestrian and recreational areas for the real object was carried out experimentally using the urban development model, which included about ten buildings with significant elevation differences. All buildings were located on the common stylobate. The range of distances between the studied structures was from 1.5 to 25 meters. The research was carried out in the Landscape wind tunnel of the Krylov State Centre. This wind tunnel can reproduce the characteristics of the atmospheric boundary layer, so it is well suited for problems in which wind effects on a person are studied. In the course of experiments using Irwin`s surface wind sensors manufactured at the Krylov Center, the distributions of mean and pulsating velocity components were determined at the height approximately corresponding to the height of pedestrians (about two meters on a full-scale scale). As a result of experimental studies, the features of the emerging flow were identified and areas were determined in which, due to the configuration of buildings, the greatest acceleration of air flow is observed. The data obtained made it possible to assess the level of pedestrian comfort in accordance with known regulatory documents.

REFERENCES

1. **Irwin H.P.A.H.** A simple omnidirectional sensor for wind-tunnel studies of pedestrian-level winds // J. Wind Eng. Ind. Aerodyn. 7 (1981). P. 219–239.
2. **Richards P.J. et al.** Wind-tunnel modeling of the Silsoe Cube // J. Wind Eng. Ind. Aerodyn. 2007. Vol. 95. P. 1384–1399.

DOI 10.53954/9785604990131_56

STUDY OF THE THREE-DIMENSIONAL AIR FLOW STRUCTURE ABOVE HELICOPTER'S LANDING SPOTS OF TYPICAL SHIP AND MARINE OBJECTS

E.F. Khrapunov, E.A. Khomenok, A.N. Novikov, S.A. Mozhaiskiy, V.V. Sokolov, S.Y. Solovev

Krylov State Research Centre
196158, Saint-Petersburg, Russia

The use of helicopters on ships and marine structures, such as offshore platforms, involves a high level of risk. One of the main risks is the complex wind patterns that occur when natural winds interact with these structures' helipads. Helicopter operations on ships and marine structures require pilots to navigate decks with various protruding elements, like superstructures, cargo containers, rescue equipment, etc. Furthermore, these operations must be carried out safely in various weather conditions. Therefore, most structures equipped with helipads undergo studies to determine the flow patterns in the helicopter's maneuvering space during the design stage [2]. This is especially important for structures that will use twin-rotor helicopters since these helicopters' upper and lower blades, which lack sufficient rigidity, may collapse during spin-up and stop, leading to an emergency. The primary aim of this research is to explain the three-dimensional, time-averaged structure of the wind patterns above the helipad. The study was conducted on a simplified model that replicates the typical features of real marine structures. Two different helipad positions were considered.

Despite the continuously increasing possibilities of numerical simulation, the main and most reliable source of information about the structure of the airflow around an object of complex geometry is a physical experiment.

In the present work, the results of studies of the flow structure over the helipads of a simplified-shaped object are presented. Experimental studies were carried out on a scale model of simplified geometry in a homogeneous air-free flow. It is well known that measurements of the three-dimensional velocity vector can be performed using various systems, but the simplest is pneumometric probes: five- and seven-hole probes. To measure air velocity in this work, a seven-hole probe created in the aerodynamics laboratory of the Krylov State

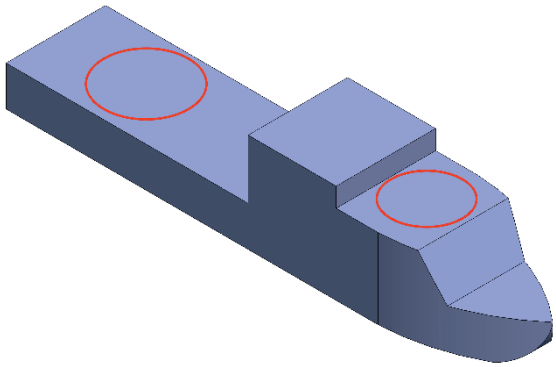

Diagram of a simplified facility with dedicated helicopter operation sites

Research Centre was used. The use of a seven-hole probe makes it possible to determine three components of the velocity vector with bevel angles in two orthogonal planes up to 70°. This range of measuring bevel angles (and therefore the component of the total velocity vector) significantly exceeds the range of five holes and similar probes available for measurement [3].

The research work focuses on the distribution of flow velocities around a simplified object's deck where a helicopter is located. The study shows that flow separation occurs at the edge of the windward side of the object, regardless of any protruding elements nearby. In some cases, the airflow sticks back to the deck if it has sufficient length. Similar patterns are observed at offshore structure sites. The airflow and superstructure interaction creates an aerodynamic wake area in the helicopter's maneuvering space. This area is characterized by relatively small average speed values but significant bevel angles in two orthogonal planes. The study also demonstrates how wind tunnel research results can be used in providing recommendations for the operation of real equipment on real objects' sites.

REFERENCES

1. **Lopez-Nunez E. et al.** Characterization of The Wind Flow on The Flight Deck of a Frigate // Proc. of 8th European Conference for Aeronautics and Aerospace Sciences (EUCASS). 2019. p. 9.
2. **Buchholz J.H.J. et al.** Structure of a Ship Airwake at Model and Full Scale // Proc of AIAA SciTech Forum. 2018. 19 p.
3. **Gerner A.A et al.** Non-nulling seven-hole probes for high angle flow measurement // Experiments in Fluids. 1984. Vol. 95. P. 95–103.

DOI 10.53954/9785604990131_58

INVESTIGATION OF SUPERSONIC BOUNDARY LAYER STABILITY WITH TRANSVERSE PRESSURE GRADIENT INDUCED BY AN INCLINED SHOCK WAVE

S.V. Kirilovskiy, T.V. Poplavskaya, A.A. Sidorenko

Khristianovich Institute of Theoretical and Applied Mechanics of SB RAS, 630090, Novosibirsk, Russia

A numerical investigation of the interaction of the boundary layer (BL) on a flat plate with a weak shock wave incident on it, generated by a wedge located above the plate, was considered in [1] in a two-dimensional setting. It has been shown that there is a marked increase in the values of the N-factors of the Tollmin–Schlichting (TS) instability in the interaction region. Another interesting test case is the interaction of the boundary layer on a flat plate with a jump generated by a thin keel protruding from the surface. As a result of this three-dimensional interaction, the induced transverse pressure gradient can lead to the development of crossflow vortices instability (CFVs) in addition to TS wave instability. As a result of this three-dimensional interaction, the induced transverse pressure gradient can lead to the development of crossflow vortices instability in addition to TS instability.

In this paper we consider the interaction of a supersonic ($M_\infty = 1.43$) BL on the surface of 0.31m long plate with an incident weak shock wave generated by a wedge located at right angles to the plate surface on the lateral surface of the computational domain (see Fig. 1*a*). The angle of rotation of the wedge θ with respect to the flow direction varied the intensity of the shock wave interacting with the BL.

This problem was solved numerically using the method of integration of the LOTRAN 3.0 software package, created in ITAM SB RAS, and the ANSYS Fluent gasdynamic package [2]. Within the framework of this approach, two tasks were solved: 1) calculation of the laminar flow of the model using the ANSYS Fluent software package (obtaining the characteristics of the main flow), and 2) stability analysis of the main flow profiles using the LOTRAN 3.0 software package.

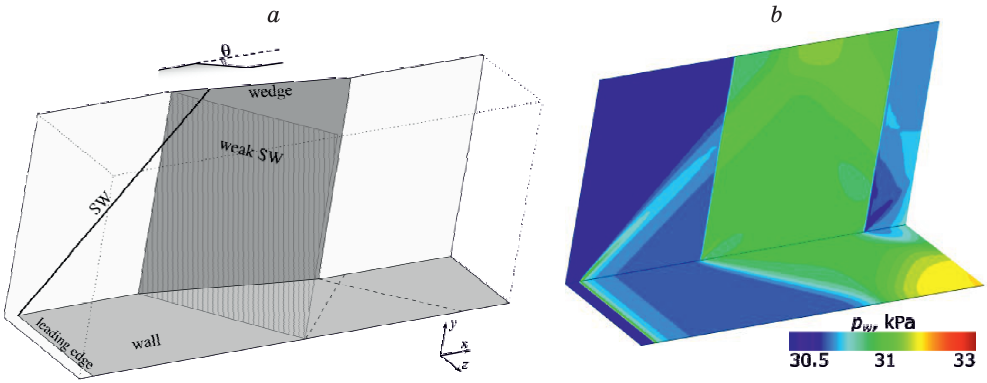

Fig. 1. Schematic representation of interaction of inclined shock wave with BL on the plate (*a*) and static pressure field on the plate surface and the lateral boundary of the computational domain (*b*).

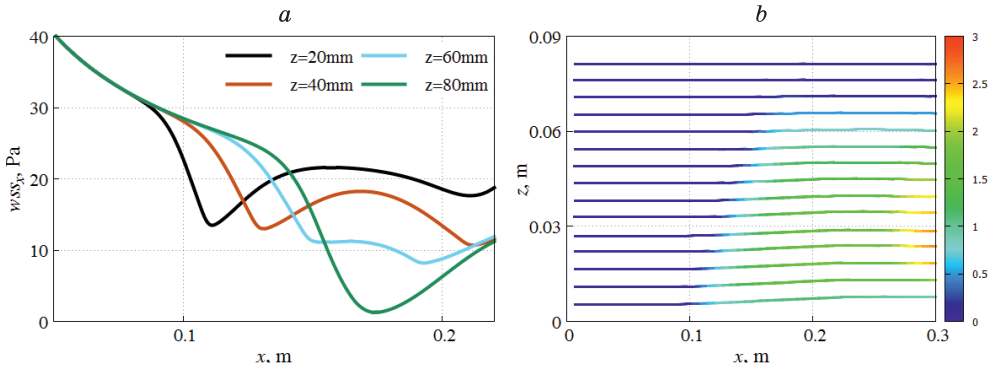

Fig. 2. Distribution of the longitudinal component of shear stresses on the plate surface in the region of interaction of the BL with the incident SW at different z (*a*) and streamlines colored by the values of *N*-factors of crossflow vortices instability (*b*): θ = 1.0°.

Figure 1*b* shows the static pressure field on the plate surface and the lateral boundary of the computational domain including a wedge located at the angle θ = 0.5°. The pressure rise behind the oblique shock wave can be seen. It is also seen that the shock wave from the plate leading edge does not affect the interaction region.

Figure 2*a* shows the longitudinal shear stress *wss* distributions for different z coordinates (z = 0 corresponds to the position of the wedge leading edge. It can be seen that a decrease in the minimum of the longitudinal component of the shear stress approaching zero value is observed when moving away from the wedge. Increasing the wedge angle leads to the appearance of negative values of *wss*, indicating the presence of separation flow zone. Moreover, increasing the wedge angle leads to a more intense interaction of the BL with the oblique shock wave. An increase in the *N*-factors for the instability of the cross-flow vortices is observed starting from θ = 1.0° just after the interaction region (Fig. 2*b*).

The work was carried out within the framework of the state assignment of ITAM SB RAS.

REFERENCES

1. **Kirilovskiy S., Poplavskaya T., Sidorenko A.** On the stability of supersonic boundary layer in interaction with weak shock waves // E3S Web of Conferences 2023. V. 459, No. 03003. P. 1–4.
2. **Boiko A.V., Demyanko K.V., Kirilovskiy S.V., Nechepurenko Y.M, Poplavskaya T.V.** Modeling of transonic transitional three-dimensional flows for aerodynamic applications // AIAA J. 2021. V. 59, No. 9. P. 3598–3610.

DOI 10.53954/9785604990131_60

FLOW STRUCTURE OF AN IMPACT UNDEREXPANDED JET WITH VORTEX GENERATORS AT THE NOZZLE EXIT

N.P. Kiselev, R.A. Styazhkin, A.A. Pivovarov

Khristianovich Institute of Theoretical and Applied Mechanics SB RAS
630090, Novosibirsk, Russia

The importance of the study of impact jets is associated with the search for methods for reducing the noise level formed as a result of intense pulsations during the interaction of a high-speed jet with a surface, for example, during takeoff/landing of an aircraft. One of these methods is the use of various vortex-generators devices at the nozzle exit – chevrons, tabs or issue of small-sized jets.

The goal of the work was to study the pulsation characteristics of an impact underexpanded jet and the possibility of their control using microjets. An experimental study of the flow of an underexpanded jet impinging with a normal plane obstacle was carried out using a vertical jet facility of the ITAM SB RAS. The jet exhausted from the sonic axisymmetric nozzle with a geometric Mach number at the exit $M_a = 1.0$ and $N_{pr} = P_0/p_c = 4$, (N_{pr} is the ratio of the pressure in the settling chamber P_0 to the ambient pressure p_c) which corresponds to an underexpanded jet. The underexpanded microjets (6 pcs.) issued from convergent axisymmetric micronozzles directed near the exit of the main nozzle tangentially to the jet boundary. The flow pictures of an impact undisturbed jet and a jet with microjets is shown in Fig. 1. The distance from the nozzle *1* exit to the obstacle *2* is $H/D_a = 4$. From the visualization it is clear that for the mode without microjets (Fig. 1, a) a strong pulsating flow mode is realized. In addition to the main system of shock waves corresponding to the barrel shock *3*, the Mach disk *4* and the reflected shock *5*, the boundary of the jet *6* takes on a wave-like appearance, and a large-scale structure *7* is formed. In the field of the jet, from the place of interaction of the jet with the obstacle, when the flow is reflected, acoustic waves 8 are emitted, directed from the obstacle to the nozzle cut and having the nature of weak waves, such as Mach waves. A pulsating interaction mechanism such as acoustic feedback loop is implemented [1]. Wave *8* from the obstacle moves towards the flow and, arriving at the nozzle exit, disturbs a thin mixing layer (~1 mm), the oscillation of the mixing layer develops and intensifies downstream, passes through a system of oblique shock waves, intensifies towards the obstacle, and closes the feedback loop.

When microjets are exhausted (see Fig. 1b), the flow pattern between the nozzle and the obstacle changes significantly: it is clear that the jet boundary is not disturbed and large-scale structures are not formed. At the same time, lines associated with artificially created streamwise vortices are clearly visible. The jet is decelerated when through standoff shock *9* (Fig. 1, b).

On the surface of the obstacle (at its center $r/D_a = 0$), a pulsation sensor measured the dynamic pressure p'_w, presented in the form of amplitude Spectrum *1* corresponds to an undisturbed impact jet, *2* – in the presence of microjets. For undisturbed jet *1*, many amplitude peaks are registered, characterized by a strong pulsating self-oscillatory flow regime. The maximum amplitude of disturbances at a frequency of 5 kHz is 23 kPa. With microjets (pos. *2*, Fig. 2), a spectrum without amplitude maxima is visible – the highest amplitude is fixed at low frequencies (60–80 Hz), which is due to the reflection of sound waves from the walls of the room or equipment of the experimental facility. It can be seen that pulsations characteristic of a self-oscillating process are not registered in this case.

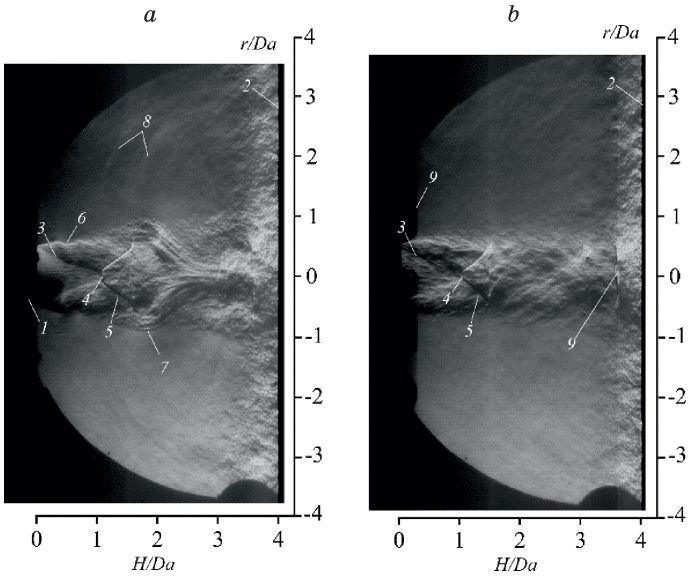

Fig. 1. Visualization of an impact jet exhausting from a sonic nozzle (*a*) and a nozzle with microjets at the exit (*b*), exposure 4 μs

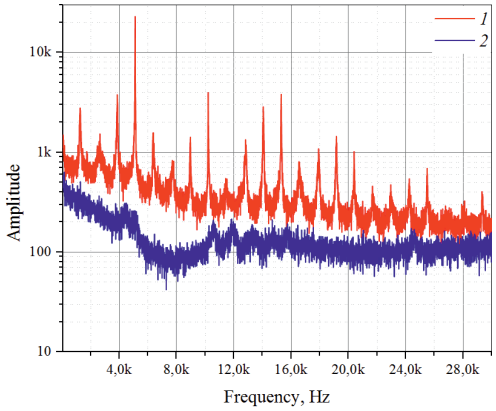

Fig. 2. Fourier amplitude spectrum, $r/D_a = 0$

The standard deviation of wall pressure pulsations is $\langle p'_w \rangle / p_c = 0.4$ for an undisturbed jet and 0.1 for a jet with microjets. Thus, the presence of microjets makes it possible to completely suppress acoustic feedback loop at a distance of four calibers and reduce pulsations in the impact jet by 4 times.

The research was carried out within the state assignment of Ministry of Science and Higher Education of the Russian Federation. The study was conducted at the Equipment Sharing Center «Mechanics» of ITAM SB RAS.

REFERENCES

1. **Powell A.** The sound-producing oscillations of round underexpanded jets impinging on normal plates // J. of Acoustic Society of America. 1988. Vol. 83. P. 515–533.

DOI 10.53954/9785604990131_62

INFLUENCE OF INLET-SECTION GEOMETRICAL PARAMETERS ON THE VORTEX STRUCTURE OF THE GAS FLOW IN THE SLOT CHANNEL

S.P. Kiselev, V.P. Kiselev, V.N. Zaikovskii, and G.V. Trubacheev

Khristianovich Institute of Theoretical and Applied Mechanics, 630090, Novosibirsk, Russia

In [1], it was shown that in a supersonic jet emanating out of a rectangular channel (see Fig. 1, *a*) there arise gas-flow disturbances visible in the schlieren photograph of the flow on the plate (see Fig. 1, *b*). These disturbances are related with the longitudinal vortices originating at the entrance to the channel and also, with the transverse compression-rarefaction waves that arise when the gas leaves the channel. The flow geometry is shown in Fig. 1, *a*. From the high-pressure cylindrical chamber (pre-chamber) 1, the air with temperature $T_0 = 300\,\mathrm{K}$ and pressure p_0 was supplied to the vertical inlet channel through a row of holes made in insert 2. The inlet channel was bounded by a central rod 3 and by the cylindrical

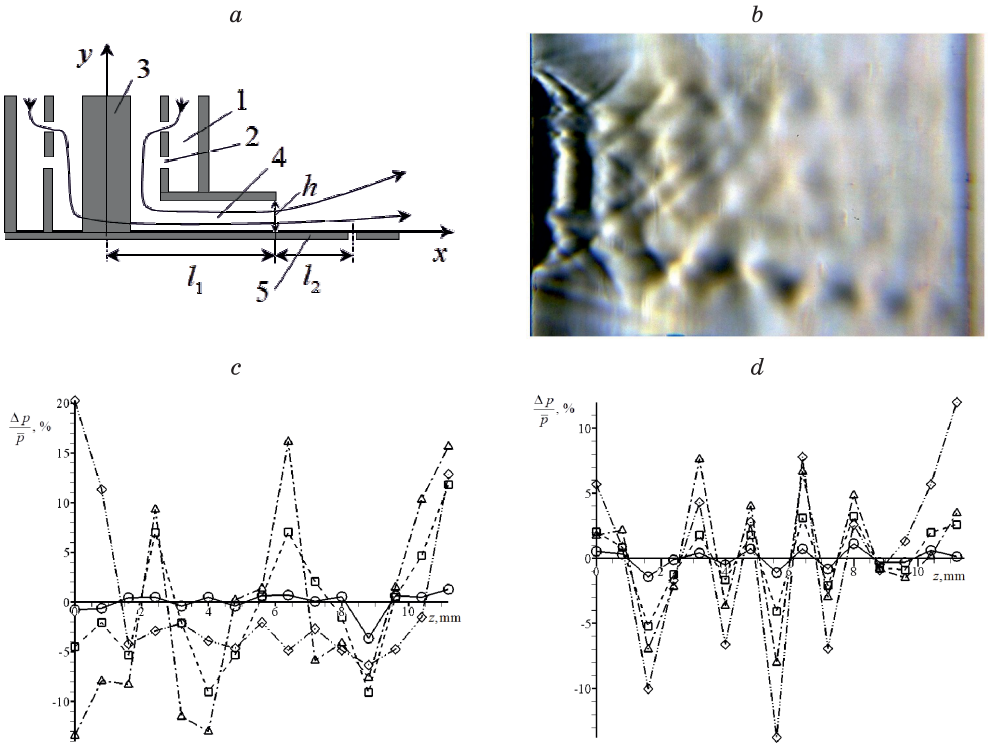

Fig. 1. Experimental setup and measured data: *a* – diagram of the experimental setup; *b* – Schlieren photograph of the gas flow (p_0 = 1.1 MPa) over the glass plate; *c* – $p(y, z)$ for B_1: p_0 = 0.18 MPa – circles; p_0 = 0.3 MPa – squares; p_0 = 0.43 MPa – triangles; p_0 = 1.1 MPa – rhombuses; *d* – $p(y, z)$ for B_2: p_0 = 0.18 MPa – circles; p_0 = 0.27 MPa – squares; p_0 = 0.36 MPa – triangles; p_0 = 0.56 MPa – rhombuses.

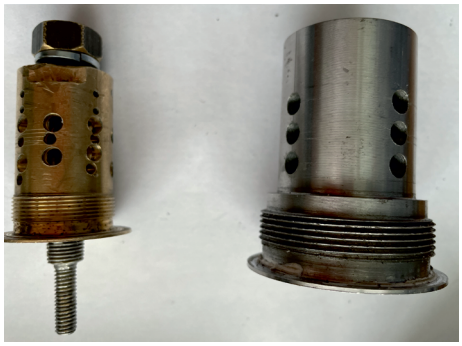

Fig. 2. Photos of the inserts: the insert B_1 is shown on the left, and the insert B_1, on the right.

insert 2. The experiments were carried out with two inserts, B_1 and B_2, which differed in diameter and in the number of made holes, but with the total area of the holes in both inserts being identical. From the vertical channel, the air flowed into the outlet rectangular channel 4, from which it was discharged into the ambient space bounded on one side by plate 5. Channel 4 had a length $l_1 = 36\,\text{mm}$ and a rectangular cross-section of width $h = 1\,\text{mm}$ and height $b = 18\,\text{mm}$.

On plate 5, at a distance of $l_2 = 12\,\text{mm}$ from the exit section of the channel, 15 pressure holes were provided, which were made in transverse direction at a distance $\Delta z = 0.8\,\text{mm}$ from each other. Using those holes, the static pressure on the plate was measured. Shown in Fig. 1, *c* and *d* are the distributions of $\Delta p / \overline{p}$ on the plate at different prechamber pressures p_0, obtained with the insert B_1 (Fig. 1, *c*) and with the insert B_2 (Fig. 1, *d*), where p is the static pressure on the plate in section $x = l_1 + l_2 = 48\,\text{mm}$, $\overline{p}$ is the average pressure, and $\Delta p = p - \overline{p}$. Figure 2 shows the inserts that were used in the experiments.

Evidently, with different inserts the amplitudes of the disturbances and the distances between the maxima of pressure disturbances on the plate are different. This result seems to be somewhat paradoxical, since in the vertical channel there is a flow moving at a low subsonic velocity. In the slot channel, the gas is accelerated to a transonic velocity, and at the exit from the channel, to a supersonic velocity $\text{M} \approx 2$. This difference in the distribution of $\Delta p / \overline{p}$ may be due to the influence of initial disturbances formed when the gas flows through the holes in two different inserts B_1 and B_2.

For testing this hypothesis, numerical calculations of the gas flows with and without insert were carried out in the geometry like that used in the experiment (see Fig. 3). The gas flow was described within the framework of the SST k – omega model of turbulence, and the numerical calculations were carried out using the FLUENT software. In the case with the insert, the gas was supplied into the vertical channel through holes with the area the same in value as in the experiment (see Fig. 3, *a*), and in the case without insert, the gas was supplied into the vertical channel from above (see Fig. 3, *b*).

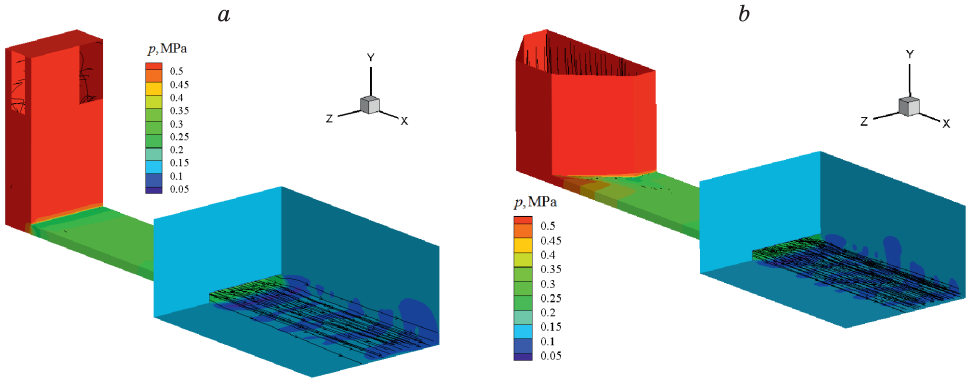

Fig. 3. Geometry of half ($z > 0$) of the computational domain, and the calculated pressure distributions and streamlines: *a* – with holes; *b* – without holes.

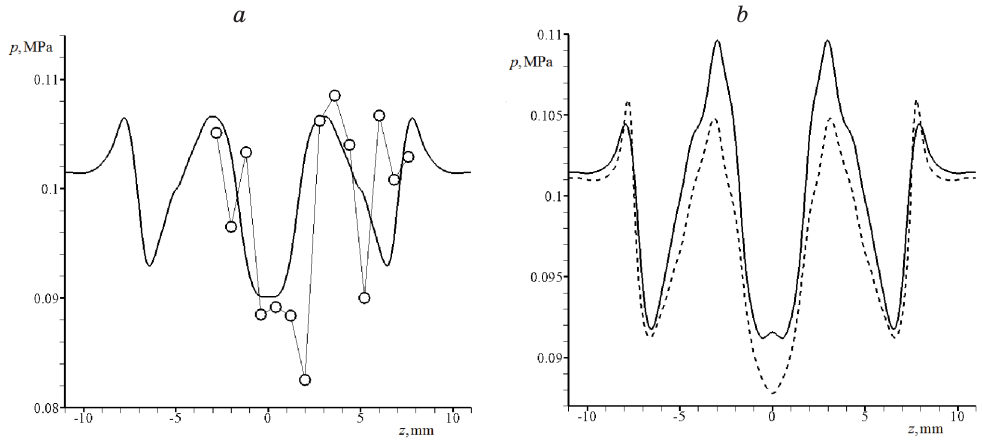

Fig. 4. Distribution of pressure in different sections y = const on the plate: *a* – in section $y = 0$, calculated and experimental data with the insert (solid line and circles, respectively); *b* – in section $y = 0.5$ mm, calculation with and without the insert (respectively the solid and dashed line).

Fig. 4 shows the distributions of pressure on the plate obtained in the numerical calculations and in the experiment held at prechamber pressure $p_0 = 0.53\,\text{MPa}$.

From Fig. 4, it follows that the results of calculation of the pressure with the insert are in satisfactory agreement with the results of measuring the static pressure on the plate in the experiment with the insert B_1. From Fig. 4, *b* it follows that the distributions of pressure on the plate obtained in the calculations with and without an insert are similar and close to each other. It follows from here that the influence of the insert on the distribution of pressure on the plate is insignificant. The difference in pressure on the plate observed in the experiment (see Fig. 1, *c* and *d*) cannot be attributed to the different number of holes in the inserts B_1 and B_2 through which the gas is supplied to the vertical channel.

Conclusion. The present paper reports results of a study of pressure disturbances in a supersonic jet emanating from a rectangular slot channel. The experiment revealed the influence of the method of gas supply at the channel entrance through various inserts on the magnitude and period of pressure disturbances on the plate. The distribution of pressure on the plate obtained in the numerical calculations of the gas flow in the channel with the insert is in satisfactory agreement with the experimental data obtained with the insert B_1. Numerical calculations show that a change of the method of gas supply into the vertical channel weakly affects the distribution of pressure on the plate.

This work was carried out within the framework of a state assignment for ITAM SB RAS.

REFERENCES

1. **Kiselev S.P., Kiselev V.P., Zaikovsky V.N., Trubacheev G.V.** Vortex flows in channels with the conditions of cold gas-dynamic spraying // Dynamics of Multiphase Media (DMS 2023): Proc. of the XVIII All-Russian seminar with international participation dedicated to the 115th anniversary of S.A. Khristianovich, September 24–27, 2023, – Novosibirsk, 2023. P. 50–51.

DOI 10.53954/9785604990131_65

NUMERICAL RESULTS BASED ON THE LINEAR STABILITY THEORY OF THE INFLUENCE OF SLOTS ON THE DISTURBANCES DEVELOPMENT IN THE SUPERSONIC BOUNDARY LAYER

G.L. Kolosov, A.A. Yatskikh, B.V. Smorodsky, A.D. Kosinov

Khristianovich Institute of Theoretical and Applied Mechanics SB RAS
630090, Novosibirsk, Russia

In recent experimental studies V.I. Lysenko et al. (ITAM SB RAS) discovered the effect of flow stabilization in a supersonic boundary layer at Mach number 2 in the presence of small extended slots on the surface of the plate. Experimental data must be confirmed by calculations, including calculations based on the linear stability theory.

The work uses linearized Navier-Stokes equations for the compressible case [1]. A system of 8th order ordinary differential equations is considered, which was solved analytically in a free flow. Next, integration was carried out according to the fourth order Runge-Kutta scheme using the Gram-Schmidt orthogonalization. To satisfy the boundary conditions, a minimum determinant was found, composed of the values of velocity and temperature amplitudes on the model wall. Average velocity and temperature profiles were taken from direct numerical simulation calculations.

It was found that for certain geometric parameters of the slots, a smaller increase of unstable disturbances is observed compared to the case of a flat plate with a smooth surface. Below are the dimensional spatial growth rates for a disturbance frequency of 16 kHz for the case of a smooth plate and a plate with slots 0.1, 0.18 mm deep in a section 95 mm from the leading edge of the model.

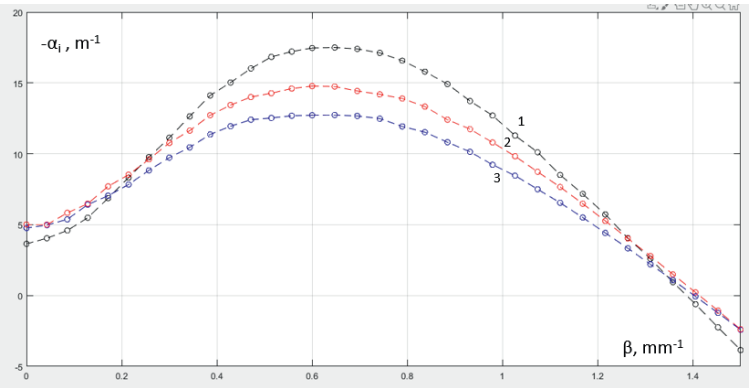

Growth rates as a function of transverse wavenumbers.

1 – smooth plate, *2* – model with slots 0.1 mm deep, *3* – model with slots 0.18 mm deep.

The study was supported by the Russian Science Foundation grant No. 23-79-10167, https://rscf.ru/project/23-79-10167/. Calculations of the average flow were performed in the FlowVision software package (TESIS LLC, https://flowvision.ru/) on the Equipment Sharing Center “Mechanics” of ITAM SB RAS

REFERENCES

1. **Mack L.M.** AGARD Report No. 709 (Special course on stability and transition of laminar flows), VKI, Brussels, 1984.

DOI 10.53954/9785604990131_66

CONTROL OF TURBULENT BOUNDARY LAYER ON AN AIRFOIL BY MASS TRANSFER THROUGH A PERMEABLE WALL (REVIEW)

V.I. Kornilov

Khristianovich Institute of Theoretical and Applied Mechanics SB RAS*, *630090 Novosibirsk*, *Russia

Further development of high-speed air transport, as well as ground and sea transportation, is hardly possible without the creation of new economical methods for controlling near-wall flows [1]. The problem of controlling a turbulent boundary layer (BL) on a wing, the drag of which reaches 2/3 of the total drag balance of a modern subsonic transport aircraft, is especially relevant. Positive (from the wall) and negative (toward the wall) air mass transfer through a permeable wall is one of the promising ways to reduce turbulent friction and aerodynamic drag of this most important element of the aircraft [2]. It is no coincidence that the possibilities and prospects for using such a control method are being studied in laboratories in dozens of countries around the world.

This work is a generalization of the experience of world research (mainly the author's) on the efficiency of both distributed (through a high-tech finely perforated section) and localized (through a slot) mass transfer on two-dimensional airfoils at subsonic flow velocities. Within the framework of dimensional theory, a set of dimensionless parameters responsible for the process of mass transfer on the airfoil under conditions of an incompressible flow around it has been determined. The problems of numerical and experimental modeling of such a flow are considered as well as calculated and experimental data are analyzed that describe the effectiveness of this control method in terms of improving the aerodynamic characteristics of the airfoil when changing a number of important parameters: the mass transfer intensity, the angle of attack of the airfoil, the width and position of the slot (or permeable section) along the airfoil chord, and also estimates the energy costs for the mass transfer process.

The results of investigations lead us to the following generalized conclusions:

– experience in solving this complex problem, the nature of which is determined by the process of interaction of an external shear flow with an array of microjets or with a single slot jet, requires close cooperation between specialists working in the field of numerical and physical modeling. An important role here belongs to the experiment, a typical diagram of which with a model of the low-speed airfoil placed in a wind tunnel is shown in Fig. 1;

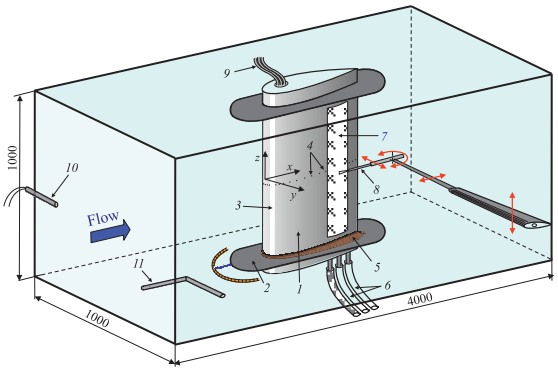

Fig. 1. Arrangement of the typical experiment with the airfoil model in the wind tunnel test section.

1 – low-speed airfoil; *2* – end plate; *3* – tripping device; *4* – pressure taps; *5* – fillet; *6* – to a compressor or to a vacuum system (on other side); *7* – perforated section; *8* – hot-wire probe or other probes; *9* – to a pressure scanner; *10* – thermocouple; *11* – Pitot-static tube. All dimensions are in millimeters.

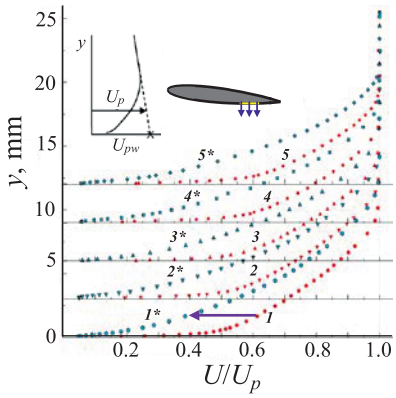

Fig. 2. Boundary layer mean velocity profiles on the side of positive mass transfer.

1; *1** – α = –2°; *2*; *2** – α = 0°; *3*; *3** – α = 2°; *4*; *4** – α = 4°; *5*; *5** – α = 6°. *1* ÷ *5* – C_b/C_s = 0; *1** ÷ *5** – C_b/C_s = 9.9 10^{-3}/4.75 10^{-3}.

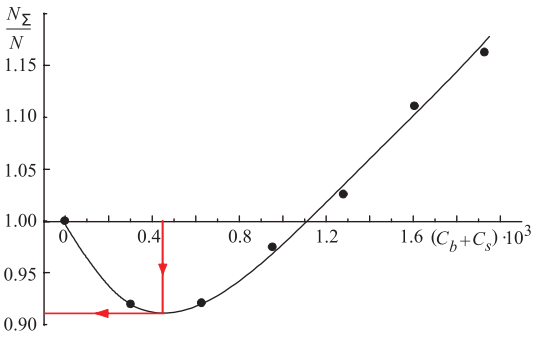

Fig. 3. Dependence of normalized power on the total intensity of mass transfer at α = 0°.

– just as in a gradient-free flow, the experimental profiles of the mean velocity in the BL for angles of attack α = ±6° on the side of positive mass transfer (Fig. 2) are less full compared to those for the basic configuration. On the contrary, in the presence of negative mass transfer, the distribution of the mean velocity along the height of the BL is of the opposite nature. Naturally, the local velocity gradient near the wall, reflecting the behavior of the friction component, decreases in the first case and increases in the second. The distribution of turbulent velocity fluctuations in these two cases is of the opposite nature;

– an assessment of the effectiveness of the combined forcing of distributed mass transfer on the airfoil BL, carried out taking into account energy costs, shows that power savings of about 9% are achieved with a total mass transfer coefficient (C_b + C_s) approximately equal to (0.4–0.5)×10^{-3} (Fig. 3). As (C_b + C_s) increases, the effectiveness of the control method decreases. When (C_b + C_s) ≥ 1.1×10^{-3} this control method becomes economically unjustified, at least when the permeable section is located in the tail of the airfoil;

– an increase in pressure due to positive mass transfer on one side of the airfoil and an increase in exhaust due to negative mass transfer on the opposite side lead to a corresponding increase in lift and ultimately to a gain in the lift-to-drag ratio of the airfoil, reaching 3 units at angles of attack α close to zero. As α increases, the effectiveness of this method of influencing the BL decreases;

– positive mass transfer is preferable to use to increase the lift of the airfoil. Negative mass transfer is more effective in reducing drag, but the effect of its use at the same values of the mass transfer coefficient is significantly weaker;

– potential of both distributed and localized mass transfer for controlling near-wall flow has not been exhausted. Even at the expense of external pressure flow resources, i.e. by supplying air through a finely perforated section on the leading edge of the airfoil, it is possible to increase the lift-to-drag ratio by two units. Further studies of the optimal relationship between positive and negative mass transfer at different angles of attack of the profile, as well as the position of the permeable section or slot along the chord, can provide a reserve for increasing efficiency. The length of the perforated section is of particular importance when using this technology on board an aircraft, where, due to the required structural rigidity, only local areas can be made permeable.

The work was performed within the framework of the State Assignment of the ITAM SB RAS.

The author expresses his sincere gratitude to Prof. Evgeny Shkvar, Dr. Ivan Kavun and Dr. Anatoly Popkov for helping in computations.

REFERENCES

1. **Abbas A., De Vicente J., Valero E.** Aerodynamic technologies to improve aircraft performance //Aerospace Science and Technology. 2013. Vol. 28, No. 1. P. 100–132.
2. **Kornilov Vladimir.** Combined blowing/suction flow control on low-speed airfoils // Flow, Turbulence and Combustion. 2021. Vol. 106. P. 81–108.

DOI 10.53954/9785604990131_69

ADDITIVE METHODS FOR FORMING FUNCTIONAL SURFACE LAYERS. COLD SPRAYING

V.F. Kosarev, S.V. Klinkov

Khristianovich Institute of Theoretical and Applied Mechanics SB RAS
630090, Novosibirsk, Russia

The paper presents main results of research related to cold gas-dynamic spraying – from discovery of phenomenon to development of equipment and scientific basis of various technologies using cold spray.

The first studies have shown that at a certain particle speed there is a transition from the process of substrate erosion to deposition process. For the first time, it was established that coatings can be grown from particles having a temperature significantly lower than their melting point. Using unheated mixtures of helium with air (nitrogen), as well as slightly heated pure air (nitrogen), to accelerate particles, coatings of most metals and many alloys on substrates of metals, glass, and ceramics were produced. In this case, powder deposition efficiency can reach relatively high values of 0.5–0.8. By heating helium jet, it is possible to obtain coatings of refractory metals (Nb, Mo и W).

Later, it was also unexpectedly discovered that high speeds should not always be of priority; coatings can also be produced at lower speeds, for example, when metalizing building materials such as brick with aluminum. Such materials are classified as not erosion-resistant, i.e. under typical cold spray conditions they are destroyed, and it is difficult to produce metal coating on them. However, due to lowering the particle velocity (for example, by reducing the stagnation pressure), continuous aluminum coatings can be obtained on such materials without the need for any preliminary surface preparation.

Today, cold spray is often called additive manufacturing (in international publications its abbreviation is CSAM – cold spray additive manufacturing). This is based on the ability to use cold spray for almost unlimited increase in volume of the compact/coating. For the successful development of this direction, a model of deposition at an angle is required (it is clear that the manufacture of a three-dimensional product will inevitably lead to a geometry far from a flat plate). The basics of such model in the frames of continuum media mechanics can be found in [1, 2]. In particular, the simulation results have shown a change in the cross-sectional profile of a single deposition track from the initial shape which is close to Gaussian to the wedge-shaped; and it was confirmed by experiments. In addition, it has been shown (by simulation and experiment) that the deposition strategy based on changing the deposition angle actually allows growing 3D objects. for example, such as walls.

Comparative simplicity of implementation of cold spray allows developing unique nozzle assemblies to solve specific problems. The first cold spray installations operated at stagnation pressure range of particle-accelerating gas of 1.5–2.5 MPa; under these circumstances the powder was introduced into the nozzle pre-chamber from a volume where pressure was maintained higher than in nozzle pre-chamber. Later, high-pressure cold spray devices were developed (4 MPa, and today even 7 MPa). To make it possible to feed powder from an open powder feeder (at atmospheric pressure), ejector nozzles were developed based on the design of a gas ejector with a central body. Currently, this development ensures

the feeding and spraying of powder from an atmospheric feeder in the range of operating air stagnation pressures of main ejecting flow up to 4 MPa.

Combining shape of nozzle exit (oblique cuts, longitudinal slits) with flow swirling in nozzle pre-chamber, it is possible to change the shape of spray spot. For example, it was shown that in certain cases it is possible to produce extremely wide strips of coatings (from 20 to 70 mm), which is difficult when using rectangular nozzles. In this case, such a wide dispersion of particles is achieved by organizing a powerful fan-shaped spreading of gas into an angle of about 60 degrees. Usage of radial nozzle makes it possible to apply coatings to the inner surface of pipes of small (40–100 mm) diameter without rotating it.

There were developed basic features of a new technology [4] for double-sided topographic metallization by about 300 μm thick copper layers produced on 300 μm thick ceramic plates made of aluminum oxide and nitride. The topological pattern was obtained by masking during deposition process, i.e. avoiding typical technological step consisting of partly removing previously attached conductive layer. Specific tests have shown that the samples can withstand thermal cycling (about 100 cycles) in the temperature range from – 60 to + 150 °C.

Thus, on basis of the discovery, in ITAM SB RAS there was developed the method for coating and additive manufacturing that has no analogues in the world, which provides a number of advantages, including: low-temperature action on sprayed arts; simple equipment and control, long service life; opportunity of collecting and reusing particles, as well as possibility of fabricating coatings with properties close to one of particle material; possibility of producing composites containing dissimilar materials: metals, ceramics, polymers; potential of increasing in coating thickness, thus, creating additive technologies.

There are technologies with application of cold spraying, being introduced into Russian Federation industry. The products are included to State Standard and are used in companies of Russian Federation (cable terminators and transition plates).

For the work “Creation of generalized theory of interaction of high-speed heterogeneous flows with an obstacle, development of technologies and equipment for gas-dynamic deposition of metals, widely used in world practice” some personnel at ITAM SB RAS (Alkhimov A.P., Klinkov S.V., Kosarev V.F., Papyrin A.N. and Fomin V.M.) were awarded the Prize of Russian Federation Government in the field of science and technology in 2010 year.

Contribution of ITAM SB RAS to the investigation of cold spray process and its place in the world is clearly illustrated by data published in the paper [1]. In this reference, based on Scopus data, an analysis of worldwide publication activity in the field of cold spray was carried out as it was at the end of 2021 year. A total number of 1944 publications were taken into account (articles – 1164, articles based on conference materials – 559, review articles – 128, chapters in monographs – 68, etc.). In between 20 countries that have contributed to research in the field of cold spray, Russia Federation ranks 6th place with 117 publications; higher are: China (486), USA (344), Canada (257), France (225) and Japan (143). Within 10 most productive institutions in the world, ITAM SB RAS ranks 6th place with 69 publications (59% of publications in Russian Federation); above are organizations from France (Universite de Technologie de Belfort-Montbeliard), China (Xi’an Jiaotong University), USA (U.S. Army Research Laboratory), Canada (University of Ottawa) and Ireland (Trinity College Dublin). Between 20 most cited publications, the monograph Cold Spray Technology / A. Papyrin, V. Kosarev, S. Klinkov, A. Alkhimov, V. Fomin // Elsevier Science, 2007 (the world’s first monograph dedicated to cold spray) with 628 citations is located on 2nd place.

REFERENCES

1. **Abu Bakar I.A., Oma N.I., Yusuf Y., Rahim T.A.** Reflection and Future Perspectives in Cold Spray Technology: A Bibliometric Analysis / Journal of Thermal Spray Technology. 2023. Vol. 32, P. 1576–1595.
2. **Klinkov S.V., Kosarev V.F., Shikalov V.S.** Control of Cold Spray Process by Changing of Nozzle Setting Angle // AIP Conference Proceedings: – S. l.: AIP Publishing, 2019. – Vol. 2125 No. 030022.
3. **Klinkov S.V., Kosarev V.F., Ryashin N.S., and Shikalov V.S.** Influence of particle impact angle on formation of profile of single coating track during cold spraying // AIP Conference Proceedings 2027, 020007 (2018)
4. **Patent** RF N2687598 Method of metallization of ceramics for welding Nepochatov Y.K., Kosarev V.F., Ryashin N.S., Melamed B.M., Shikalov V.S., Klinkov S.V., Krasnyi I.B., Kumacheva S.A. Bulletin N 14 15.05.2019.

DOI 10.53954/9785604990131_72

NONLINEAR WAVE INTERACTION AT THE EXISTENCE OF LONGITUDINAL DISTURBANCE IN THE FLAT PLATE SUPERSONIC BOUNDARY LAYER

A.D. Kosinov, M.V. Piterimova, Yu.G. Yermolaev, A.V. Shmakova, B.V. Smorodsky, N.V. Semionov, A.A. Yatskikh

Khristianovich Institute of Theoretical and Applied Mechanics SB RAS
Novosibirsk 630090, Russia

Summary. The report discusses the results of experimental studies of the development of a wave train in a longitudinal vortex in the boundary layer of a flat plate at Mach numbers of 2 and 2.5. The spatial-temporal amplitude distributions, frequency-wave spectra of pulsations and their wave characteristics were obtained in the linear and weakly nonlinear phase of the high frequency wave train development in a homogeneous and inhomogeneous boundary layer under conditions of a fixed power of a local source of controlled disturbances.

Introduction. The impact of weak shock waves in the form of an N-wave on the leading edge of a flat plate with a sharp leading edge generates a stationary longitudinal wake in the supersonic boundary layer [1]. The resulting flow is become inhomogeneous in the transversal direction. Its changes the mechanisms of the laminar-turbulent transition in the supersonic boundary layer in comparison with its homogeneous state. It is known that longitudinal wakes (streaks) either tighten the transition in the boundary layer downstream or shift it upstream, as noted in [2, 3]. Knowledge of the mechanisms of interaction of unstable disturbances usually significantly facilitates the solution of problems of numerical modeling of the laminar-turbulent transition and prediction of its position in the boundary layer. Two methods are used for the process modeling: direct numerical simulation based on the Navier-Stokes equations and calculations using the wave approach of the hydrodynamic stability theory. Experimental data are required when compared with theory. The introduction of artificial wave trains into the supersonic boundary layer makes it possible to obtain the experimental data required for comparison with calculations [4]. This is realized by analyzing the spatial-temporal amplitude distributions, frequency wave spectra of pulsations and their wave characteristics in the linear and weakly nonlinear phase of the development of a wave train in a homogeneous and inhomogeneous boundary layer, subject to a fixed power of the local source of controlled disturbances. Data analysis allows us to determine possible mechanisms of wave interaction in a homogeneous and inhomogeneous boundary layer on a flat plate and compare them with each other. This is the main goal of the current cycle of research begun in [4].

Experiment setup and results. The experiments are carried out in the supersonic wind tunnel T 325 of the ITAM SB RAS at Mach numbers 2 and 2.5. The scheme of experiments with the introduction of controlled disturbances into an inhomogeneous boundary layer is shown in the figure. This setup was implemented in a series of experiments at Mach numbers 2 and 2.5. The figure shows a specific experimental setup at Mach number 2.5. Here it is indicated: 1 and 2 – falling weak shock waves; 3 – generator of weak shock waves; 4 – source of controlled disturbances; 5 and 6 – relative changing of mass flow in sections $x = -10$ and $x = 60$ mm.

At Mach number 2, the conditions for introducing artificial disturbances along the Z coordinate were different, which influenced the nature of the development of the wave train.

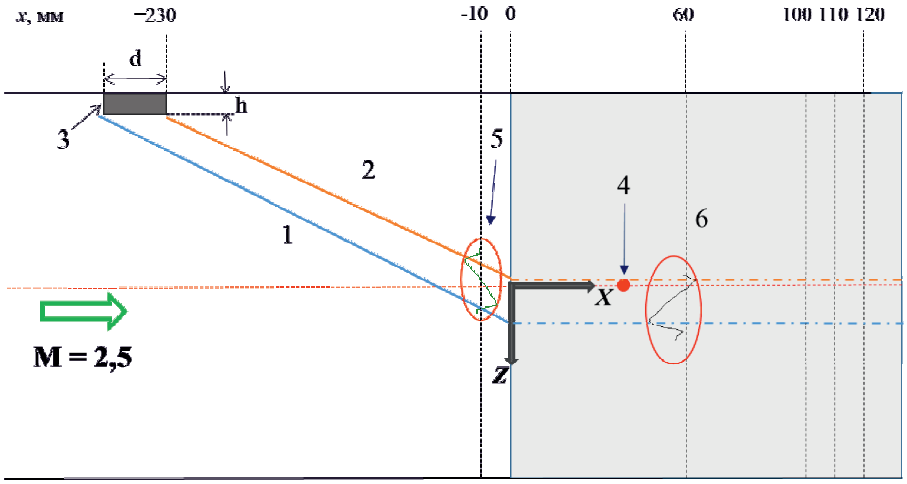

Fig. Conducting experiments at Mach number 2.5.

1 and *2* – incident weak shock waves, *3* – generator of weak shock waves, *4* – source of controlled disturbances, *5* and *6* – relative changing of mass flow in sections $x = -10$ and $x = 60$ mm.

For the experimental conditions carried out in the T 325 wind tunnel on a flat plate model, calculations were carried out using the linear stability theory within the framework of the full Lise-Lin system. The wave characteristics of inclined mass flow disturbances were obtained for frequencies of 10, 20, 30 and 40 kHz. In this work, these results are used to analyze experimental data and partially for comparison with them.

Estimates of the wave spectra of stationary inhomogeneities and experimental data on wave characteristics and disturbance spectra made it possible for the first time to propose options for wave interaction for the oblique breakdown regime of boundary layer transition.

Note that at Mach number 2 it was possible to identify two mechanisms of interaction of disturbances in an inhomogeneous boundary layer: subharmonic resonance and oblique breakdown. At Mach number 2.5, depending on the experimental conditions, only oblique breakdown mechanism can be observed. Possible reasons for this are discussed in the report.

Acknowledgments. This work was supported by the Russian Science Foundation (№ 22-19-00666, https://rscf.ru/project/22-19-00666/). The study was conducted at the Equipment Sharing Center «Mechanics» of ITAM SB RAS.

REFERENCES

1. **Vaganov A.V., Ermolaev Yu.G., Kolosov G.L., Kosinov A.D., Panina A.V., Semionov N.V.** Impact of incident Mach wave on supersonic boundary layer // Thermophysics and Aeromechanics. 2016. V. 23, No 1. P. 43–48. DOI: 10.1134/S0869864316010054.
2. **Egorov I.V., Ngoc Hai Duong, Nhu Can Nguyen *et al.*** Numerical Simulation of the Influence of a Mach Wave on the Laminar–Turbulent Transition in a Supersonic Boundary Layer. // Doklady Physics. 2022. V. 67, No. 5. P. 144–147. https://doi.org/10.1134/S1028335822050019.
3. **Piterimova M.V., Kosinov A.D., Semionov N.V., Yatskikh A.A., Kocharin V.L., Yermolaev Yu.G.** Experimental study of effect of a pair of weak shock waves on laminar-turbulent transition in the boundary layer of flat plate at Mach number 2 // Siberian journal of physics. 2022. V. 17, No 2. P. 30–40. (In Russ.) https://doi.org/10.25205/2541-9447-2022-17-2-30-40.
4. **Kosinov A.D., Piterimova M.V., Shmakova A.V., Semenov N.V., Ermolaev Yu.G.** Experimental study of evolution of controlled perturbations in a longitudinal vortex generated in a boundary layer on a flat plate at a mach number M = 2 // Journal of Applied Mechanics and Technical Physics. 2023. V. 64, No. 4. P. 656–666. DOI: 10.1134/S0021894423040119.

DOI 10.53954/9785604990131_74

LTT AND REGIMES OF COMBUSTION OF HYDROGEN MICROJETS

V.V. Kozlov

Khristianovich Institute of Theoretical and Applied Mechanics, SB RAS, 630090, Novosibirsk, Russia

Abstract. Results of experimental studies of diffusion combustion of hydrogen microjets performed in recent years are presented. Specific features of the hydrogen flow structure and hydrogen combustion are studied for various shapes of the nozzle, jet exhaustion velocity, and direction of gravitation. Hydrogen combustion in mixtures with other gases and periodic actions on microjets (in the case considered, by external acoustic disturbances, is also considered.

Introduction. At the moment, the main matter used for energy production is fossil fuels. Alternative technologies of energy production from renewable energy sources have found various applications during the last decades and are still under development. One of such technologies is hydrogen power engineering, which implies burning of hydrogen extracted from water, and water resources on the Earth are almost unlimited. The reaction product is water again, which is an environmentally friendly product. Hydrogen power engineering has not yet gained numerous applications because of technical problems caused by fire and explosion hazards of hydrogen. Methods of hydrogen extraction, transportation, and storage are still subjects of academic research and design activities. Therefore, it is of interest to study the combustion of hydrogen jet flows formed by various burners and nozzles. The present paper describes the results of studying the combustion of hydrogen microjets. Microjets are understood as flows from nozzles with a plane or circular cross section and with the transverse size smaller than 3 mm. Some preliminary investigations were performed to study the dynamics of "macrojet" flows, where particular attention was paid to hydrodynamic instability typical for such flows, which determines the flow structure and, correspondingly, the burning character. In particular, experimental results showed that breakup of a round jet and its transition to the turbulent mode depend to a large extent on the initial velocity profile at the nozzle exit. In the case of the top-hat (U-shaped) velocity distribution, the Kelvin–Helmholtz instability prevails, leading to comparatively rapid turbulization of the flow. In the case of a parabolic velocity profile at the nozzle exit, the jet remains laminar up to a large distance and retains its range. The results of studying jet combustion under various conditions (nozzle shape, initial velocity distribution, and external effects on jet combustion) were reported in [1–3]. It is also of interest to consider promising methods of controlling hydrogen jet flows and hydrogen combustion. One of such methods is periodic excitation of the jet by external acoustic disturbances. Such an approach to combustion regime modification was used, e.g., in [4–5]. The results showed that a controlled periodic action on the hydrogen jet significantly affects the vortex structure of the flow and intensity of hydrogen mixing with ambient air, including emission of nitrogen oxides at an optimal frequency of acoustic excitation. The results mentioned above and other experimental data on hydrogen combustion in large-scale jet flows form the basis for experimental investigations of the dynamics, flow instability, and hydrogen combustion at small scales (microjets).

Research Methods. The present experiments were performed on the jet setup based at the Khristianovich Institute of Theoretical and Applied Mechanics of the Siberian Branch of

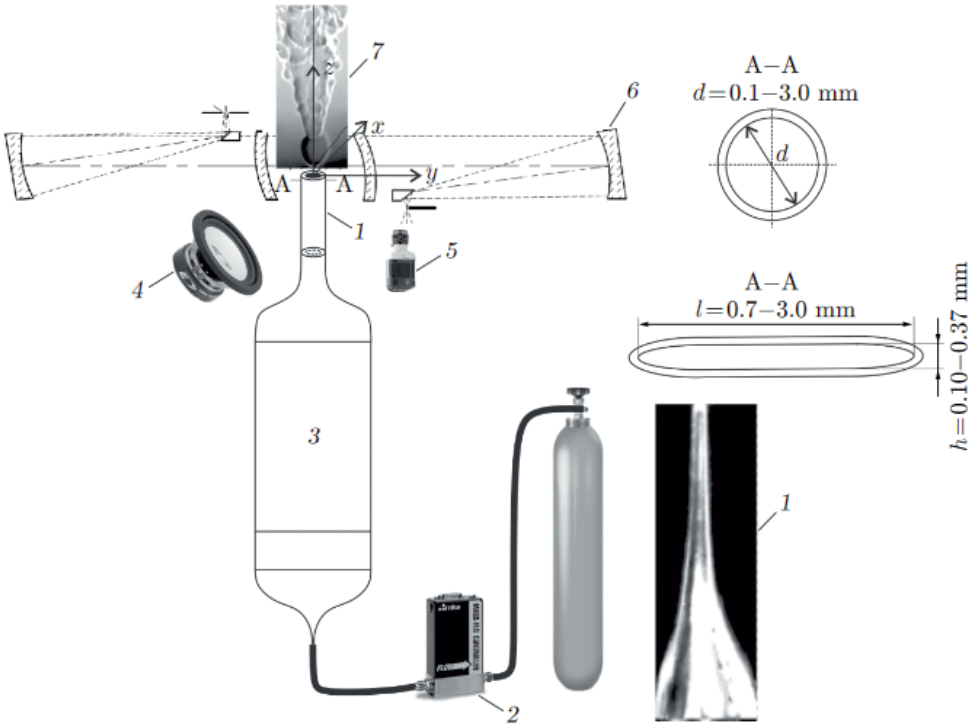

Figure 1. Setup for studying hydrogen microjet combustion: (1) nozzle, (2) flow rate controller, (3) settling chamber, (4) loudspeaker, (5) camera, (6) shadowgraph, and (7) microjet.

the Russian Academy of Sciences (ITAM SB RAS) with the use of circular or slotted nozzles with various cross-sectional sizes at the exit. Figure 1 shows the general setup diagram, which was varied depending on the investigation purposes. Hydrogen was injected into the setup from a gas holder through a reductor, and the gas flow rate was controlled by a flow rate controller. The minimum inhomogeneity of the jet flow and background perturbations was ensured by a honeycomb and deturbilization grids located ahead of the nozzle (the diagram in figure. 1 refers to a slotted nozzle with a variable cross section). To study the influence of the external periodic action on the microjet development and combustion, it was excited by acoustic oscillations generated by a dynamic loudspeaker located near the nozzle exit.

Experimental Results. The experimental data on diffusion combustion of hydrogen microjets reported in the present paper were usually obtained by shadowgraphy with recording of the picture by a video camera. We studied:

1. Flame Structure in the Case of Diffusion Combustion of Hydrogen Microjets [5]
2. Effect of the Jet Orientation in the Gravity Field on its Diffusion Combustion [4].
3. Dependence of Diffusion Combustion of Hydrogen Microjets on the Method of Jet Ignition [8]
4. Specific Features of Hydrogen Combustion in a Cocurrent Jet [6]
5. Diffusion Combustion of a High-Velocity Microjet [8]

This study was supported by the Russian Science Foundation (Grant No. 22-19-00151 https://rscf.ru/project/22-19-00151/).

REFERENCES

1. **Kozlov V.V., Grek G.R., Litvinenko Yu.A.** Visualization of Conventional and Combusting Subsonic Jet Instabilities // Eds. by Kozlov V.V., (Dordrecht: Springerbook, 2015).
2. **Oh J., Heo P., Yoon Y.** Acoustic Excitation Effect on NOx Reduction and Flame Stability in a Lifted Non-Premixed Turbulent Hydrogen Jet with Coaxial Air // Intern. J. Hydrogen Energy 34, 2009. P. 7851–7861.
3. **Kim M., Choi Y., Oh J., Yoon Y.** Flame Vortex Interaction and Mixing Behaviors of Turbulent Non-Premixed Jet Flames under Acoustic Forcing // Combust. Flame 156, 2009. P. 2252–2263.
4. **Kozlov V.V., Vikhorev V.V., Grek G.R. et al.** Diffusion Combustion of a Hydrogen Microjet at Variations of its Velocity Profile and Orientation of the Nozzle in the Field of Gravitation // Combust. Sci. Technol. 191 (7), 2019. P. 1219–1235.
5. **Shmakov A.G., Kozlov V.V., Litvinenko M.V., Litvinenko Yu.A.** Effect of Inert and Reactive Gas Additives to Hydrogen and Air on Blow-Off of Flame at Hydrogen Release from Microleakage // Intern. J. Hydrogen Energy 46 (2), 2021. P. 2796–2803. DOI: 10.1016/j.ijhydene.2020.10.088.
6. **Kozlov V.V., Litvinenko M.V., Litvinenko Yu.A. et al.** Combustion of Round Hydrogen Microjet in Concurrent Flow // J. Engng Termophys 30 (2), 2021. P. 1–12.
7. **Kozlov V.V., Grek G.R., Korobeinichev O.P. et al.** Combustion of Hydrogen in Round and Plane Microjets in Transverse Acoustic Field at Small Reynolds Numbers as Compared to Propane Combustion in the Same Conditions. Pt 1 // Intern. J. Hydrogen Energy. 41 (44), 2016. P. 20231–20239.
8. **Kozlov V.V., Grek G.R., Kozlov G.V., Litvinenko Y.A., Shmakov A.G.** Experimental study on diffusion combustion of high-speed hydrogen round microjets // International Journal of Hydrogen Energy. Vol. 44. No. 1, 2019. P. 457–468.

DOI 10.53954/9785604990131_77

APPLICATION OF NON-CONTACT VIDEOGRAMMETRY METHOD FOR INVESTIGATION MOTION AND DEFORMATION PARAMETERS OF AIRCRAFT WING CONSOLE DURING FLIGHT

V.P. Kulesh, K.A. Kurulyuk, G.E. Nonkin, I.V. Senyuyev

Central Aerohydrodynamic Institute named after prof. N.E. Zhukovsky (TsAGI), 140180, Zhukovsky, Russia

Creation and refinement of new aircraft models involves numerous tests on the ground and in flight. Under the influence of distributed aerodynamic and mass-inertial forces, the shape of the wing and other structural elements of the aircraft in flight undergoes noticeable changes, which can affect on the flight characteristics of the aircraft [1]. Most experimental investigations of an aircraft motion and deformation in an air flow are carried out in wind tunnels on elastic and dynamically similar aircraft models. However, the structural and load scheme of the model inevitably differs from the scheme of the full-scale wing, which entails a difference in the aerodynamic and load characteristics between the model and the real full-scale wing [2]. Therefore, it is necessary to measure parameters of motion and deformation of the aircraft wing, which carried out during a real flight.

Non-contact optical methods, in particular, digital videogrammetry methods (VGM), have recently proven themselves well in measuring distributed deformation fields of models in the wind tunnels. The possibility to extract information from hundreds and thousands points on the surface of a model from a single image simultaneously provide the high information value of the VGM method. For past decades, in TsAGI (Central Aerohydrodynamic Institute) optical methods of videogrammetry has been actively applied and improved in wind tunnels and at experimental stands [3, 4].

The essence of the method is following: one can determine 3 spatial coordinates X,Y,Z of object point knowing only its 2 response coordinates u,v in the digital image. In general formulation, the task of coordinates recovering is underdetermined. In world practice, to solve the problem of ambiguous coordinates recovering a method of stereo photo is commonly used, which implies obtaining not only one image of the surface of object, but two ones from two cameras separated by a distance. Combining data from such two images allows enclosing the operating system of equations. However, in real experimental conditions it is not always possible to locate two cameras at the desired points.

The main purpose of this work was to provide non-contact measurements of motion parameters and deformation of the console and wing controls of a medium-range passenger aircraft in flight by the method of videogrammetry with a specialized monogrammetry system (with one camera).

The objectives of the work were:

- adaptation of the videogrammetry method to the object and test conditions, including hardware and software;
- development of a monogrammetry VGM measuring system for installation and operation on board of a full-scale aircraft in ground and flight tests;
- development of a method for rapid calibration of the VGM system in ground conditions;
- measurement of motion parameters and deformations of the wing console of the aircraft in ground tests and in flight.

With the help of the developed VGM system, trial ground measurements of the deformation parameters of the console under the action of hydraulic power drivers and free movement of the flaps were completed. In the first flight there were made measurements in 42 flight regimes and in the second flight – in 106, including takeoff, cruising and landing regimes.

The paper presents a brief description of the videogrammetry method, features of calibration and results processing. Numerical parameters of bending deformation and torsion of the wing console, aileron and spoilers are obtained. It was found that the deflection of the wing console in cruising regimes was 850–900 mm.

In general, an experience of usage the videogrammetry method for measuring the parameters of motion and deformation of structural elements of a full-scale aircraft in flight considered to be successful and can be recommended for further application in flight tests.

REFERENCES

1. **Gorbushin A.R., Ishmuratov F.Z., Nguyen V.N.** Studying dependence of "rigid" aerodynamic models elastic deformations on their geometric and design parameters. Aerospace mai journal. 2022, vol. 29, no. 2, pp. 45–60.
2. **Kuruliuk D.V.** Programmnoe obespechenie dlya avtomatizacii provedeniya prochnostnyh ispytanij. Avtomatizatsiya v promyshlennosti, 2017, no. 4, pp. 51–53.
3. **Kuruliuk K.A., Kulesh V.P.** Non-contact measurement of helicopter device position in wind tunnels with the use of optical videogrammetry method. AIP Conference Proceedings 18, International Conference on the Methods of Aerophysical Research, ICMAR 2016: Proceedings of the 18th International Conference on the Methods of Aerophysical Research. 2016. P. 030006. 13.
4. **Busarova M.V., Zhelonkin S.V., Kulesh V.P., Kuruliuk K.A.** Application of optical videogrammetry technique for normal deformation fields of aircraft fuselage panel meausring. Aerospace mai journal. 2020, vol. 27, no. 2, pp. 52–60.

DOI 10.53954/9785604990131_79

EFFECT OF ARTIFICIALLY INDUCED PERTURBATIONS ON THE TRANSITION DURING THE INTERACTION OF SHOCK WAVE WITH A BOUNDARY LAYER

A.I. Kutepova, D.V. Khotyanovsky, A.A. Sidorenko

Khristianovich Institute of Theoretical and Applied Mechanics SB RAS
630090, Novosibirsk

The problem of the development of an artificially introduced thermal perturbations in a supersonic boundary layer on a flat plate was solved using direct numerical simulation. The HyCFS-R computer code [1] developed at the ITAM SB RAS was used. This code uses multi-level parallelization: computational domain decomposition and MPI messages to transfer data between compute nodes, Nvidia CUDA for the graphics coprocessor, and OpenMP thread parallelization on each compute node. Numerical calculations were carried out on the hybrid computing cluster "Aero" of the Research Equipment Sharing Center of the ITAM SB RAS using two computing nodes and four Nvidia Tesla V100 graphic coprocessors. Parallel computational methods and the cluster make it possible to quickly and efficiently obtain the results of three-dimensional unsteady numerical simulations with resolution of the vortex flow structure.

The flow parameters in the numerical simulation correspond to the parameters in experiments performed using a T-325 ITAM SB RAS wind tunnel [2]: the flow Mach number M = 1.45, the stagnation pressure P_0 = 55 kPa, the stagnation temperature T_0 = 290 K, and the wall temperature T_w = 290 K. Numerical calculations were carried out in the computational domain, which was a parallelepiped with a total number of cells of 52 million. Thermal perturbations are represented by a drastic change in surface temperature and are induced in the form of rectangular periodic pulses of the wall temperature in a region 3 and 2 mm in the longitudinal and the transverse directions, respectively. A detailed description of the source parameters and its study in a supersonic boundary layer is presented in the article [3]. To study the issue of flow control using local thermal action, the problem of shock wave boundary layer interaction was solved. The shock wave was established using boundary conditions at the upper boundary of the computational domain.

To study the issue of the evolution of unstable temperature perturbations, the influence of the amount of energy in the source pulse on the appearance and the characteristics of the development of introduced perturbations was investigated. For this purpose calculated cases differing in the duration of the heat source pulse were considered. The values D_1 = 0.5 and D_2 = 0.1 were chosen for the first and second calculated cases, respectively.

The figure shows the spectrogram of pressure pulsations obtained on the line z = 0. It can be seen that for both calculated cases, after introducing a rectangular signal with a fundamental frequency of 16.7 kHz, the first and second harmonics appear. Harmonics appear much more clearly for the case D_2 = 0.1. An increase in pulsations across the entire frequency spectrum is observed in the region of the separation bubble. This turns out itself better in the case of D_2 = 0.1 where this zone has a greater extent. The spectral recording clearly show how the spectrum is filled during flow turbulization in each calculated case.

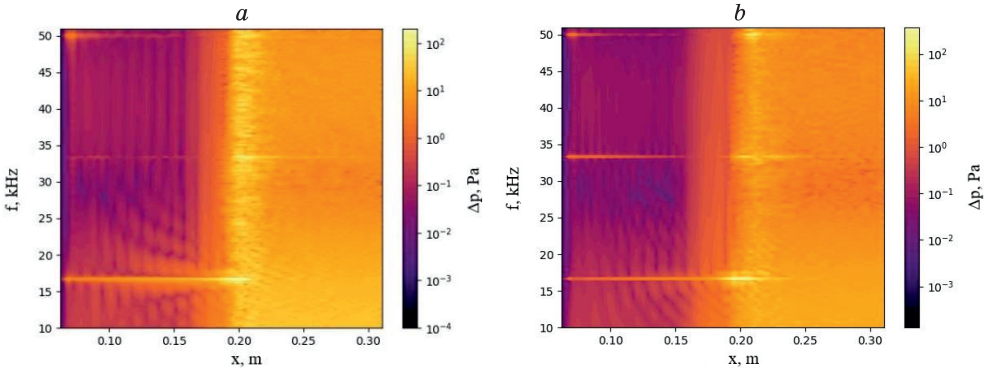

Spectrogram for two calculated cases with different pulse durations of the heat source

a) $D_1 = 0.5$ and b) $D_2 = 0.1$

Thus such a different process of filling the spectrum and the occurrence of additional frequencies in the calculated case $D_2 = 0.1$ leads to more suppression of the separation region. When the pulse duration was reduced by a factor of 5, the size of the separation region decreased by almost 1.4.

REFERENCES

1. **Shershnev A., Kudryavtsev A., Kashkovsky A., Khotyanovsky D.** HyCFS, a high-resolution shock capturing code for numerical simulation on hybrid computational clusters // AIP Conf. Proc. 1770, 11 (2016)
2. **Polivanov P.A., Sidorenko A.A., Maslov A.A.** The influence of the laminar-turbulent transition on the interaction between the shock wave and boundary layer at a low supersonic Mach number // Technical Physics Letters 41, 933–937 (2015)
3. **Kutepova A.I., Khotyanovsky D.V., Sidorenko A.A.** Numerical simulation of the development of perturbations induced by a periodic heat source in a supersonic boundary layer // Journal of Applied Mechanics and Technical Physics, 2023, Vol. 64, No. 5, pp. 853–857

DOI 10.53954/9785604990131_81

OPTIMAL DISTURBANCES OF THREE-DIMENSIONAL AERODYNAMIC BOUNDARY LAYERS

S.A. Kuznetsova, A.V. Boiko, K.V. Demyanko, G.V. Zasko, Yu.M. Nechepurenko

Marchuk Institute of Numerical Mathematics RAS,
119333, Moscow, Russia

The authors of the present report develop a technique for computing the spatial optimal disturbances of three-dimensional boundary layers; such disturbances play a key role within the bypass transition scenario. The proposed technique is implemented in LOTRAN software package, also designed by the authors [1, 2], which is widely used for both scientific and engineering purposes (see, e.g., [3–6]). As input, LOTRAN takes a laminar-turbulent flow data obtained using ANSYS Fluent or any other CFD code. Then, disturbance propagation lines are constructed on the flow-exposed body, and flow slices are constructed along these lines (the slices are normal to the flow-exposed surface). The downstream propagation of small disturbances of the main flow is studied along the slices, with the linearized equations of heat and mass transfer of a viscous compressible medium [2] being used. The streamwise initial-value problems are solved numerically for computing the optimal disturbances [7]. The numerical method [7] represents an original modification of the known implicit schemes, where the numerical solution is projected at each integration step onto the invariant subspace of physically relevant modes. This method eliminates the contribution from modes propagating upstream and growing downstream at large rates. As a result, the matrix of the fundamental system of solutions is found, and the optimal disturbance is computed via the singular value decomposition of the matrix.

We present the results for the following two configurations. The first one, (a), is the swept wing [5] (–5° angle of attack, NACA 67 1-215 profile, and 45° sweep angle). The second one, (b), is the prolate spheroid [1] (10° angle of attack, and 6:1:1 axis ratio). The maximum energy amplification of disturbances is computed as a function of the streamwise coordinate x (the local coordinate along the slice) at spanwise wavenumbers β, which are corresponding to the propagation of crossflow vortices (Fig. 1).

For both configurations, we found that, in addition to the global maximum in the spanwise wavenumber, there is a local maximum corresponding to an optimal disturbance with

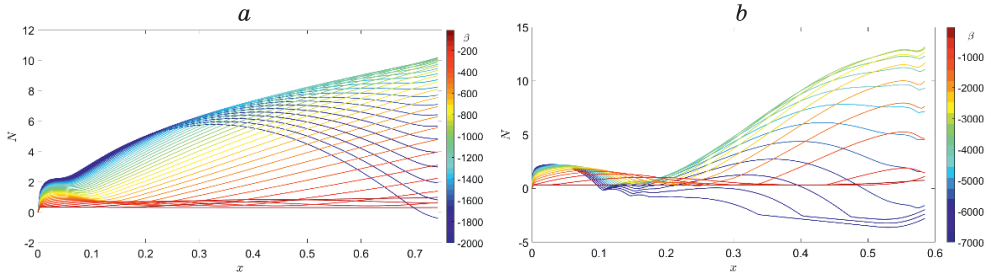

Fig. 1. Natural logarithm of the energy amplification for the optimal disturbances along one of the disturbance propagation lines. The curves of different colors correspond to the different values of β. (a): the swept wing; (b): the prolate spheroid.

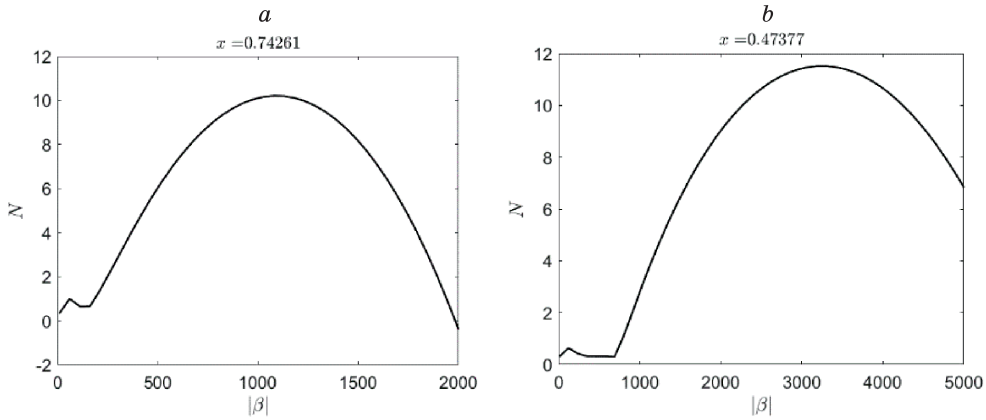

Fig. 2. The dependence of the natural logarithm of energy amplification for the optimal disturbances on |β| at fixed *x*. (a): the swept wing; (b): the prolate spheroid.

small spanwise wavenumber (Fig. 2). Note that the disturbance corresponding to the local maximum does not contain modes growing downstream. The obtained result is in qualitative agreement with the experimental data [8] on a swept wing; for a body of revolution, such a result is obtained for the first time.

This research is supported by the Russian Scientific Foundation (grant No. 22-11-00025).

REFERENCES

1. **Boiko A.V., Demyanko K.V., Kirilovskiy S.V., Nechepurenko Y.M., Poplavskaya T.V.** Modeling of transonic transitional three-dimensional flows for aerodynamic applications // AIAA J. 2021. Vol. 59, No. 9. P. 3598–3610.
2. **Boiko A.V., Demyanko K.V., Nechepurenko Y.M.** On computing the location of laminar-turbulent transition in compressible boundary layers // Russ. J. Numer. Anal. Math. Modelling. 2017. Vol. 32, No. 1. P. 1–12.
3. **Boiko A.V., Demyanko K.V., Inozemtsev A.A., Kirilovskiy S.V., Nechepurenko Yu.M., Paduchev A.P., Poplavskaya T.V.** Determination of the laminar-turbulent transition location in numerical simulations of subsonic and transonic flows past a flat plate // Thermophysics and Aeromechanics. 2019. Vol. 26, No. 5. P. 629–637.
4. **Poplavskaya T.V., Boiko A.V., Demyanko K.V., Kirilovskiy S.V., Nechepurenko Y.M.** Numerical simulation of the transition to turbulence in subsonic and transonic flows // J. of Physics: Conf. Series, 2019. Vol. 1359. Art. 012068.
5. **Kirilovskiy S.V., Boiko A.V., Demyanko K.V., Ivanov A.V., Nechepurenko Y.M., Poplavskaya T.V.** Numerical simulation of the laminar-turbulent transition on a swept wing in a subsonic flow // J. of Physics: Conf. Series, 2019. Vol. 1359. Art. 012070.
6. **Kirilovskiy S.V., Boiko A.V., Demyanko K.V., Nechepurenko Y.M., Poplavskaya T.V., Sidorenko A.A.** On integrating the LOTRAN 3.0 package into the ANSYS fluent CFD software // AIP Conf. Proc. 2019. Vol. 2125. Art. 030098. P. 1–6.
7. **Zasko G.V., Boiko A.V., Demyanko K.V., Nechepurenko Yu.M.** Simulating the propagation of boundary-layer disturbances by solving boundary-value and initial-value problems // Russ. J. Numer. Anal. Math. Modelling. 2024. Vol. 39, No. 1.
8. **Boiko A.V.** Swept-Wing Boundary Layer Receptivity to a Steady Free-Stream Vortex Disturbance // Fluid Dynamics. 2002. Vol. 37. P. 37–45. doi.org/10.1023/A:1015126631538.

DOI 10.53954/9785604990131_83

3D PARAMETRIC OPTIMIZATION TECHNOLOGY OF A SUPERSONIC PASSENGER AIRCRAFT AERODYNAMIC DESIGN USING FLYPOINT PARAMETRICA AND LS-TECH FRAMEWORK

L. Lavrishcheva[1], N. Staroverov[1], V. Novoselov[1], D. Strelets[2]

[1] LS-Technologies, 198206, St. Petersburg, Russia

[2] Moscow Aviation Institute (MAI), 125993, Moscow, Russia

Today, the three-dimensional aerodynamic optimization of airframe elements and the complete aircraft configuration is still an important, relevant and also very challenging task in the aviation industry. One of the main issues in the optimization of complex curvilinear surfaces such as aircraft wings, engine nacelles, tail and fuselage geometry is the parameterization of these objects [1–3]. Nowadays it is still very difficult to obtain a digital fully parametric model of an aircraft body with all the components. Computer-aided design (CAD) systems, in its turn, do not make it possible to create a representation of such complex objects with a single curvilinear surface in such a way that allows to change the geometry of the model in a wide range of parameter variation. Furthermore, a special problem concerns the presence of large number of parameters in the initial mathematical description of the aircraft model. For example, a typical parametrical description of isolated aircraft wing has more than 100 independent parameters, which cannot be controlled directly by the optimizer because of their large number and surface oscillations that will inevitably occur on curved surfaces in the process of parameter variation [4].

The lack of 3D CAD capabilities for effective parametrization of aircraft components and many years of research in the field of geometry parameterization led to the creation of the Flypoint Parametrica, specialized software, based on its own geometric modeling kernel, which fundamentally gives engineers complete freedom in the choice of the control parameters of the model and the complete control over the shape of the product. An example of the shape modification of the supersonic passenger aircraft (SPA) wing model in Flypoint Parametrica is shown in Figure 1.

However, the optimization process is not limited to the creation of a 3D parametric model and imposes additional requirements on the efficiency operation of each element of the optimization workflow [5]. The presented technology eliminates the process of manual geometry refinement, as well as the processes of meshing, CFD-solver configuration and results postprocessing are fully automated within the optimization cycle thanks to the program platform LS-TECH Framework.

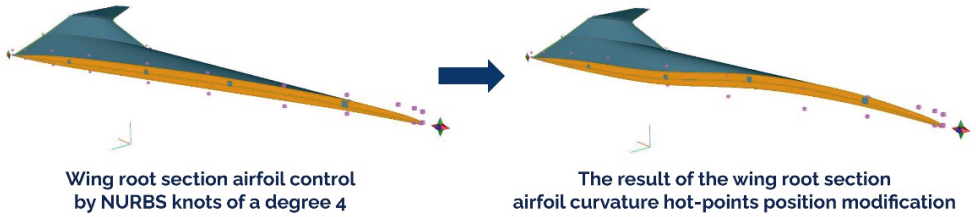

Fig. 1. SPA wing parametric model modification in Flypoint Parametrica

Fig. 2. Comparison of the initial (green) and optimized (blue) wings (top view and front view)

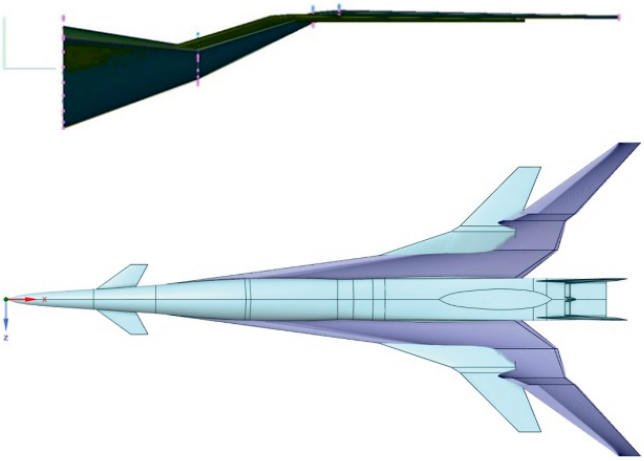

Fig. 3. Combining the geometry of the optimized wing with the fuselage (the original wing is shown in gray-blue color)

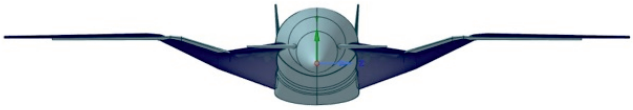

In the presented work the wing shape optimization of a supersonic passenger aircraft in cruise flight mode was conducted in order to increase lift-to-drag ratio (L/D) with the constraint of the level-flight lift force of the aircraft above the provided value. The set of parameters describing the leading-edge sweep angle and wing aspect ratio was identified as control parameters. The numerical simulation of the airflow around the SPS was carried out in the Ansys Fluent CFD solver, and Ansys optisLang was used as an optimizer. The adaptive optimization algorithm based on metamodeling approach allowed to achieve optimal wing shape in 225 iterations with increase in lift-to-drag ratio by 4.7 % with satisfaction of all imposed design and aerodynamic constraints. A comparison of the original and optimized models is shown in Figure 2 and 3.

REFERENSES

1. **Sun Y., & Smith H**. (2019). Low-boom low-drag optimization in a multidisciplinary design analysis optimization environment. Aerospace Science and Technology, 2019. P. 94.
2. **Kirz J.** Surrogate Based Shape Optimization of a Low Boom Fuselage Wing Configuration. AIAA Aviation 2019 Forum.
3. **Kozelkov A.S., Strelets D.Yu., Sokuler M.S., and Arifullin R.H.** Application of Mathematical Modeling to Study Near-Field Pressure Pulsations of a Near-Future Prototype Supersonic Business Aircraft. Journal of Aerospace Engineering. Vol. 35. Issue 1. 2022.
4. **Official LS-Technologies website**. URL: https://ls-technologies.ru/.
5. **Lavrishcheva L.** Numerical simulation of the flow around marine objects and development of the optimization technology of the marine propeller shape. 2018. Ph.D Thesis. URL: https://disser.spbu.ru/files/2018/disser_lavrisheva.pdf

DOI 10.53954/9785604990131_85

WAYS TO IMPROVE THE DYNAMIC CHARACTERISTICS OF THE OSCILLATORY SYSTEM OF A SOUND GENERATOR

I.V. Lebedev, D.P. Pavlov, A.Ya. Sterlin, A.V. Furman

Federal Autonomous Institution "Central Aerohydrodynamic Institute", Zhukovsky, Russia

Modern aircraft are subjected to intense sound pressure fluctuations caused not only by engine noise but also by turbulent environmental effects during flight. These fluctuations cause vibrations in the structure, leading to aircraft skin and power element fatigue fractures and equipment failures. Operational experience has shown the necessity to account for acoustic fatigue, starting at loads of 130 to 135 decibels (dB). And at loads above 160 dB, acoustic fatigue is one of the primary factors determining the structural integrity of aviation and spacecraft.

Despite the development of computational techniques for examining the acoustic resistance of aircraft and spacecraft equipment, the most accurate and reliable current methods still rely on experimental studies.

To conduct such investigations in a laboratory setting, facilities such as reverberation chambers are utilized. A key component in these facilities, which determines their operating characteristics, is sound generators.

During acoustic strength testing of modern aircraft in order to achieve operational frequencies of 1000–1200 Hz it is necessary to develop a domestic high-frequency sound generator. This requires not only structural enhancements but also research into the effects of speed and displacement feedback on the dynamic performance of the generator's valve assembly. These developments will expand the frequency range of the mobile part of the modulator.

REFERENCES

1. **Nikolaev V.S., Kaurova N.F.** "Installations for Testing Structures of Aerospace Aircraft for Acoustic Strength," Review No. 565, Publication Department of the Central Aerohydrodynamic Institute (TsAGI), Moscow, Russian Federation, 1979, 195 pg.
2. **Patent 2742283** of the Russian Federation, IPC G10K7/06, "Gas flow modulator," by A.Ya. Sterling, A.V. Furman, S.K. Kim, S.A. Kutsenko and G. E. Dyadchenko, applicant and patent holder at TsAGI (Central Aerohydrodynamic Institute). Application No. 2020120957, filed on 06.25.20, published on 02.04.21 Bulletin No. 4.
3. **Patent No. 26946** of the Russian Federation, IPC G 10 K 7/06. "Electro-pneumatic sound generator" by A.Ya. Sterling, A.V. Furman, S.K. Kim and N.V. Zverev, Applicant and Patent Holder of TsAGI, Application No. 2018142901, filed on 05.12.18, published on 07.08.19, Bulletin No. 22.
4. **Patent No. 2707587** of the Russian Federation, IPC class G 10K7/06. "A method for generating sound for the testing of structures and apparatus for implementing the same" by A.Ya. Sterling, A.V. Furman, S.K. Kim and S.A. Kutsenko, applicant and patent owner of TsAGI (TsAGI – Central Aerohydrodynamic Institute). No. 2018142903, filed on 05.12.18, published on 28.11.19, Bulletin No. 34.

DOI 10.53954/9785604990131_86

THE INVESTIGATON OF NON SINGLE-PHASE IN AN AIR-COOLING WING TUNNEL USING OPTICAL METHODS IN CONFORMITY WITH ICE FORMATION PROBLEM OF AIRCRAFTS

E.A. Liverko, S.I. Inshakov

Central Aerohydrodynamic Institute named by N.E. Zhukovskiy (TsAGI)
140180, Zhukovskiy, Russia

Currently the problem of ice-covering in aircraft is extremely relevant, since ice on the surface of an aircraft, especially, leads to loss of stability, a decrease in the load-bearing properties of the wing and an increase in resistance to damage in general. The results of this work present studies of a two-phase flow created in an air-cooling wing tunnel (hereinafter referred to as ACT) of the TsAGI FAU using contactless optical methods.

The flow of droplets of supercooled liquid was simulated by injecting water through nozzles located in the ACT prechamber. The two-phase flow was ignited by a laser plane created using a cylindrical lens attachment. It was assumed that the intensity of scattered light is proportional to the concentration of scattering centers, and that made it possible to assess the uniformity of the droplets distribution in the flow. Fig. 1(*a*) shows the layout of the measuring system. The camera with lens and pulsed laser were synchronized using a pulse generator. The shooting was carried out in 9 ACT operating modes, with different flow rates and water consumption, and 500 frames were taken for each mode.

Fig. 1 (*b*) shows a diagram of light scattering on a droplet with a diameter of 1 μm according to the Mie theory. In our case, the edges of the frame were at angles of 120–150° to the laser plane. It follows from the diagram that the intensity of light from the edges of the frame differed from each other by an order of magnitude. This effect was not taken into account in this work [1]–[2].

Fig. 2 (*a*) shows a snapshot of particles in the ACT illuminated by a laser plane. Before processing of these data, the cross section of the laser plane beam was normalized to its thickness, which makes it possible to take into account its ellipsoidal shape in this section. The processing itself was carried out in the Matlab environment, and consisted of averaging the light intensity pixel by pixel throughout the entire video sequence separately for each mode, respectively [3]. Further, normalization was carried out to the maximum value, which made it possible to assess the uniform fillability of particles in the frame area and present data from 0 to 100 % (where 0 are pixels in which there are almost no particles, and 100 are

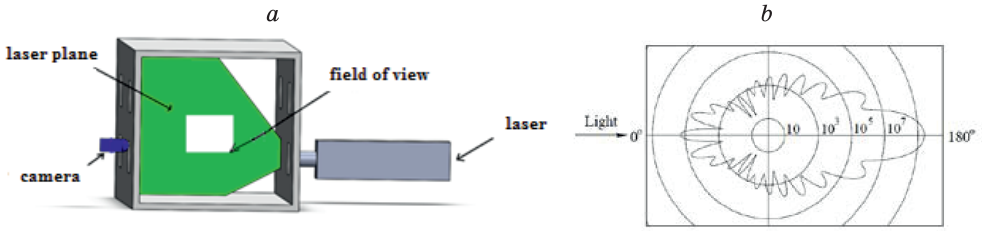

Fig. 1. Scheme of measuring system (*a*) and diagram of light scattering on a droplet

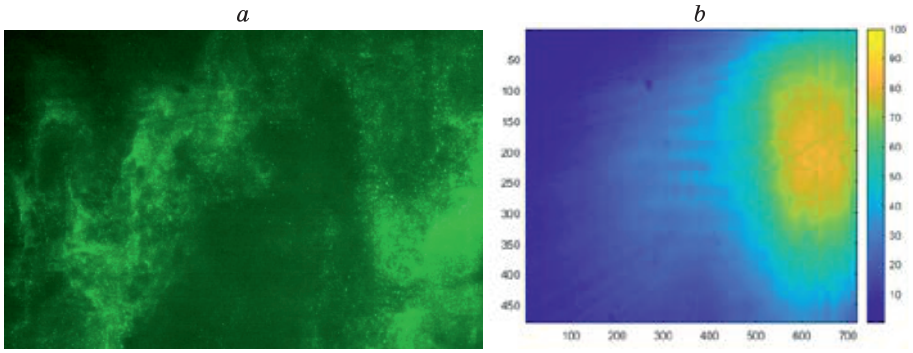

Fig. 2. Original image (*a*) and processing of operating mode (*b*)

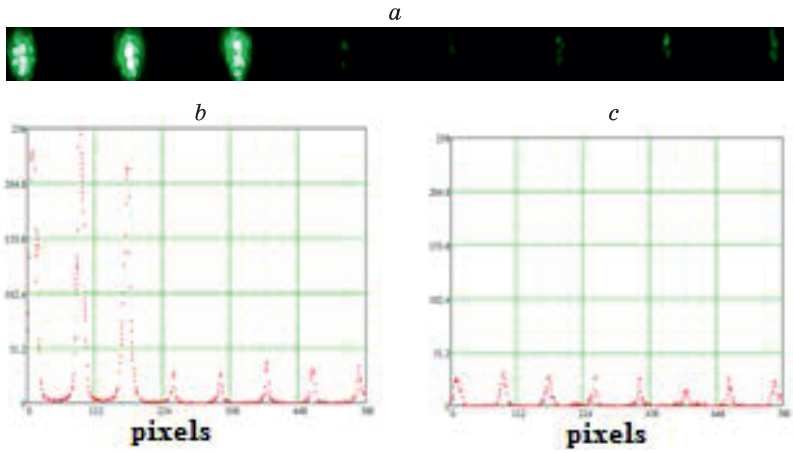

Fig. 3. Original frame of a non-uniform light plane (*a*), unnormalized frame (*b*), normalized frame (*c*)

pixels in which the probability of encountering a particle is maximum). Fig. 2 (*b*) shows an example of such processing for a flow speed of 100 m/s and a water flow rate of 80 g/s.

To take into account the inhomogeneity of the light plane associated with the quality of the cylindrical lens, normalization was carried out. The heterogeneity was modeled by a neutral light filter, and the scattering centers were modeled by a grating. Fig. 3 (*a*) demonstrates the original frame of a non-uniform light plane, Fig. 3 (*b*) shows an unnormalized frame, and Fig. 3 (*c*) exhibits a normalized frame.

At the next stage, droplet sizes were measured using the shadow method. In this case, a camera with a microscopic lens and a light source (a pulsed laser with an attachment in which a lens is located to create a diverging beam of light) were positioned on the same optical axis. The particles cast shadows that were captured by the camera. Using the Canny algorithm [4]–[5], drop shadows were detected in images, and then shadows that did not fall into the depth of the field imaged space of the lens were rejected. Culling was based on comparing the maximum intensity gradient of each shadow with a predefined threshold value [6]. The maximum of histogram of particle size distribution was within the limits of 15–22 mkm.

As a result of the work carried out, the size of the droplets was measured and particles equitability of the ACT working section was assessed.

REFERENCES

1. **Bryukhanova V.V., Samokhvalov I.V.** Laser polarization probing, Tomsk, 2007
2. **Khvostikov I.A.** "The theory of light scattering and its application to issues of transparency of the atmosphere and fogs", Advances in Physical Sciences, Vol. 24, issue 2, 1940
3. **Klimkov Yu.M.** Applied laser optics., 1985
4. **Vlasov A.V., Tsapko I.V.** "Modification of the Canny algorithm applied to the processing of radiographic images", Bulletin of Science of Siberia, Vol. 4 (10). 2013
5. **Vijayaranil S., Vinupriya M.** «Performance Analysis of Canny and Sobel Edge Detection Algorithms in Image Mining», International Journal of Innovative Research in Computer and Communication Engineering, Vol. 1, Issue 8, 2013
6. **Lee S.Y., Kim Y.D.** «Sizing of spray particles using image processing Technique», KSME International Journal, Vol. 18. No. 6, 2004

DOI 10.53954/9785604990131_89

EFFECT OF SLOT DEPTH AND ORIENTATION ANGLE ON SUPERSONIC BOUNDARY LAYER STABILIZATION+

V.I. Lysenko, B.V. Smorodsky, A.D. Kosinov, A.A. Yatskikh

Khristianovich Institute of Theoretical and Applied Mechanics, SB RAS
630090, Novosibirsk, Russian Federation

For the first time, a study of the effect of longitudinal (orientation angle φ = 0) slots with different depth *h* (corresponding to Reynolds number Re_h = 0–2000) on the stability of the supersonic (M = 2) boundary layer on a flat plate to natural disturbances of the first (vortex) mode of instability (determining the laminar-turbulent transition at M = 2) was carried out.

The influence of surface slots (grooves) with a depth of *h* = 0.18 mm (Reynolds number by depth $Re_h \approx 1000$) with different angles of their orientation φ = 0, 30, 45, 90° on the stability of the supersonic boundary layer (M = 2) on a flat plate to natural disturbances of the first mode of instability was also investigated.

Experimental Setup. The experiments were carried out in the wind tunnel T-325 of the ITAM SB RAS at free-stream $M_\infty = 2$. The test model was a heat-insulated steel flat plate, which was fixed at a zero angle of attack.

Over the working-surface segment of 53–165 mm (i.e. throughout the whole width of the plate), the plate was provided with a groove 4.3 mm deep. The inserts-plates with different slots could then be mounted flush in the groove. A series of inserts-plates with longitudinal rectangular slots (with an orientation angle of φ = 0) of different depths *h* = 0, 0.1, 0.15, 0.18, 0.26 and 0.32 mm and a series of inserts with rectangular slots with a depth of *h* = 0.18 mm and different orientation angles of slots φ = 0, 30, 45, 90° were made. The width of each slot was s = 0.6 mm, slot spacing *t* = 1.2 mm.

The boundary-layer stability to natural disturbances was studied by a constant resistance hot-wire anemometer operated with a single-wire sensor made of 10-μm diameter tungsten wire 1.5 mm in length.

Measurements of the downstream disturbance amplification were performed in the layer of maximal fluctuations across the boundary layer, corresponding approximately to the condition of *E* = const, where *E* is the mean diagonal voltage across the hot-wire bridge (i.e. along the line of a constant value of the mean mass flux). Spatial growth rates of perturbations $-\alpha_i$ are obtained depending on frequency *f* for different values of depth *h* of slots and angles of their orientation.

Results. It is obtained that such disturbances can be stabilized by longitudinally located slots with a small depth ($Re_h < 2000$), and the greatest stabilization will be at Reynolds number by slot depth $Re_h \approx 1000$.

It is also obtained that as the angle of orientation of the slots decreases (from φ = 90° to 0), the maximum spatial growth rates of the disturbances decrease. And at φ = 0 and 30° they are already less than the corresponding value for a smooth plate. The obtained results show that disturbances of the first mode in the supersonic boundary layer can be stabilized by slots with a small depth (at $Re_h \approx 1000$) and small angles of their orientation (φ ≈ 0–40°).

The research was financially supported by the Russian Science Foundation (Project No. 23-79-10167, https://rscf.ru/project/23-79-10167/).The study was conducted at the Equipment Sharing Center «Mechanics» of ITAM SB RAS.

DOI 10.53954/9785604990131_90

INVESTIGATION OF THE INTERACTION OF THE PAIR OF SUPERSONIC COUNTER-ROTATING VORTICES WITH DIFFERENT INTENSITY

A.I. Lukyanov, A.M. Shevchenko, A.S. Shmakov

Khristianovich Institute of Theoretical and Applied Mechanics SB RAS, 630090, Novosibirsk, Russia

The paper presents results of experimental and numerical study of the flow field in the near-wake behind of two rectangular wings, installed at a different angles of attack. In [1–3] results were acquired for co-rotating and counter-rotating vortices with equal intensity. The aim of present work was to study of the interaction of the pair of counter rotating vortices with unequal intensity and to validate the CFD-package FlowVision 3.13.02 [4] for simulations of flow fields with large gradients of flow parameters.

A pair of longitudinal vortices was generated by two rectangular-shaped half-wings with sharp leading and trailing edges, chord length b = 30 mm and half-spans of 75 and 95 mm, installed at the angle of attack of 5 and 10 deg respectively. Wings thickness at the tip chord were – 0,4 mm. Wings were installed coaxially. Distance between tip chords, measured at the span direction, was 30 mm.

The experiments were carried out in the supersonic wind tunnel T-325 of ITAM SB RAS at Mach number of 3 and 4. During the experiments Pitot pressure measurements were performed using five Pitot probes, installed with increments of 6 mm.

Computations were conducted with laminar flow assumption, using CFD-package FlowVision 3.13.02 at computational cluster AERO of the Equipment Sharing Center «Mechanics» of ITAM SB RAS. Computational domain was a rectangular prism with dimensions as follows: length of 155 mm, height of 120 mm, width of 200 mm; and consisted of 3,7 mil. cells. Computations were conducted with Mach number of 2, 3 and 4.

Vortex core is defined as area with the maximum of the circumferential Mach number $M_{YZ} = \sqrt{M_Y^2 + M_Z^2}$ at the boundary and minimum at the center. Besides, minimum of the Pitot pressure and maximum of the vorticity was found at the vortex center. Intensity of the vortex was estimated by longitudinal vorticity, maximum value of which corresponds to central part of vortex core.

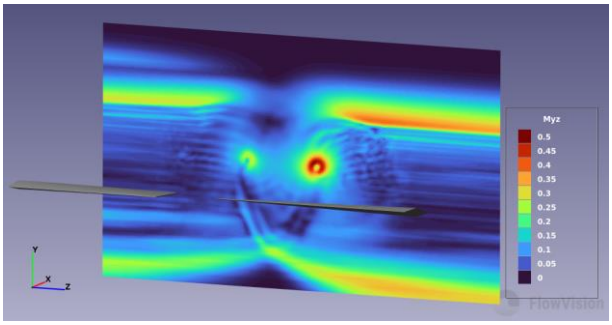

Fig. 1. Circumferential Mach number map at M = 3.

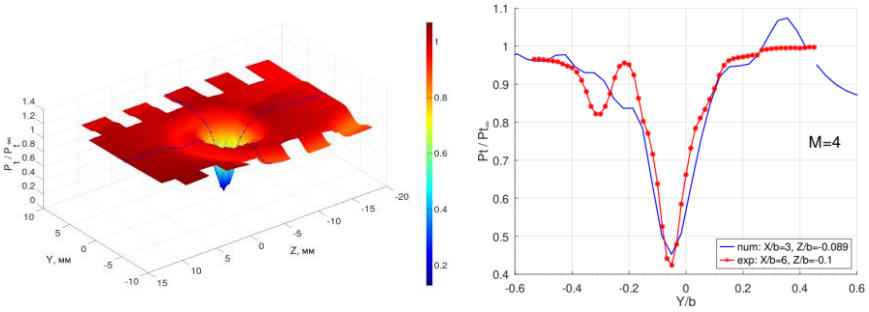

(a) (b)

Fig. 2. Distribution of the Pitot pressure P_t. (a) experimental isosurface at M = 3; (b) comparison between numerical and experimental data at M = 4.

Comparison between experimental and numerical data shows that data, acquired from numerical simulation does not contradict with experimental data. This allows to qualitatively determine coordinates of the central part of vortex core and full pressure deficit in it (Fig. 2b).

It is shown that interference of the vortices leads to redistribution of the velocity profiles: asymmetry of the tangential velocity relative to the core, vertical velocity increases in area between the vortices cores and decreases in areas, closer to the root chords of wings. Also, vortex core of a lesser intense vortex displaced upward relative to vortex core of a greater intense vortex at all Mach numbers.

It is obtained that vortices cores positioned with systematic offset to the root chords of the wings. It is found that with increasing Mach number both cores move downward and intensity of the longitudinal vortices decreases.

The research was carried out within the state assignment of Ministry of Science and Higher Education of the Russian Federation. The study was conducted at the Equipment Sharing Center «Mechanics» of ITAM SB RAS. Computations was performed using FlowVision 3.13.02 provided by “TESIS” company.

REFERENCES

1. **Konstantinovskaya T.V., Borisov V.E., Davydov A.A., Lutsky A.E., Shevchenko A.M.** Interaction of Two Counter-Rotating Supersonic Vortices // Physical-Chemical Kinetics in Gas Dynamics. 2020. V. 21, № 1.
2. **Borisov V.E., Davydov A.A., Konstantinovskaya T.V., and Lutsky A.E.** Numerical Simulation of Two Streamwise Supersonic Vortices Interaction // AIP Conference Proceedings 2351, 030002 (2021)
3. **Shmakov A.S., Shevchenko A.M.,** Interaction of a pair of vortex wakes at Mach 3 // Int. Conf. on the Methods of Aerophys. Research (ICMAR 2020) (Novosibirsk, Russia, November 1-7, 2020): AIP Conference Proceedings. 2021. Vol. 2351. Art. 040012. 4 p. https://doi.org/10.1063/5.0052013.
4. https://flowvision.ru/ru/

DOI 10.53954/9785604990131_92

INFLUENCE OF DISTRIBUTED HYDROGEN INJECTION AND COMBUSTION ON SUPERSONIC BOUNDARY LAYER STABILITY AND TRANSITION

V.I. Lysenko, S.A. Gaponov, B.V. Smorodsky, A.N. Semenov, S.O. Morozov, A.V. Starov

Khristianovich Institute of Theoretical and Applied Mechanics, SB RAS
630090, Novosibirsk, Russian Federation

This study recorded the influence of the distributed injection of hydrogen through a permeable surface and its combustion on the stability and transition of a supersonic boundary layer. The laminar base flow for a multicomponent flat-plate boundary layer was computed using the computational fluid dynamics solver *Ansys Fluent* with chemistry for free-stream Mach number M = 2. Linear stability theory equations for a reactive gas mixture were derived in the local parallel base flow approximation. The influence of the distributed injection and diffusion combustion of hydrogen in the supersonic boundary layer on the position of the laminar-turbulent transition was estimated using the linear stability theory based e^N-method. Calculated and experimentally obtained dependencies of the relative transition Reynolds number on the relative mass flow rate of injected hydrogen were compared.

Results. First, calculations according to linear theory found a double reversal in the maximal amplification rate magnitudes of perturbations, wherein at first they increased, then decreased to zero, and then rose again, at increased rate of mass flow of injected hydrogen.

Also it was found (Fig. 1) that depending upon the flow conditions around the body (flow parameters), the hydrogen diffusion flame could accelerate or decelerate the transition in the supersonic M = 2 boundary layer, when compared to absence of hydrogen burning. Two counteracting effects compete: heat supply by combustion exerts stabilizing influence, while low-molecular-weight gas (H_2) blowing from the surface exerts destabilizing influence. Depending on the interplay of these two factors, it was possible to obtain boundary-layer flow stabilization (that is, the stabilizing effect of heat supply to the boundary layer

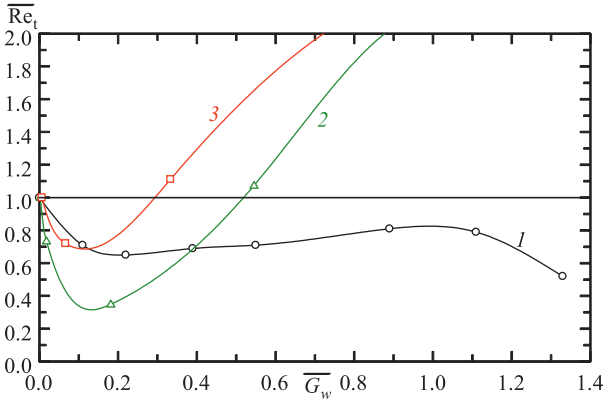

Fig. 1. Relative Reynolds number of transition $\overline{\mathrm{Re}}_t$ in experiment (*1*) and in computation (*2*-*3*) versus the relative mass flux of the injected hydrogen $\overline{G}_w$: T_w=600 K (*2*), T_w=900 K (*3*); T_0=300 K.

prevailed over the destabilizing effect of hydrogen blowing) or destabilization (that is, the destabilizing effect of hydrogen injection prevailed over the stabilizing effect of heat supply to the boundary layer).

This research study was supported by the Russian Science Foundation, No.22-21-00017. The experimental research was performed at the Institute of Theoretical and Applied Mechanics using the equipment at the Centre of Cooperative Use “Mechanics”.

DOI 10.53954/9785604990131_94

A FLAT JET NOZZLE INTEGRATION WITH THE SUPERSONIC CIVIL AIRCRAFT PLANE WITH A LOW LEVEL OF SONIC BOOM

A.V. Lysenkov, V.S. Gorbovskoy, G.N. Lavrukhin, I.S. Matyash, A.A. Saveliev, A.V. Shenkin

The Central Aerohydrodynamic Institute named after N.E. Zhukovsky, 140180, Zhukovsky, Russian Federation

Now, various countries of the world perform the works to create a new generation of supersonic civil aircraft (SCA). The possibility to develop a new generation of SCA is closely connected with solving the problems of these aircraft impact on the environment. First of all, environmental problems are caused by the need to reduce the noise on the ground at take-off/landing regimes and the sound impact in cruising supersonic flight over populated areas. For aircraft with a supersonic cruising flight velocity, from the standpoint of economic efficiency, it is advisable to use a turbojet of a small bypass ratio.

The configuration with the power plant on the upper surface of the airframe allows to form the lower surface of the airframe with taking into account the minimization of sound impact. In addition, this configuration allows to use airframe design elements for shielding the mixing zone of the jet with the outer flow and, accordingly, for reducing the noise of jet engines at take-off/landing modes. In the 2000s, TsAGI, together with CIAM, proposed a scheme of a flat sector nozzle with an oblique exit [1]. It shown in Fig. 1.

Experimental and computational investigations of aerodynamic and acoustic characteristics [2–4] have shown that a flat sector nozzle with an oblique exit with a mixer-ejector noise-suppressing system permits to achieve a level of the noise-suppressing about 6-9 EPNdB.

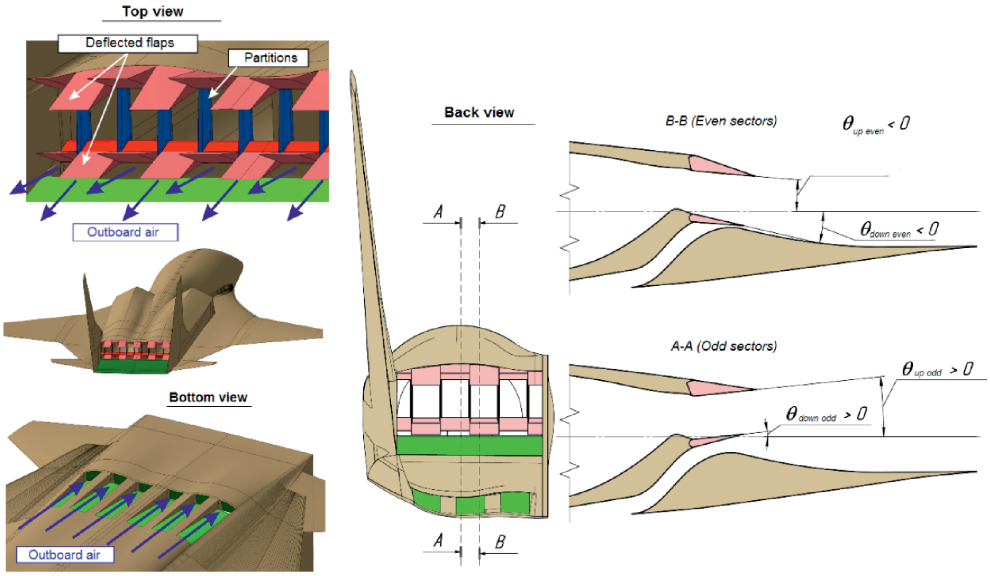

Fig. 1. Scheme of a flat sector nozzle with an oblique exit

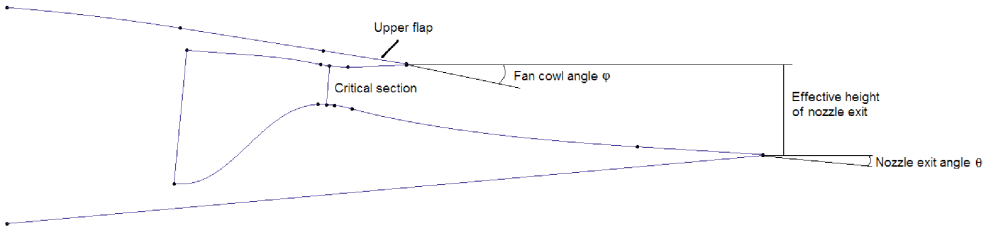

Fig. 2. Cross-section of a typical flat nozzle with an oblique exit

This paper considers the characteristics of a flat nozzle with a retracted noise-suppressing system in a wide range of M numbers.

The following features common to flat nozzles can be distinguished:

- the effective thrust losses of isolated flat (rectangular) nozzles are higher than the thrust losses of equivalent round nozzles because of angular effects on the inner and outer surfaces of flat nozzles;
- the aerodynamic efficiency of flat nozzles in configurations can be higher than the efficiency of round nozzles in the cases of their nonoptimal configuration or the negative interference between the external flow and jets and the airframe elements;
- in the case of an optimal configuration of round nozzles (minimal negative interference), their effective thrust losses are lower than the thrust losses of equivalent flat nozzles.

The effective thrust losses [5], including the external drag from the tail part of the nacelle, depend on the fan cowl angle of the aircraft tail part φ (Fig. 2). As the angle φ increases, the external drag increases, because the flow accelerates on the outer surface and the projection of the area perpendicular to the X axis increases. In addition, at large fan cowl angles φ, a shock is generated on the trailing edge of the upper flap. It can lead to negative effects on other elements of the aircraft and to the flow separation of the under the shock.

On the other hand, when the fan cowl angle φ decreases (when the critical section is shifted upwards) and aircraft lower surface is fixed, the effective height of the nozzle exit and the angle of nozzle exit θ increase. This can lead to a growth of internal losses in an unregulated nozzle in both supersonic and pre- and transonic flight regimes. To obtain the most effective configuration, it is necessary to choose the optimal fan cowl angle φ.

When choosing the optimal parameters of a flat jet nozzle, it is possible to realize acceptable values of nozzle effective thrust losses. In subsonic and supersonic regimes, the thrust losses for a flat nozzle in the configuration will be 0.5 % greater, and in transonic regimes – 1–2 % more than for a round nozzle.

REFERENCES

1. **Mironov A.K., Krasheninnikov S.Y., Pavlyukov E.V., Zhitenev V.K., Kazhan V.G., Shenkin A.V.** A flat sector nozzle to suppres the noise generated on the ground by an administrative supersonic aircraft. Proceedings of TsAGI, issue 2710, 2013 (Russian language).
2. **Bykov A.P., Gorbovskoy V.S., Kazhan A.V., Kazhan V.G., Shenkin A.V.** Computational and experimental studies of a light supersonic business aircraft nozzle aerodynamics // TVF, vol. LXXXIX, No. 3–4 (720–721), 2015, pp. 38–50 (Russian language).
3. **Gorbovskoy V.S., Kazhan A.V., Kazhan V.G., Shenkin A.V.** Computational studies of thrust characteristics of a supersonic passenger aircraft nozzle using computational gas dynamics methods // Bulletin of MAI. 2019. T. 26. No. 4. Pp. 7–16 (Russian language).
4. **Gorbovskoy V.S., Kazhan A.V., Kazhan V.G., Samokhin V.F., Shenkin A.V.** Investigation of the aerodynamics of a supersonic nozzle with a noise-suppressing system // Scientific notes of TsAGI, 2020, vol. LI, No. 4, pp. 56–72 (Russian language).
5. **Lavrukhin G.N., Ivankin M.A., Talyzin V.A.** Aerogasodynamics of jet nozzles. Vol. I, II, III. – M.: Fizmatlit, 2017 (Russian language).

DOI 10.53954/9785604990131_96

CHEMICAL REACTION RATE COEFFICIENTS CALCULATION USING MACHINE LEARNING ALGORITHMS

Z. Maksudova, A. Savelev, E. Kustova

Saint Petersburg State University, Saint Petersburg, Russia
st076791@student.spbu.ru, aleksey.schumacher@gmail.com, e.kustova@spbu.ru

Calculating the rate coefficients of chemical reactions that rely on temperature and all possible electronic-vibrational states of the reagents is a crucial step in determining the hydrodynamic characteristics of nonequilibrium gas flows in the state-to-state approximation. The most precise values are often produced with the use of molecular dynamics and quantum chemistry methods [1, 2], however these techniques are very computationally demanding and cannot be included into computational codes directly. This research reports on the efforts that the process of calculating reactions rate coefficient values in air can be sped up, and the obtained approaches can be further scaled to predict rates of physicochemical processes for other reactions at any temperature.

A generalised formula for coefficient rates of dissociation and exchange reactions which takes into account vibrational and electronic states of all reagents was obtained in work [3]:

$$k^{ex,diss}_{V_r \to V_p} = B \exp\left(-\frac{\Delta E_{V_r \to V_p}\, \Theta\left(\Delta E_{V_r \to V_p}\right)}{k} \left(\frac{1}{T} + \frac{1}{U}\right) \right),$$

$$\Delta E_{V_r \to V_p} = E_a + E_p - E_r,$$

Where k is the Boltzmann constant, V_r, V_p are the internal states of the reagents and reaction products, E_r, E_p are the corresponding energies, $\Theta(x)$ is the Heaviside function, E_a is the activation energy of the reaction, T is the temperature in Kelvin, U is the parameter of the model having the dimension of temperature, B is the normalising factor, which is the most time-consuming in modelling due to the need to summarise exponents for all possible vibrational and electronic states of all reaction participants [3].

The presented problem can be solved by using Neural Networks or Nonlinear Regression. In the one-dimensional case, the reaction temperature, reaction type (e.g., N_2 + O or $O_2 + O_2$), and the sequence of vibrational level energy values for the molecules O_2, NO, and N_2 were used as input data (see Fig. 1). In the case of taking into account electron-vibrational excitation, the dimensionality is increased by the corresponding number of reaction participants for which we consider the electronic state. The data generation was performed according to the anharmonic oscillator model based on the papers [1, 2, 4, 5, 6].

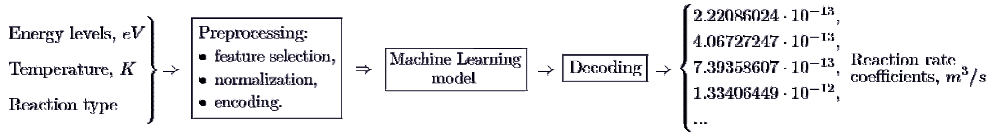

Fig. 1. General scheme of the model in the case of accounting for the vibrational state of the reagent.

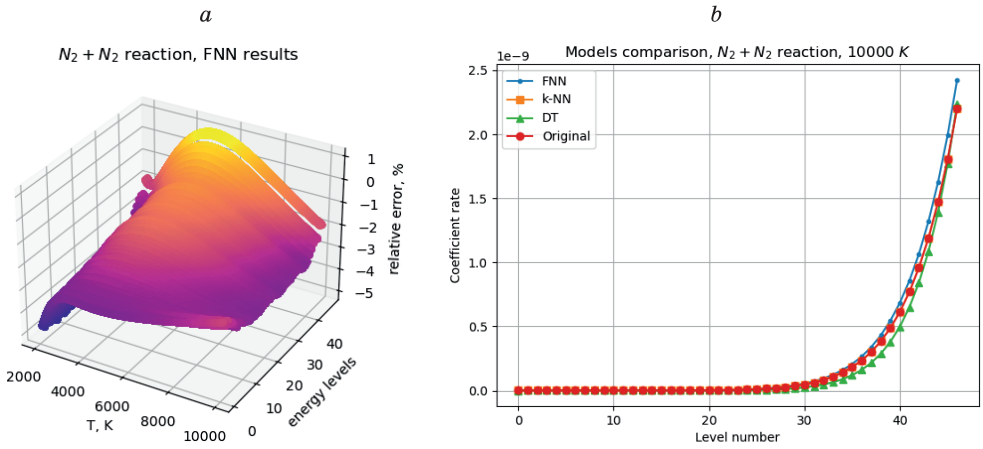

Fig. 2. Plot of percentage relative error test score (left) and predicted with different models coefficient rates(right) for N_2+N_2 dissociation reaction.

Based on the nonlinear dependence of the input features and the target real vector, it was decided to use the k-Nearest-Neighbours (k-NN) and Decision Tree (DT) regression algorithms [7] to begin with. As a result, although k-NN gives low Mean Absolute Percentage Error (MAPE), the time taken for prediction increases according to the size of the trained data, so due to specificity this algorithm may not be a perfect choice to make fast predictions. DT gives a significant gain in prediction speed but has a higher MAPE value because tree structures tend to overtrain. The problem of inaccuracy of the DT algorithm could be solved by ensembling models, but this will significantly increase the computation time.

At the same time, by automating the process with Feedforward Neural Networks (FNN) [7, 8], one can obtain a computationally efficient tool to perform coefficient rates calculations according to the state-to-state approach for temperatures above 2000 K. Thus, when using neural networks it is possible to achieve computational acceleration by a factor of 10 and more, while having MAPE loss lower than acceptable 10 % in our production (see Fig. 2).

REFERENCES

1. **Armenise I., Esposito F.** Dissociation–recombination models in hypersonic boundary layer O_2\O flows. Chemical Physics 398 (2012) 104–110.
2. **Armenise I., Esposito F., Capitta G., Capitelli M.**. O–O_2 state-to-state vibrational relaxation and dissociation rates based on quasiclassical calculations. Chemical Physics 351 (2008) 91–98.
3. **Kustova E., Savelev A.** Generalised model for state-resolved chemical reaction rate coefficients in high-temperature air. Journal of Physics: Conference Series 1959 (2021) 012033.
4. **BaluckramV.T. and Andrienko D.A.** First-principle simulation of vibrational activation and dissociation in oxygen shock flows. AIAA Paper 2021-0447.
5. **Esposito F., Armenise I., Capitelli M.** N-N_2 state to state vibrational-relaxation and dissociation rates based on quasiclassical calculations. Chemical Physics 331 (2006) 1–8.
6. **Armenise I., Esposito F., Capitelli M.** Dissociation-recombination models in hypersonic boundary layer flows. Chemical Physics 336 (2007) 83–90.
7. **Pedregosa F., Varoquaux G., Gramfort A., Michel V., Thirion B., Grisel O., Blondel M., Prettenhofer P., Weiss R., Dubourg V. and others.** Scikit-learn: Machine learning in Python. The Journal of machine Learning research. Vol 12 (2011), 2825–2830.
8. **Paszke A., Gross S., Massa F., Lerer A., Bradbury J., Chanan G. and others.** PyTorch: An Imperative Style, High-Performance Deep Learning Library. In Advances in Neural Information Processing Systems 32 (2019), 8024–8035.

DOI 10.53954/9785604990131_98

AUTOMATED TEST BENCH FOR MEASURING MASS, COORDINATES OF MASS AND MOMENTS OF INERTIA

V.S. Manvelyan, V.V. Petronevich, V.V. Lytov, S.V. Dytskov

Central Aerohydrodynamic Institute named after prof. N.E. Zhukovsky (TsAGI), 140180, Zhukovsky, Russia

One of the key parameters to control the movement of aircraft are mass, coordinates of mass and moment of inertia [1].

The impressive development and proliferation of various types UAVs requires the improvement of their control systems, which makes it necessary to develop automated measuring test bench to measure seven static and dynamic parameters – mass, three coordinates of center of mass and three moments of inertia.

In recent years, TsAGI has developed theoretical and applied solutions for solving a set of problems related to test bench development. Unique measuring instruments and standards have been created for metrological certification, which allows us to speak about the leading position of TsAGI in the field of complex solutions to problems of measuring the static and dynamic parameters of aircraft [2].

The study is devoted to a review of TsAGI's developments in the field of measuring the static and dynamic parameters and the application of these developments to various types of UAVs weighing up to 100 kg.

REFERENCES

1. **Bazhenov S.G.** Basics of Flight Dynamics, 2021, Moscow, FIZMATLIT, 432 p. ISBN 978-5-9221-1906-1.
2. **Bogdanov V.V., Dytskov S.V., Manvelyan V.S., Petronevich V.V.** Theoretical Aspects of Industrial Products Coordinates of the Center of Mass and the Tensor of Inertia Measurement in Dynamic Mode. TsAGI Scientific Notes. – 2022. – T. 53, № 5. – C. 66–73. – EDN RCNJJO.

DOI 10.53954/9785604990131_99

EFFECT OF LONGITUDINAL VORTEX ON THE TURBULENT STRUCTURE OF THE BOUNDARY LAYER

V.V. Markin, P.A. Polivanov

Institute of Theoretical and Applied Mechanics SB RAS
630090, Institutskaya 4/1, Novosibirsk, Russia

The improvement of the take-off and landing characteristics of perspective aircrafts is possible through the use of active boundary layer control (BLC) methods. Currently, there are various approaches to active BLC: blowing/suction of the boundary layer, heat transfer from the wall, different type of plasma source and etc. One of the most energetically advantageous methods is an air-jet vortex generator, which is actively being investigated [1]. A longitudinal vortex leads to a change of the boundary layer velocity profile by supplying kinetic energy from the upper layers of the flow to the surface. In addition, the longitudinal vortex leads to a change the unsteady characteristics of the turbulent boundary layer. Nevertheless despite the fact that there is a rich experience of studying and applying air-jet vortex generators, at the moment there is no consensus on the physical mechanism of the effects of such devices for delay and suppression of flow separation. Separated flow is a significantly unsteady phenomenon, therefore the equilibrium of the incoming turbulent boundary layer should be one of the key physical mechanisms of the influence. In this paper, the flow behind an air-jet vortex generator is experimentally studied to determine the effects of a longitudinal vortex on unsteady structures developing in a turbulent boundary layer.

The experiments were carried out in a T-503 NSTU wind tunnel with test section with a diameter of 1.2 m at an incoming velocity of 25 m/s. There was a model in the test section of the wind tunnel, which was a flat plate with dimensions of 1470×740×16 mm. The vortex generating device was a pressure buffer chamber (dimensions 40×20×5 mm) with a nozzle installed inside the plate. The nozzle of the air-jet vortex generator was located at a distance of 500 mm from the leading edge of the plate. The vortex generator nozzle had inclination angles of 45° to the surface of the plate (downstream) and 45° to the longitudinal axis of the plate, as a result of which a longitudinal vortex generated above the plate.

The flow parameters were measured using a stereo-PIV, which made it possible to obtain the values of three components of the flow velocity in several sections behind the vortex generator.

Figure 1 shows the different defect fields (the difference between the case with the BLC turned on and off) of the components associated with the Reynolds stresses and included in the Reynolds-averaged Navier–Stokes equation for the longitudinal momentum equation (a) and the energy equation (b). The data are obtained in vertical cross-section of the flow behind the air-jet vortex generator. The data obtained point a significant influence of the longitudinal vortex not only on the average flow in the boundary layer, but also on the processes of turbulence generation and dissipation.

Data processing included POD and correlation analysis, the construction of Reynolds stress fields and turbulence invariants, in addition, the scales of vortex structures were estimated. As a result of the research, it was found that the adding of a vortex into the flow leads to the destruction of large-scale turbulent structures in the area behind the vortex generator

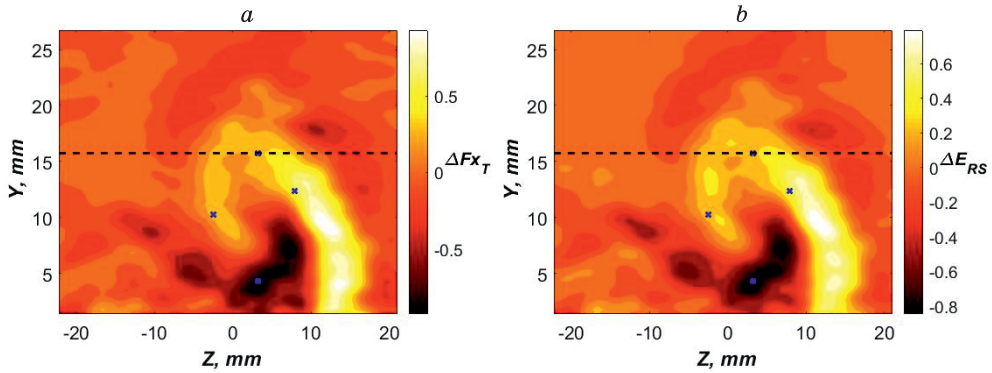

Fig. 1. a) Defect of dynamic pressure (P_{dyn}) and b) defect of the dissipative term of the energy equation (E_{RS}).

and an increase in the isotropy of turbulence. It was found that an increase in the total pressure in the jet contributes to a local increase in the dynamic pressure in the boundary layer due to more efficient mixing.

REFERENCES

1. **Greenblatt D., Wygnanski I.D.** The control of flow separation by periodic excitation // Progress in Aerospace Sciences. – Vol. 36, No. 7. 2000. P. 487–545.

DOI 10.53954/9785604990131_101

IMPLEMENTATION OF THE "ADAPTIVE" BOUNDARY LAYER SUCTION FOR SUPPRESSING THE SEPARATION IN A CURVED DUCT

I.S. Matyash

140180, TsAGI FAU, Zhukovsky, Moscow region, Russian Federation

The integrated powerplant is considered a promising solution in terms of reducing the noise of a modern civil aircraft. Sometimes, in this case, a curved duct of the inlet is used to supply air to the engine. The duct curvilinearity often leads to the flow separation and, as a result, to total pressure losses, high levels of non-uniformity and flow fluctuations at the engine entrance. It significantly affects the gasdynamic stability of the engine. The non-uniformity and flow fluctuations are strictly regulated [1], however, sometimes the separation does not permit to meet these limits. Therefore, the study and application of methods to control the separation is an actual problem.

In the presented work, an "adaptive" suction of the boundary layer is used for suppressing the separation. The adaptation is achieved by choosing the suction gap size according to the separation zone width (in the circumferential direction) [2]. In this case, the part of the boundary layer that separates because of the boundary layer thickness growth will be sucked off through the suction system. It allows us to hope for the elimination of separation.

The curved duct M2129 has been chosen as the base model [3]. The results of an extensive computational study are presented. A RANS equation system closed by the SST turbulence model is solved. The gap length and its position in the duct are varied. The flow parameters at the duct exit section are calculated for different flow regimes and different flow rates through the duct. The influence of the suction system on the parameters at the duct exit section is estimated. Curvilinear ducts with different basic geometric parameters are considered. The results of using a suction system for curved ducts in a wide range of geometric

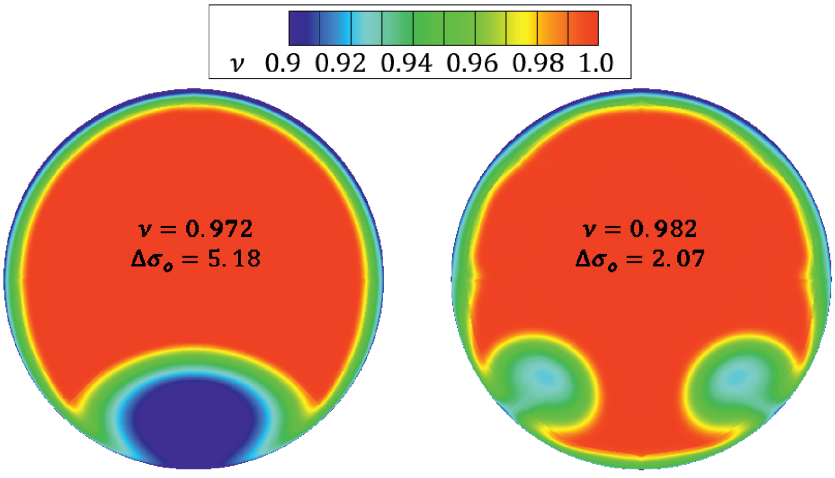

Distribution of the total pressure recovery coefficient in the measuring section, on the left – the base duct, on the right – the duct with the suction system

parameters confirm the effectiveness of the proposed system, which reduces the total pressure losses and flow non-uniformity (see figure).

The estimation of total pressure fluctuations in a curved duct is also an important problem. It was shown in [4–5] that such an estimation can be performed in calculations using vortex-resolving methods. In this work, the IDDES method [6] has been used to perform a non-stationary calculation on one regime. The numerical results have confirmed the results of stationary calculations and have also demonstrated a decrease in the level of total pressure fluctuations by 40 % using the proposed suction system.

REFERENCES

1. **Aerodynamics** and flight dynamics of aircraft // Edited by G.S. Byushgens. Moscow – Beijing: China Aviation Publishing House, 1995, 772 p.
2. **Matyash I.S.** Improving the efficiency of the boundary layer suction system in a curved duct // Scientific notes of TsAGI. 2023. Vol. LIV, No. 3, pp. 62–73.
3. **GARTEUR AD/AG-43.** Application of CFD to high offset intake diffusers. Final report, GARTEUR TP-173, 107 p. http://garteur.org/wp-content/reports/AD/AD_AG-43_TP-173_OPEN.pdf.
4. **Lyubimov D.A.** Investigation of throttling effect on pressure fluctuation spectra in a paired supersonic inlet using vortex-resolving methods // Math. simulation. 2023. Vol. 35, No. 9, pp. 61–76.
5. **Novogorodtsev E.V.** Numerical study of total pressure fluctuations in the inlet with sharp edges using the vortex-resolving SBES method // Bulletin of MAI. 2019. Vol. 26, No. 3, pp. 17–31.
6. **Bakhne S., Vlasenko V.V., Matyash S.V., Mikhailov S.V., Molev S.S., Troshin A.I.** Simulation of turbulent flows based on the IDDES approach using the zFlare program // Computational mechanics of continuous media. 2023. Vol. 16, No. 2, pp. 203–218.

DOI 10.53954/9785604990131_103

NUMERICAL ANALYSIS OF FLOW IN DUCTS WITH DIFFERENT METHODS OF DECELERATING SUPERSONIC FLOW

I.I. Mazhul

Khristianovich Institute of Theoretical and Applied Mechanics SB RAS, 630090, Novosibirsk, Russian Federation

Interest in studying the processes of decelerating of supersonic flows in the spatial ducts is associated with the possibility of their use in the creation of various kinds of technical devices. In this regard, comparative studies of the interaction of shock waves in relation to flat, axisymmetric, and spatial ducts are relevant, in particular, in terms of achieving the required integral flow characteristics in the exit section. The study of supersonic flows with three-dimensional interaction of shock waves with each other and the reflection of the resulting shocks from the walls is also of independent theoretical interest.

In present work, are numerically study the features of the flow in a configuration containing an entrance converging section with an angle of inclination of the compression wedges $\delta_w = 8°$, and then a section of a constant cross-section (see Fig. 1). Configurations with a relative exit cross-section area $\bar{A}_{ex} = A_{ex}/A_0 = 0.49$ (where A_0 is the entrance cross-section area) are considered and a comparative analysis of the flow characteristics is carried out under the assumption of flat, conical or spatial flow. In the latter case, an internal channel is considered, the initial section of which is formed by four wedges intersecting each other in pairs at the corners of the configuration.

A comparison was also made of the integral characteristics of the flow (the degree of pressure increase $\bar{p}_{ex} = p_{ex}/p_{in}$, the total-pressure recovery factor $\sigma_{ex} = P_{0ex}/P_{0in}$, where p_{in} and P_{0in} are the static and total pressure in the free-stream flow) in the exit section of the studied configurations with different types of flows in the internal channel. The considered configurations are applicable, for example, to the frontal air intakes of supersonic aircraft, so the results of the study may be of interest when designing the tract of their engine. Numerical computations were carried out using the ANSYS Fluent software package based on solving the Reynolds-averaged Navier–Stokes equations and the k-ω SST turbulence model.

An example of the flow structure in the studied configurations is presented in Fig. 1 at the free-stream Mach number M = 2.5 in the form of a distribution of lines of constant Mach numbers in the vertical plane of symmetry, as well as in cross-sections x = const. In the vertical plane of symmetry, shocks 1 and 2 occur due to compression of the flow an entrance section, which are then reflected on the axis of symmetry in the form of shocks 3 and 4. In the case of a conical configuration, this reflection is irregular with the formation of a Mach disk (Fig. 1*b*). A more complex flow structure is observed for a configuration with a square cross-section (Fig. 1*c*, *d*), where the interaction of four shock waves induced by the bow compression wedges takes place. Here, the surfaces of shocks 1 and 2 have a triangular shape, limited by the leading edges of the compression wedges and the side arrow-shaped lines of their pairwise intersection at the dihedral angles. Along these intersection lines, three-dimensional irregular interaction of adjacent shocks (for example, shocks 1 and 1', Fig. 1*d*) occurs to form reflected shocks (shocks 1*a* and 1*b*). Due to the incidence of the primary reflected shock 1*a* on the vertical plane of symmetry and its reflection, a flow feature appears here in the form of a shock wave 5.

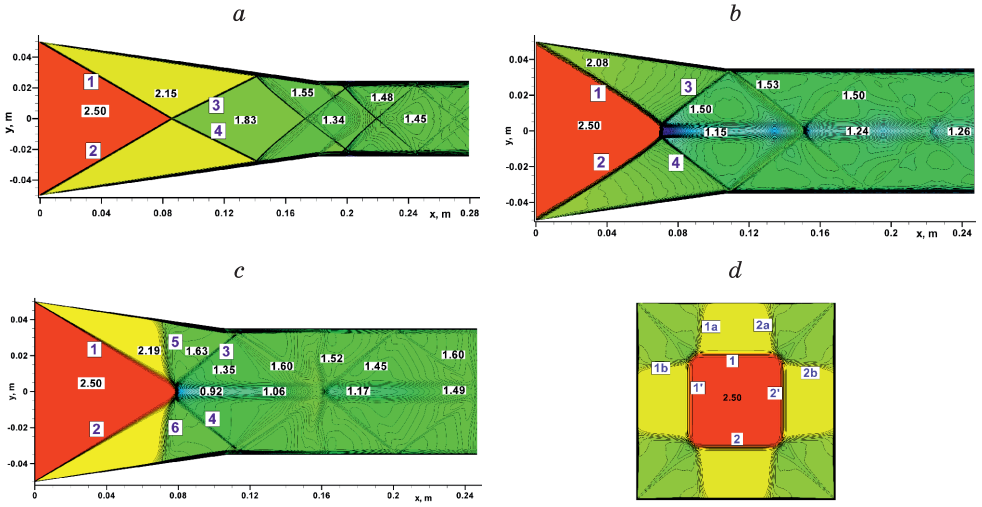

Fig. 1. Flow structure in configurations at M = 2.5.

a) – flat, *b*) – conical, *c*) with a square cross section, *d*) – cross section at x = 0.05 m, 1–6 – shock waves.

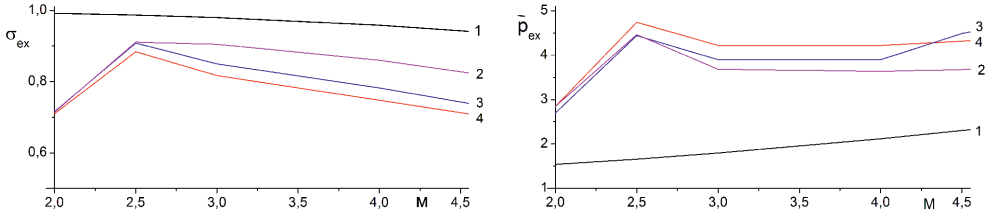

Fig. 2. Integral flow parameters in the exit cross-section of the configurations.

1 – wedge δw = 8°, 2 – flat channel, 3 – conical channel, 4 – rectangular channel.

The integral characteristics of the flow in the range M = 2–4.5 in the channel exit section are presented in Fig. 2. Here, for comparison, data are presented in the case of flow around a flat wedge with an angle δ_w = 8°, which takes place on the bow of the configuration. Note that at M = 2 all configurations flow around with a bow shock at the entrance section, which leads to a drop in the values of $\bar{p}_{ex}$ and σ_{ex}. The data presented shows that, in terms of total pressure loss, conical and rectangular channels provide similar values of σ_{ex}, although in the latter case slightly higher values of pressure increase $\bar{p}_{ex}$ may occur.

The work was carried out within the framework of a state assignment.

DOI 10.53954/9785604990131_105

APPROXIMATE AND NUMEICAL SOLUTION OF THE PROBLEM OF PENETRATION OF COMPACT AND SEGMENTED PROJECTILES INTO A HALF-SPACE

A.E. Medvedev, I.I. Shaballin, and E.I. Kraus

Khristianovich Institute of Theoretical and Applied Mechanics, Siberian Branch, Russian Academy of Sciences, 630090, Novosibirsk, Russia

The formation of cavities and craters by a high-velocity impact of a compact or segmented projectile onto a massive target (half-space) is considered. Structural materials are usually polycrystalline materials possessing an internal mesostructured; however, all material characteristics except for density and dynamic hardness are not important for determining the crater depth. In the present study, it is shown that crater formation by an impact is a self-similar process. Based on solving a self-similar problem, analytical curves of the crater depth are derived for compact and segmented projectiles.

The process of crater formation by a compact projectile was considered within the framework of a rigid-plastic model of a solid. For high impact velocities, the problem of penetration into a target can be modeled on the basis of the strong explosion model [1, 2]. The energy equal to the kinetic energy of the flying projectile is released at the impact point at the initial time. A strong shock wave propagates over the half-space after the impact. At a certain distance from the shock wave, the target material transforms to a plastic state (Tresca criterion). The boundary of this transition is the boundary of the crater. It is demonstrated that penetration of a compact projectile into a massive target is described by a self-similar dependence of the dimensionless crater depth on the kinetic energy of the projectile

$$L_p \big/ \tilde{d}_0 = K\left(\rho_u v_0^2 \big/ H\right)^{1/3}, \tag{1}$$

where L_p is the crater depth, $\tilde{d}_0 = d_0 \left(1.5\lambda\right)^{1/3}$ is the effective diameter of the projectile, ρ_u is the projectile density, $\lambda = l_0 / d_0$ is the aspect ratio of the projectile (l_0 is the cylindrical projectile length and d_0 is the projectile diameter), v_0 is the impact velocity, and H is the dynamic hardness of the target material. The dimensionless parameter K is found by solving a self-similar problem of a strong explosion [2] or from comparisons with experimental data. The curve described by Eq. (1) and comparisons with experimental data [3] are shown in Fig. 1.

Interaction of solid and segmented rods with massive blocks is studied numerically and analytically. Numerical results are compared with experimental data for verification of material parameters under dynamic conditions. Numerical results are found to be in qualitative and fairly realistic agreement with experimental data, such as a nonmonotonic dependence of the depth of the cavity generated by segmented rods on the gap between the segments. It is shown that the efficiency of the action of segmented rods is always higher than that of solid rods with a similar mass penetrating with an identical velocity into a semi-infinite target.

The dimensionless penetration depth L_p / l_0 is obtained as a function of the projectile aspect ratio λ and velocity v_0:

$$L_p / l_0 = \lambda^{-2/3} K\left(\rho_u v_0^2 / H\right)^{1/3}. \tag{2}$$

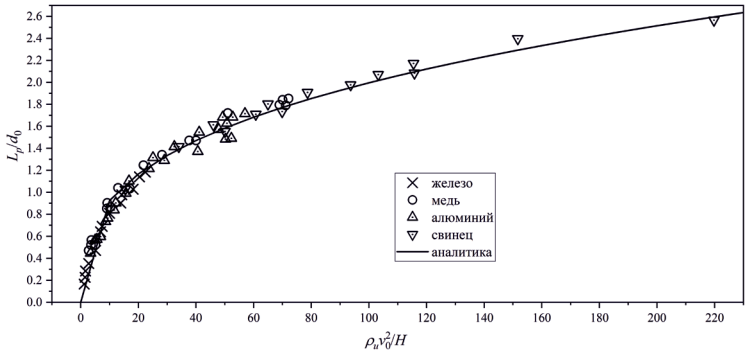

Fig. 1. Normalized penetration depth L_p/d_0 of a compact projectile into a massive target versus the parameter $\rho_u v_0^2/H$ for various metals (symbols [3] and self-similar curve (1).

The process of penetration of a solid projectile with an aspect ratio $\lambda_0 N$ and segmented N projectiles with an aspect ratio λ_0 into a massive target is considered. The depths of penetration of N segmented projectiles $L_p^{(N)}$ and of the solid projectile L_p are

$$L_p^{(N)} = L_p^{(1)} \sum_{i=1}^{N} i^{-1/3} \quad \text{and} \quad L_p = L_p^{(1)} N^{1/3}, \tag{3}$$

where $L_p^{(1)}$ is the depth of penetration of one projectile with an aspect ratio λ_0. A comparison of these values shows that

$$L_p^{(N)} > L_p, \text{ because } \sum_{i=1}^{N} i^{-1/3} > N^{1/3}. \tag{4}$$

The depth of penetration of segmented projectiles is greater than the depth of penetration of a solid projectile. This difference increases with increasing distance between the segments during the impact.

Thus, the following results were obtained in the present analytical and numerical studies:

1) It was shown that the penetration depth depends on the dynamic hardness of the target and on the projectile density;
2) A functional dependence of the depth of penetration into a massive target on the velocity and size of the compact projectile was derived;
3) It was shown that the depth of penetration of segmented projectiles is greater than the depth of the cavity generated by a solid projectile with the same kinetic energy;
4) A functional dependence of the penetration depth of a solid projectile on the projectile aspect ratio and impact velocity was derived.

REFERENCES

1. **Sedov L.I.** Methods of Similarity and Dimension in Mechanics, 8th edition, Nauka, Moscow, 1977, 440 pp.
2. **Medvedev A.E. and Shabalin I.I.** Analytical presentation of Zlatin's modeling curve, Fiz. Mezomekh. 1999, Vol. 2, No. 5, P. 105–107.
3. **Belyakov L.V., Vitman F.F., and Zlatin N.A.** On the process of the impact of deformable bodies and its modeling. II (Modeling the impact of a sphere on a half-space), Zh. Tekh. Fiz., 1963, Vol. 33, No. 8, P. 990–995.

DOI 10.53954/9785604990131_107

THE STRUCTURE OF A FREE SUPERSONIC JET EXHAUSTING AT ANGLE TO THE FREESTREAM DIRECTION

I.V. Menshchikova, V.I. Zapryagaev, I.N. Kavun

Khristianovich Institute of Theoretical and Applied Mechanics SB RAS, Novosibirsk, Russia

The searching for ways to reduce the drag of an aircraft is a relevant problem of aerodynamics. One of the ways of drag reduction was described in [1, 2]. In these papers, it was shown that drag coefficient can both decrease and increase in the presence of the engines turned on, but the causes of flow changes were not described in detail. It is reasonable to carry out the study to reveal the physical mechanism of this phenomenon.

In this paper the results of the research are presented. The structure of the single jet interacting with the freestream at the non-axial direction is described. The freestream Mach number is $M_\infty = 2$. The jet with the following parameters was studied: Mach number at nozzle exit is $M_a = 3.5$, $Npr = 1000$ ("Nozzle pressure ratio" is the ratio of total pressure at nozzle exit to the static pressure in the surrounding space of the jet, $Npr = p_{0a}/p_\infty$). The angle between freestream direction and jet flow direction is 30°.

The results of experimental and numerical studies of the shock-wave structure of the single free jet exhausting into motionless medium are presented in fig. 1. Fig 2 shows the flow picture of jet interaction with the freestream $M_\infty = 2$. The line is the location of the cross section. Schematic of the jet interacting with the freestream is shown in fig. 3. It is labeled: 1 – nozzle; 2 – expansion fan, which front characteristic forms the Mach cone; 3 – barrel shock; 4 – reflected shock; 5 – conventional external boundary of jet mixing layer; 6 – windward side shock; 7 – reversal flow; 8 – expansion fan; 9 – λ-shock.

The calculation results are in satisfactorily correspondence to experimental data (fig. 1), which shows that simulation model is appropriate to the physical phenomenon under study. The jet under the influence of the freestream (fig. 2) deviates from its original direction and deforms downstream. The typical features of this type of the flow are the windward side shock and reversal flow on the leeward side (see fig. 3).

The research was carried out within the state assignment of Ministry of Science and Higher Education of the Russian Federation, and using the equipment of the Equipment Sharing Center "Mechanics" of ITAM SB RAS.

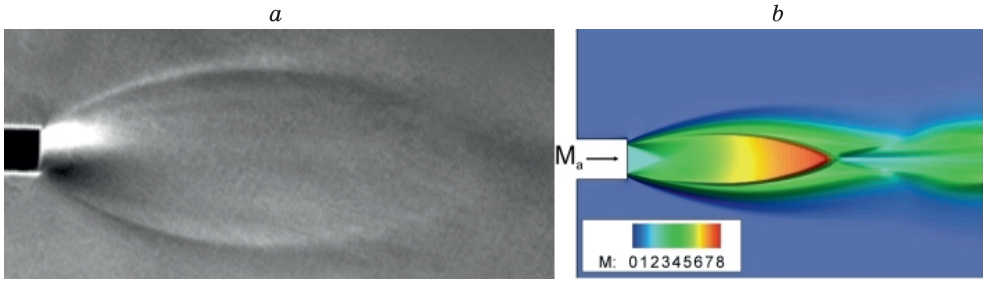

Fig. 1. Single free jet: *a* – Schlieren photo of the jet exhausting into the motionless medium, $M_a = 2.8$, $Npr = 356$; *b* – numerical calculation.

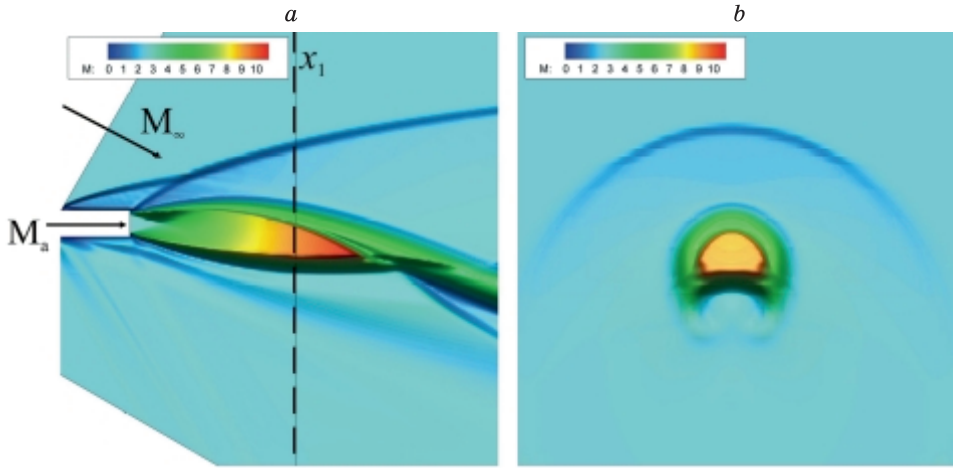

Fig. 2. The flow picture of jet interaction with the incoming flow $M_\infty = 2$: *a* – longitudinal section; *b* – cross section.

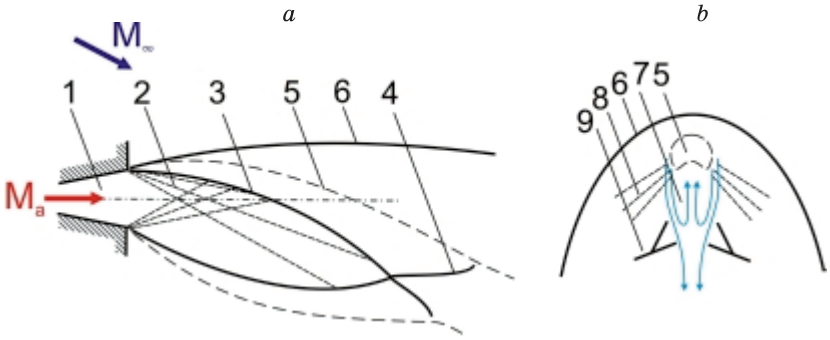

Fig. 3. Scheme of the jet interacting with the freestream: *a* – longitudinal section; *b* – cross section.

REFERENCES

1. **Andreev V.N., Borovkov A.I., Voynov I.B., Drozdov S.M., Dyadkin A.A., Kazakov M.I., Kazakov M.N., Mikhaylov M.V.** Aerogasdynamics behavior of the escape system separable nose assembly with operating propulsion system// Space Engineering and Technology. 2014, no. 4(7), pp. 10–20.
2. **Dyadkin A.A., Kazakov M.I., Mikhaylov M.V., Andreev V.N., Kozlovskiy V.A.** A study of the abort rocket unit plume effects on the aerodynamics of the separation unit// Space Engineering and Technology. no. 4(19). pp. 16–28.

DOI 10.53954/9785604990131_109

THE STUDY OF CHANGES IN THE STRUCTURE OF ERYTHROCYTE MEMBRANES EFFECT ON THE LATERAL DIFFUSION OF LIPIDS AND THE TRANSFER OF GAS MOLECULES THROUGH IT

P.V. Mokrushnikov[1], V.Ya. Rudyak[1, 2]

[1]Novosibirsk State University of Architecture and Civil Engineering (Sibstrin), 630008, Novosibirsk, Russia

[2]Institute of Thermophysics SB RAS, 630090, Novosibirsk, Russia

Changes in the structure of plasma membranes affect the functions of membranes and cells. Some of these changes can lead to the development of pathologies in the body, which makes the task of studying the effect of changes in the structure of membranes on their functions relevant and extremely important from a practical point of view. It has now been established that when stress hormones and androgens interact with plasma membranes, their structure changes [1, 2]. A change in the structure (conformation) of plasma membranes means a change in the secondary, tertiary and quaternary structures of membrane proteins, the phases of the lipid bilayer, the relocation of proteins and lipids throughout the bilayer, and a change in their morphology. At the same time, the interactions between proteins and lipids in the plasma membranes change, and a stationary quasiperiodic network of protein-lipid domains associated with the cytoskeleton is formed. In these domains, lipids adjacent to proteins are more strongly attracted to proteins that have changed their conformation. This, in turn, leads to a change in the mechanical stress field in the membrane [1, 2]. The initiators of the formation of protein-lipid domains are membrane proteins that change their conformation during the interaction of the membrane with hormones [1]. Structural changes in membranes lead to various consequences. In particular, to changes in the lateral diffusion of lipids and the formation of a specific mechanism for the transfer of gas molecules through the membrane. This, in turn, affects other cell functions, such as exocytosis and endocytosis, and the transport of oxygen molecules by erythrocytes. The purpose of this work is to study the effect membrane structural changes on the lipids lateral diffusion and the gas molecules transport across the membrane and to develop two corresponding mechanical models.

As the first, a model of lateral diffusion of lipids in a heterogeneous native cytoplasmic membrane is discussed. The model being developed is based on the idea that the various types of diffusion previously observed experimentally [3] are caused by the appearance in the membrane, as a result of structural transitions, of a network of stationary periodically located protein-lipid domains associated with the spectrin-actin-ankyrin network. As a result, the corresponding lipid diffusion equation is formulated. Using the Fourier transform method, a solution to the equation of diffusion of a particle in an inhomogeneous flat infinite layer is obtained, the diffusion coefficient of which is described by a function periodic in coordinates. It has been shown that in this case advection-diffusion of lipids occurs along the membrane. If these domains are the same, then this advection-diffusion can be observed as super and subdiffusion, when the root-mean-square displacement of particles depends nonlinearly on time. At the same time, the average displacement of the molecule is zero.

In the case when not all membrane proteins associated with the spectrin-actin-ankyrin network change their conformation equally when interacting with ligands, two sublattices of

heterogeneities arise in the membrane. In this case, advection-diffusion can be observed as hop diffusion, when periods of nonlinear diffusion of lipids are replaced by periods of joint advection and nonlinear diffusion, in which the average displacement of molecules along the membrane is not equal to zero. Criteria for observing advection-diffusion of lipids in the form of hop diffusion were analytically obtained.

The following model discusses the transfer of gas molecules through the erythrocyte membrane by kinks-solitons. Previously, a hypothesis has already been expressed about the possibility of transfer of gas molecules through the lipid bilayer by kinks [4], which are usually called bends that occur in the hydrocarbon chain of phospholipids. Kinks are formed due to thermal vibrations of the chain. This idea, however, has very obvious shortcomings. First, the fluctuation nature of kink formation indicates the obvious instability of such a mechanism. It is also not clear what results in the directed movement of these kinks along the hydrocarbon chain. In the model developed in this work, it is shown that as a result of the simultaneous action of transverse mechanical stresses compressing the membrane and tensile longitudinal mechanical stresses, not just kinks arise, but kinks-solitons running along the hydrocarbon chain of phospholipids. It is shown, that the compressive transverse stresses must be greater than a certain value. The proposed model explains the sharp increase in membrane permeability for gases during the passage of an erythrocyte through a microcapillary network, when compressive transverse mechanical stresses increase sharply. The model is consistent with the previously experimentally established fact that native erythrocyte membranes in the bloodstream are in a state of structural transition, when small changes in blood pH, hormone concentrations, and temperature dramatically change the biomembranes conformation and their functions by changing the mechanical stress field in the biomembrane [1, 2].

The study was supported by a Megagrant from the Ministry of Science and Higher Education of the Russian Federation (Agreement No. 075-15-2021-575).

REFERENCES

1. **Mokrushnikov P.V., Panin L.E., Panin V.E., Kozel'skaya A.I., Zaitsev B.N.** Structural transitions in erythrocyte membranes (experimental and theoretical models). Novosibirsk, Sibstrin Publ., 2019. 286 p. (rus).
2. **Mokrushnikov P.V.** Mechanical Stresses in the Lipid Bilayer of Erythrocyte Membranes // Lipid Bilayers: Properties, Behavior and Interactions. Edited by Mohammad Ashrafuzzaman. – NY: Nova Science Publishers, 2019. p. 43–91.
3. **Fujiwara T.K., Iwasawa K., Kalay Z., Tsunoyama T.A., Watanabe Y., Umemura Y.M., Murakoshi H., Suzuki K.G.N., Nemoto Y.L., Morone N., Kusumi A.** Confined diffusion of transmembrane proteins and lipids induced by the same actin meshwork lining the plasma membrane // Mol. Biol. Cell. 2016. Vol. 27, No. 7. P. 1101–1119.
4. **Subczynski W.K., Hyde J.S., Kusumi A.** Effect of alkyl chain unsaturation and cholesterol intercalation on oxygen transport in membranes: a pulse ESR spin labeling study // Biochemistry. 1991. Vol. 30, No. 35. P. 8578–90.

DOI 10.53954/9785604990131_111

VISUALIZATION OF LAMINAR-TURBULENT TRANSITION BY INFRARED THERMOGRAPHY

V.E. Mosharov, V.N. Radchenko, I.V. Senyuev

Central Aerohydrodynamic Institute
140180, Zhukovsky, Russia

Infrared thermography (IRT) is increasingly used to visualize the laminar-turbulent transition (LTT). IRT is based on recording the intrinsic thermal radiation of investigated surface in the infrared (IR) range. Modern thermal imaging technology allows to measure temperature differences of less than 0.1 °C, that makes it possible to use IR imagers to visualize the laminar-turbulent transition. The LTT can be detected due to the difference in the recovery temperatures of the laminar and turbulent boundary layers, which can be 0.5–3 °C, depending on flow speed. However, the application of this approach requires very low thermal conductivity of the model material .

Most researchers prefer to detect LTT based on a sharp increase in convective heat transfer in a turbulent boundary layer. The application of this approach requires either the heating/cooling of investigated surface or the changing of free flow temperature . In this case, it is possible to obtain sufficient temperature differences in the laminar-turbulent transition zone even on surfaces with not very high heat-insulating properties. If the model is metal, its surface can be covered by a polymer film or by a thick paint coating. The best result is achieved by making inserts from heat-insulating material on investigated surface. In closed-circuit wind tunnels, the flow temperature increases usually that provides visualization of the LTT.

If the thermophysical properties of the model is constant over the surface, the surface temperature will reflect the heat flux distribution. In practice, the consistency of the thermophysics of the model is not ensured, and the structure of the model is often become visible on the thermal image: parts made of different materials, internal cavities, pressure tapes etc.

The thermal imager acquires the radiant energy flux from the surface, which consists of the model's intrinsic radiation plus the radiation of surrounding objects reflected from the surface. In addition, if the wind tunnel has a closed test section, then the model radiation is attenuated by the window on the one hand, on the other hand the radiation of the window and the radiation of wind tunnel environment reflected by the window are added.As a result, unless the model is a blackbody and/or the window is absolutely transparent, the detected thermal radiation will have a significant background component. This reduces the contrast of LTT images. IR camera software interprets the recorded signal as black body radiation with some emissivity (inputted by operator).

The laminar-turbulent transition does not occur instantly; the LTT has an onset and an end. There is a known technique for processing of experimental data [1] when the dependence of Stanton number (St) on x (or Re_x) is plotted in logarithmic coordinates, then the laminar, transient and turbulent regions are interpolated by linear dependencies, and the x coordinates of the intersection points of these linear interpolations are taken as coordinates of the onset (X_t) and the end (X_T) of the transition. Despite the temperature measured by IR camera cannot be interpreted as a heat flux, this technique can be successfully applied for temperature distribution analysis (see Fig. 1).

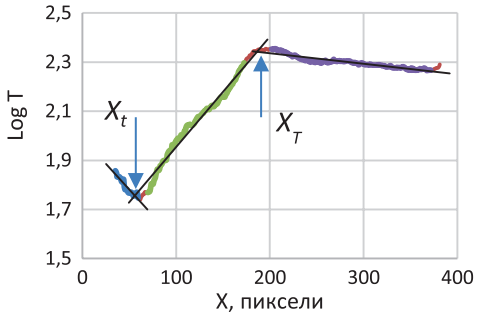

Fig. 1. Finding of the onset X_t and the end X_T of the LTP on the engine nacelle model (Fig. 3).

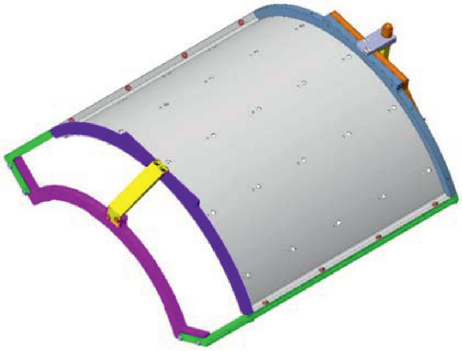

Fig. 2. Calibration arrangement.

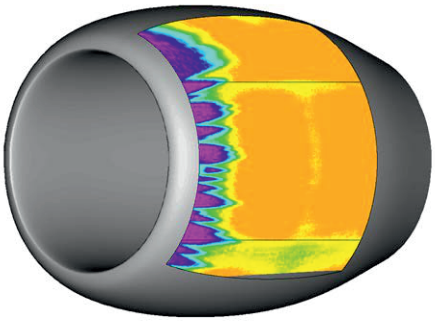

Fig. 3. 3D models of the engine nacelle with temperature distribution.

Thermal images are perspective, therefore, an essential point of IR visualization (like any other visualization) is the presentation of visualization results on the surface of 3D model [2]. Linking the position of the LTT to the real model coordinates is provided by transforming a flat image onto a three-dimensional mathematical surface of the model. The problem is solvable if the three-dimensional geometry of the object and a set of marker points (minimum 9) with known coordinates on the mathematical model and on the perspective image are known. Any specific points of the model can use as these marker points, but it is better to apply optically distinguishable points to the model surface and measure their three-dimensional coordinates. In the visible wavelength range this problem is easily solved, but in IR range this problem is more difficult. Markers can be made of metal, for example of aluminum foil, since metal in IR range has low emissivity and is essentially a mirror. But in the conditions of thermodynamic equilibrium, such markers will not be distinguishable. Another approach is to install special arrangement with markers on the surface of the model. This arrangement must be installed in strictly determined position with respect to the surface of the model. The calibration arrangement for the engine nacelle model is shown in Fig. 2. The markers on this arrangement are made as the holes. This approach requires spatial stability of the model position during experiment. Changing the spatial position of the model requires recalibration. An example of a thermal image transformed onto a 3D model is shown in Fig. 3.

REFERENCES

1. **Bertin J.** Hypersonic Aerothermodynamics, AIAA Education Series, J.S.Przemieniecki Series Editor –in-Chief, AIAA, 1994, 412 p.
2. **Mosharov V.E. Radchenko V.N., Senyuev I.V., Tsipilev N.S.** Liquid crystal coating application in aerodynamic experimental testing for skin friction visualization // Uchyonye zapiski TsAGI, 2021. Vol. LII, No. 5, P. 42–61.

DOI 10.53954/9785604990131_113

A STUDY OF THE FLOW OF CARBON DIOXIDE IN HETEROGENEOUS SATURATED POROUS MEDIA TAKING INTO ACCOUNT THE FORMATION OF GAS HYDRATES

N.G. Musakaev, S.L. Borodin

Tyumen Branch of the Khristianovich Institute of Theoretical and Applied Mechanics SB RAS, 625026, Tyumen, Russia

One of the most promising methods for reducing carbon dioxide emissions into the Earth's atmosphere is the sequestration of this substance. Currently, sequestration technology mainly includes three methods: carbon dioxide burial in geological reservoirs, marine sequestration and mineral carbonation [1]. Underground carbon dioxide storage appears to be the most viable method for large-scale reduction of CO_2 emissions. The main arguments in favor of this method of CO_2 storage are the simple technology concept and the large storage volume. Various authors propose methods for organizing the storage of carbon dioxide in porous reservoirs, including in gas hydrate form. The main sites for introducing technology for organizing underground gas hydrate storage of carbon dioxide can be depleted hydrocarbon deposits, since they are well studied, the characteristics of the deposits and their geometric dimensions are known, and some infrastructure is available. One of the factors determining the effectiveness of the underground gas hydrate CO_2 storage technology is the reservoirs heterogeneity. In this regard, it is important to mathematically model the processes occurring during the flow of carbon dioxide in zonally heterogeneous saturated porous media, taking into account the formation of gas hydrates.

The work considers the following problem statement. Let there be a porous reservoir consisting of two zones with different permeability and initially saturated with methane and water. Carbon dioxide with a constant temperature T_e is pumped into the reservoir through a well at a constant pressure p_e. In this case, T_e is lower than the equilibrium temperature of carbon dioxide hydrate formation for pressure p_e, and the thermodynamic conditions in the porous medium after the start of CO_2 injection into it allow the formation of CO_2 hydrate. When mathematically modeling the studied process assumptions have been accepted similar to those presented in [2]. The heat exchange of the considered region of the porous medium with the surrounding rocks is additionally taken into account. The mathematical model of non-isothermal gas-liquid filtration, written in a two-dimensional axisymmetric approximation, taking into account the formation of gas hydrates, includes equations of conservation of mass and energy, Darcy's law, equations of state for gas and water, and the condition of phase equilibrium. Based on the proposed mathematical model, a software product has been developed for conducting computational experiments on the burial of carbon dioxide in gas hydrate state in a zonally heterogeneous porous reservoir. An analysis of the influence of carbon dioxide injection parameters and porous reservoir characteristics on the distributions of hydrodynamic and temperature fields in the reservoir, as well as on the intensity of gas hydrate formation, was carried out.

The research was funded by the Russian Science Foundation (project No. 24-29-00093), https://rscf.ru/project/24-29-00093/.

REFERENCES

1. **Cao X., Wang H., Yang K., Wu S., Chen Q., Bian J.** Hydrate-based CO_2 sequestration technology: Feasibilities, mechanisms, influencing factors, and applications // Journal of Petroleum Science and Engineering. 2022. Vol. 219. 111121.
2. **Musakaev N.G., Borodin S.L.** Mathematical Modeling of the Gas Hydrate Formation Process in a Zonal Heterogeneous Porous Reservoir // Lobachevskii Journal of Mathematics. 2021. Vol. 42, No. 9. P. 2205–2210.

DOI 10.53954/9785604990131_115

EXPERIMENTAL INVESTIGATION OF THE UNDEREXPANDED GAS JET WAVE STRUCTURE IN THE PRESENCE OF LIQUID PHASE

A.Yu. Nesterov, V.M. Boiko, S.V. Poplavski

Khristianovich institute of theoretical and applied mechanics SB RAS, 630090, Novosibirsk, Russia

Liquid spraying devices, or nozzles, are widely used in industrial applications for many purposes. A wide variety of constructive designs of such devices can be divided into classes according to the physical mechanism used for atomization, and one them is the class of pneumatic nozzles. Here, the liquid is dispersed by a high-velocity gas flow, which allows to form a fine spray, including the cases of viscous liquids atomizing or highly concentrated sprays. Also, the design has a number of technological advantages, for example, comparatively low liquid pressure in the supply channel [1]. One of the pneumatic nozzle designs is a coaxial nozzle with external mixing, here the liquid is supplied along the jet axis to the gas nozzle cutoff. This design is of scientific interest, since it is the simplest nozzle configuration, as well as practical, because these results allows to evaluate the processes taking place during the liquid spraying by the nozzles used in industry. In the cases of viscous media or high liquid flow rates, it seems promising to atomize liquid by supersonic gas jets, which allows substantial increasing of the droplet aerodynamic load [2]. However, the interaction of supersonic jets with the dispersed phase is a complex phenomenon from the point of view of gas dynamics as well as atomization processes. It was shown [3] that the interaction of a gas-liquid jet with the wave structure of the gas shell leads to noticeable changes both in the spray and the gas phase structure: the deflection of the Mach disk upstream and sharp increasing of the concentration of droplets behind it. It is followed by the formation of a bow shock on the cloud of particles and its shift in the nozzle direction with the droplets concentration rising. These data were obtained by analyzing the visualization patterns and droplet velocity profiles on the jet axis. It should be noted that the visualizing allows to obtain data on the wave structure only at minimal droplet concentrations in the spray, whereas droplet velocity profiles is not provide complete information about the structure of the jet in the two-phase region. This information can be obtained by analyzing the velocity fields of droplets; however, this technique has not previously been applied to the problem of changing the wave structure of a gas jet in a gas-liquid core. Thus, the aim of this work is to study of the wave structures of a supersonic underexpanded gas jet in its gas–liquid core of a coaxial nozzle of external mixing experimentally using new diagnostic techniques.

The work was performed at the gas-liquid stand setup of ITAM SB RAS, designed for testing pneumatic nozzles at gas and liquid pressures in a pre-chamber up to 8 atm. A detailed description of the setup is given in [3], it consists of a jet module with a nozzle unit, supplied by gas and liquid, and a receiving tank for used liquid. The liquid can be supplied either from a vessel under certain pressure or recirculation system with intake from a tank. As diagnostic tools, a set of methods consists of shadowgraphy, including AVT-visualization [4], as well as a laser Doppler anemometer with direct spectral analysis [5] was used, it allows to measure the droplets velocity in highly concentrated gas-liquid jets. The instrument can be used to obtain velocity profiles as well as velocity fields when moving the test sample in both directions. The described set is used to study supersonic flows of water and a viscous

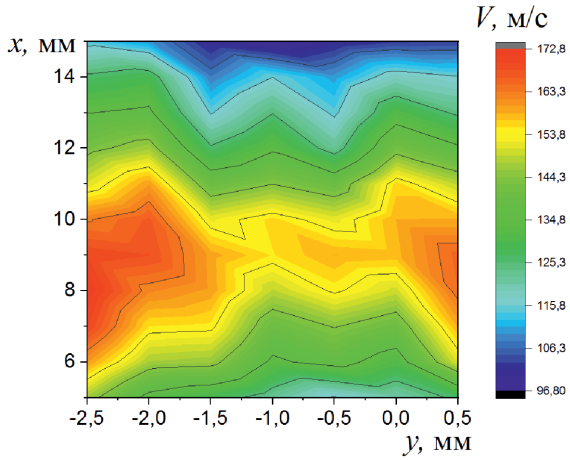

Droplets velocity field in the vicinity of the shock, Npr6, liquid flow rate is 44 g/s, viscous mixture

mixture simulating the viscosity of fuels. The profiles and two-dimensional fields of drops velocity in the gas-liquid core of the jet were obtained (the example of the velocity field – in the picture). It is shown that the droplet velocity profile similar to the gas velocity profile of a supersonic underexpanded jet is reproduced in the two-phase region of the jet with a number of specific features. At liquid flow rates of less than 5 g/s, an artifact behind the bow shock was detected, clearly noticeable in the Npr8 mode. As the rate grows, the artifact disappears. The deflection of the Mach disk observed in the visualization pictures at high fluid flow rates does not detected due to the alignment of the droplet concentration profile in the cross section of the jet. The results obtained by spraying a viscous liquid differ from the data for water mainly by the greater droplets inertia, so the gas velocity significantly differs from the data obtained on droplets.

The work was performed in the framework of the budget project of ITAM SB RAS (№ АААА-А19-119051590050-2).

REFERENCES

1. **Vitman L.A., Katsnelson B.D., Paleev I.I.** Atomization of liquid by nozzles. Moscow, Leningrad: Gos. Energ. Izd., 1962. 265 p.
2. **Andryushkin A.Yu.** Liquid dispersion by the supersonic gas-dynamic technique (survey) // Constr. from the comp. mat. 2011. № 3. P. 5–27.
3. **Boiko V.M., Nesterov A.Yu., Poplavski S.V.** Spray influence on the gas-dynamic structure of a supersonic underexpanded jet // Thermophysics and aeromechanics. 2022. Vol. 29, № 3. P. 311–325.
4. **Boiko V.M., Orishich A.M., Pavlov A.A., Pikalov V.V.** Methods of optical diagnostics in aerophysical experiments. Novosibirsk, 2009. 450 p.
5. **Poplavski S.V., Nesterov A.Yu., Boiko V.M.** Development and application of the laser Doppler anemometer with direct spectral analysis for studying high-velocity multiphase flows // Thermophysics and aeromechanics. 2020. Vol. 27, № 4. P. 555–563.

DOI 10.53954/9785604990131_117

FEATURES OF THE INFLUENCE OF INCOMING EXTERNAL DISTURBANCES ON THE STRUCTURE OF THE SEPARATED FLOW OF WING MODELS

A.M. Pavlenko, N.S. Alpatskiy, B.Yu. Zanin

Khristianovich Institute of Theoretical and Applied Mechanics SB RAS
Institutskaya str., 4/1, Novosibirsk, 630090, Russia

The work is devoted to studying the influence of incoming external disturbances on the structure of separated flow around models of aircraft wings depending on the angle of attack and oncoming flow velocity. Using the visualization method with soot-oil coatings, flow patterns near the surface of the models were obtained for each flow regime. Quantitative data were obtained and the structure of the flow behind the source of external disturbances was determined using the hot-wire anemometry method. It was found that, under certain conditions, incoming external disturbances can significantly reduce the areas of local and global separation on the surface of the wings, up to complete reattachment of the flow.

Flow separation is a physical phenomenon that occurs when gases or liquids move over a solid surface or, conversely, when a body moves in a stationary liquid or gas, which consists in the fact that the flow stops moving along the surface and moves away from it. General information about separated flows can be found in the monograph [1]. Viscosity and pressure change along the surface are two factors that are decisive for the occurrence of flow separation. These factors lead to a slowdown in the flow of liquid or gas, followed by an increase in the downstream boundary layer and the formation of a reflux flow. As a result of these processes, the fluid inhibited in the boundary layer is carried out into the external flow, and the boundary layer is pushed away from the body. Such conditions arise when flowing around an airplane wing. The study of flow separation is a very urgent task, since this phenomenon is accompanied by a decrease in lift and an increase in drag, which can lead to a rapid loss of altitude, stalling the aircraft into a tailspin and, accordingly, is unfavorable for the operation of aircraft. When flying at low altitudes in the surface boundary layer, aircraft can enter areas where the atmosphere is highly disturbed. In addition, during flight, an aircraft may enter zones of turbulent wake vortices behind obstacles, behind other aircraft, or behind the topography of the earth's surface. Therefore, studying the influence of these factors on the flow is of great practical importance. The purpose of the presented fundamental research was to study the influence of incident external disturbances on three-dimensional separation structures arising on the surface of wing models of various shapes.

All experiments on the research topic were carried out in the subsonic wind tunnel T-324 ITAM named after S.A. Khristianovich SB RAS (Novosibirsk) [2]. The dimensions of the test section of the square section are 1×1 m^2 and 4 m long. A fleecy thread was used as a source of disturbances, which was installed in front of the wing model upstream (Fig. 1). The hot-wire anemometry technique was used to obtain quantitative data on the flow structure behind the disturbance source. The diameter of the thread was about 1.5 mm. Three wing models were used in the experiments: a straight wing, a V-shaped wing and a trapezoidal wing. The angles of attack varied in the range from $\alpha = 0°$ to $\alpha = 20°$. The oncoming flow velocity was set in the range of 10–25 m/s and was controlled using a Pitot-Prandtl nozzle connected to an electronic micromanometer using a pneumatic track. The Reynolds number

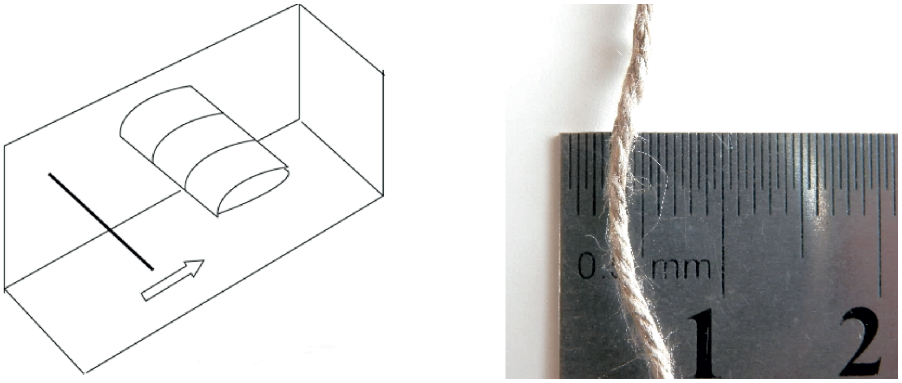

Fig. 1. Diagram of the location of the source of generation of external disturbances in front of the model in the test section of the wind tunnel and the dimensions of the thread.

ranged from $0.8*10^5$ to $6.4*10^5$. The main method for obtaining experimental data was the soot-oil coating method [3].

Three series of experiments were carried out on three models of wings devoted to the study of the separation structure in the presence and absence of oncoming external disturbances. In experiments with a straight wing model, it was found that incoming external disturbances can eliminate global flow stall. Additionally, on a straight wing, the effect of the swept angle on the flow separation was studied. It was also found that the swept angle leads to a decrease in the local separation area, and the influence of disturbances from the thread led to the almost complete elimination of the local separation bubble at low angles of attack.

In studies on a V-shaped wing model, it was found that incoming external disturbances can also lead at low angles of attack to a significant reduction in local separation bubbles and the elimination of global flow separation from the leading edge at a supercritical angle of attack.

In experiments with a trapezoidal wing model, it was discovered that the turbulent trace from the thread can significantly change the structure of the separation flow. Large-scale vortices are significantly reduced in geometric size, and the area of attached flow on the model surface increases. At low angles of attack, local separation bubbles gradually decrease in size until they disappear completely as the distance between the source of external disturbances and the wing decreases.

The results of hot-wire measurements of the flow behind the thread were also obtained. The structure of the flow behind the disturbance source was studied.

This work was carried out within the framework of the Program of Fundamental Scientific Research of State Academies of Science for 2024-2026 (project 124021400038-1). The work was carried out using the Equipment Sharing Center «Mechanics» of ITAM SB RAS.

REFERENCES

1. **Chang P.K.** Separation of Flow. Pergamon Press, New York 1970, 796 p.
2. **Bagaev G.I., Golov V.K., Medvedev G.V., Polyakov N.F.** T-324 Low Speed Wind Tunnel with Reduced Turbulence // Aerophysical Research. Novosibirsk. 1972. I. 1. P. 5–8.
3. **Kornilov V.I.** Spatial near-wall turbulent flows in angular configurations. Novosibirsk, 2013. P. 431.
4. **Pavlenko A.M., Zanin B.Yu., Katasonov M.M.** Flow around a small-sized UAV model in a turbulent trace // Proc. of 19 Int. Conf. on the Methods of Aerophys. Research (ICMAR2018): AIP Conference Proceedings. 2018. Vol. 2027. Art. 040004. 7 p. doi.org/10.1063/1.5065278.

DOI 10.53954/9785604990131_119

WAYS TO IMPROVE THE CONSTRUCTION OF THE SOUND GENERATOR MODULATOR

D.P. Pavlov, I.V. Lebedev, A.Ya. Sterlin, A.V. Furman

Federal Autonomous Institution "Central Aerohydrodynamic Institute", Zhukovsky, Russia

In the mid-20th century, the use of turbojet engines led to an increased acoustic impact on aircraft and the emergence of the problem of structural fatigue in aircraft due to acoustic loads. Acoustic loads may be caused not only by engine noise but also by turbulent boundary layers, shock waves, flows around cavities, and other phenomena. These vibrations can cause fatigue fractures in the aircraft skin and power structures, equipment failures and damage, leading to increased operating costs and limited product lifecycle. Consequently, acoustic fatigue testing of samples is essential.

To conduct such studies in a laboratory environment, reverberation chamber facilities are used, with sound generators being the key component that determines the operational characteristics of these facilities.

Currently, there is a need for the development and creation of a promising domestic sound generator (SG). Nowadays, French and American models are used in domestic ventures. The Russian high-frequency SG is intended to replace foreign analogues, in order to enhance the testing capabilities of aviation and space-related equipment. This requires:

1) modernization of magnetic system design to increase magnetic induction in the gap;

2) optimization of valve assembly of moving part:

– mass reduction of movable cylinder;

– minimization of heat generation during valve assembly reciprocating movement and enhancement of convective heat transfer;

– decrease in electromagnetic resistance forces experienced during valve assembly movement;

– mitigation of mechanical friction forces.

REFERENCES

1. **Nikolaev V.S., Kaurova N.F.** "Installations for Testing Structures of Aerospace Aircraft for Acoustic Strength," Review No. 565, Publication Department of the Central Aerohydrodynamic Institute (TsAGI), Moscow, Russian Federation, 1979, 195 pg.
2. **Patent 2742283** of the Russian Federation, IPC G10K7/06, "Gas flow modulator," by A.Ya. Sterling, A.V. Furman, S.K. Kim, S.A. Kutsenko and G.E. Dyadchenko, applicant and patent holder at TsAGI (Central Aerohydrodynamic Institute). Application No. 2020120957, filed on 06.25.20, published on 02.04.21 Bulletin No. 4.
3. **Patent No. 26946** of the Russian Federation, IPC G 10 K 7/06. "Electro-pneumatic sound generator" by A.Ya. Sterling, A.V. Furman, S.K. Kim and N.V. Zverev, Applicant and Patent Holder of TsAGI, Application No. 2018142901, filed on 05.12.18, published on 07.08.19, Bulletin No. 22.
4. **Patent No. 2707587** of the Russian Federation, IPC class G 10K7/06. "A method for generating sound for the testing of structures and apparatus for implementing the same" by A.Ya. Sterling, A.V. Furman, S.K. Kim and S.A. Kutsenko, applicant and patent owner of TsAGI (TsAGI – Central Aerohydrodynamic Institute). No. 2018142903, filed on 05.12.18, published on 28.11.19, Bulletin No. 34

DOI 10.53954/9785604990131_120

SCIENCE OF THE STRENGTH OF MATERIALS OR WHAT IS NOT TAUGHT IN UNIVERSITIES

M.G. Petrov

Aeronautical Research Institute named after S.A. Chaplygin, 630051, Novosibirsk, Russia

Mechanics currently dominates in the calculations of the strength and durability of structures, as well as in the analysis of the strength characteristics of materials. Mechanics considers only the external side of the failure process, successfully solving a number of specific tasks necessary for practice. The result of the observed behavior of the material is what happens inside it. And this is considered by the science of the strength of materials based on condensed matter physics.

The various sides of the strength problem are very closely interrelated. In general, this is an interdisciplinary problem solved by combining knowledge and methods of mechanics, physics and physical material science [1]. Such fields of knowledge as the theory of vibrations, rheology of materials, thermodynamics of the solid state and general kinetic theory are intertwined here. And each of them relates to the strength and fracture of structures. Therefore, all problems should be solved in a complex, from the standpoint of ideas about what a material is and why it is destroyed. And the material is an atomic-molecular structure in thermal motion, and it is destroyed as a result of stochasticity and anharmonicity of thermal vibrations of atoms in a solid. This is the root from which to proceed.

To demonstrate which approaches should be used in the analysis of construction failure, a calculated assessment of the durability of the composite shell of the "Titan" bathyscaphe was carried out, according to the magnitude of the circumferential stresses on its inner contour [2]. The calculations are performed using the following expressions:

$$\sigma_r = \frac{a^2 b^2 (p_0 - p_i)}{b^2 - a^2} \cdot \frac{1}{r^2} + \frac{p_i a^2 - p_0 b^2}{b^2 - a^2}, \quad \sigma_\theta = -\frac{a^2 b^2 (p_0 - p_i)}{b^2 - a^2} \cdot \frac{1}{r^2} + \frac{p_i a^2 - p_0 b^2}{b^2 - a^2}.$$

At an internal pressure of $p_i = 0$, the formulas take the form:

$$\sigma_r = -\frac{b^2 p_0}{b^2 - a^2}\left(1 - \frac{a^2}{r^2}\right), \quad \sigma_\theta = -\frac{b^2 p_0}{b^2 - a^2}\left(1 + \frac{a^2}{r^2}\right),$$

where a is the inner radius, b is the outer radius, and r ($a \le r \le b$) is the current radius from the shell axis. The greatest circumferential stresses σ_θ act on the inner contour of shell, where the radial σ_r are zero. Therefore, the calculation is based on circumferential stresses proportional to the external pressure p_0 as for uniaxial compression. The inner diameter of the shell is assumed to be 2000 mm. The wall thickness of the composite shell of the bathyscaphe was 127 mm.

The processing of test results of specimens (thermal activation analysis) cut from carbon fiber reinforced plastic panels for aviation purposes was carried out using the fracture kinetic concept (FKC) according to the following formulas similar to expressions for plastic

flow rates [1]. The rate of failure as the inverse of durability was represented by the expression

$$\dot{\omega} = A\exp(B\,|\,\sigma\,|)\,,$$

where $A = \nu_0 \exp[-U_0/(RT)]$, $B = \gamma/(RT)$, ν_0 is the characteristic Debye frequency, the inverse of the average period of thermal vibrations of atoms in a solid, and $|\,\sigma\,|$ is the absolute value of compression stresses. Integrating this expression for constant and linearly varying stresses leads to the formulas

$$\omega = \omega_0 + A\exp(B\,|\,\sigma_0\,|)t \text{ and } \omega = \omega_0 + A\exp(B\,|\,\sigma_0\,|)\frac{\exp(BDt)-1}{BD},$$

where ω_0 is the damage at the beginning of the time step t, $|\sigma_0|$ is the compression stress at the beginning of the time step, $D = \mathrm{d}|\sigma|/\mathrm{d}t$ is the loading rate substituted into the equation with the corresponding sign. The second term in the formulas is the increment of damage in the time step.

The initial fracture activation energy (FAE) $U0$ is assumed to be equal to 155.3 kJ/mol and corresponds to a previously determined value [3]. The structurally sensitive coefficient γ in parameter B is assumed to be constant. Its values in KFC are associated with the concentration of internal stresses resulting from the structural heterogeneity of the material, and the absolute temperature T determines the energy going to failure.

The loading program, based on the operating conditions, assumed a slow increase in pressure to 40 MPa and a decrease in temperature from 20 to 0 °C when the bathyscaphe descended to a depth of 4000 m for 2.5 hours with similar conditions when it returned to the ocean surface. The time spent at this depth was assumed to be 20 minutes. The activation volume γ was assumed to be constant and was adjusted when processing the test results of the specimens for the thickness of the non-working layer with a perpendicular direction. The calculation was carried out using a mathematical model describing the general flow of the binder material (creep) from the point of view of the science of strength of materials [3, 4].

The calculation was performed in time steps with duration of 60 seconds, assuming a constant temperature on the step value, and a linearly varying depth. For failure probability of 0.5, only 65 dives to a depth of 4000 m with a wall thickness of 127 mm can be considered safe. By increasing the thickness of the shell to 150 mm, its durability increases by more than 20 times. But it is necessary to take into account the scatter in the strength characteristics of the material and the consequences that the fracture of the single most critical structural element can lead to. The probability of failure of such elements should be at least 1 %, taking into account the confidence limits [5].

If we take the statistics of the highest stresses $|\sigma_{max}|$ that the tested specimens withstood, then it is clearly insufficient. Therefore, instead of 2.3, for the failure probability of 1 %, we subtract three standard deviations $|\sigma_{max}|$ from the center of scattering of the values of their FAE and determine its position corresponding to the failure probability of 0.14 %. The value of U_0 remains the same, only the coefficient γ changes. Thus, we obtain the force dependence of the FAE for a given probability, according to which the calculation is performed. In this case, the calculation showed 7–8 safe dives to a given depth. Further operation of the bathyscaphe under the same conditions should result in its fracture, which can occur during any next dive.

So, the use of FKC, in which the temperature is explicitly included in the equations, makes it possible to solve the problems of predicting the durability of composite materials as well as metal alloys under changed temperature and force conditions. Its application shows how to approach the strength of materials in general and fatigue failure in particular [1, 4]. Then the problems that have not yet been solved by the methods of mechanics are solved.

REFERENCES

1. **Petrov M.G.** Strength and durability of structural components: an approach based on models of material as a physical medium. Saarbrücken, 2015. 472 p. [In Russian]
2. **Timoshenko S.P., Goodier J.N.** Theory of Elasticity (3rd ed.). New York, 1970. 608 p.
3. **Petrov M.G.** Mathematical Modeling of Failure and Deformation Processes in Metal Alloys and Composites // American Journal of Physics and Applications. 2020. 8(4). P. 46–55.
4. **Petrov M.G.** Fracturing of Solids as a Thermodynamic Process // Alloys. 2023. 2(3). P. 122–139. Available at: https:/doi.org/10.3390/alloys2030009.
5. **14 CFR Part 25.** Airworthiness Standards: Transport Category Airplanes.

DOI 10.53954/9785604990131_123

SIMULATION FEATURES OF RUNNING PROPELLERS IN CONDITIONS OF AIRFRAME INTERFERENCE

E.A. Pigusov

Central Aerohydrodynamic Institute named after N.E. Zhukovsky
140180, Zhukovsky, Moscow Region, Russian Federation

The aerodynamic design of propeller-driven aircraft equipped with a twin-engine propulsion system, despite quite a lot of research experience, is a difficult task. The use of a twin-engine propeller propulsion system is typical for aircraft of local air lines of the commuter category and regional aircraft of the transport category, where an acceptable flight economy should be ensured when flying over fairly short distances (up to 1000–1500 km) and operation from relatively short runways, while high cruise speed is not required. For aircraft of these classes, the typical aerodynamic layout is a conventional tube-and-wing configuration with the placement of engines on the wing and a single vertical tail, with the placement of a stabilizer on the fuselage or on top of the vertical tail. It should be noted that for economic reasons, these aircraft are equipped with a manually operated flight control system with minimal introduction of electronics, which imposes higher requirements on the flying skills of flight crew.

In a typical aerodynamic layout, blowing the airframe with jets of propellers makes it possible to increase the load-bearing characteristics and efficiency of the control surfaces on the tail located in the wake of the propellers. At the same time, the tail may lose its effectiveness due to an increase in the angle of flow bevel due to the deflected wing high-lift devices during blowing [1]. Another problem for twin-engine aircraft is engine failure, which leads to an increase in the drag coefficient, a decrease in the lift coefficient and, accordingly, an increase in yawing and rolling moments. This problem is aggravated by unidirectional rotation of the propellers in case of engine failure of the so-called “critical” engine, for example, the propellers rotate clockwise and in case of failure of the right engine, the vertical tail and rudder turn out to be outside the area of blowing by jets of propellers and, accordingly, lose their effectiveness. Under these conditions, it is quite difficult to fend off the emerging “parasitic” moments, and the accompanying losses in aerodynamic characteristics complicate the stability and controllability of an airplane with a failed engine. As a result, when designing aircraft, the layout parameters (increased tail dimensions, etc.) and the power plant (thrust margin) are chosen that are not optimal in terms of performance in cruising flight mode, which leads to a decrease in the flight performance of the aircraft. Thus, taking into account the features of the integration of a propeller-driven propulsion system into a layout at the early stages of design can allow for a qualitative improvement in flight performance. Experimental studies are currently being conducted to simulate the operation of propellers in wind tunnels, but conducting such studies at the initial stages of design is difficult due to the high cost and complexity. In addition, geometric similarity can be provided in wind tunnels, but similarity in numbers Reynolds Re, Mach M and Strouhal Sh is difficult. Common methods for calculating the effect of blowing on the aerodynamic characteristics of aircraft are mainly based on the impulse theory, which does not fully describe the physical phenomena occurring during this process. The use of computational fluid dynamics methods in relation to this problem can significantly expand the capabilities of the researcher, but also has a

number of limitations, such as the specifics of setting boundary conditions, significant computational power is also required in both non-stationary and quasi-stationary settings, and the lack of reliable validation data obtained from a wind tunnel or flight experiment.

In this paper, the main modern aspects of the running propellers simulation in conditions of interference with the airframe are considered, both using a wind tunnel and a numerical experiment. Approaches to computational studies of the interference of propellers and airframe are presented. The features of the behavior of the aerodynamic characteristics of a twin-engine aircraft in cruising and takeoff and landing configurations, including when modeling the failure of one of the engines, are shown. A comparison of the test results obtained in a low-speed wind tunnel and calculated by computational fluid dynamics is given.

REFERENCES

1. **Chernousov V.I., Krutov A.A., Pigusov E.A.** Three-dimensional visualization of flow pattern near transport airplane model with operating propellers in wind tunnel // Journal of Physics: Conference Series. 2020. Vol. 1697, No. 012216. https://doi.org/10.1088/1742-6596/1697/1/012216.

DOI 10.53954/9785604990131_125

TO THE DEFINING OF THE OBLIQUE BREAKDOWN MECHANISM IN THE BOUNDARY LAYER ON A FLAT PLATE AT MACH 2

M.V. Piterimova, A.D. Kosinov

Khristianovich Institute of Theoretical and Applied Mechanics SB RAS
630090, Novosibirsk, Russia

Introduction. Experimental study of the mechanisms of disturbances interaction in boundary layers is an important task for the theoretical description of wave processes of laminar-turbulent transition (LTT) [1, 2]. Two essential methods are applicable for modeling LTP: direct numerical simulation and calculations based on the wave approach of the hydrodynamic stability theory. For comparison with numerical results, experimental data, which can be obtained by introducing controlled disturbances into the supersonic boundary layer, are required [3]. This paper presents the results of oblique breakdown mechanism identification in a supersonic boundary layer on a flat plate, the flow in which is distorted by a longitudinal disturbance generated at the sharp leading edge by a pair of weak shock waves. This work is a follow of the research cycle begun in [4].

Experimental set up. The experiments are carried out in the T-325 supersonic wind tunnel of the ITAM SB RAS at M = 2 and $Re_1 = (8.00 \pm 0.04) \times 10^6$ m^{-1}. The measurements are conducted using a constant-temperature hot-wire anemometer. To generate weak shock waves, a two-dimensional inequality located on the test chamber sidewall was used. The dimensions of the inequality are the following: a length is 150 mm, a thickness is approximately 0.13 mm, and a width in the direction of the oncoming flow is 2.5 mm. The model is a steel flat plate with a cylindrical leading edge with a radius of (0.039 ± 0.002) mm. Controlled disturbances with a frequency multiple of 10 kHz were introduced into the flow locally from the model surface by a high-frequency glow discharge located inside the model. The direct component of the output signal of the hot-wire anemometer E is measured by a multimeter, and the variable part of the voltage is digitized by a 12-bit analog-to-digital converter (ADC) with a sampling rate of 750 kHz. At each probe position, four full measurements were performed (including four digital pulsations oscillogram measurements with a length of 16384 points in each full measurement to fill the ADC buffer to 2^{16} points), synchronized with the source of controlled disturbances. A detailed description of the experiments and data processing is given in [5].

Results. As a result of the work, the wave characteristics of disturbances were assessed using experimentally obtained phase spectra based on the transverse wave number β (the results are given in the table).

Estimation of controlled disturbances wave characteristics

n	*f*, kHz	β, rad/mm	α_r, rad/mm	χ, °
1	20	–0,8	0,48	–59.1
2	20	–1,7	0,40	–76.8
3	0	0,9	0,06	86,6

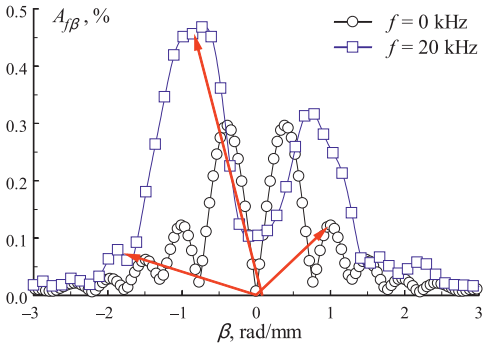

Fig. 1. Wave spectra of a stationary disturbance at x = 60 mm and the fundamental harmonic at x = 100 mm.

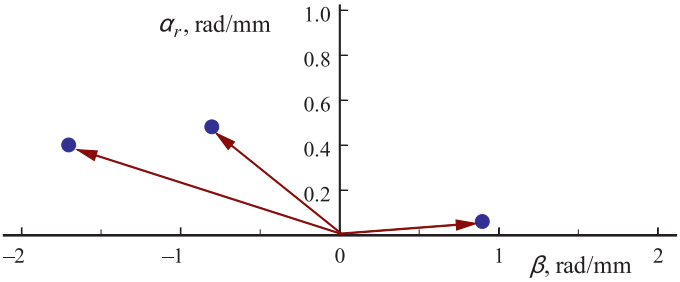

Fig. 2. Assumed triplet for the interaction of the fundamental wave and a stationary disturbance.

Typical resonant wave triplets have been identified. Figure 1 shows the wave spectra of a stationary disturbance at x = 60 mm and the fundamental harmonic at x = 100 mm. To form up the triplet (Fig. 2), data from the table were used. The arrows in Fig. 1 indicate the peaks involved.

The results obtained made it possible to identify oblique breakdown mechanism in a wave train under conditions of flow inhomogeneity and to propose conditions for the resonance fulfillment, which are given in the table. In accordance with it, an estimate of the wave number for a stationary disturbance is proposed based on the magnitude of the x coordinate where the measurements were made: $\alpha_r = \frac{2\pi}{x}$.

Conclusion. The results obtained made it possible to identify oblique breakdown mechanism in a wave train under conditions of flow inhomogeneity and to evaluate the conditions for resonance. The wave number of the longitudinal component of the wave vector for a stationary disturbance is estimated based on the value of the x coordinate where the measurements were made.

Acknowledgments. The research was supported by the Russian Science Foundation № 22-19-00666, https://rscf.ru/project/22-19-00666/. The study was conducted at the Equipment Sharing Center «Mechanics» of ITAM SB RAS.

REFERENCES

1. **Boiko A.V., Grek G.R., Dovgal A.V., Kozlov V.V.** The Origin of Turbulence in Near-Wall Flows. Springer-Verlag Berlin Heidelberg, 200. 268 p.

2. **Zhigulev V.N. and Tumin A.M.** Origin of Turbulence. Novosibirsk, 1987. 282 p.
3. **Mayer C.S.J., Wernz S. and Fasel H.F.** Numerical investigation of the nonlinear transition regime in a Mach 2 boundary layer // J. Fluid Mech., 2011, Vol. 668. P. 113–149.
4. **Kosinov A.D., Piterimova M.V., Shmakova A.V., Semionov N.V., Ermolaev Yu.G.** Experimental study of evolution of controlled perturbations in a longitudinal vortex generated in a boundary layer on a flat plate at a Mach number M = 2 // Journal of Applied Mechanics and Technical Physics. 2023. Vol. 64, No. 4. P. 656–666.
5. **Kosinov A.D., Semionov N.V., Piterimova M.V., Yatskikh A.A., Yermolaev Yu.G., Smorodsky B.V., Shmakova A.V.** Features of the wave train development in a longitudinal disturbance of a supersonic boundary layer // Journal of Applied Mechanics and Technical Physics. 2023. ONLINE FIRST.

DOI 10.53954/9785604990131_128

DETERMINATION OF VELOCITY PULSATIONS CHARACTERISTICS IN MIXING LAYER OF SUBSONIC JET BY VARIOUS METHODS

A.A. Pivovarov, I.N. Kavun, N.P. Kiselev, A.S. Pevzner

Khristianovich Institute of Theoretical and Applied Mechanics SB RAS, 630090, Novosibirsk, Russia

At present, despite of long lasting research, there is still no complete understanding of turbulent motion dynamics in gas jet flows, so studying the pulsations characteristics in the high-speed jets mixing layer is an urgent task. Contactless panoramic measurements of velocity pulsations are in demand for studying jet streams. In the work the results obtained using a pressure pulsation sensor and a panoramic laser PIV method is presents.

Experiments to study subsonic jets were carried out on the Vertical Jet Installation and on the jet module of the T-326 blow-down wind tunnel at the ITAM SB RAS. An axisymmetric flooded jet exhausted at a regime of $M_a = 0.85$ from a profiled nozzle with a radius at the cut $R_a = 30$ mm.

Numerical calculation of the jet flow was performed in the ANSYS Fluent software package. The Favre-averaged Navier-Stokes equations were solved in an axisymmetric formulation using the two-parameter *k-ω SST* turbulence model. The values of velocity fluctuations were calculated from the value of turbulent kinetic energy k, are determined by the turbulence model.

Velocity root-mean-square pulsations values level profiles in the mixing layer at points of two sections $x/R_a = 3$ and $x/R_a = 4$ are presented in Fig. 1. It can be seen that the change nature in pulsations agrees satisfactorily with each other when comparing the results obtained by using various methods.

The contours of the relative average velocity with the streamline in the mixing layer of the subsonic jet are shown in Fig. 2. The color shows the relative speed values in accordance with the scale shown at the figure top part. The data were obtained by averaging 500 instantaneous velocity fields distributions.

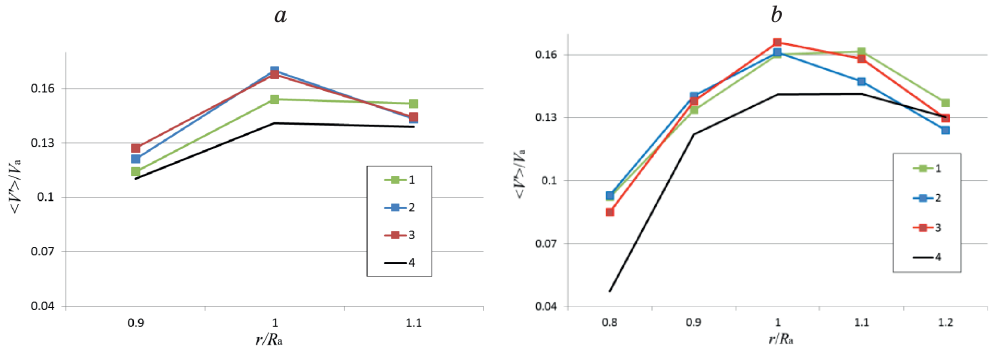

Fig. 1. Velocity pulsations relative root-mean-square values level at various points of the jet mixing layer in the cross section $x/R_a = 3$ (*a*), $x/R_a = 4$ (*b*).

1 – reconstructed velocity pulsation values based on pressure pulsation sensor data, *2* – PIV data from 500 instantaneous velocity field measurements, *3* – PIV data with increased values number to $30 \cdot 10^3$, *4* – ANSYS Fluent (*k-ω SST*) numerical calculation results.

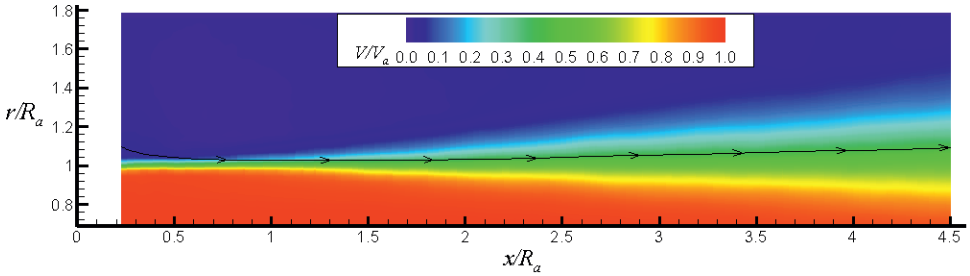

Fig. 2. Mean velocity field with a streamline along which the root-mean-square pulsations levels were calculated.

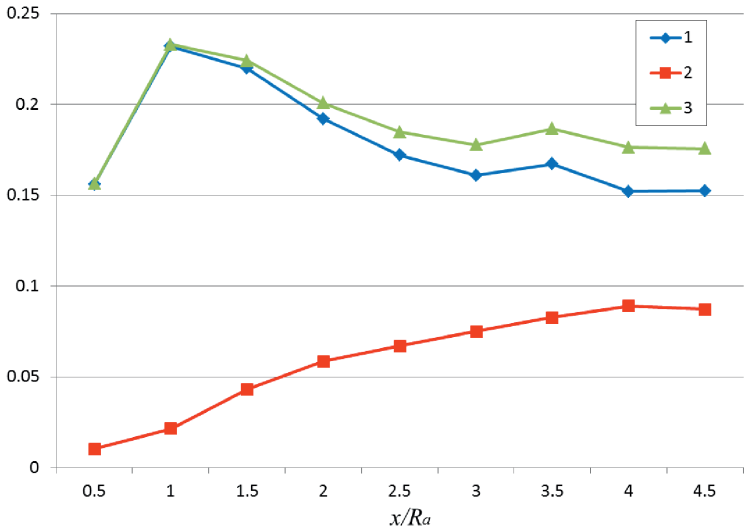

Fig. 3. Pulsations relative root-mean-square values level for various components of the velocity vector and absolute velocity in the jet mixing layer longitudinal direction.

1 – velocity longitudinal component pulsations $\langle V_x'\rangle/V_a$, *2* – velocity radial component pulsations $\langle V_r'\rangle/V_a$, *3* – absolute velocity pulsations $\langle V'\rangle/V_a$.

In Fig. 3 shows the longitudinal profiles of the relative root-mean-square values of the pulsations of the velocity vector components and the absolute velocity pulsations along the streamline flowing into the mixing layer from the space surrounding jet near the nozzle exit. According to the curves in the graph from Fig. 3, it can be noted that the main contribution to the pulsations is made by the longitudinal component V_x of the velocity in the section from $x/R_a = 0.5$ to $x/R_a = 2.0$. Downstream from the nozzle exit, the radial velocity component pulsations V_r monotonically increase and reach 50 % of the absolute velocity pulsations level V.

Data on root-mean-square velocity deviations in various sections inside the free subsonic jet mixing layer were obtained. A comparison of velocity root-mean-square pulsations levels obtained by using the PIV method and those reconstructed from data from a pressure pulsation sensor at various points in the mixing layer of jet was carried out.

The research was carried out within the framework of the Program of Fundamental Scientific Research of the state academies of sciences in 2024–2026. The study was conducted at the Joint Access Center «Mechanics» of ITAM SB RAS.

DOI 10.53954/9785604990131_130

QUADROCOPTER FOR STUDYING ATMOSPHERIC TURBULENCE

P.A. Polivanov, G.A. Berkon, V.V. Markin

Khristianovich Institute of Theoretical and Applied Mechanics SB RAS
630090, Institutskaya 4/1, Novosibirsk, Russia

Measuring wind characteristics in the atmospheric boundary layer is an important task not only for meteorological problems, but also for various issues related to ecology, wind energy, construction, etc. One of the most modern methods for measuring wind conditions is various acoustic (sodar) and optical (lidar) wind detection systems [1]. The advantage of such systems is the possibility of contactless measurement of the atmosphere in a wide range of altitudes, up to ≈1 km for sodar and ≈10 km for lidar systems. One of the disadvantages of such systems is the limitation in spatial resolution, which can be tens of meters or more. This problem arises especially acutely in the study of atmospheric turbulence. To solve this problem it is possible by using multirotor aerial vehicles equipped with a pitot tube [2] or other measuring system. The problem with this approach is the need to turn the aircraft into the wind. Another approach was used in [3] in which the atmospheric boundary layer was studied using a DJI drone. The main idea is to determine the velocity and direction wind based on the angle of the quadcopter without the use of additional measuring systems. The drone in position holding mode needs the groundspeed to be zero, respectively the true airspeed should be equal to the wind speed and be opposite to it. In this case the airspeed of the quadcopter is determined by the angle of inclination of the drone. The disadvantage of work [3] is the use of a non-specialized quadcopter with a complex shape, which significantly complicated data analysis. The goal of this paper is to design a specialized weather drone with aerodynamics optimized for studying wind characteristics, including atmospheric turbulence.

To solve this problem computational and experimental studies were carried out on the effect of the quadcopter shape (ball, teardrop-shaped and keel-shaped) on the accuracy of determining the direction and velocity of the wind. During these studies the aerodynamic characteristics of the quadcopter without propellers and with rotating propellers with a fuse-

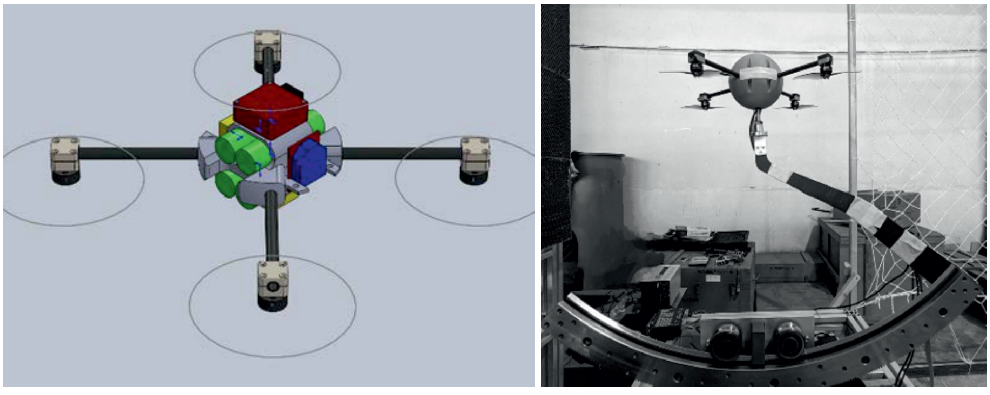

Fig. 1. a) Sketch draw and b) photo of the meteodrone

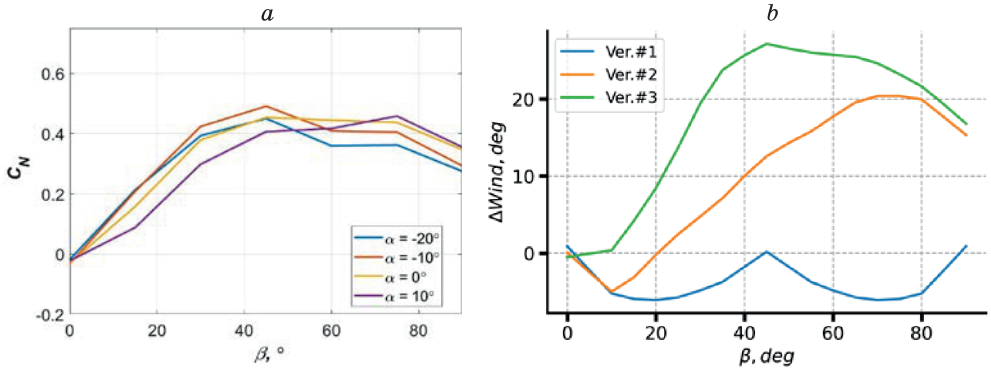

Fig. 2. a) Coefficient of side force and b) the difference between the wind direction and the tilt direction of the quadcopter depending on the side-slip angle

lage of various shapes were determined. After which a prototype of a meteodrone was design and assembled (Fig. 1a). The prototype was used to perform research on the response of a drone to gusts of wind simulating atmospheric turbulence. For this purpose a multifan aerodynamic stand was used [4] (Fig. 1b), which makes it possible to generate complex air flow, similar of atmospheric turbulence.

An example of the data is shown in Fig. 2. The dependence of the coefficient of side force on the side-slip angle for the fin-shaped version of the fuselage is shown in Fig. 2.a. It is clearly seen that with increasing side-slip angle there is a sharp increase in side force, which stops at a side-slip angle of about 40°. In Fig. 2b shows the uncertainty in detecting wind direction for various radome configurations depending on the side-slip angle of the drone. It is clearly seen that at small side-slip angles the uncertainty in detecting the wind direction weakly depends on the shape of the fuselage. But for large side-slip angles for elongated shapes (ver. 3), the uncertainty in determining the wind direction can reach ≈30 degrees, which must be taken into account when using non-specialized drones when studying wind characteristics.

As a result not only a meteodrone was designed and created that allows for research of wind conditions, but also a method for its dynamic calibration was developed, which allows it to be used for studying atmospheric turbulence

REFERENCES

1. **Sterlyadkin V.V., Gorelik A.G., Shchukin G.G.** Review of methods and means of wind sensing of the atmosphere // Problems of remote sensing, propagation and diffraction of radio waves: III All-Russian Armand readings: Youth school. – Murom, 2013. – pp. 24–42 (in Russian)
2. **Fuertes F.C., Wilhelm L., and Porté-Agel F.** Multirotor UAV-Based Platform for the Measurement of Atmospheric Turbulence: Validation and Signature Detection of Tip Vortices of Wind Turbine Blades // J. Atmos. Oceanic Technol. 2019. 36, 941–955, https://doi.org/10.1175/JTECH-D-17-0220.1.
3. **Shelekhov A., Afanasiev A., Shelekhova E., Kobzev A., Telminov A., Molchunov A., Poplevina O.** High-Resolution Profiling of Atmospheric Turbulence Using UAV Autopilot Data // Drones. 2023; 7(7):412. https://doi.org/10.3390/drones7070412
4. **Berkon G.A., Polivanov P.A.** Development of a multi-fan stand "Aerosten" for the study of small UAVs. // "NPO-2023" Publishing house of NSTU, 2023. – P. 140–145. (in Russian)

DOI 10.53954/9785604990131_132

NUMERICAL SIMULATION OF DISTRIBUTED BLOWING ON A BODY OF REVOLUTION IN A SUPERSONIC FLOW

A.N. Popkov, V.I. Kornilov

Khristianovich Institute of Theoretical and Applied Mechanics SB RAS, 630090, Novosibirsk, Russia

Improvement of aerodynamic efficiency and increasing flight range and payload, as well as reducing both fuel costs and direct operating costs of an aircraft are one of the urgent tasks of applied research in recent decades. Blowing of air or other gases into turbulent boundary layer through a high-tech finely perforated wall [1] seems to be one of the effective ways to reduce local skin friction and aerodynamic drag of the bodies of revolution (BRs). However, the efficiency of using this approach under the conditions of flow around such bodies in a supersonic flow still remains unknown due to the lack of any research [2].

This work is a continuation of studies carried out at subsonic velocities [2]. It was undertaken in a supersonic flow with the aim of studying the efficiency of air blowing on the BR with an aspect ratio of 25.3 at its axisymmetric flow around. To organize distributed blowing, a perforated section 76 mm long, a flush-mounted (with the main BR surface) was used. The frontal boundary of section was located at a distance of 901.3 mm (x/L = 0.342) from the BR tip. The parameters of the perforated material itself are: degree of permeability (open cross-sectional area of the holes) 22 %, average diameter of staggered holes 0.3 mm.

ANSYS Fluent software package was used to solve the task. The computations are made for the unit number of Reynolds $\mathrm{Re}_1 = 15.3 \times 10^6$ 1/m, which corresponds to the flight mode at $\mathrm{M}_\infty = 2$ at a height of 10 km. The mathematical modeling of the blowing process was carried out in a three-dimensional approach. The maximum number of cells in the calculated region is 13.2 million. The computational grid was refined so that the known parameter y^+ in the near-wall layer was not higher than 40. With a lower magnitude in the y^+, the flow structure in near wall region is significantly detailed and becomes insignificant.

The results of studies of the mean flow parameters in the boundary layer with changes of the blowing intensity, as well as the aerodynamic drag C_x of the BR and its components C_{xp} and C_f, give the opportunity to be noted the following:

– streamlines and Mach number contour in the vicinity of the blowing region, presented in Fig. 1*a* for intermediate blowing intensity $\mathrm{M}_b/(\mathrm{M}_b)\mathrm{max} = 0.3$, show the flow structure to be largely similar to that which is formed when flow around a body with an obstacle located on its surface. A microjet array can be considered as a liquid transversely located obstacle that has a braking effect on the primary flow. This leads to a corresponding increase in pressure upstream. As a result, such structural flow features as a flow separation, frontal and rear recirculation regions, and other peculiarities are formed in the analyzed region. These features become especially noticeable with increasing blowing intensity (Fig. 1*b*), which is confirmed by the wave structure of the flow. It follows from it that an increase in the blowing intensity leads to the formation of a shock wave in front of the blowing region, rarefaction waves that arise at the flow around a near-wall layer pressed away from the surface, a shock wave in the region where the separated flow attaches, and other flow features;

– distributed blowing through a perforated section of the BR surface ensures a significant gain not only in friction drag C_f, but also in the total aerodynamic drag C_x of the body as

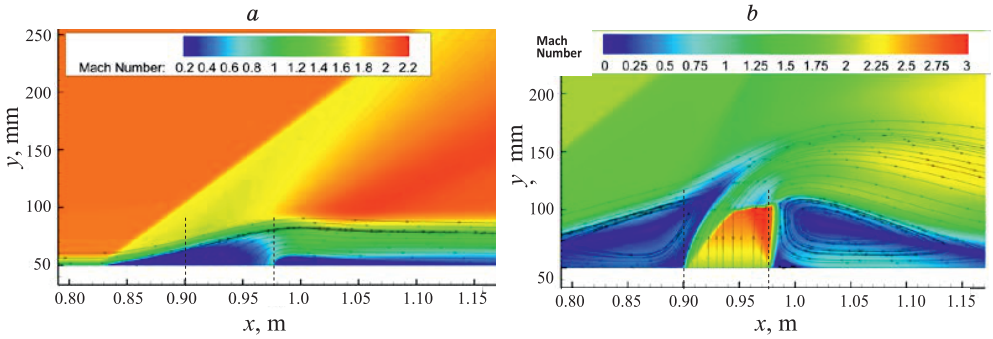

Fig. 1. Streamlines and Mach number contour in the vicinity of the blowing region at $(M/M_b)max = 0{,}3$ (*a*) and $(M/M_b)max = 1{,}0$ (*b*).

Frontal and rear boundaries of perforated section are shown by the dashed lines.

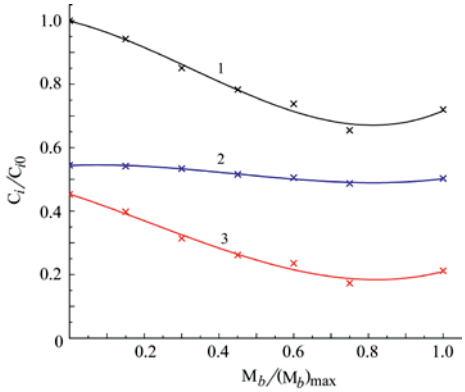

Fig. 2. Dependence of normalized values of total aerodynamic drag of the BR (1) and its components caused by pressure force (2) and friction force (3) as functions of normalized blowing intensity.

Lines are approximation of computed values.

compared to that for the base configuration. A stable decrease in C_x value, which is of great practical interest, is observed up to $M_b/(M_b)max = 0.75$ and reaches approximately 34 %. However a complex flow structure is formed over the blowing region at a minimum C_x value, the mechanism of which is not entirely clear. The result obtained here also requires a correct assessment of the energy costs for the injection process. This is important, since under conditions of significant blowing intensity, the gain in the BR drag can significantly decrease until it disappears completely.

Analogous studies carried out for the BR with an equivalent conical head part reveal a qualitative similarity in the behavior of the aerodynamic drag C_x of the body and its components C_{xp} and C_f versus the blowing intensity.

This work was carried out within the frame of a state assignment.

REFERENCES

1. **Kornilov V.I.** Current state and prospects of researches on the control of turbulent boundary layer by air blowing // Progress in Aerospace Sciences. 2015. Vol. 76. P. 1–23.
2. **Kornilov V.I., Popkov A.N.** State and prospects of researches on the control of turbulent boundary layer by air blowing on a body of revolution (review) // J. Applied Mechanics and Technical Physics. 2023. Online-First, eLIBRARY ID: 54386974 https://www.elibrary.ru/item.asp?id=54386974 (in Russian).

DOI 10.53954/9785604990131_134

VISCOSITY OF HYBRID NANOFLUIDS WITH CARBON NANOTUBES. MOLECULAR DYNAMIC SUMULATION

V.Ya. Rudyak[1], S.L. Krasnolutskii[1], E.V. Lezhnev[1, 2]

[1]*Novosibirsk State University of Architecture and Civil Engineering, 630008, Novosibirsk, Russia*

[2]*Novosibirsk State Technical University, 630073, Novosibirsk, Russia*

The unusual properties of nanofluids have been successfully studied for more than twenty-five years. They are already actively used or are planned to be used in various biomedical, cosmetological or thermophysical technologies, in the creation of new materials, in tribology, in pharmacology, etc. [1–4]. In recent years, along with conventional nanofluids, carbon nanotube nanofluids (CNTs) and hybrid nanofluids have been actively studied [5–8]. Quite significant data have already been accumulated here. In particular, it has been experimentally shown that the properties of hybrid nanofluids differ significantly from those of conventional nanofluids with spherical nanoparticles and from those of nanofluids with CNTs. Hybrid nanofluids are an extremely complex object. Their properties depend on the concentration of nanoparticles and CNTs, on the size and material of the nanoparticles, and on the properties of the base liquid. The difficulty also lies in the fact that the morphology of the hybrid fluid is extremely complex. On the one hand, nanoparticles with characteristic sizes from one to one hundred nanometers are mesoobjects. On the other hand, the diameter of CNTs falls well within this gap, while their length can reach tens of micrometers. In addition, CNTs can be single-wall and multi-wall. In some cases, it is necessary to use various dispersants, which further complicates the situation. For this reason, despite the large number of publications on the study of the thermophysical properties of hybrid nanofluids, there is still a lack of understanding of the reasons determining these properties. This is due, in particular, to the fact that publications actually present data on completely different nanofluids, the properties of which are not only difficult to compare, but often impossible. Nevertheless, applications require a clear understanding of the causes that cause changes in certain properties of nanofluids. Here, of course, systematic experiments performed on nanofluids of the same class (on the same base fluids, nanoparticles, dispersants, etc.) are necessary. At the same time, experiments do not reveal the mechanisms of transport processes in such complex dispersed liquids, which is necessary to create nanofluids with specified controlled properties. The transport processes in fluids are determined by the corresponding transport coefficients. Since the latter are of a molecular nature, it is possible to identify their features only using appropriate methods. The optimal tool of this kind is the method of molecular dynamics.

The purpose of this work is to systematically model and study the viscosity of hybrid nanofluids with single-walled carbon tubes and copper nanoparticles using the molecular dynamics method. The identification of the features of the transport processes of hybrid nanofluids required their systematic comparison with the properties of nanofluids with CNTs and nanofluids with conventional nanoparticles. For this reason, the article simultaneously studies the properties of nanofluids with CNTs and nanofluids with copper and carbon nanoparticles. Benzene was used as the base fluid in all studied nanofluids. In hybrid nanofluids, CNTs of the armchair type with chirality (8.8) were used, and their length was 14.6 nm. The volume concentration of CNTs was 1–2 %, and the concentration of nanoparticles varied from 1 to 5 %. When studying the viscosity of nanofluids with CNTs, the length

of the latter varied from 1.1 to 14.6 nm, and their mass concentration from 1 to 15 %. The nanoparticle sizes were 1.4, 2.5 and 3.2 nm. The maximum concentration of copper and carbon nanoparticles was 5.8 %.

The shear viscosity coefficient was determined by the fluctuation-dissipation theorem, known in the literature as the Green–Kubo formula [9, 10]. All calculations were performed at atmospheric pressure and temperature of 25 °C. The interaction of benzene and carbon molecules with each other was determined by the Lennard-Jones potential. The interaction of benzene molecules with graphite or copper nanoparticles was described by the Rudyak–Krasnolutskii potential [11]. The Rudyak–Krasnolutskii–Ivanov potential is used as the interaction potential of graphite or copper nanoparticles [12].

It was found that the viscosity coefficient of all studied hybrid nanofluids increases with increasing concentration of both CNTs and nanoparticles. It is significantly higher than the corresponding values for nanofluids with CNTs and nanoparticles. The viscosity coefficient of nanofluids with CNTs increases with increasing concentration and this increase is significantly higher than predicted by the corresponding theories for coarse dispersed liquids (see [13] and etc.). The viscosity of nanofluids with CNTs at a given concentration increases with increasing their length. It was further established that the viscosity of nanofluids with CNTs at fixed mass concentrations is higher than the corresponding values for nanofluids with spherical particles. The viscosity coefficient of a nanofluid with copper particles at the same volume concentrations is higher than that of a nanofluid with carbon particles. It has been shown that the main reason for the increase in the viscosity of the nanofluid compared to the corresponding value for the base fluid is the structuring of the molecules of the base fluid near nanoparticles or CNTs. This structuring is determined by the parameters of the interaction potential of the base fluid molecules with nanoparticle atoms or CNTs and their surface area.

The work is supported by the Russian Science Foundation (Grant No. 20-19-00043).

REFERENCES

1. **Li J., Zhang X., Xu B., Yuan V**. Nanofluid research and applications: A review // Int. Com. Heat and Mass Transfer. 2021. Vol. 127. P. 105543.
2. **Zhao J., Huang Y., He Y., Shi Y**. Nanolubricant additives: A review // Friction. 2021. Vol. 9. No. 5. P. 891–917.
3. **Pordanjani A.H., Aghakhani S.. Afrand M., Mahmoudi B., Mahian O., Wongwise S**. An updated review on application of nanofluids in heat exchangers for saving energy // Energy Convers. Manag. 2019. Vol. 198. P. 111886.
4. **Rudyak V.Ya., Minakov A.V.** Modern Problems of Micro and Nanofluidics, Science, Novosibirsk, 2016, 296 p.
5. **Rudyak V.Ya., Dashapilov G.R., Minakov A.V., Pryazhnikov M.I**. Comparative characteristics of viscosity and rheology of nanofluids with multi-walled and single-walled carbon nanotubes // Diamond & Related Mat. 2023. Vol. 132. P. 109616.
6. **Rudyak V.Ya., Pryazhnikov M.I., Minakov A.V., Shupik A.A.** Comparison of thermal conductivity of nanofluids with single-walled and multi-walled carbon nanotubes. Diamond & Related Mat. 2023. Vol. 139. P. 110376.
7. **Suneetha S., Subbarayudu K. Reddy P.B.A**. Hybrid nanofluids development and benefits: A comprehensive review // J. Ther. Eng. 2022. Vol. 8, No. 3. P. 1–11.
8. **Babar H., Ali H.M.** Towards hybrid nanofluids: Preparation, thermophysical properties, applications, and challenges // J. Mol. Liquids. 2019. Vol. 281. P. 598–633.
9. **Allen M.P., Tildesley D.J.** Computer Simulation of Liquids. Oxford University Press, 1987.
10. **Rudyak V.Ya**. Fluctuation-dissipation theorems and transport coefficients of the gases, liquids and nanofluids // J. of Physics: Conference Series. 2020. V. 1560. P. 012002.
11. **Rudyak V.Ya., Krasnolutskii S.L .** Simulation of the thermal conductivity of a nanofluid with small particles by molecular dynamics methods // Technical Physics. 2017. V. 62. No. 10. P. 1456–1465.
12. **Rudyak V.Ya., Krasnolutskii S.L., Ivanov D.A.** 2012. The interaction potential of nanoparticles. Doklady Physics. V. 57. P. 33–35
13. **Einstein A**. A new determination of molecular dimensions. Ann. Phys. 1906. Bd. 19. S. 289–300.

DOI 10.53954/9785604990131_136

MOLECULAR DYNAMICS SIMULATION OF FLUID AND NANOFLUID RHEOLOGY IN NANOCHANNELS

V.Ya. Rudyak, T.A. Rafalskaya

Novosibirsk State University of Architecture and Civil Engineering, Leningradskaya, 113, Novosibirsk, 630008, Russia

Interest in nanofluids appeared more than twenty years ago and was initiated by their possible thermophysical applications. Later it turned out that the area of their applicability is much wider and includes biomedical, pharmacological, and cosmetic technologies; the first results of their use in the oil and gas industry have already appeared [1–3]. One of the actively implemented applications of nanofluids is tribology. It appears that the use of nanoparticles to create lubricants is extremely promising for various reasons. Quite a lot of publications has already accumulated here, which you can get acquainted with through reviews [4–7]. The problems that arise here are manifold. From a practical point of view, the issue of the viscosity and rheology of the nanofluids used is extremely important. Today, it has been experimentally reliably established that approximately a quarter of conventional nanofluids in volume have non-Newtonian rheology, although the base fluids were Newtonian fluids [8, 9]. In modern devices, the thickness of the lubricant film varies, ranging from several nanometers. It is easy to see that the shear rates are quite high. But with increasing shear rate, even ordinary Newtonian fluids become non-Newtonian [10]. In addition, the interaction of fluid molecules with the walls of sufficiently small channels can also change the viscosity [11]. It is almost impossible to measure viscosity and determine the rheology of fluids and nanofluids in nanochannels. The only constructive method for studying them is molecular simulation. Molecular dynamics simulation of the viscosity and rheology of benzene and nanofluids based on it in nanochannels is the goal of this work. The main task was to determine the dependence of the viscosity and rheology of the base fluid and nanofluids on the distance between the moving walls (height) of the channel, which varied from 6 to 30 nm.

Simulation of the viscosity and rheology of benzene and nanofluids was carried out using the so-called nonequilibrium molecular dynamics method in the version with simulation of Couette shear flow between two plates [12]. The simulation was carried out in the LAMMPS package at atmospheric pressure and a temperature of 298 K. A Langevin thermostat was used to stabilize the flow. The channel walls were modeled by copper atoms located at the nodes of a face-centered crystal lattice. The walls were given constant velocities having opposite directions; a close to linear profile of the average molecular velocity was established in the channel, from which the shear rate $\dot{\gamma}$ and the corresponding shear stresses τ were determined. The viscosity coefficient η was calculated from the shear stress of the fluid: $\eta = \tau / \dot{\gamma}$.

To create the nanofluid, copper particles with a diameter of 3 and 6 nm were used, their concentration varied from 2 to 6 %. The interaction of benzene molecules and copper atoms was described by the Lennard-Jones potential. The interaction of nanoparticles with benzene molecules and with copper walls was described by the Rudyak-Krasnolutskii potential [13], and the interaction of nanoparticles with each other by the Rudyak-Krasnolutskii-Ivanov potential [14]. The number of benzene molecules varied from 5000 to 33000, nanoparticles – from 2 to 20.

As a result of systematic simulation, it was established that the base fluid is Newtonian over a wide range of shear rates. In this case, in the channel of maximum height (30 nm), viscosity of based fluid is in good agreement with the value experimentally observed in the volume. However, starting from a certain critical shear rate, the rheology of benzene, even in such a relatively large channel, changes. Benzene becomes a pseudoplastic fluid.

With decreasing channel height, the viscosity of benzene increases, and in a channel of minimum height (6 nm), it almost doubles. Simultaneously with a decrease in the height of the channel, the critical shear rate of change in its rheology also decreases. At the same time, with increasing shear rate, the difference between the viscosity of benzene in channels of different heights quickly decreases. For example, at a shear rate of $5 \cdot 10^7$ s^{-1}, the viscosity of benzene in a 6 nm channel is 1.75 times higher than in a 30 nm channel, and at a shear rate of $8 \cdot 10^{10}$ s^{-1} the increase of viscosity is only 1.08 times.

In the second part of the report, the viscosity and rheology of nanofluids was studied. It is shown that in channels with heights of 30, 24 and 12 nm, the nanofluid at low shear rates is also Newtonian. Its viscosity is well described by a quadratic function of the particle concentration, and the smaller the particle size, the greater it is. In all cases, the value of the viscosity coefficient is significantly higher than that predicted by classical theories for coarse fluids (Einstein, Batchelor, etc.). Further, with a decrease in the channel height and an increase in the shear rate, all nanofluids become pseudoplastic. The corresponding critical shear rates are determined and their dependence on the channel height and nanoparticle concentration is obtained. Finally, the mechanisms of change in the rheology of nanofluids are discussed.

The work was supported by the Russian Science Foundation (grant No. 20-19-00043).

REFERENCES

1. **Li J., Zhang X., Xu B., Yuan V**. Nanofluid research and applications: A review // Int. Com. Heat and Mass Transfer. 2021. Vol. 127. P. 105543.
2. **Yaqoob S.B., Adnan R., Khan R.M.R., Rashid M.** Gold, silver, and palladium nanoparticles: A chemical tool for biomedical applications // Front. Chem. 2020. Vol. 8 P. 376–392.
3. **Rubbi F., Das L., Habib K., Aslfattahi N., Saidur R., Alam S. Ul.** A comprehensive review on advances of oil-based nanofluids for concentrating solar thermal collector application // J. Mol. Liq. 2021. Vol. 38. P. 116771.
4. **Kong L., Sun J., Bao Y.** Preparation, characterization and tribological mechanism of nanofluids // RSC Adv. 2017. Vol. 7. P. 12599–12609.
5. **Paul G., Hirani H., Kuila T., Murmu N.C.** Nanolubricants dispersed with graphene and its derivatives: an assessment and review of the tribological performance // Nanoscale. 2019. Vol. 11. P. 3458–3483.
6. **Zhao J., Huang Y., He Y., Shi Y.** Nanolubricant additives: A review // Friction. 2021 Vol. 5. P. 891–917.
7. **Ouyang T., Lei W., Tang W., Cheng L., Shen Y.** Synergistic low friction effect and mechanism of inorganic fullerene-like tungsten disulfide and talcum at the interface of steel tribo-pairs under severe conditions // Applied Surface Sci. 2022. Vol. 585. P. 152570.
8. **Sharma A.K., Tiwari A.K., and Dixit A.R.** Rheological behaviour of nanofluids: A review // Renewable and Sustainable Energy Reviews. 2016. Vol. 53, P. 779– 791. DOI: 10.1016/j.rser.2015.09.033.
9. **Minakov A.V., Rudyak V.Ya., Pryazhnikov M.I.** Rheological behavior of water and ethylene glycol nanofluids with oxide nanoparticles // Colloids and Surfaces: Physicochemical and Engineering Aspects. 2018. Vol. 554. P. 279–285.
10. **Rudyak V.Ya., Belkin A.A., Rafalskaya T.A.** Molecular dynamics modeling rheology of nanofluids // J. Technical Physics Letters. 2023. Vol. 49. No. 10. P. 1–4.
11. **Rudyak V.Ya., Belkin A.A.** Molecular-dynamics simulation of fluid viscosity in nanochannels // Nanosystems: Physics, Chemistry, Mathematics. 2018. No. 9. P. 349–355.
12. **Rapaport D.C.** The art of molecular dynamics simulation // Cambridge University Press, Cambridge. 2004. P. 549.
13. **Rudyak V.Ya., Krasnolutskii S.L.** Diffusion of nanoparticles in rarefied gas // J. of Technical Physics. 2002. T. 72. No. 7. P. 13–20.
14. **Rudyak V.Ya., Krasnolutskii S.L., Ivanov D.A.** On the interaction potential of nanoparticles // Reports of the Academy of Sciences. 2012. T. 442. No. 1. P. 54–56.

DOI 10.53954/9785604990131_138

EXPERIMENTAL STUDY OF SUBSONIC BOUNDARY LAYER DISTURBANCES AND CONTROL OF THEIR DEVELOPMENT

I.A. Sadovskiy

Institute of Theoretical and Applied Mechanics. S. A. Khristianovich, Siberian Branch of the Russian Academy of Sciences 630090, Novosibirsk, Russian Federation

Suction of liquid or gas from the surface of a streamlined body is a universal tool for controlling the development of disturbances in the shear layer, including natural disturbances. Reducing the intensity of natural disturbances can delay the laminar-turbulent transition and reduce friction resistance. In [1], a study was carried out of the effect of gas suction through a transversely located slit on the development of natural wave disturbances in the boundary layer of a flat plate. The authors found that disturbances are most effectively suppressed at the linear and weakly nonlinear stages of development.

The development of material processing techniques makes it possible to obtain permeable surfaces that have the property of hydrodynamic smoothness, i.e. flow around such surfaces is equivalent to flow around smooth, impenetrable analogues. Permeable surfaces treated in this way can serve as the basis for organizing distributed gas suction from the surface, and in the unused state, the surface through which gas is removed flows around as smooth.

This paper presents the results of fundamental research on the control of self-disturbances using a hydrodynamically smooth surface in the boundary layers of straight and swept wings. A study was carried out of disturbances both developing naturally and amplified by an external acoustic field. This method of amplifying disturbances has been widely tested and used, including in works [2, 3]. Experimental studies were carried out using the T-324 wind tunnel of the ITAM SB RAS. To carry out measurements in the flow, a hot-wire anemometer equipped with a single-filament sensor was used.

The first set of experiments was carried out using a straight wing model, with a cross section of NACA 0012 with a maximum thickness of 60 mm. In the wing, at a distance of 312 mm from the leading edge, there was an aluminum hydrodynamically smooth permeable surface through which suction was carried out. The dimensionless suction coefficient was 0.019. The distributed impact on disturbances at the linear and nonlinear stages of development was studied. The amplitude of nonlinear disturbances in the area of influence of suction was an order of magnitude greater than the amplitude of linear ones. After activating gas suction through the surface, the amplitude of both disturbances developing naturally at the linear and nonlinear stage of development, and those amplified by acoustics, decreased to minimal values and did not increase in the measurement area. The separation of the boundary layer that occurs at a distance of 435 mm from the leading edge was also eliminated. Thus, the amplitude of disturbances at the linear stage of development was reduced by 10 times, amplified by acoustics by 20 times. The amplitude of disturbances at the nonlinear stage of development was reduced by two orders of magnitude.

The next series of experiments was carried out using a model representing a section of a swept wing with a chord of 807 mm, a span of 950 mm and a sliding angle of 30°. In this setting, among other things, the question of the required intensity of distributed impact to

obtain a sustainable effect of reducing the amplitude of disturbances was investigated. It turned out that in this setting, to reduce the amplitude of average velocity pulsations from 12 to 3 % U_∞ at the end of the measurement region, it is enough that the suction coefficient is $C_s = 0{,}029$. To suppress acoustically amplified disturbances from 13 to 0,3 % U_∞ the suction intensity was increased to $C_s = 0{,}043$.

To test the hypothesis that the main contribution to the suppression of disturbances comes from the elimination of separated flow, setups were implemented both with the presence of a local separation bubble and continuous flow. The results obtained give grounds to assert that the effectiveness of the distributed impact on the flow through a hydrodynamically smooth surface in terms of suppressing the growth of disturbances is due not only to the addition of a separated flow, but in general to a change in the flow stability parameters.

The research was supported by the Russian Science Foundation №23-29-00670,https://rscf.ru/en/project/23-29-00670/

REFERENCES

1. **Kozlov V.V., Levchenko Y.A., Scherbakov V.A.** Development of perturbations in the boundary layer during slit suction // Scientist. zap. TSAGI. – 1978. – Vol. 9. – No. 2. – P. 99–105.
2. **Dovgal A.V., Kozlov V.V., Simonov O.A.**. Sound excitation of boundary layer vibrations on a swept wing // TsAGI Research Notes. 1989. Vol. 20. – No. 6. – P. 21–26.
3. **Mangiarotty R.A., Bohn A.** Wind tunnel study of acoustical disturbance effect on controlled laminar flow // AIAA J. 1980. Vol. 18, No. 7.

DOI 10.53954/9785604990131_140

END PLATES INFLUENCE ON SQUARE PRISM DRAG COEFFICIENT

S.D. Salenko, I.S. Konovalov, Yu.A. Gosteev

Novosibirsk state technical university
630092, Novosibirsk, Russia

During study aerodynamics and aeroelasticity of building structures elements, it is often necessary to study sectional models of extended prismatic structures. In this case, the flow pattern of a large prism elongation must be reproduced on a relatively small elongation prism. End plates are often used for this purpose. There are problems of assigning the optimal end plates diameter D and correct introduction of corrections for recalculation of obtained results for a given (in the limit infinite) elongation.

Within of the bridge suspension aerodynamic characteristics investigations, wind tunnel force tests and numerical computations of a square prism cross flow with elongation $\lambda = 7.7$ with several variants of round end plates having relative diameter $D/H = 0…5.1$. The side of the square prism $H = 78$ mm. both in experiments and in computations were carried out. Input flow parameters: Reynolds number $Re \approx 10^5$, turbulence intensity $\varepsilon = 0.35$ %.

Fig. 1 shows a vortex structures visualization near the models obtained numerically by detached eddy simulations DES. As can be seen, the end plates presence (in this case with $D/H = 2.5$) suppresses the large end vortices development, and horseshoe-shaped vortices appear near the end sections of the prism (Fig. 1, b).

It is known that the finite elongation model has significantly smaller aerodynamic coefficients values, in particular, the drag coefficient c_d, compared to the infinite elongation model [1]. End plates using brings the flow closer to two-dimensional flow and increases the effective elongation of the model [2], but at present it is difficult to identify an unambiguously approved methodology for recalculating the characteristics of bluff bodies obtained on the sectional model to the characteristics of the body with infinite elongation. In this paper, a method developed on acceptable assumptions about the distribution of the drag coefficient over the span of the prism was used.

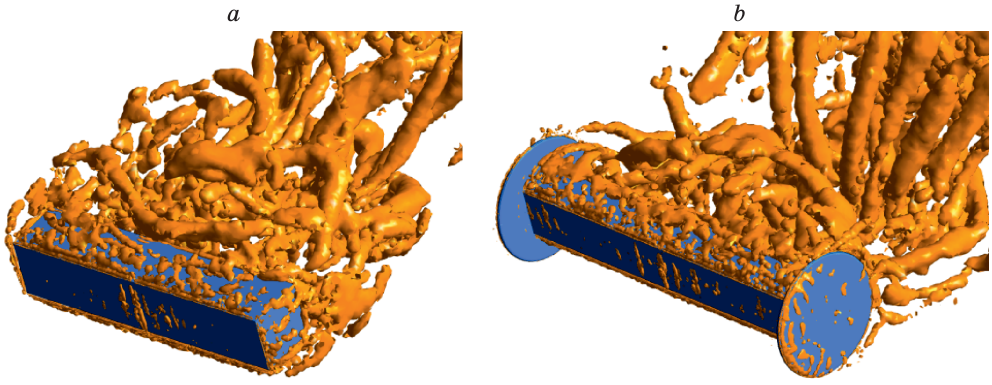

Fig. 1. Instantaneous iso-surface of the Q-criterion at $Q = 0.2Q_{max}$ around of the model without (*a*) and with end plates (*b*) ($D/H = 2.5$).

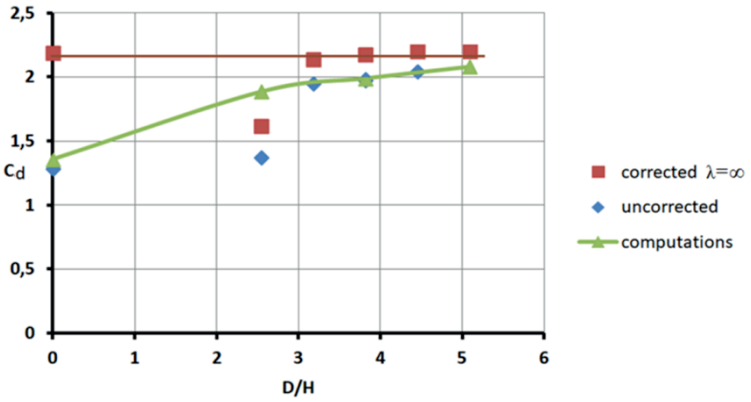

Fig. 2. Comparison of experimental and calculated drag coefficient values of a square prism.

Fig. 2 shows a comparison of wind tunnel force test results with the numerical calculation results depending on the relative end plates diameter. The experimental results are shown with and without corrections for model elongation and relative end plates diameters. In general, note a good agreement between the experimental and calculated results, as well as falling out of the general experimental trend of the point corresponding to the above-mentioned case $D/H = 2.5$. It should be noted that when testing this model variant in a wind tunnel, a pronounced bistability of the flow was observed. In this case, the lift force fluctuations amplitude spontaneously changes several times with time. Such an effect was not observed in the calculations.

The work results show that the adopted methodology for introducing corrections makes it possible to recalculate the results obtained experimentally or numerically with relatively small elongation to a given (in the limit infinite) elongation. The scatter of the c_d values for $\lambda = \infty$ calculated on the basis of data for models with effective elongation $\lambda = 7.7\ldots13.5$ does not exceed ±4 %. The average value of $c_d = 2.17$ for all variants (except for bistable flow) lies within the range of c_d values according to numerous sources and normative documents.

REFERENCES

1. **Cowdrey C.F.** A Note on the Use of End Plates to Prevent Three-dimentional Flow at the Ends of Bluff Cylinders // London: Her Majesty's Stationery Office, 1963, No. 683.
2. **Wenyong Ma, Bocheng H., Deqian Zh., Meng Lu and Haiyun Li.** Effect of the presence of end plates and aspect ratio on the aerodynamic forces on circular cylinders in various flow regimes // Fluid Dynamics Research. 2019. Vol. 51, 21 pp. DOI: 10.1088/1873-7005/ab2ff7.

DOI 10.53954/9785604990131_142

ENHANCED ANTICANCER CYTOTOXIC EFFECT OF CO-TREATMENT WITH COLD ATMOSPHERIC PLASMA JET AND GOLD NANOPARTICLES

I. Schweigert, M. Biryukov, A. Polyakova, N. Krychkova, E. Gorbunova, O. Koval, E. Milakhina, P. Gugin, Dm. Zakrevsky

Khristianovich Institute of Theoretical and Applied Mechanics, 630090, Novosibirsk, Russia

Efficient and biologically safe mode of cold atmospheric plasma jet (CAPJ) is crucial for the development of CAPJ-based anticancer therapy. In the experiment and numerical simulations, by changing the pulse duration of a positive-pulsed (PP) voltage, we found the optimal helium CAPJ modes with a regular streamer propagation and a maximum safe discharge current at $T < 42$ °C [1,2]. These CAPJs substantially suppressed the viability of cancer cells. To enhance a cytotoxic effect of CAPJ treatment, gold nanoparticles (NPs) were added to the cells before and after the CAPJ exposure. Combination of CAPJ, generated with the PP voltage, and gold nanoparticles decreased the viability of NCI-H23 epithelial-like lung adenocarcinoma, A549 lung adenocarcinoma, BrCCh4e-134 breast adenocarcinoma and uMel1 uveal melanoma cells. Polyethylene glycol-modified nanoparticles with attached fluorescent labels were used to visualize the uptake of NPs. The treatment with optimal CAPJ modes in combination with modified NPs, bearing the cancer-addressed molecules and therapeutics may be the next strategy of strengthening the CAPJ-based antitumor approaches. We also studied the molecular basis for selectivity of the cytotoxic response of lung adenocarcinoma cells to CAPJ [3].

For CAPJ with the PP voltage, the effect of the pulse length on streamer propagation is shown in Fig. 1 (experiment) and Fig. 2 (simulations). The applied voltage and the current were measured on a shaved mouse skin during exposure to the PP voltage CAPJ. For a pulse length $\tau = 7$ μs, the current I is registered in each voltage cycle and I = 4.8 mA. For $\tau = 14$ μs, the current frequency on the treated skin is a half of the voltage frequency $f_I = f/2$ and I = 2.2mA (He flow, v = 9 L/min, nozzle-surface gap, d = 2.5 cm). The fluorescent labels (FAM) were attached to NPs covered with polyethylene glycol (PEG) to visualize the penetration of NPs into the cancer cells under CAPJ exposure. NP-PEG-FAM (20 nM) were added to the cells immediately (0 h) or 0.5–4 hours after the CAPJ treatment. Flow cytometry analysis of the cells was made one hour later. Data in Fig. 3(a) are presented as MFI

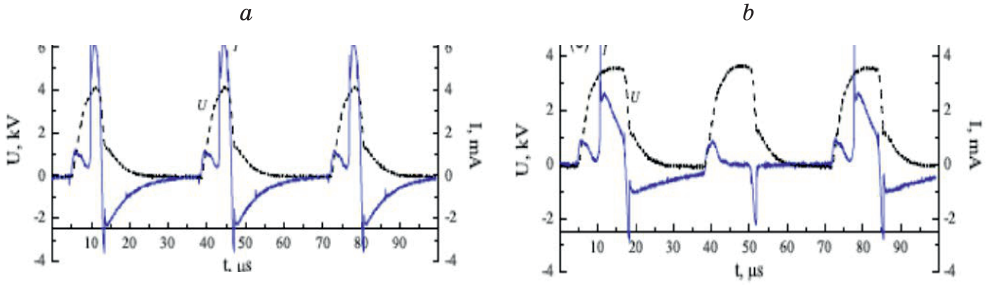

Fig 1. Voltage at U-electrode and current measured on mouse skin exposed to CAPJ with PP voltage with different τ, $f = 30$ kHz, $U = 3.8$–4 kV, (a) $\tau = 7$ μs, (b) $\tau = 14$ μs.

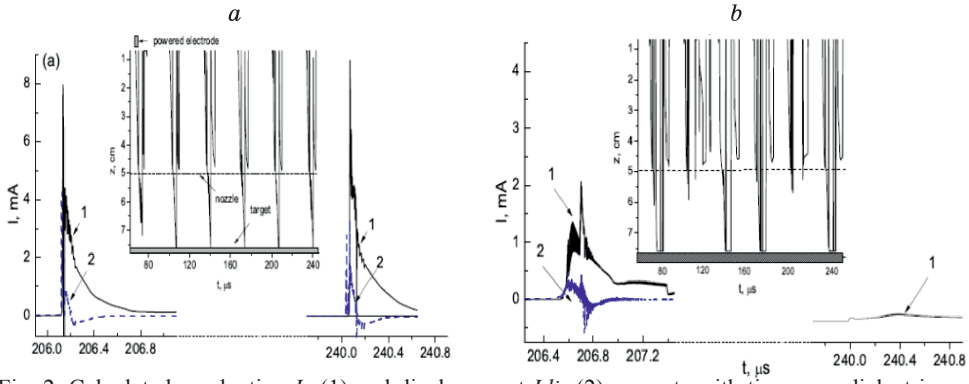

Fig. 2. Calculated conduction *Ic* (1) and displacement *Idis* (2) currents with time near dielectric surface, PP voltage, $U = 4$ kV, $f = 30$ kHz, $\tau = 7$μs (*a*) and $\tau = 14$μs (*b*). Inserts show the streamer head propagation with time from U-electrode (z = 0) to the target (z = 7.7 cm) during six voltage cycles.

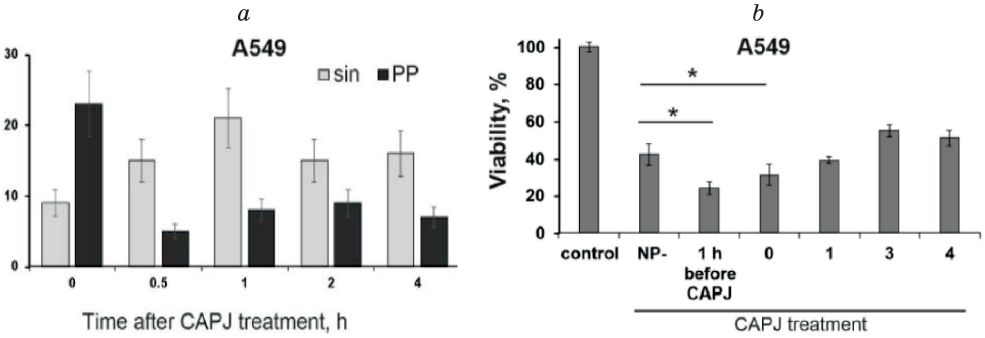

Fig. 3. Visualization of NPs uptake by cells with CAPJ-stimulation (*a*) and viability of cancer cells after co-treatment (*b*).

(mean fluorescence intensity) in FAM channel between CAPJ-treated NP accumulation and passive NP entering.

Changes in the viability of 1 min CAPJ-exposed A549 cells under different NP addition times are shown in Fig. 3(b). The addition of NPs enhanced the cytotoxic effect of CAPJ exposure, the magnitude of which correlated with the mode of maximal NP penetration.

This work was supported by Russian Science Foundation Grant number 22-49-08003.

REFERENCES

1. **Schweigert I.V., Zakrevsky D.E., Gugin P.P., Milakhina E.V., Biryukov M.M., Keidar M. and Koval O.A.** *Plasma Sources Sci. Technol.,* 2022. Vol. 31, P. 114004.
2. **Schweigert I.V., Zakrevsky D.E., Milakhina E.V., Aleksandrov A.L., Biryukov M.M. and Koval O.A.** *Plasma Physics Reports*, 2023. Vol. 49. No. 11. P. 1358.
3. **Biryukov M., Semenov D., Kryachkova N., Polyakova A., Patrakova E., Troitskaya O., Milakhina E., Poletaeva J., Gugin P., Ryabchikova E., Zakrevsky D., Schweigert I. and Koval O.** Biomolecules, 2023. Vol. 13. No. 11, P. 1672.

DOI 10.53954/9785604990131_144

IMPACT OF WEAK SHOCK WAVES ON THE BOUNDARY LAYER OF A FLAT PLATE WITH A VARIABLE SWEPT ANGLE OF THE LEADING EDGE AT M=2

N.V. Semionov, A.D. Kosinov, L.V. Afanasev, Yu.G. Yermolaev, A.A. Yatskikh

Khristianovich Institute of Theoretical and Applied Mechanics, Siberian Branch, Rusian Academy of Sciences, 630090, Novosibirsk, Russia

Studies of the laminar-turbulent transition are of significant practical interest and have a wide range of engineering applications. It is known that the transition of the boundary layer depends on the level and type of disturbances in the free flow. In the test section of wind tunnels, in addition to acoustic pulsations, the process of flow around models can be affected by quasi-stationary disturbances in the form of weak shock waves (SW), generated by irregularities of the nozzle inserts or walls of the test section. The purpose of these studies is to identify the degree of influence of weak shock waves incident on the leading edge on the flow in the boundary layer when the sweep angle changes.

The experiments were carried out in the supersonic low-noise T-325 wind tunnel of the ITAM SB RAS at Mach number M = 2. Two models of a flat plate were used with a leading edge blunting radius of 2.5 mm and with a model rotation mechanism that made it possible to change the sweep angle along the leading edge directly during the experiment. The first model is a flat plate with an initial zero sweep angle (when the model was rotated, the sliding angle of the leading edge changed from 0 to 25°), in the second model the initial sweep angle was 35° and could vary from 35° to 60°. For introducing a pair of weak shock waves into the flow, a "two-dimensional" roughness, mounted vertically on the side wall of the wind-tunnel test section, was used. The dimensions of the roughness were as follows: length (across the flow) ≈ 150 mm, width (in down-stream direction) 7 mm, and thickness 0.13 mm. Measurements of the mean mass flow rate and its pulsations in the flow were carried out using a constant-temperature hot-wire anemometer; in some cases, a Pitot probe was used. The experimental setup and measurement technique are described in detail in [1, 2].

To estimate the intensity of incident shock waves, measurements were made in the free-stream flow ahead of the leading edge of the models. The distributions of the rms pulsations $\langle m' \rangle$ and the mean mass flux ρU normalized by the rate of the incoming flow as dependent over the transverse coordinate z are measured for each series of experiments. A disturbance in the form of an N-wave is recorded in the free flow in front of the models. The evolution of disturbances in the free-stream flow at various distances from the generator of weak shock waves on the wall of the test section of the wind tunnel is presented in [2]. It is shown that the level of disturbances from inhomogeneity in the free flow remains practically unchanged. The results of visualization of a pair of weak shock waves generated by a two-dimensional irregularity on the wall of the test section of a supersonic wind tunnel using the shadow method with a Foucault knife and the interference method of the adaptive imaging transparency of absorption saturation (AVT SA) are presented in [3].

In the boundary layer of the models, measurements of the flow characteristics were carried out for the case of a smooth wall of the test section of the T-325 wind tunnel and with an installed generator of weak shock waves. The results are presented comparing these two cases. Using a constant-temperature hot-wire anemometer, flow patterns in the boundary

layer of the plate were obtained at sweep angles of the leading edge $\chi = 0$, $\chi = 5°$, $\chi = 15°$, $\chi = 20°$ and $\chi = 25°$ for the first model of the flat plate. It was found that when a pair of weak shock waves falls on the leading edge of the plate, the generation of a pair of longitudinal vortices is observed in the boundary layer, accompanied by an increase in the level of pulsations and a change in the spectral composition of disturbances. When the sweep angle of the leading edge of the plate was varied from 0 to 25 degrees, a widening of the vortex in the supersonic boundary layer, occurring due to the action of the incident "catching-up" weak shock wave, was observed. The width of the vortex generated by the trailing edge of the N-wave varied from 2 ± 0.5 mm to 3.5 ± 0.5 mm, and the width of the vortex generated by the trailing edge of the N-wave, from 2 ± 0.5 mm to 4.5 ± 0.5 mm. Using a pitot tube, flow patterns in the boundary layer of the plate were obtained at sweep angles of the leading edge $\chi = 0$, $\chi = 5°$, $\chi = 15°$. It was found that when the leading edge sweep angle changes from $\chi = 0°$ to $\chi = 15°$, an increase in the width of the disturbed region in the transverse direction z is observed. The disturbed "peak to peak" region increases from 1 mm at $\chi = 0°$ to 2.5 mm at $\chi = 15°$.

In the second series of experiments, studies were carried out for the second model of a flat plate. Also, for two cases, a comparison was made of the flow pattern in the boundary layer of the plate at sweep angles of the leading edge $\chi = 35°$, $\chi = 40°$, $\chi = 45°$ and $\chi = 50°$ for the second model of a flat plate. For the first time, it was experimentally obtained that when the sweep angle along the leading edge changes from 35 to 45 degrees, a decrease in the intensity of the effect of weak shock waves on the flow in the boundary layer is observed. When the sweep angle along the leading edge increases to 50 degrees, it is found that there is no influence of weak shock waves on the flow in the supersonic boundary layer of the swept plate. Thus, at sweep angles of more than 45 degrees, it can be assumed that weak shock waves are not able to influence the flow in the boundary layer.

This work was financially supported by the Russian Science Foundation (Grant No. 22-19-00666, https://rscf.ru/en/project/22-19-00666).The study was conducted at the Equipment Sharing Center «Mechanics» of ITAM SB RAS.

REFERENCES

1. **Kocharin V.L., Kosinov A.D., Yatskikh A.A., Ermolaev Yu.G., Semionov N.V., Piterimova M.V., Shevelkov S.G., Minin O.P.** The impact of weak shock waves on the flow in the boundary layer of a flat plate with a variable sweep angle of the leading edge // Thermophysics and Aeromechanics. 2019. Vol. 26, No. 6. P. 803–809. DOI: 10.1134/S0869864319060027
2. **Kosinov A.D., Semionov N.V., Yatskikh A.A., Kocharin V.L., Shmakova A.V.** Influence of the leading-edge bluntness radius of a plate on the response of flat-plate boundary layer to an N-wave at Mach number M = 2 // Thermophysics and Aeromechanics. 2023. Vol. 30. No. 2. P. 227–237. DOI: 10.1134/S086986432302004
3. **Pavlov Al.A., Golubev M.P., Kosinov A.D., Pavlov A.A. Visualization of interaction of Mach waves with a bow shock //** Proceedings of the XXV Conference on High-Energy Processes in Condensed Matter (HEPCM 2017): AIP Conference Proceedings. – Vol. 1893. No. 1. – S. l.: AIP Publishing, 2017. – 030068 p. DOI: 10.1063/1.5007526

DOI 10.53954/9785604990131_146

ON THE LAMINAR-TURBULENT TRANSITION OF SUPERSONIC BOUNDARY LAYER ON SWEPT WINGS

N.V. Semionov, A.D. Kosinov, A.N. Semenov, B.V. Smorodsky, S.A. Shipul

Khristianovich Institute of Theoretical and Applied Mechanics, Siberian Branch, Rusian Academy of Sciences, 630090, Novosibirsk, Russia

Research on the turbulence beginning and the development, based on the obtained data, of new engineering methods for predicting of the transition position and the transition control in spatial boundary layers is the focus of attention of specialists in many countries. Such studies are of practical interest, since these flows are realized around the swept wing of an aircraft. The transition to turbulence in high-speed flows is determined by many parameters, many of which are not fully understood, which leads to problems in the development of physics-based prediction methods. The purpose of this work is to study the influence of the Mach number, unit Reynolds number, external disturbances, as well as small angles of attack on the transition location on swept wings in a supersonic flow.

The experiments were carried out in the supersonic low-noise T-325 wind tunnel of the ITAM SB RAS at Mach numbers M = 2 – 4. Two models of a wing with a lenticular profile were used. The first model is a wing with a 3 % profile and swept angles of the leading and trailing edges $\chi = 45°$, in the second model the sweep angle of the leading edge is 72°, the trailing edge is 58°. The study of the evolution of disturbances and determination of the position of the laminar-turbulent transition were carried out on the upper surface of the model using a constant-temperature hot-wire anemometer, in some cases with a Pitot tube. The experimental setup and measurement technique are described in detail in [1–4].

Studies have been carried out of the influence of a unit Reynolds number on the laminar-turbulent transition in the supersonic boundary layer of swept wings at M = 2 and 2.5. It is shown that the laminar-turbulent transition in the supersonic boundary layer of the swept wing with a subsonic leading edge occurs earlier than on the model with a supersonic leading edge for the same free-stream parameters. An increase in the unit Reynolds number Re_1 leads to an increase in the transition Reynolds number Re_{tr} on the wing model with $\chi = 45°$. A change in a unit Reynolds number has less impact on the transition position in the boundary layer of the swept wing with a subsonic leading edge, in contrast to a model of the wing with a supersonic leading edge. The reason for this effect may be the determining role of stationary disturbances in the process of laminar-turbulent transition on the model of the swept wing with a subsonic leading edge.

Experimental studies have been carried out on the influence of external vortex disturbances on the position of the laminar-turbulent transition in the supersonic boundary layer of swept wings at M = 2 and 2.5. Vortex disturbances were generated by a wire installed in front of the nozzle inserts in the subsonic part of the flow. The wire diameter varied from 0.9 to 3 mm. It is shown that for a wire diameter of 3 mm, the maximum influence of vortex disturbances on the position of the transition is noted (20 % destabilization of the boundary layer is obtained). Reducing the wire diameter leads to an increase in the transition Reynolds number. And already at d = 0.9 mm the influence of vortex disturbances is not fixed on the transition location.

A comparison of the transition Reynolds numbers obtained on the wing model with a swept angle $\chi = 72°$ with the results of measurements on the model with $\chi = 45°$ shows that

destabilization of the flow with increasing sweep angle is recorded only in the case of an undisturbed flow (absence of a source of vortex disturbances). Similar results were obtained when studying the influence of the Mach number on the position of the transition on swept wings. The transition Reynolds numbers for a wing with $\chi = 45°$ were higher only at $M = 2$ and 2.5, where, as shown in [5], low-noise regimes are realized. With an increased noise level in the test section of the wind tunnel, the effect of the sweep angle on the position of the transition point is not recorded.

Experimental data were obtained and the results were generalized on the influence of small angles of attack and Mach number on the position of the laminar-turbulent transition on swept wings at Mach numbers from 2 to 4. Changing the angle of attack has a strong effect on the transition Reynolds number for all Mach numbers. An increase in the Mach number led to a decrease in the transition Reynolds number. It is shown that the laminar-turbulent transition in the boundary layer on a wing with a subsonic leading edge is more sensitive to changes in the angle of attack compared to the case of flow around a model of a wing with a supersonic leading edge. The calculations of the mean flow in a supersonic boundary layer and those according to the linear theory of hydrodynamic stability are performed under the experimental conditions for the wing with the leading-edge sweep angle of 72°. Analysis of calculated and experimental data makes it possible to conclude about the governing role played by stationary disturbances in the laminar-turbulent transition process on a model of a swept wing with the leading-edge swept angle of 72° under the conditions of the experiments carried out in this study.

REFERENCES

1. **Ermolaev Y.G., Kosinov A.D., Semenov A.N., Semionov N.V., Yatskikh A.A.** Effect of unit Reynolds number on the laminar-turbulent transition on a swept wing in supersonic flow // Thermophysics and Aeromechanics. 2018. Vol. 25. No. 5. P. 659–665.
2. **Ermolaev Y.G., Kosinov A.D., Kocharin V.L., Semenov A.N., Semionov N.V., Shipul S.A., Yatskikh A.A.** Experimental study of the influence of external disturbances on the position of the laminar-turbulent transition on swept wings at M = 2 // Thermophysics and Aeromechanics. 2021. Vol. 28. No. 3. P. 319–325.
3. **Kosinov A.D., Semionov N.V., Yermolaev Y.G., Smorodsky B.V., Kolosov G.L., Yatskikh A.A., Semenov A.N.** The influence of moderate angle-of-attack variation on disturbances evolution and transition to turbulence in supersonic boundary layer on swept wing // Journal of Aerospace Engineering. 2020. Vol. 234. No. 1. P. 96–101.
4. **Kosinov A.D., Kocharin V.L., Liverko A.V., Semenov A.N., Semionov B.V., Tolkachev S.N., Yatskikh A.A.** Effect of small angles of attack on turbulence generation in supersonic boundary layers on swept wings // Fluid Dynamics. 2023. Vol. 58. No. 3. P. 371–380.
5. **Kosinov A.D., Semionov N.V.** The laminar-turbulent transition experiments in supersonic boundary layers // AIP Conf. Proc. 2019. V. 2125. P. 030105

DOI 10.53954/9785604990131_148

MULTI-TEMPERATURE MODELING OF NON-EQUILIBRIUM GAS-SOLID INTERACTIONS

L. Shakurova, E. Kustova

Saint-Petersburg State University,
199034, St. Petersburg, Russia

There exists a need for accurate and self-consistent models that can capture effects of non-equilibrium gas interactions with solid bodies surfaces. Such models are crucial, for example, for analyzing gas flows near space vehicles re-entering planetary atmospheres and rarefied flows in microchannels. The models are required to capture physical effects during particles scattering by the surface and consider the impact of gas rarefaction. Additionally, it is essential to incorporate heterogeneous processes at the gas-solid interface in modeling. This includes catalytic effects, ablation, and ionization reactions. Capturing these complex multi-physics phenomena through rigorous modeling enables accurate prediction of near-surface gas flow properties, including the total heat flux at the surface.

Recently, we developed an approach based on kinetic boundary condition that allows us to capture some of the effects mentioned above within the framework of continuum modeling [1, 2, 3]. More precisely, the approach enables derivation of a closed set of slip boundary conditions for the case of a gas described on the basis of a detailed state-to-state approximation. The expressions were specifically developed under strong vibrational and chemical non-equilibrium conditions, neglecting electronic excitation. The following non-equilibrium surface processes were accounted for: adsorption, desorption, vibrational excitation/deactivation due to wall impinging, as well as heterogeneous recombination/dissociation.

Despite the numerous benefits of the approach under the state-to-state model, practical applications of the developed conditions face certain limitations. This is mostly due to the extremely high computational cost associated with the state-specific modeling, particularly in the case of polyatomic molecules and non-one-dimensional flows. Although the reduction to multi-temperature (MT) models may have limitations in capturing the influence of internal molecular excitation on gas properties, these constraints can be overcome by employing hybrid approaches [4].

Multi-temperature models are widely used for modeling non-equilibrium flows around solid bodies; however, slip conditions are commonly not applied. An exception is the consideration of wall catalytic effects based on simplified models, e.g. in [5, 6, 7]. Regarding existing MT models for boundary conditions, expressions can be found in work [8]. However, these conditions do not correctly incorporate heterogeneous processes, as highlighted in [2, 3]. Thus, under the multi-temperature approximation, the general formulation of the developed approach and the expressions for slip boundary conditions are required. The present work is dedicated specifically to the latter.

In the present study, we obtain multi-temperature expressions for velocity slip, temperatures jumps and the species wall mass fluxes, which incorporate heterogeneous processes. It should be emphasized that the expressions are obtained for the case of temperatures defined for each vibrational mode of molecular species, including the electronic temperature for electrons. The development of such models is essential for ionized flows,

where the ion-electron recombination is almost perfectly catalyzed. The vibrational temperatures jumps in the developed models capture the change in the molecular vibrational state due to the wall impinging and provide its impact on the flow near solid parameters. The slip conditions are used in numerical simulations, and a comparison with state-specific expressions is provided.

This work is supported by the Russian Science Foundation (project № 23-19-00241).

REFERENCES

1. **Shakurova, L., Kustova, E.** State-specific boundary conditions for nonequilibrium gas flows in slip regime // Phys. Rev. E. 2022. Vol. 105. Art. 034126.
2. **Shakurova, L., Armenise, I., Kustova, E.** State-specific slip boundary conditions in non-equilibrium gas flows: Theoretical models and their assessment // Physics of Fluids. 2023. Vol. 35. Art. 086109.
3. **Shakurova, L., Kustova, E.** Slip boundary conditions for gas mixture flows with state-to-state vibrational-chemical kinetics // AIP Conference Proceedings. 2024. Vol. 2996. Art. 130002.
4. **Kosareva, A., Kunova, O., Kustova, E., Nagnibeda, E.** Hybrid approach to accurate modeling of coupled vibrational-chemical kinetics in carbon dioxide // Physics of Fluids. 2022. Vol. 34. Art. 026105.
5. **Hao, J., Wang, J., Lee, C.** Numerical study of hypersonic flows over reentry configurations with different chemical nonequilibrium models // Acta Astronautica. 2016. Vol. 126. P. 1–10.
6. **Candler, G. V.** Rate effects in hypersonic flows // Annual Review of Fluid Mechanics. 2019. Vol. 51. P. 379–402.
7. **Yu, M., Qiu, Z., Takahashi, Y.** Numerical investigation of surface catalytic effect on the plasma sheath of a hypersonic re-entry capsule // Physics of Fluids. 2023. Vol. 35. Art. 056106.
8. **Kiryutin, B. A., Tirskii, G. A.** Slip boundary conditions on a catalytic surface in a multicomponent gas flow // Fluid Dyn. 1996. Vol. 31. P. 134–143.

DOI 10.53954/9785604990131_150

HEAT AND MASS TRANSFER IN PLANE-PARALLEL SHEAR COMPRESSIBLE GAS FLOWS

V.I. Shalaev, S.T. Kalugin, G.V. Toloko, V.A. Tokarev

Moscow Institute of Physics and Technology
16 Gagarin street, Zhukovsky, Moscow Region, Russia, 140180

In this report, on the base of Naiver-Stocks equations three classic plane-parallel compressible viscous gas flows in a channel with the width l under actions of the longitudinal motion of the lower plate with the velocity U, at the presence of the transverse mass transfer $\rho v = q_0 = const$ (ρ is the gas density, v is the transverse velocity), and the pressure gradient $p_x = const$ are considered. It is assumed, the longitudinal flow velocity $u(y)$ and the enthalpy $h(y)$ depend only on the transverse coordinate y. The first problem is considered before by other methods [1 – 3], other two problems are not solved earlier.

Solutions contain two integrals: one presents the enthalpy as a velocity function and another is impulse equation integral. For the first problem, which is an analog of Couette flow ($p_x = q_0 = 0$) the solution has the following dimensionless form:

$$\overline{h}(V) = \beta\left(a + bV - V^2\right) = \beta R(V), \quad f(V) = \int \frac{R^{3/2}(V)\,dV}{R(V) + H_s} = AY + B,$$

$$V = \frac{u}{U},\ Y = \frac{y}{l},\ \beta = \frac{\Pr U^2}{2h_0},\ H_S = \frac{h_S}{\beta},\ f(1) = B,\ A = f(0) - f(1),\ a = \frac{\overline{h}_1}{\beta},\ b = \frac{1+\beta}{\beta} - a,$$

$$AY + B = f(V) = \frac{(2V-b)\sqrt{R(V)}}{4} + \left(\frac{\Delta}{8} - H_S\right) arc\sin\frac{2V-b}{\sqrt{\Delta}} +$$

$$+ H_S\sqrt{\frac{H_S}{\Delta_1}}\left[arctg\frac{\sqrt{\Delta_1}\left(V - \frac{b}{2}\right) - \frac{\Delta}{2}}{2\sqrt{H_S R(V)}} + arctg\frac{\sqrt{\Delta_1}\left(V - \frac{b}{2}\right) + \frac{\Delta}{2}}{2\sqrt{H_S R(V)}}\right];\ \Delta = b^2 + 4a,\ \Delta_1 = \Delta + 4H_S.$$

For the analog of the Couette-Poiseuille flow ($q_0 = 0$) the analytical integral for the enthalpy equation exists only for thermally insulated unmoving wall , when b =0. In this case, the boundary condition for the enthalpy on the unmoving wall is $dh(1)/dy = 0$, and the full solution has the form:

$$\overline{h}(V) = \beta R(V) = \beta\left(a - V^2\right), \quad P = \frac{p_x l^2}{\mu_0 U\left(1 + h_s\right)\sqrt{\beta}}, \quad A = f(0) - f(1) - \frac{1}{2}P, \quad B = f(1),$$

$$\frac{1}{2}PY^2 + AY + B = f(V) = \frac{V\sqrt{a - V^2}}{2} + \left(\frac{a}{2} - H_S\right) arc\sin\frac{V}{\sqrt{a}} +$$

$$+ \frac{H_S^{3/2}}{2\sqrt{a_1}}\left[arctg\frac{\sqrt{a_1}V - a}{\sqrt{H_S\left(a - V^2\right)}} + arctg\frac{\sqrt{a_1}V + a}{\sqrt{H_S\left(a - V^2\right)}}\right].$$

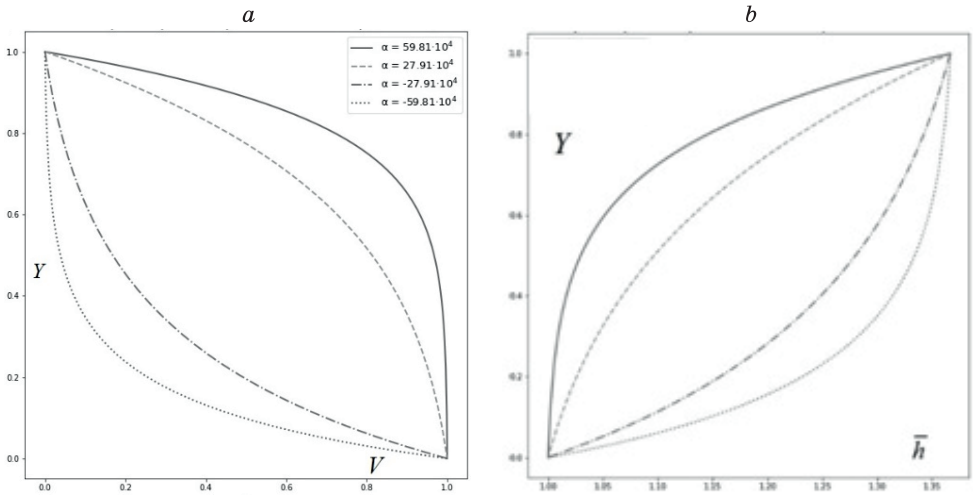

Fig. 1. Compressible Couette flow with transverse mass transfer.

a) velocity distributions; *b*) enthalpy distributions;

The third considered problem corresponds to the compressible Couette flow with the constant transversal mass transfer $\rho v = q_0 = const$ through permeable walls and $p_x = 0$. At arbitrary Prandtl number ($\mathrm{Pr} \neq 2$), the enthalpy related with the velocity by equations:

$$\bar{h}(s) = \beta\left[a + bs^{\mathrm{Pr}} + cs^2\right] = \beta R(s), \quad s = V + A,$$

$$a = -\left\{\frac{A^{\mathrm{Pr}} - \bar{h}_1(1+A)^{\mathrm{Pr}}}{\beta} - c\left[A^{\mathrm{Pr}}(1+A)^2 - A^2(1+A)^{\mathrm{Pr}}\right]\right\}\left[(1+A)^{\mathrm{Pr}} - A^{\mathrm{Pr}}\right]^{-1},$$

$$b = D = \left[\frac{1-\bar{h}_1}{\beta} - c(1+2A)\right], \quad \left[(1+A)^{\mathrm{Pr}} - A^{\mathrm{Pr}}\right]^{-1}, \quad c = -\frac{1}{2-\mathrm{Pr}}.$$

At $\mathrm{Pr} = 2$, $\beta = U^2/h_0$ the solution for the enthalpy is singular:

$$R(s) = a - s^2 \ln s + bs^2,$$

$$a = -(1+2A)^{-1}\left[\frac{A^2 - \bar{h}_1(1+A)^2}{\beta} + A^2(1+A)^2 \ln\frac{1+A}{A}\right], \quad b = \frac{1-\bar{h}_1}{\beta} + (1+A)^2\ln(1+A) - A^2\ln A$$

The impulse equation solution is represented as the integral:

$$f(s) = \int \frac{R^{3/2}(s)\,ds}{(R(s)+H_S)s} = \alpha Y + B, \quad \alpha = \frac{v_0 l}{\mu_0(1+\bar{h}_S)\sqrt{\beta}}, \quad f(1+A) = B, \quad f(A) - f(1+A) = \alpha$$

At an arbitrary Prandtl number the integral has not an analytical form. Analytical solution exists only at Pr = 1. Dimensionless velocity and enthalpy profiles at Pr=0,72, $\beta = 2{,}95 * 10^{-4}$ and different values of α obtained on the base of numerical calculations are presented in Fig. 1*a* and 1*b*.

REFERENCES

1. **Grodzovsky G.L.** Viscous gas flow between two moving parallel walls and two rotating cylinders. Applied Mathematics Journal, 1955. V. 19. P. 99–102.
2. **Ghmulin E.M.** Viscous gas flow two moving parallel plates. TsAGI Scientific Notes. 1971. V. 2. No. 4. P. 31–37.
3. **Golubkin V.N., Sizyh G.B.** On compressibleCouetteflow. TsAGI Scientific Notes. 2018. V. 49. No. 1. P. 27–38.

DOI 10.53954/9785604990131_152

NUMERICAL STUDY OF SECONDARY FRACTURE OF A DIESEL FUEL DROP

A.A. Shebeleva, A.V. Shebelev, A.V. Minakov

Siberian Federal University
660041, Krasnoyarsk, Russia

To date, there are a large number of experimental works in field of studying destruction of a droplet when it suddenly enters gas flow. This is due to rather extensive applied significance of this research, for example, in field of engine building, chemical industry, fuel energy, in field of oil and gas industry waste utilization, etc. Experiments are carried out with different liquids, and process of droplet deformation, fracture dynamics, and disintegration are studied. All these stages of droplet fracture process are best observed in experiments with passing shock waves [1–4]. To study the secondary fragmentation of a droplet, it is important to observe deformation process from the moment droplet enters flow, so experiments are performed using shock tubes and various ways to visualize process [1–2].

At present, all problems related to resolution of small scales of droplet destruction process are available only for numerical simulations. This study used a numerical technique based on a combination of the VOF method to resolve the interface, LES model to describe turbulence, and adapted meshes to more accurately describe interface. This technique allows us to correctly describe behavior of moving boundary and main turbulent scales that are involved in droplet breakup. A detailed description of numerical methodology for calculating droplet breakup in flow behind shock wave is presented in [3–4].

This paper presents results of numerical simulation of viscous drop of diesel fuel fracture in flow behind shock wave. Computational domain is a parallelepiped with dimensions 3×3×5 cm, on one faces of which condition of entrance with a fixed value of velocity was set. On the other faces conditions of free exit were set. At initial moment of time at a distance of 5 mm from entrance to computational region was placed a spherical droplet of size d_0 = 2.8 mm, which is affected by a passing shock wave generating an air flow with velocity u_g = 78.3 m/s, which corresponds to the Weber number We = 1081. Destruction of a viscous diesel fuel droplet at low temperature t = –45 °C: ρ_l = 846 kg/m^3, μ_l = 0.428 Pa·s was studied. Air was considered as gas: ρ_g = 1.7 kg/m^3, μ_g =1.789·10^{-5} Pa·s. Surface tension coefficient was equal to σ = 0.027 N/m.

Figure 1 shows dynamics of development of fracture process arising from interaction of air flow with diesel droplet. Pictures are presented in frontal projection. As can be seen, at time 1133 μs, initially spherical droplet has transformed into a liquid disk from which a thin film located at bottom of droplet (left) is blown into flow direction. At time 1139 μs, a disruption of droplet surface integrity is observed. Further, film continues to break down, but liquid ring is still intact. After reaching a time of 1251 μs, a similar film breakdown is observed, but on the other side of droplet (right). Throughout calculation, we observe breakup of central part of droplet into smaller droplets. Liquid ring moves through flow, gradually thinning, and is last to collapse. In this case, induction time of diesel droplet destruction is $t \approx$ 1135 μs. For basic research, an important quantitative parameter is mass transport induction period $t_i = 0.36 \cdot (d_0 / u_g) \cdot (\rho_l / \rho_g)^{0.5}$ = 287 μs. The dimensionless induction period $T_i = t_i / t_{0m}$ is the ratio of the massonos induction period to the time constant $t_{0m} = (d_0 / u_g) \cdot (\rho_l / \rho_g)^{0.5}$ =

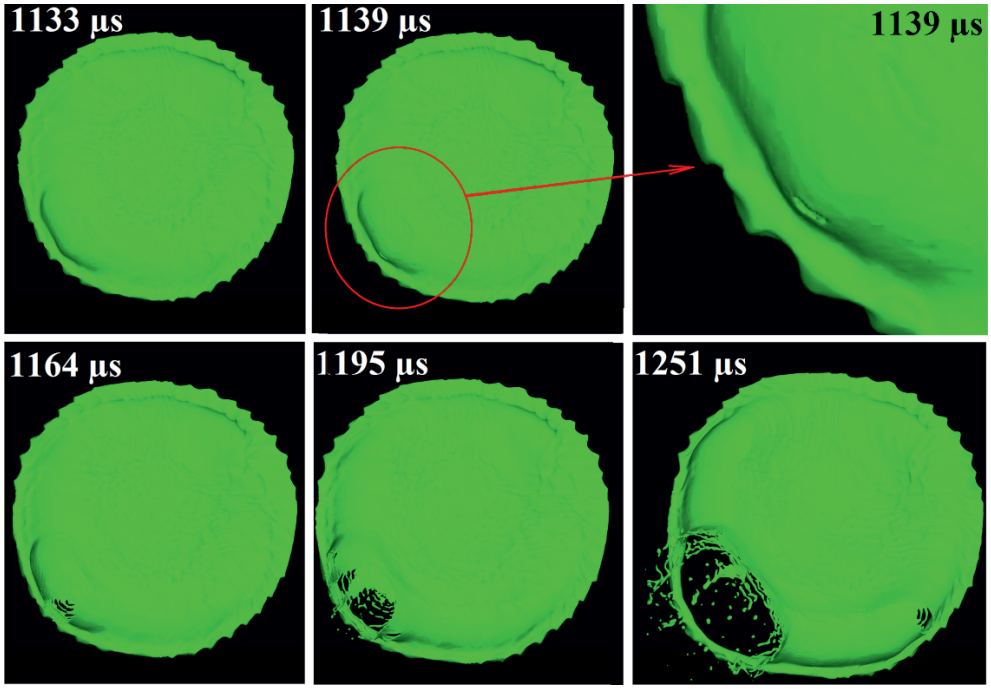

Fig. 1. Frontal projection of the process of destruction of a drop of diesel fuel at various points in time.

= 797.7 μs, in this case the dimensionless induction time T_i = 0.36. Also, the dependence of the ratio of the maximum degree of deformation of the droplet core before the beginning of its destruction to the initial size d_{max}/d_0 = 2.6 is obtained.

The reported study was carried out with the support of the "Krasnoyarsk Regional Fund for Support of Scientific and Scientific-Technical Activities" within the framework of the scientific project "Study of the characteristics of secondary crushing of coal water slurries containing petrochemicals in order to improve technologies for its combustion in Arctic conditions" No. 20231113-06407.

REFERENCES

1. **Boiko V.M., Poplavski S.V.** On the dynamics of droplet acceleration at the early stage of velocity relaxation in the shock wave // Combustion Explosion and Shock Waves. 2009. Vol. 45. No. 2. P. 198–204.
2. **Boiko V.M., Poplavski S.V.** Experimental study of two types of stripping breakup of a drop in the flow behind the hock wave // Combustion Explosion and Shock Waves. 2012. Vol. 48. No. 4. P. 440–445.
3. **Poplavski S.V., Minakov A.V., Shebeleva A.A.** An early stage of the drop interaction with shock wave: airflow, deformation, destruction // Journal of Physics: Conference Series. 2019. doi:10.1088/1742-6596/1359/1/012032.
4. **Poplavski S.V., Minakov A.V., Shebeleva A.A., Boyko V.M.** On the interaction of water droplet with a shock wave: Experiment and numerical simulation // International journal of multiphase flow. 2020. Vol. 127. Art. 103273. https://doi.org/10.1016/j.ijmultiphaseflow.2020.103273

DOI 10.53954/9785604990131_154

INVESTIGATION OF THE INFLUENCE OF THE GAP SIZE BETWEEN THE SECTIONS OF THE OIL COOLER ON ITS EFFICIENCY

A.R. Shigapova

Kalashnikov Izhevsk State Technical University
426069, Studencheskaya str., 7, Izhevsk, Russia

At the present stage of industrial development, great attention is paid to careful production, which means that technologies developed many years ago need to be modernised and improved.

Equipment engines used in industry operate on the principle of compression and expansion of working media, so their operation involves heating of these media. Therefore, a common technical solution is the use of special convective heat exchangers for excess heat removal, the design of which significantly affects the thermal efficiency of such devices. One of the most effective schemes of such heat-exchange apparatuses are devices of «radiator» type, representing a complex collector from a set of internal plates-collectors with small-sized internal channels of complex shape and developed external surface. Oil coolers can be referred to this type of devices [1–6].

The main structural element of oil coolers is an aluminium or copper tube of rectangular cross-section, finned on the outer surfaces. The finning is necessary to increase the effective heat transfer area through which the heat is dissipated to the environment. One of the most effective finning techniques is planing or warp cutting. Heat-exchange tubes made by this method have significant dimensions and, consequently, higher mass of the product, and the frequency of finning, as well as the basic geometric characteristics of a single fin – significantly affect the thermal efficiency of the device and its metal intensity. At the same time, the issues of studying the thermal efficiency of oil coolers, as well as the issues of thermal modes of their operation in general remain insufficiently studied [1, 4, 6]. Thus, the object of research is an industrial oil cooler.

The work is aimed at the study of the optimal value of the gap between the slats of the oil cooler.

The conjugate problem of heat exchange between heated hydraulic oil, plates of oil cooler and cold flow of air blown by a fan is considered. The flow of heat-conductive incompressible liquid (conditional hydraulic oil with density 1100 kg/m^3, molar mass 48,61 kg/mol, dynamic viscosity coefficient 0.11 Pa*s and thermal conductivity coefficient 0.11 Pa*s. 11Pa*s and thermal conductivity coefficient 0.41 W/(m*K)) in channels of small size [2, 3] with heat transfer to the wall of the aluminium slat of the oil cooler [4–6] and turbulent ($20000 < Re < 400\,000$) spatial flow of air in the gap between the slats of the oil cooler. The geometrical model of a unit section of the oil cooler (plates) is presented in [1], the general scheme of the device is presented in [1–6].

The mathematical model of fluid media motion is based on the Navier-Stokes equations. The system of equations describing the motion of continuous media, in general case, has the form:

$$\frac{\partial \rho}{\partial t} + \frac{\partial \rho u_i}{\partial x_i} = 0 \qquad (1)$$

$$\frac{\partial \rho u_i}{\partial t} + \frac{\partial \rho u_i u_j}{\partial x_j} = -\frac{\partial p}{\partial x_i} + \frac{\partial}{\partial x_j}\left(\mu\left(\frac{\partial u_i}{\partial x_j} + \frac{\partial u_j}{\partial x_i}\right) - \frac{2}{3}\mu\frac{\partial u_k}{\partial x_k}\delta_{ij}\right) + F_i \quad (2)$$

$$\frac{\partial \rho E}{\partial t} + \frac{\partial \rho E u_j}{\partial x_j} = -\frac{\partial p u_j}{\partial x_j} + \frac{\partial u_i \tau_{ij}}{\partial x_j} + \frac{\partial q_j}{\partial x_j} + F_i u_i \quad (3)$$

$$p = \rho RT, \quad (4)$$

In the system of equations (1)–(4) the following assumptions are adopted: ρ – density of the medium; u_i components of the velocity vector u; p – pressure; μ – dynamic viscosity coefficient; F_i – external mass force, given for the refrigerant to account for gravity; $E = C_v T + 0.5u_i^2$ – total specific energy of the medium; $H = E + \frac{p}{} = C_p T + 0.5u_i^2 = h + 0.5u_i^2$ – total specific enthalpy; $\tau_{ij} = 2\mu S_{ij} - \frac{2}{3}\mu\frac{\partial u_k}{\partial x_k}\delta_{ij}$ – viscous stress tensor; $S_{i,j} = \frac{1}{2}\left(\frac{\partial u_i}{\partial x_j} + \frac{\partial u_j}{\partial x_i}\right)$ strain rate tensor; $q_j = \lambda\frac{\partial T}{\partial x_j}$ heat flux; λ heat transfer coefficient of the medium; T – temperature.

Modelling of heat transfer processes in the oil cooler plate is carried out on the basis of the heat conduction equation:

$$\rho c_p \frac{\partial T}{\partial t} = \nabla \cdot (\lambda \nabla T). \quad (5)$$

The Metnter SST turbulence model [7] is used to close the system of conservation equations. The boundary conditions are set as follows: at the inlet to the region and at the upper boundary, the velocity and temperature of the impinging flow (air temperature T = 20 °C, air velocity V = 10 m/s), oil pressure and temperature (temperature To = 60 °C, liquid pressure – 1 MPa) were set; at the outlet, the zero gradient condition for the velocity and temperature, and a fixed pressure value for oil (0.3 MPa) were defined At solid impermeable surfaces, the sticking and non-flow conditions are set. At the oil/aluminium and aluminium/air interfaces, a boundary condition of genus IV is used.

The system of partial derivatives (1)–(5) thus constructed on the basis of the conservation equations is solved approximated by the finite-volume method within the framework of the quasi-stationary formulation. Discretisation of the obtained system of equations in space is carried out by hexagonal elements. For discretisation of non-viscous flows, a counter-flow scheme of the 2nd order of accuracy is applied, and for viscous flows, a centred scheme of the 2nd order of accuracy is used. The system of difference equations is solved by the algebraic multigrid method, for acceleration of convergence of which the conjugate gradient method is used.

As a result of calculations the distribution fields of physical quantities are obtained, the heat transfer coefficients of oil and aluminium are estimated, integral thermophysical characteristics of the air flow before and after passing the section of the oil cooler depending on the value of the varying distance between the sections (slats) are obtained. Analysis of the obtained thermophysical characteristics, including the obtained temperature profiles, made it possible to identify the optimal, from the point of view of thermal efficiency of the oil cooler, value of the gap between the slats of the oil cooler.

REFERENCES

1. **Armyanin A.Yu., Baymetova E.S., Hval'ko M.E.** Peculiarities of the thermal regime of an oil cooler with a developed external surface // Chemical physics and mesoscopy, 2022, vol. 24, no. 1, pp. 93–103.
2. **Baimetova E.S.** Numerical simulation of hydrodynamic processes in a multichannel collector. Trudy MAI, 2023, no. 130. DOI: 10.34759/trd-2023-130-08
3. **Baimetova E.S., Koroleva M.R.** Research of conjugate heat transfer in a collector of a complex shape of an external fins // В книге: XXI International Conference on the Methods of Aerophysical Research (ICMAR 2022). Abstracts . Novosibirsk, 2022. С. 13–14.
4. **Baymetova E.S., Chernova A.A., Koroleva M.R., Kelemen M.** Optimization of the developed outer surface of an industrial oil cooler // MM Science Journal. 2021. 2021. June. P. 4764–4768.
5. **Menter P.F.R., Kuntz M., Langtry R.** "Ten years of industrial experience with the SST turbulence model," In: Hanjalić, K. (ed) Proc. 4th. Int. Symp. on Turbulence, Heat and Mass Transfer. Begell House, 2003, 8 p.

DOI 10.53954/9785604990131_157

NUMERICAL SIMULATION OF TURBULENT FLOWS IN HYCFS SOLVER

G.V. Shoev, A.A. Shershnev, D.P. Polevshikov, T.Y. Shkredov, A.V. Kashkovsky, A.N. Kudryavtsev

Khristianovich Institute of Theoretical and Applied Mechanics SB RAS 630090, Novosibirsk, Russia

Hybrid Compressible Flow Solver (HyCFS) is a software that solves numerically the Euler and Navier–Stokes–Fourier equations. HyCFS [1] is being developed at the Khristianovich Institute of Theoretical and Applied Mechanics, and it was originally dedicated to simulate the inviscid or laminar flows. HyCFS was successfully used to simulate various flows such as external flows around bodies, internal flows, jets, plumes, chemically reactive flows, non-equilibrium flow, etc. However, recently a necessity for simulating turbulent flows occurred. The Spallart–Allmaras model was chosen as the starting point for this direction, because this model has only one equation and it was used in the literature showing acceptable numerical results.

In this paper, we describe implementation of the standard Spallart–Allmaras model in the HyCFS flow solver for the structured and unstructured hexa-mesh. Numerical strategy for the solution of the governing equations is as follows. The inviscid fluxes are computed using HLLC [2, 3] approximate Riemann solver with the left and right parameters interpolated with the MUSCL reconstruction of the second order. The viscous fluxes are computed differently: central difference scheme is used for the structured mesh and, so-called, lmk-algorithm [4] is used for the unstructured mesh. The source terms describing generation and destruction of turbulence are computed using the flow parameters in cell centers. The minimum wall distance is computed by solving the Eikonal equation. The first derivatives in the source terms are computed in the cell centers using central difference scheme for the structured mesh and Green-Gauss theorem for the unstructured mesh. Time integration is performed using the explicit Runge–Kutta TVD method of the second order with the local time step.

Three NASA test cases were used to verify HyCFS for the structured mesh: 2D Zero Pressure Gradient Flat Plate Verification Case [5], 3D Bump-in-channel Verification Case [6], 2D Coflowing Jet Verification Case [7]. An excellent agreement between the HyCFS and CFL3D/FUN3D numerical solutions was obtained. Three additional test cases are planned to simulate using both structured and unstructured meshes: Axisymmetric Shock Wave Boundary Layer Interaction near M = 7 [8], flat plate [9], 3D ONERA M6 Wing Validation Case [10].

REFERENCES

1. **Shershnev A.A., Kudryavtsev A.N., Kashkovsky A.V., Shoev G.V., Borisov S.P., Shkredov T.Yu., Polevshchikov D.P., Korolev A.A., Khotyanovsky D.V., Kratova Yu.V.** A numerical code for a wide range of compressible flows on hybrid computational architectures // Supercomputing Frontiers and Innovations. 2022. Vol. 9. No. 4. P. 85–99.
2. **Batten P., Leschziner M.A., Goldberg U.C.** Average-state jacobians and implicit methods for compressible viscous and turbulent flows // Journal of Computational Physics. 1997. Vol. 137, No. 1. P. 38-78.
3. **Toro E.F., Spruce M., Speares W.** Restoration of the contact surface in the HLL-Riemann solver // Shock Waves. Vol. 4. No. 1. P. 25–34.

4. **Wang Z.J.** A fast nested multi-grid viscous flow solver for adaptive cartesian/quad grids // International Journal for Numerical Methods in Fluids. 2000. Vol. 33. No. 5. P. 657–680.
5. https://turbmodels.larc.nasa.gov/flatplate.html
6. https://turbmodels.larc.nasa.gov/bump3d.html
7. https://turbmodels.larc.nasa.gov/shear.html
8. https://turbmodels.larc.nasa.gov/axiswblim7_val.html
9. **Marsilio R., Grillo D.** Implementation and validation of the spalart-allmaras turbulence model for high speed flows // ICAS 2002 congress. https://www.icas.org/ICAS_ARCHIVE/ICAS2002/PAPERS/R40.PDF
10. https://turbmodels.larc.nasa.gov/onerawingnumerics_val.html

DOI 10.53954/9785604990131_159

EXPERIMENTAL STUDY OF THE APPLICABILITY OF OVERSUCTION CRITERIA IN THE THREE-DIMENSIONAL BOUNDARY LAYER OF A SWEPT WING

S.N. Tolkachev, S.A. Baranov, A.Ph. Kiselev, D.S. Sboev

Central Aerohydrodynamic Institute
140180, Zhukovsky, Russia

Introduction. Boundary layer suction is an effective and versatile laminarization method that works well with various laminar-turbulent transition mechanisms. The efficiency of laminarization depends on the magnitude of suction. Selection of the optimal value is a complex task that takes into account the gain in drag, the weight and size characteristics of the suction system, as well as the energy consumption for suction.

The concept of oversuction is found in the literature – the application of such an influence that leads to destabilization of the flow. Physically, the process of oversuction is similar to the flow around a roughness element with the formation of counter-rotating vortices. For the flat plate and straight wing models, various criteria have been proposed: some based on diagrams (Ellis and Poll [1]; Pfenninger [2]; Goldsmith [3]), others developed criterion values (MacManus and Eaton [4, 5]; Campe [6]). The question arises about the applicability of these criteria for a three-dimensional boundary layer on a swept wing, which was studied in this work.

Experimental conditions. The experiments were carried out in the low-turbulence wind tunnel T-124 of the Central Aerohydrodynamic Institute (TsAGI). To simulate a three-dimensional boundary layer implemented on a swept wing, a configuration was chosen using a swept plate, above the upper plane of which a negative pressure gradient is created using a curved wall, and the shape of the side walls corresponds to the calculated streamlines.

The sweep angle of the model is 35°, span 998 mm, chord 2100 mm, thickness 20 mm. The model is made of plexiglass. Its front edge has the shape of an ellipse with a major semi-axis of 80 mm. The X axis is orthogonal to the leading edge of the model and is measured from it. The first and second sections were used in the experiments, and the remaining sections were plugged to avoid the influence of uncontrolled injection on the flow stability. The first panel with large-diameter holes (d_{hole} = 0.5 mm, located in the nodes of a rectangular lattice with a pitch of 5 mm in the transversal direction and 4 mm in the along-stream direction: a total of 3 rows of 93 holes). The second panel with holes of small diameter (d_{hole} = 0.06 mm, arranged in a checkerboard pattern with a step of 0.5 mm both in the transversal direction and in the direction along the flow: a total of 20 rows of 920 holes). During an optical study of the quality of perforation, it was found that the actual parameters of the first panel corresponded to the drawing, and in the second panel only 37 % of the holes turned out to be working. The middle positions of the perforated panels were located at positions along X = 304 mm; 404 mm; 504 mm; 654 mm and 814 mm.

Most studies of the laminar-turbulent transition have been carried out in the range of free-stream velocities of 28–33 m/s. The influence of suction on stationary disturbances and pulsations of speed 21 m/s. The freestream velocity in the experiment was Ufs = 28.6 m/s. The study of the boundary layer structure was carried out using hot-wire anemometry.

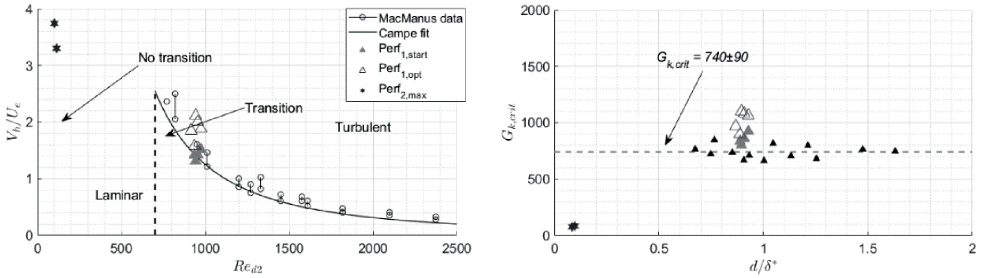

Fig. 1. Regimes corresponding to oversuction, implemented in the experiment.

V_h – suction speed in the hole; U_e – velocity at the outer region of the boundary layer; $\mathrm{Re}_{d2} = U_e d/\nu$; $G_k = (1/\nu)Q_h^{2/3}(\partial U/\partial y)_w^{1/3}$; Q_h – volumetric air flow through one hole; ν – kinematic viscosity; d – hole diameter; δ^* – displacement thickness; $\mathrm{Perf}_{1,\mathrm{start}}$ – extrapolated oversuction value obtained in the experiment on the first perforated plate; $\mathrm{Perf}_{1,\mathrm{opt}}$ – oversuction value obtained in the experiment on the first perforated plate; $\mathrm{Perf}_{2,\mathrm{max}}$ – maximum suction value obtained in the experiment on the second perforated plate.

Results. When the first perforated panel was activated, the oversuction regime was achieved. The second perforated panel led to flow stabilization throughout the entire available range of suction speeds.

The experimental results obtained were compared with the existing oversuction criteria mentioned in the introduction. Two of them have shown their validity (see Fig. 1): the one proposed by Campe [6] based on the approximation of data obtained by MacManus and Eaton in [4], and the engineering approach, which was given by MacManus and Eaton in [5], by the critical value G_k.

The physical influence of suction through the holes was manifested in the selective suppression of long-wave stationary disturbances (λ_Z = 11–14 mm) and the selection and even some enhancement of the short-wave mode (λ_Z = 4.26 mm) at high air flow rates.

EFERENCES

1. **Ellis J.E., Poll D.I.A.** Laminar and laminarizing boundary layers by suction through perforated plates//2“d European Forum on Laminar Flow Technology, 1996.
2. **Pfenninger W.** Laminar Flow control, laminarization, Special Course on concepts of drag reduction//AGARD Report No. 654, 1977.
3. **Goldsmith J.** Critical laminar suction parameters for suction into an isolated hole or a singlerow of holes// Rep. BLC-95. Northrop Aircraft., 1957.
4. **MacManus D.G., Eaton J.A., Barrett R.V., Rickards J., Swales C.** Mapping the flow field induced by a HLFC perforation using a high resolution LDV//34th Aerospace Sciences Meeting and Exhibit. – 1996.
5. **MacManus D.G., Eaton J.A.** Measurement and analysis of the flowfields induced by suction perforations// AIAA Journal, 1998.
6. **Campe R.** A two-dimensional model for the conceptual design for a LFC equipped sailplane//Msc thesis report, 2004.

DOI 10.53954/9785604990131_161

COMPUTATIONAL AND EXPERIMENTAL STUDIES OF THE NEAR FIELD OF THE SUPERSONIC CIVIL AIRCRAFT MODEL IN THE WT T-112

S.N. Tolkachev, S.A. Baranov, G.V. Biryukov, V.S. Gorbovskoy, A.V. Zabrodin, S.I. Konovalov, V.E. Mosharov, V.N. Radchenko, D.S. Sboev

Central Aerohydrodynamic Institute
140180, Zhukovsky, Russia

Introduction. Recently, there has been increased interest in a new generation of supersonic civil aircraft (SCA), which during flight will provide a low level of sonic boom (SB) on the ground. Direct experimental studies of SB are complicated by the need to implement a large distance from the model to the wall with measuring devices and, in fact, can only be performed during a flight experiment, which is associated with a high level of material costs. However, experimental techniques have already been developed that make it possible to obtain estimates of SB levels at a large distance from the model based on the results of measuring the disturbed pressure field near the experimental model [1].

An experimental study of the pressure distribution in the "near field" region near an aircraft model is a very non-trivial task. The level of disturbances from models designed to ensure a low level of SB becomes comparable to the level of disturbances present in the test section of the wind tunnel, which significantly complicates the interpretation of the results.

Experimental conditions. As part of this work, on an experimental stand located in the test section of the T-112 TsAGI wind tunnel with a cross section of 600×600 mm, pressure distribution measurements were carried out at two Mach numbers (1.5 and 1.78) in the "near field" from the SCA model on the measuring wall, installed flush with the wall of the test section of the wind tunnel. SCA model with a length of 304.7 mm, a span of 114.9 mm and a height of 31 mm was located from the nearest wall at a distance of 195 mm on a knife-shaped holder. Using a set of special inserts, it was possible to achieve an angle of attack of the model of 3.24°; 3.5°; 3.76°; 3.98°. Obtaining near-field characteristics for these regimes will make it possible to assess the influence of a vertical gust of wind when it affects the model on the SB value.

The measuring wall allows you to implement two methods of recording pressure distribution: pneumometric (3 rows of 128 pressure measurement points) and pressure sensitive paint (PSP), which make it possible to obtain the pressure distribution over the entire surface of the measuring panel. The PSP method is indirect, restoring the distribution of absolute pressure, is sensitive to surface temperature, but, on the other hand, is panoramic with a fairly high spatial resolution. Combining the two techniques makes it possible to significantly expand the experimental capabilities for studying the "near field". To isolate the pressure distribution from the SCA model in the near field region against the background of natural disturbances in the test section of the wind tunnel, the subtraction technique was used. It is based on the linearity of disturbances, due to their rather small amplitude. The wind tunnel was launched with an empty test section, which made it possible to determine the structure and amplitude of the wind tunnel's own disturbances.

The pressure distributions near the SCA model measured using the above-mentioned methods in the "near field" are not direct and are not suitable for a direct assessment of the

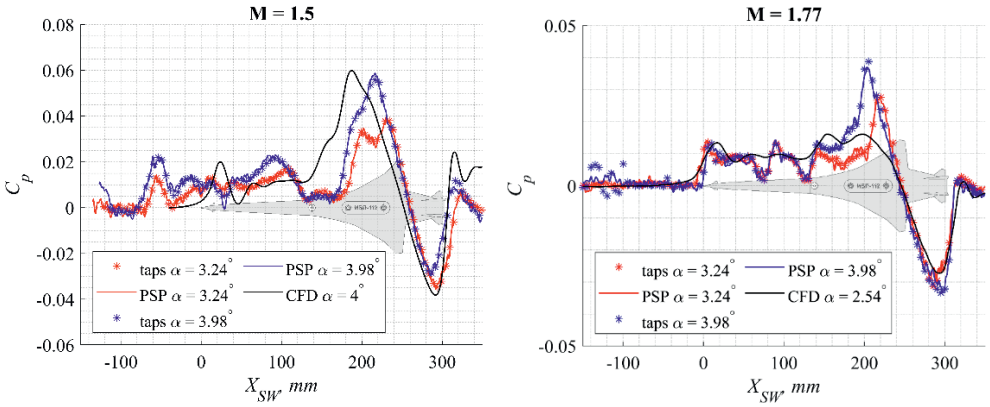

Fig. 1. Comparison of the distribution of the pressure coefficient C_p on the measuring wall on the first line of pneumatic taps at M = 1.5 (left figure) and 1.77 (right figure).

taps – pneumometry results; *PSP* – results obtained using PSP; *CFD* – results obtained by calculation.

SB level, since they reflect the result of the interaction of shock waves with a developed turbulent boundary layer present on the measuring wall. For this reason, the concept of a computational and experimental method has been adopted, the essence of which is to simultaneously calculate the experimental configuration using Computational Fluid Dynamics (CFD) methods, taking into account the developed turbulent boundary layer and comparison with experimental results.

Results. The level of pressure disturbances from the SCA model during the experiment was comparable to the natural level of disturbances in the working part of the wind tunnel. To isolate the disturbances created by the SCA model, a subtraction technique was used, previously successfully used at TsAGI. The results obtained by the two methods coincided with each other to within a constant accuracy. The data obtained using PSP have been corrected.

In the M = 1.5 regime (left figure in Fig. 1), a high level of disturbances was observed that were not compensated by the subtraction method, making it difficult to interpret the results obtained and compare them with the calculation. The structure of disturbances in the region of the tail shock in the experiment qualitatively coincides with the calculation results.

In the M = 1.78 regime (right figure in Fig. 1), the quality of the experimental results is significantly higher than those obtained at M = 1.5. When comparing the experimental results with the calculations, the pressure disturbance levels are in good agreement. Apparently, the main differences are due to the difference in the angle of attack of the model in calculations and in experiments, and disturbances that are not compensated by the subtraction method also have a negative impact.

Acknowledgments. The work is prepared in the implementation of the program for the creation and development of the World-Class Research Center “Supersonic” for 2020-2025 funded by the Ministry of Science and Higher Education of the Russian Federation (Grant Agreement of May, 17, 2022, № 075-15-2022-1023).

REFERENCES

1. **Zhilin Yu.L.** O svyazyvanii blizhnego i dalnego polej v zadache o zvukovom udare [On the coupling of near and far fields in the sonic boom problem] // Uchenye zapiski TsAGI – TsAGI Science Journal 1998. Vol. 29, № 3–4. P. 111–122.

DOI 10.53954/9785604990131_163

INVESTIGATION OF POSSIBILITY OF COLD SPRAYING UNDER PROTECTION OF DEPOSITS AGAINST AMBIENT AIR

S.Yu. Usynin, S.V. Klinkov, V.F. Kosarev

Khristianovich Institute of Theoretical and Applied Mechanics SB RAS
630090, Novosibirsk, Russia

At cold spraying (CS), a wide range of materials, both substrates and powders, are used. Some materials, such as titanium and its alloys, react strongly with oxygen when the air is utilized as working gas. As an alternative to air, nitrogen or helium can be used, resulting in oxidation to be minimized. However, at the typical standoff distance (SoD) during for cold spraying (z_{ns} = 30 mm), there is an intense mixing of ambient air into nitrogen or helium jet and, thus, oxygen can reach the substrate and coating. As a result, under condition of high temperatures, the substrate itself and the particles (moving in jet or sitting on coating surface) are covered with an oxide film. The presence of oxide films affects deposition efficiency and coating quality. As a protection against oxidation, one could propose a modernization of the outer shape of the typical cold spray working nozzle with adding shielding disk. There have been no studies on the protection of the spray zone against the external environment under cold spray conditions, but there are a small number of published works devoted to the study of this possibility in related disciplines such as plasma spraying and laser cladding [1], which makes this topic relevant. The aim of this work is to numerically investigate the possibility of protecting the spray zone against ambient air. In this study, the Ansys Fluent is used to simulate the flow pattern, with special attention to be paid to nitrogen and oxygen concentrations, temperatures, and velocities.

The main parameters of the problem corresponded to the conditions of typical experimental ones. The supersonic jet was formed using an axisymmetric de Laval nozzle 145 mm long with critical and exit cross-section diameters of 2.8 mm and 6.5 mm, respectively. A cylindrical aluminum plate, with a radius of 30 mm and a thickness of 5 mm, was used as the substrate; diameter of shielding disk was 26 mm. The substrate axis coincided the nozzle axis. The nozzle did not move relative to the substrate, so that there were stationary parameters in the flow of supersonic jet on the substrate. The distance from the nozzle exit to the substrate (SoD) varied from 30 mm down to the distance, at which the space between the disk and the substrate is completely filled with nitrogen. Pure nitrogen was used as the working gas. The posed problem is solved in axisymmetric formulation. The k–ω SST turbulence model was chosen to close the Navier-Stokes equations. The input conditions are nitrogen stagnation pressure of 3.75 MPa and temperature of 573 K. The jet outflow is into the ambient space with air pressure of 0.1 MPa and temperature of 300 K. Fig. 1 shows the mass fraction of nitrogen at different SoD distances.

The calculation results show that at the standard distance 30 mm (a), the area of pure nitrogen covering the substrate surface is smaller than the nozzle exit diameter. As the nozzle approaches the substrate, where SoD = 5 mm (b) and 4 mm (c), this area and the height of the gas layer increases due to protection. If the nozzle is set at a distance of 3 mm (d), the space between the shielding disk and the substrate is filled with nitrogen only i.e. without oxygen.

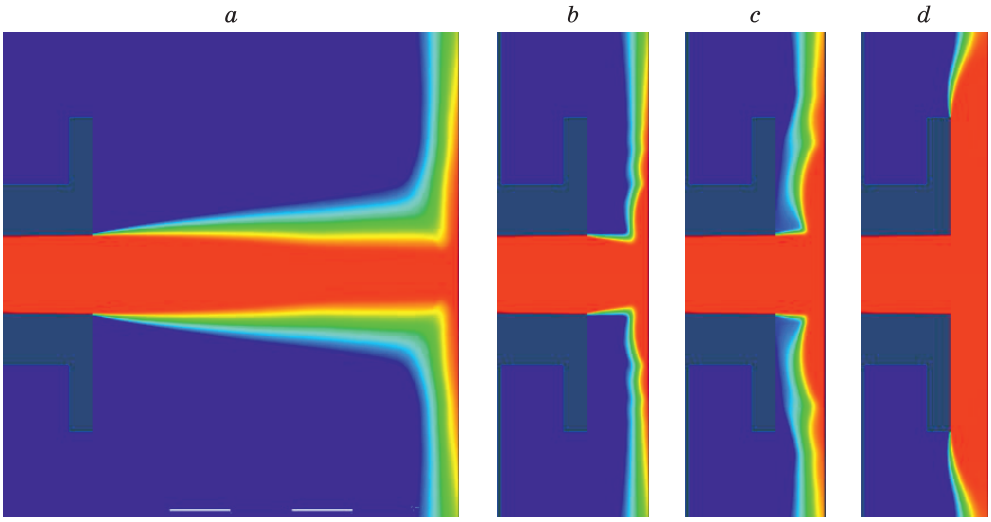

Fig. 1. Mass fraction of nitrogen at different distances.

a – 30 mm, b – 5 mm, c – 4 mm, d – 3 mm.

Hence, the calculation results confirm the effectiveness of the proposed cold spray nozzle design modernization, which in the future will help to avoid oxidation of coating and substrate materials.

The research was carried out within the state assignment of Ministry of Science and Higher Education of the Russian Federation.

REFERENCES

1. **Patent No 2105084 RF.** Protection device of zone of gas-powder laser welding-up of metals from external medium and method of protection of zone of gas-powder laser welding-up of metals from environment (versions) / Kovalev O.B., Bedenko D.V. Appl. No 2019108105. Date of filing: 21.03.2019. Date of publ.: 01.09.2020.

DOI 10.53954/9785604990131_165

THE INFLUENCE OF MAGNETIC FIELD ON THE FLOW STRUCTURE NEAR SUBMILLIMETER ARC DISCHARGE IN TRANSVERSE MAGNETIC FIELD

M.A. Yadrenkin, Yu.V. Gromyko, V.P. Fomichev

Khristianovich Institute of Theoretical and Applied Mechanics
630090, Novosibirsk, Russia

For the active control of subsonic and supersonic wall currents, active control methods, including magnetoplasmic techniques, have been employed. These methods involve the generation of volumetric electromagnetic forces within an ionized gas subjected to a magnetic field [1, 2]. Surface electric discharges of various types are utilized to induce local ionization of the flow. Recent studies have focused on developing miniature actuators based on an arc discharge that moves within an external magnetic field [3]. This paper examines a method that utilizes a submillimeter arc discharge to create volumetric electromagnetic forces. This method enables the localized manipulation of the flow near the streamlined surface within the gas region, with dimensions comparable to the thickness of the boundary layer.

This paper presents the experimental findings regarding the impact of magnetic field strength on the flow structure when discharge plasma is subjected to a magnetic field at pressures ranging from 1300 Pa to atmospheric conditions. The investigations were conducted in both stationary gas and supersonic flow scenarios. A submillimeter arc discharge lasting between 10 and 50 microseconds was generated between two circular electrodes, positioned flush with the dielectric surface at a distance of 2.2 mm. Alternatively, a line of electrodes was arranged perpendicular to the flow. A generator was employed to produce electric current pulses, characterized by a high-voltage igniting pulse lasting less than 1 microsecond, followed by a low-voltage working voltage pulse with adjustable duration, enabling gas breakdown and subsequent discharge combustion with reduced energy release. To create a permanent magnetic field of up to 0.3 T, rare-earth magnets of varying thicknesses were integrated into the working surface. The magnetic field was oriented perpendicular to the surface, resulting in the movement of the discharge along the surface.

The visualization of the observed phenomena was conducted using a shadow method in conjunction with a high-speed camera. Additionally, the particle image velocimetry (PIV) technique was employed, and the measurement area was coated with soot particles. The laser knife plane was positioned at various sections, perpendicular to the surface, both in the direction of the discharge movement and transversely. The restoration of the velocity field was accomplished through the utilization of cross-correlation adaptive algorithms, employing continuous window displacement, a single grid division, and deformation of the computational domain. With precise process synchronization, accurate to at least 100 ns, and excellent repeatability, averaged velocity fields of tracer particles were obtained, comprising 50-100 pairs of frames, with a high level of detail. These measurements provided data on the three-dimensional configuration of the resulting flow, including information on the dynamics of the shock wave pattern that emerges immediately after the gas breakdown.

The presented figure illustrates the flow structure 230 microseconds after the initiation of electric breakdown, showcasing different magnetic field strengths. The characteristic flow patterns arise from the movement of gas under the influence of electromagnetic forces, leading to the formation of a low-density cavity in the region of initial energy release. Figures (*a*)

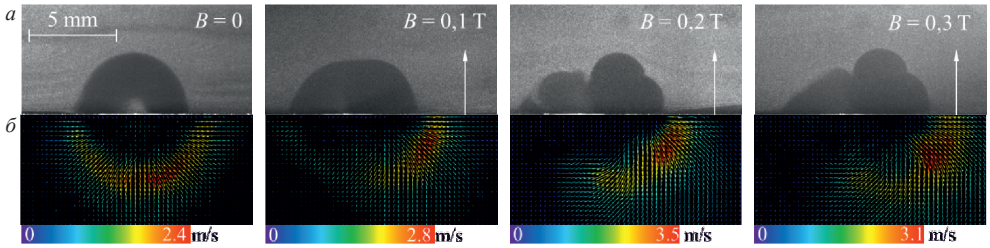

The flow structure formed during the movement of a pulsed electric discharge in a magnetic field: distribution of tracer particles in the plane of the laser knife (*a*) and PIV measurement results (*b*).

depict the distribution of tracer particles, while figures (*b*) display the corresponding velocity fields obtained through the PIV method, represented as a mirror image. It is observed that the initially homogeneous spherical shape of the cavity, formed without a magnetic field, undergoes transformation into a complex vortex structure due to electromagnetic forces. Following the attenuation of the discharge, the cavity continues to expand and propagate in the direction of the initial force. Subsequently, the cavity experiences collapse, characterized by a disruption of its integrity and uniformity. The study establishes that the magnitude of the magnetic field influences the decay rate of the flow, attributed to increased local Reynolds numbers and early turbulence. This assumption is supported by the maximum values of instantaneous gas velocity measured using the PIV method.

Overall, this paper presents the evolution of wall flow resulting from the movement of submillimeter electric discharge plasma under the influence of electromagnetic forces at varying magnetic field strengths. The findings suggest that this type of actuator can effectively manipulate the structure of wall flow during the flow of both subsonic and supersonic air around a plane.

The research was carried out with funding from the Russian Science Foundation Grant No. 23-29-00825 https://rscf.ru/project/23- 29-00825/.

The study was conducted using equipment provided by the Shared-Use Center “Mechanics” (ITAM SB RAS)

REFERENCES

1. **Yang Hs.** et al. Research Progress of hypersonic boundary layer transition control experiments. // Adv. Aerodyn. 4, 18 (2022). https://doi.org/10.1186/s42774-022-00105-1
2. **Joussot R.** et al. Aerospace Lab, 10 (2015) https://doi.org/10.12762/2015.AL10-04
3. **Moralev I.** et al. // J. Phys. D: Appl. Phys. 53:42 2020. P. 425203 https://doi.org/10.1088/1361-6463/ab9d5a

DOI 10.53954/9785604990131_167

DEVELOPMENT OF AN APPROACH TO MODELLING THE GAS DYNAMICS OF LASER PLASMA IN A FLOW

V.I. Yakovlev, T.A. Korotaeva

Khristianovich Institute of Theoretical and Applied Mechanics, Siberian Branch of Russian Academy of Sciences, 630090, Novosibirsk, Russia

One of the main directions of plasma aerodynamics is the development of computational models that make it possible to predict the structure of flows with energy absorption in the flow. When using optical discharge plasma, there are certain difficulties due to the fact that laser plasma is formed in different modes of optical discharge propagation [1]. Each corresponds to a dominant mechanism of plasma front transfer, depending on the energy parameters of the laser beam and the conditions of its focusing; the mode may change during the pulse duration. For example, in a study [2] of laser plasma in the process of absorption of a CO2 laser beam, it was revealed that the light supported detonation wave (LSDW) mode at peak pulse power transforms into the fast ionization wave (FIW) mode in the power absorption "plateau" region. A feature of the LSDW mode is the formation of a high-speed microjet plasma flow in the direction of the laser beam [3]. As a result, the volume of the LSDW plasma, in addition to energy, acquires momentum in the direction of the laser beam, and the FIW plasma absorbs the remaining half of the energy of the laser pulse without the formation of plasma flows in the axial direction.

This work proposes a new approach to creating a computational model for determining the dynamics of gas-thermodynamic parameters of an optical discharge plasma, taking into account the features of the above modes of optical discharge propagation. Analysis of the physics of discharges shows that, firstly, the duration of the early stage of the appearance of primary electrons is significantly less than the total duration of the laser pulse. Secondly, the speed of discharge propagation is significantly higher than the characteristic scale of the speed of gas-dynamic disturbances. Therefore, in the computational model it is possible to use a hydrodynamic approach, in which plasma regions are energy (heat) sources that have a certain set of spatiotemporal parameters, as was used in numerous computational studies, for example, in [4]. However, it is necessary to take into account the features of laser discharges. In the LSDW mode, a plasma flow is formed in the direction of the laser beam, while in the FIW mode, energy is absorbed without the formation of a directed plasma flow. Therefore, in this work, the model of an energy source in a subsonic argon flow (Fig. 1) contains two (*1*, *2*) regions of laser energy absorption during two characteristic time intervals of the laser pulse. Their energy- and spatio-temporal parameters are determined on the basis of experimental data from recording the dynamics of energy absorption and visualizing the structure of the plasma glow. The value of the mo-

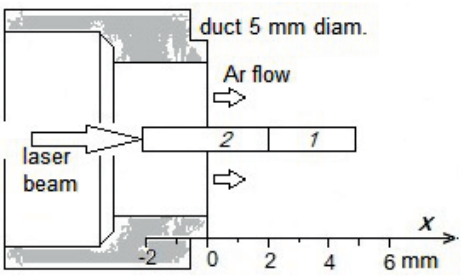

Fig. 1. Scheme of the energy source.

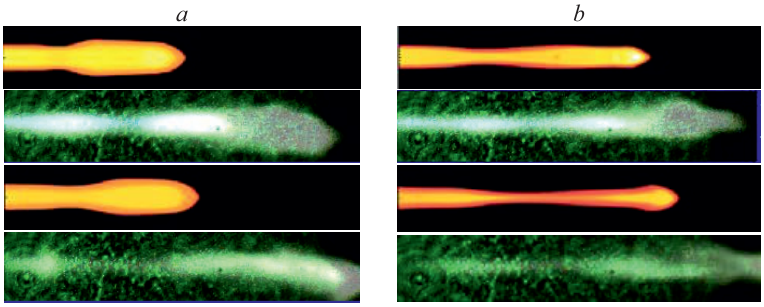

Fig. 2. Results of luminosity calculations (above), without (*a*) and accounting (*b*) the plasma momentum. The experiment is below.

mentum of the microjet plasma flow, calculated on the basis of the analytical approach [3], was also used. In the initial stage of 0–1 μs in region *1*, the LSDW mode occurs, with the absorption of half the pulse energy. In the subsequent stage of 1–2.5 μs in region *2* (including 1), the second half of the energy is absorbed without the formation of directed flows, an analogue of the FIW mode.

Numerical modeling of laser energy supply into a subsonic argon flow was carried out for a non-stationary problem in an axisymmetric formulation using the ANSYS FLUENT software package. The Reynolds-averaged Navier-Stokes equations were solved, supplemented by the k-ω SST turbulence model. The supply of energy and momentum is realized by specifying additional terms for the equations of conservation of energy and momentum. For this purpose, a so-called user-defined function was written in the C programming language, which specified the spatiotemporal parameters of the region of the simulated laser plasma and the features of the LSDW and FIW modes. An example of the results obtained is presented in Fig. 2. The temperature field obtained in the calculations is converted into the relative luminosity parameter S/S_{max}. On the left are the results of calculations (t = 4 and 6 μs) of the S-field with energy supply without taking into account the plasma momentum, on the right – with it taken into account. Below the calculated data are frames of visualization of the glow in the time intervals of their registration (4.16–5.16 μs and 6.25–7.25 μs). A comparison of the calculation and experimental results shows that the influence of the plasma momentum is manifested in the formation of a more extended plasma structure. The head part is an LSDW plasma, and the wake behind it is caused by the absorption of energy in the FIW mode; the energy supply stops after 3 μs. The axial speed reaches values of up to 3.6 km/s; As a result of the acceleration of the LSDW plasma, the transverse size of the waist decreases. The downstream displacement of the plasma boundary is close to the calculation taking into account the LSDW regime. The calculation results also made it possible to determine characteristic trends in the dynamics of the plasma structure and parameters. The speed and temperature reach their maximum values during the period of absorption of laser pulse energy. Subsequently, the plasma is separated, advancing its head part downstream due to the increased speed in the LSDW mode.

Thus, the main result of this study is that an approach has been developed to create a computational model for determining the dynamics of an optical discharge plasma, which has been confirmed in a comparative analysis of experimental and calculated data.

REFERENCES

1. **Prokhorov A.M., Konov V.I., Ursu I. and Mikheilesku I.N.** Laser Beam Interaction with Metals Nauka Moscow (1988)

2. **Yakovlev V.I., Shulyatyev V.B., Yadrenkin M.A., and Gimon T.A.** Optical Discharge Regimes Sustained by a Continuously Pumped, Q-Switched Pulsed CO2 Laser // Bulletin of the Lebedev Physics Institute, Vol. 50, Suppl. 10, pp. S1108–S1119 (2023). Russian Text © The Author(s), 2023, published in Kvantovaya Elektronika, Vol. 53, No. 6, pp. 475–483. (2023).
3. **Thomas P.D.** Jet flowfield behind a laser supported detonation wave // *AIAA J*. Vol. 15. No. 10. P. 1405 (1977)
4. **Zudov V.N., Tretyakov P.K., Tupikin A.V., Yakovlev V.I.** Supersonic flow around a heat source // Izv. Akad. Nauk, Mekh. Zhidk. Gaza **38** (5), 140 (2003).

DOI 10.53954/9785604990131_170

FREE FLOW DISTURBANCES FROM TWO-DIMENSIONAL ROUGHNESS OF DIFFERENT SIZES IN A SUPERSONIC TURBULENT BOUNDARY LAYER ON A WALL

A.A. Yatskikh, N.V. Semionov, A.D. Kosinov, Y.G. Yermolaev, L.V. Afanasev

Khristianovich Institute of Theoretical and Applied Mechanics SB RAS
630090, Novosibirsk, Russia

Free-stream disturbances can significantly influence the laminar-turbulent transition of the boundary layer. In [1, 2], it was found that disturbances of the free-stream flow generated from roughness on the wall of the test section of a wind tunnel of a small height compared to the turbulent boundary layer lead to a significant distortion of the mean and pulsating flow in the boundary layer on a streamlined model. The occurrence of longitudinal stationary disturbances (streaks) in the boundary layer was discovered, in the region of which early turbulization of the flow is possible. The problem of predicting the shape, amplitude and location of disturbances generated in a free flow above a turbulent boundary layer when flowing around roughness of various sizes on a smooth wall at supersonic flow speeds is of fundamental and practical importance.

The purpose of this work is to determine the influence of the geometric dimensions (width, height) of a two-dimensional roughness on the wall of the test section of a wind tunnel on the disturbances generated in a free supersonic flow. The main data were obtained using numerical simulation in the FlowVision software package. Calculations were carried out in a two-dimensional formulation for flow parameters close to the experimental case. To model the turbulent boundary layer on the wall, the Spalart–Allmaras turbulence model was used. The thickness of the boundary layer significantly exceeded the height of the studied irregularities. When constructing the computational grid, the near-wall region was resolved, as well as the region of disturbances from two-dimensional roughness. To verify the calculation results, experimental data are presented. The results of experimental measurements of the mean and pulsation characteristics of the flow are presented. Experimental studies were carried out in the T-325 wind tunnel of the ITAM SB RAS. Two-dimensional roughness of various heights was installed on the wall of the test section. Disturbances from non-uniformity were recorded using a hot-wire probe of a constant temperature anemometer. The results of studies on the influence of the height and width of the generator on the amplitude of stationary disturbances of the free flow are presented.

The study was financially supported by the Russian Science Foundation (project no. 22-19-00666, https://rscf.ru/project/22-19-00666/). The work was carried out at the Equipment Sharing Center “Mechanics” of the Institute of Theoretical and Applied Mechanics of the Siberian Branch of the Russian Academy of Sciences. Numerical simulation was performed using the FlowVision software (https://flowvision.ru/).

REFERENCES

1. **Ermolaev Y.G., Kosinov A.D., Kocharin V.L., Semenov A.N., Semionov N.V., Shipul S.A., Yatskikh A.A.** Experimental study of the influence of external disturbances on the position of the laminar-turbulent transition on swept wings at M = 2 // Thermophysics and Aeromechanics. – 2021. – Vol. 28. No. 3. – P. 319–325.
2. **Kosinov A.D., Semionov N.V., Yatskikh A.A., Kocharin V.L., Shmakova A.V.** Influence of the leading-edge bluntness radius of a plate on the response of flat-plate boundary layer to an N-wave at Mach number M = 2 // Thermophysics and Aeromechanics. – 2023. – Vol. 30. No. 2. – P. 227–237.

DOI 10.53954/9785604990131_171

INFLUENCE OF LONGITUDINAL SLOTS OF DIFFERENT HEIGHTS ON THE SURFACE OF A PLATE ON THE GROWTH OF LOCALIZED DISTURBANCES IN THE SUPERSONIC BOUNDARY LAYER

A.A. Yatskikh, V.I. Lysenko, B.V. Smorodsky, G.L. Kolosov

Khristianovich Institute of Theoretical and Applied Mechanics SB RAS
630090, Novosibirsk, Russia

To control the laminar-turbulent transition in boundary layers, it is advisable to influence the early stages of the development of disturbances. One of the possible ways to tighten the laminar flow regime is to modify the surface, in which the change in the global flow pattern is insignificant, while the flow inside the boundary layer is modified. The possibility of using such approaches is being actively studied both for the case of subsonic flow speeds [1–2] and at high speeds [3–5]. For the case of high flow velocities, many works are devoted to studying the influence of micro-profiling on stabilizing the growth of second-mode disturbances. In particular, studies were carried out for the case of slots (small hollow in the surface of the model); a number of works showed the possibility of stabilizing the growth of disturbances of the second mode, while the first mode was destabilized. Also worth highlighting are recent works devoted to studying the possibility of using low-height depressions on the surface of a swept wing to stabilize the growth of cross-flow instability disturbances [6].

In recent experiments (V.I. Lysenko and colleagues) in the T-325 wind tunnel of the ITAM SB RAS at Mach number 2, stabilization of the growth of natural disturbances in the boundary layer of a plate with extended slots of longitudinal orientation was discovered. In this work, under experimental conditions, a numerical simulation of the development of disturbances in the boundary layer on a flat plate with longitudinal slots of varying depths that are periodic in the transverse direction (no more than the thickness of the boundary layer) is carried out. Data from numerical modeling of the development of localized disturbances are presented, wave analysis is carried out, and the wave characteristics of the development of disturbances are determined. It was found that longitudinal slots of small depth can reduce the growth of boundary layer disturbances compared to the case of a smooth plate.

The study was financially supported by the Russian Science Foundation (project no. 23-79-10167, https://rscf.ru/project/23-79-10167/). The work was carried out at the Equipment Sharing Center “Mechanics” of the Institute of Theoretical and Applied Mechanics of the Siberian Branch of the Russian Academy of Sciences. Numerical simulation was performed using the FlowVision software (https://flowvision.ru/).

REFERENCES

1. **Grek G.R., Kozlov V.V., Titarenko S.V.** An experimental study on the influence of riblets on transition // J. Fluid Mech., 1996, 315, 31–49.
2. **Grek G.R., Kozlov V.V., Titarenko S.V., Klingmann B.G.B.** The influence of riblets on a boundary layer with embedded streamwise vortices // Phys. Fluids. 1995, 7(10), 2504–2506.
3. **Fedorov A.V., Novikov A.V., Semenov N.N.** Toward optimal wavy surface shape for high-speed boundary layer stabilization // Int J. Fluid Mech. Res., 2020, 47(4), 329–335.
4. **Lukashevich S.V., Morozov S.O., Shiplyuk A.N.** Experiments on the development of natural disturbances in a hypersonic boundary layer on surfaces with microgrooves // Experiments in Fluids. 2021, 62, art. 155. 14 p.
5. **Bountin D., Chimitov T., Maslov A., Novikov A., Egorov I., Fedorov A., Utyuzhnikov S.** Stabilization of a hypersonic boundary layer using a wavy surface // AIAA J. 2013, 51(5), 1203–1210.
6. **Fedorov A., Novikov A.** Stabilization of crossflow mode by grooves on a supersonic swept wing // Theor. Comput. Fluid Dyn. 2023, 37, 261–268

Content

САМОСТОЯТЕЛЬНОЕ ЭЛЕКТРОННОЕ ИЗДАНИЕ

Научное издание

Международная конференция по методам
аэрофизических исследований
1–5 июля 2024 г.,
Новосибирск, Россия
Тезисы докладов
Часть I

На английском языке

INTERNATIONAL CONFERENCE ON THE
METHODS OF AEROPHYSICAL RESEARCH
July 1–5, 2024
Novosibirsk, Russia
Abstracts
Part I

Ответственный за выпуск А.В. Бойко
Технический редактор Н.М. Райзвих

Минимальные системные требования:
Тип компьютера, процессор, сопроцессор Pentium 4
Оперативная память (RAM) 512 Мб
Необходимо на винчестере 10 Гб
Операционные системы Widows XP
Дополнительные программные средства Adobe Acrobat 7.0

Сибирское отделение РАН
630090, просп. Акад. Лаврентьева, 17

ICMAR

ISBN 978-5-6049901-3-1